Imperial College London

Imperial College London

Department of Physics

Towards physical realisations of Quantum Thermodynamics

Author:
Zoë Holmes

Supervisors:
Dr. Florian Mintert, Dr. Janet Anders & Dr. David Jennings

A thesis submitted for the degree of

Controlled Quantum Dynamics

November 1, 2020

Copyright declaration

The copyright of this thesis rests with the author. Unless otherwise indicated, its contents are licensed under a Creative Commons Attribution-Non Commercial 4.0 International Licence (CC BY-NC). Under this licence, you may copy and redistribute the material in any medium or format. You may also create and distribute modified versions of the work. This is on the condition that: you credit the author and do not use it, or any derivative works, for a commercial purpose. When reusing or sharing this work, ensure you make the licence terms clear to others by naming the licence and linking to the licence text. Where a work has been adapted, you should indicate that the work has been changed and describe those changes. Please seek permission from the copyright holder for uses of this work that are not included in this licence or permitted under UK Copyright Law.

Declaration of originality

I hereby declare that the content of this thesis is my own work. The research has been developed during my PhD at Imperial College London under the guidance of my supervisors Florian, Janet and David. All published work of others has been appropriately acknowledged and referenced.

Abstract

Quantum thermodynamics seeks to extend the laws of thermodynamics to equilibrium and non-equilibrium systems on the nano-scale. Over the last decade a large body of theoretical research into quantum thermodynamics has been produced; however, experimental research is yet to catch up with the impressive lead set by theory. This is especially true of quantum information theoretic approaches which have proven an effective means of incorporating quantum effects into thermodynamics but seem resistant to experimental implementation. This thesis aims to counter this shortcoming by proposing concrete physical realisations of quantum thermodynamics to help bridge the gap between theory and experiment.

This task is approached directly in chapter 2 by constructing an experimental implementation of a fluctuation relation developed from a quantum information theoretic perspective. Our proposal involves the autonomous evolution of a trapped ion and uses a tapered laser beam to implement a position dependent AC Stark shift. In order to test the fluctuation relation we convert the abstract framework of an autonomous quantum Crooks equality into quantum Crooks equalities for coherent, squeezed and cat states. These new relations highlight the physical origins and implications of coherence induced corrections to classical fluctuation relations and prompt a discussion on the interplay between coherence and irreversibility.

In chapter 3 we turn our attention to Gibbs' iconic thought experiments on the work that can be extracted from the mixing of gases. Here we argue that optomechanical setups, involving a cavity in which a membrane is inserted, provide a suitable platform both to generalise such thought experiments to the quantum regime and to explore quantum thermodynamic signatures of distinguishability. We find, in contrast to classical thermodynamics, that the work that can be extracted from the mixing of the two photon gases varies continuously with their distinguishability. Finally, we demonstrate that the bunching of photons, arising from their Bosonic character, generates an energetic footprint that does not exist in classical thermodynamics.

Contents

1 Introduction **13**

2 Coherent fluctuation relations: from the abstract to the concrete **21**
2.1 Introduction . . . 21
2.2 Background . . . 22
2.2.1 Non equilibrium classical thermodynamics . . . 22
2.2.2 The classical Crooks equality . . . 23
2.2.3 Quantum fluctuation relations . . . 25
2.3 The fully quantum Crooks equality . . . 27
2.4 Derivation . . . 33
2.4.1 Gibbs map . . . 33
2.4.2 Time reversal . . . 34
2.4.3 Global Invariance . . . 35
2.4.4 Factorisability . . . 36
2.4.5 Main derivation . . . 37
2.4.6 General comments on structure of the FQC . . . 38
2.5 Quantum corrections to the classical Crooks equality . . . 42
2.5.1 Coherent state Crooks equality . . . 43
2.5.2 Squeezed state Crooks equality . . . 47
2.5.3 Cat state Crooks equality . . . 49
2.6 Autonomous quantum Crooks equality . . . 51
2.6.1 Autonomy and approximate factorisability . . . 51
2.6.2 Error bounds . . . 53
2.6.3 Verification of bounds . . . 54
2.7 Experimental proposal . . . 56
2.7.1 Experimental parameters . . . 59
2.7.2 Experimental techniques . . . 60
2.7.3 Experimental outlook . . . 61
2.8 Conclusions . . . 63

3 An optomechanical piston setup to probe thermodynamic signatures of distinguishability **66**
3.1 Introduction . . . 66
3.2 Classical Gibbs mixing . . . 67
3.3 Quantum Gibbs mixing . . . 69
3.4 Optomechanical piston setup . . . 76

3.4.1 Hamiltonian . . . 78
3.4.2 Calculation of the dynamics . . . 80
3.4.3 Initial states . . . 81
3.4.4 Work output . . . 82
3.5 Optomechanical Gibbs mixing analysis . . . 83
3.6 Optomechanical Gibbs mixing analysis . . . 85
3.7 Bunching enhanced energy transfer . . . 89
3.8 The role of photonic bunching . . . 90
3.9 Experimental outlook . . . 96
3.9.1 Quantum Gibbs mixing with PBS membrane . . . 96
3.9.2 Indistinguishability enhanced energy transfer to BS membrane . . . 98
3.10 Discussion and outlook . . . 103

Bibliography **120**

A Evidence of hostility **121**

B Coherent fluctuation relations **123**
B.1 Comment on role of heat bath . . . 123
B.2 Squeezed state Crooks equality derivation . . . 124
B.3 Cat state Crooks equality derivation . . . 127

C An optomechanical piston setup to probe thermodynamic signatures of distinguishability **129**
C.1 Displacement of PBS membrane for more realistic parameters . . . 129
C.2 Higher order effects . . . 129

List of Figures

1.1 **Coarse-grained photo of city.** When the exposure time of a photo is long as compared to the dynamics captured, the resulting image is coarse-grained and captures the average behaviour of the system. In this long exposure photo of a city at night we can tell that the road on the right (left) contains cars moving away from (towards) us and get a sense of the average occupancy of the buildings in the background. An understanding of the precise microscopic dynamics of every subcomponent, in this case each car and each person in the city, is unnecessary to understand this average behaviour. Image is taken from [1]. 14

2.1 **Full quantum fluctuation relation setup.** (a). Here we sketch the Hilbert space of a system with a Hamiltonian that varies between regions. By evolving the support of the control between regions, a change in system Hamiltonian is induced. In the forwards driving process, the setup is evolved from region i to f and vice versa for the reverse. (b). The total setup consists of a system, heat bath, work store, and control system (dashed circles). We can reduce this to a bipartite system (solid ovals) by using a single hybrid work store and control system, that we will call a 'battery' B and by setting aside the thermal bath and viewing it rather as an implicit means of preparing a thermal state. The arrows denote the systems which exchange energy. 28

2.2 **Sketch of forwards and reverse dynamics.** The blue lines represent the energy level splitting of the two level system as a function of position x. The battery states that are prepared at the start of the protocols (red/green) and the measurements that are performed at the end of the protocols (yellow/purple) are indicated by solid lines. The evolved states of the battery at the end of the driving process as sketched as dashed lines. 30

2.3 **Relation between states.** In the forwards process, the state $|\phi_i\rangle$ is prepared, evolves (indicated by the wiggly arrow) and the state $|\phi_f\rangle$ is measured. In the reverse process, the state $|\phi_i\rangle$ is prepared, evolves and the state $|\psi_f\rangle$ is measured. As indicated by the solid lines, the state $|\psi_i\rangle$ ($|\phi_f\rangle$) is related to the state $|\phi_i\rangle$ ($|\psi_f\rangle$) by the mapping specified in Eq. (2.28). 32

2.4 **Understanding the off-diagonal Crooks equality.** The process of increasing the splitting of a two level system in the presence of a harmonic oscillator battery. The left and right figures cover the cases when the two level system starts in the excited (a) and ground (b) states respectively. The see-saw like mechanism, highlighted by the red arrows, ensures energy conservation and maps changes in the system energy onto that of the battery. A superposition of battery states is raised or lowered 'as one' and as such the coherences evolve in the same manner as the populations. 40

2.5 **Coherent state Crooks equality deviations.** The purple line indicates the average energy, $\hbar\omega_T$, of a quantum harmonic oscillator in a thermal state at temperature T. The grey line shows the classical limit in which $\hbar\omega_T$ tends to k_BT. The blue dotted line and red dashed line indicate the thermal and quantum contributions to $\hbar\omega_T$ respectively, as specified by Eq. (2.98). These energies are given in units of k_BT and are plotted as a function of χ, Eq. (2.83). 46

2.6 **Squeezed state Crooks equality deviations.** We plot the prefactor q, Eq. (2.127), as a function of χ for coherent states and squeezed displaced states. The red, purple and blue lines plot $r = 1$, $r = 0$ (i.e. the coherent state case) and $r = -1$ respectively. The grey line indicates the classical limit in which $q = 1$. As indicated by the black Wigner plot insets, in a) the prepared and measured squeezed displaced battery state are displaced with respect to position only, that is the displacement is real $\alpha_{i,f} = \Re(\alpha_{i,f})$ and $\mu_{i,f} = \Re(\mu_{i,f})$; whereas in b) the state is displaced with respect to momentum only, that is the displacement is purely imaginary $\alpha_{i,f} = \Im(\alpha_{i,f})$ and $\mu_{i,f} = \Im(\mu_{i,f})$. 48

2.7 **Cat state Crooks equality deviations.** We plot $q := \frac{\Delta\tilde{E}}{W_q}$ as a function of χ for cat states. As indicated by the insets, in a) the prepared and measured battery states consist of superpositions of coherent states with opposite phase, specifically $|\phi_i\rangle = |\mathrm{Cat}_i\rangle \propto |\delta/2\rangle + |-\delta/2\rangle$ and $|\phi_f\rangle = |\mathrm{Cat}_f\rangle \propto |\delta/2+1\rangle + |-\delta/2-1\rangle$. In b) the prepared and measured states consist of superpositions of different displacements with the same phase, specifically $|\phi_i\rangle = |\mathrm{Cat}_i\rangle \propto |-2\rangle + |-2-\delta\rangle$ and $|\phi_f\rangle = |\mathrm{Cat}_f\rangle \propto |2\rangle + |3\rangle$. In both figures the dark blue line indicates $q(\chi)$ for coherent states. . . . 50

2.8 **Verification of error bounds.** We plot the error measures for evolution under the total Hamiltonian with the position dependent level splitting interaction and a harmonic oscillator battery. In the main figures, the solid (dashed) lines plot D (ϵ) and the insets plot $1 - R$. In (a) the coherent state Crooks equality data is shown in purple and squeezed state Crooks equality data shown in red ($r = -1$) and blue ($r = 1$). In (b) the data for cat states prepared and measured either side of the interaction, $|\psi_i\rangle = |\phi_f\rangle \propto |\alpha\rangle + |-\alpha\rangle$, is shown in red and the data for cat states prepared and measured on a single side of the interaction region, $|\psi_i\rangle \propto |-\alpha\rangle + |-(\alpha+1)\rangle$ and $|\phi_f\rangle \propto |\alpha\rangle + |\alpha+1\rangle$, is shown in blue. In this simulation we have used the following parameters: $x_i = -4$, $x_f = 4$, $\hbar\omega = 1$, $E_i = 1$, $E_f = 2$ and $k_BT = 1$. Both plots are a function of $-\alpha_i = \alpha_f$ the displacement of the prepared/measured state. The displacement parameters, $\alpha_{i,f}$, and the positions x_i and x_f, are given in units of dimensionless position $X = \sqrt{\frac{2m\omega}{\hbar}}x$. 55

2.9 **Sketch of trapped ion proposed implementation.** An ion (red wavepacket) is trapped in an elongated trap (grey line) which drives its evolution through the trap (indicated by red arrow). An off-resonance laser is applied perpendicularly across one half of the trap (blue oval). The laser beam has an intensity profile with a flat central region (blue line in oval). The trapped ion experiences a position dependent AC Stark shift (pair of blue lines) as it travels autonomously through the laser beam. The red dashed line indicates the spread of the ion and the black dashed line the width of the elongated trap. Here we show the ion at the start of the autonomous evolution stage of the protocol. The preparation and measurement stages of the protocol are sketched in Fig. 2.10. 58

2.10 **Preparation and measurement techniques**. Here we sketch, for the forwards protocol, the preparation (a) and measurement (b) stages of the coherent state trapped ion implementation. (a) To prepare the ion in a coherent state the ion is first cooled to the motional ground state with respect to an initial harmonic trapping potential, shown here in blue. The center of the trapping potential is then shifted non-adiabatically. The new trapping potential after the shift is shown in grey. The ion will remain in the ground state with respect to the old potential but will be in a coherent state with respect to the new trapping potential. (b) The measurement to find the overlap between some test coherent state (the blue Gaussian) and the evolved state of the ion (the dashed red wavepacket) effectively runs the preparation process in reverse. First, the trap potential is shifted such that were the evolved state equal to the test state then after the shift the evolved state would be in the ground state with respect to the new trapping potential. The old potential from the evolution process is shown in grey and the new shifted potential is shown in blue. Secondly, a projective measurement is made to find the overlap between the evolved state and the ground state of the new trapping potential. The laser beam that induces the AC Stark shift is indicated in both figures by the blue oval. 60

2.11 **Alternative position dependent potentials**. We plot the predicted quantum deviation q deduced from the transition probabilities between coherent states, using Eq.(2.127), for different choices of $E(x)$ which we plot in the inset. The turquoise circles indicate q for the usual 'flat ends' potential, the purple squares q for a $\sin(x)^2$ potential, and the red triangles q for a purely linear potential. The predicted analytical form of $q = \frac{\tanh(\chi)}{\chi}$ (also sketched in Fig. 2.6) is plotted in blue and the classical limit in which $q = 1$ is plotted in grey. In this simulation we have chosen the following physically plausible parameters, $x_i = -2$, $x_f = 2$, $E_i = 1$MHz, $E_f = 2$MHz, $\alpha_i = -5$ and $\alpha_f = 4$. The displacement parameters $\alpha_{i,f}$ and the positions, x_i and x_f, are given in units of dimensionless position. 62

3.1 **Gibbs mixing.** (a) Two types of gas, a 'red' gas and a 'yellow' gas, are initially confined to two halves of a box of volume $2V$. To draw work from the mixing of the two gases, a pair of semi permeable membranes is inserted, with red (yellow) particles passing through the red (yellow) membrane while being confined by the yellow (red) membrane. (b) The membranes are held in place with two springs, allowing them to move. Since each membrane confines one gas, which exerts a pressure on it, the gases compress the springs, performing work and mixing in the volume between the springs. (c) Eventually the membranes are pushed to the far edges of the vessel and the two gases are fully mixed. The expansion of each of the two ideal gases from V to $2V$, while in thermal contact with a heat bath at temperature T, can be used to draw work. 67

3.2 **Gibbs mixing generalisation to gases containing uneven particle numbers.** (a) Two types of gas, a 'red' gas containing $2Nx$ particles and a 'yellow' gas containing $2N(1-x)$ particles, are initially confined to volumes $2Vx$ and $2V(1-x)$ respectively. The two gases are at the same temperature and pressure. To draw work from the mixing of the two gases, a pair of semi permeable membranes is inserted, with red (yellow) particles passing through the red (yellow) membrane while being confined by the yellow (red) membrane. (c) Eventually the membranes are pushed to the far edges of the vessel and the two gases are fully mixed. The expansion of each gas while in thermal contact with a heat bath at temperature T, can be used to draw work. 68

3.3 **Quantum Gibbs mixing.** a) Initially (left) there are N particles of an ideal gas in state $|\uparrow\rangle$ and N particles of another non-interacting ideal gas in state $|\theta\rangle$, confined in two volumes V separated by a solid barrier. Let λ, $|\psi\rangle$ and $|\psi_\perp\rangle$ denote the eigenvalue and eigenstates of $\frac{1}{2}|\uparrow\rangle\langle\uparrow| + \frac{1}{2}|\theta\rangle\langle\theta|$. The initial state (left) can be unitarily rotated to the state (right) in which there are $2N\lambda$ particles of an ideal gas in state $|\psi\rangle$ occupying volume $2V\lambda$ and $2N(1-\lambda)$ particles of a gas in state $|\psi_\perp\rangle$ occupying volume $2V(1-\lambda)$ separated by a barrier. The inverse unitary transforms this final state (right) back into the initial state (left). Both processes are isentropic and so the transformations require no work or heat exchanges. b) A gas containing $2N$ particles in the state ρ_{mix} can be divided into two gases containing N particles in state the $|\psi\rangle$ and N particles in the state $|\psi_\perp\rangle$ using a pair of semi-permeable membranes that can perfectly distinguish $|\psi\rangle$ and $|\psi_\perp\rangle$ particles. This separation process requires work and the converse mixing process produces work as shown in Fig. 3.2. 72

3.4 **Peres' argument against magic membranes.** 1) Two gases in non-orthognal states $|\uparrow\rangle$ and $|\theta\rangle$ (indicated by the vertical arrows and diagonal arrows) are initially confined to two halves of a box of volume $2V$. To set up a proof by contradiction we suppose have a pair of *fictional* membranes that can perfectly distinguish between these non-orthogonal states, with vertical (diagonal) particles passing through the vertical (diagonal) membrane while being confined by the diagonal (vertical) membrane. 1) to 2) Following the same protocol as in Fig. 3.1 we can extract the work by mixing the gases with these fictional membranes. 2) to 3) The fully mixed state can written as a mixture of orthogonal states given by its eigen-decomposition. Having established the basis of this eigen-decomposition, which we sketch with horizontal and vertical arrows respectively, we switch the original membranes for a pair of physically realisable semipermeable membranes that can perfectly distinguish the the gas particles in this orthogonal basis (again sketched by horizontal and vertical dashes). 3) to 4) Work is done on the gas to divide it into its orthogonal components. 4) to 1) Finally, to complete the cycle the newly separated state is transformed back to the initial state. Since these states have the same entropy this step can be performed using a unitary operation requiring no work or heat exchanges. The net extracted work in the cycle is given by $W_{\text{gain}} - W_{\text{cost}}$. 73

3.5 **Semi-classical work extraction protocol.** 1) We start with $p(\psi_1)2N$ particles of a gas in state $|\psi_1\rangle$ and $p(\psi_2)2N$ particles of a gas in state $|\psi_2\rangle$, confined in two volumes $p(\psi_1)2V$ and $p(\psi_2)2V$ separated by a pair of membranes which measure in the orthogonal basis $\{|m_1\rangle, |m_2\rangle\}$. 1) to 2) The ψ_1 and ψ_2 gases are each separated into their orthogonal m_1 (red) and m_2 (yellow) components using the inverse of the classical Gibbs mixing protocol (Fig. 3.2) incurring work costs $W_{\text{cost 1}}$ and $W_{\text{cost 2}}$ respectively. 2) to 3) The pairs of vessels containing gases in states m_1 and m_2 are combined at no work cost. 3) to 4) The two vessels, one containing gas particles in the state m_1 and the other containing gas particles in the state m_2, are mixed using the classical Gibbs mixing protocol and allowing work to be extracted. 75

3.6 **Optomechanical setup.** A microscopic membrane is inserted into a cavity and allowed to oscillate. The displacement of the membrane from the mid-point of the cavity is denoted by X_M and the creation operator for this mechanical mode is $M^\dagger$. The transmission rate between the horizontally (vertically) polarised photon modes on the left hand side of the membrane, $L_H^\dagger$ ($L_V^\dagger$), and horizontally (vertically) polarised modes on the right, $R_H^\dagger$ ($R_V^\dagger$), is determined by the constant λ_H (λ_V). The force exerted per horizontally (vertically) polarised photon on the membrane is given by g_H (g_V). When the membrane is a perfect BS it interacts identically with horizontally and vertically polarised modes and thus $\lambda_H = \lambda_V$ and $g_H = g_V$. When the membrane is a perfect PBS, the membrane reflects all vertically polarised photons and thus $\lambda_V = 0$. It follows that for a PBS membrane the vertically polarised photons exert a greater force on the membrane than the horizontally polarised photons and therefore $g_V > g_H$. 78

3.7 **Time averaged displacement of PBS membrane.** We plot the time averaged displacement of the PBS membrane normalised by the mean number of photons per gas, $\frac{\langle X_M \rangle}{\langle N \rangle}$, and shade the normalised standard deviation of this displacement, $\frac{\sqrt{\langle X_M^2 \rangle - \langle X_M \rangle^2}}{\langle N \rangle}$, as a function of the distinguishability θ of the photons in the left cavity from the photons in the right cavity. In a) the photons are initially in a Fock state with $n = 1$ photons per cavity (light blue squares) and $n = 100$ photons per cavity (dark blue circles) and the membrane is in a thermal state at temperature $k_B T = \omega_M$. In b) both the photons and the membrane are initially in a thermal state at the same temperature $k_B T = \omega$ (peach diamonds) and $k_B T = 100\omega$ (red triangles), to ensure there is no temperature gradient such that the work output and fluctuations can be attributed solely to mixing. In both plots the following parameters were chosen to illustrate the thought experiment: $\lambda/\omega_M = 2$, $g_V/g_H = 6$ and $\omega = 10\omega_M$. All distances are given in units of $\frac{\hbar g_V}{m\omega_M^2}$. 84

3.8 **Change in energy of PBS membrane.** We plot the time averaged change in energy of the PBS membrane to first order in g_H and g_V, normalised by the expected number of photons per gas squared, as a function of the distinguishability of the photons in the left cavity from the photons in the right cavity. We plot the data for when the photons are initially in a Fock state with $n = 1$ photons per cavity (light blue squares) and $n = 100$ photons per cavity (dark blue circles) and for when the photons are initially in a thermal state at temperature $k_B T = \omega$ (peach diamonds) and $k_B T = 100\omega$ (red triangles). The inset magnifies the data for $\theta \leq \pi/8$ to highlight that the energy transfer does not vanish as $\theta \to 0$. All energies are given in units of $\frac{\hbar^2 g_V^2}{m\omega_M^2}$. In this plot $\lambda/\omega_M = 2$, $g_V/g_H = 6$, $\omega = 10\omega_M$. 87

3.9 **Temperature dependence.** The mixing work $W_M/\langle N \rangle$, Eq. (3.54), to first order in g_H and normalised by the average photon gas number $\langle N \rangle$. For perfectly distinguishable gases ($\theta = \pi/2$, solid red) $W_M/\langle N \rangle$ grows as a function of the photon state temperature T, Eq. (3.46), and is zero for indistinguishable gases ($\theta = 0$, not shown). For higher temperatures the slope becomes the same as that of the classical Gibbs mixing work per particle W_{dist}/n, Eq. (3.2), for distinguishable gases (solid black). Also shown is the full energy transfer to the membrane given by $\Delta \bar{H}_M$ in Eq. (3.55) for perfectly distinguishable gases (dark blue dashed) and for perfectly indistinguishable gases (light blue dotted). Again in the high temperature regime, both slopes become the same as the classical mixing work (solid black) and hence the energy transfers to the membrane grows linearly with the photon gas thermal state temperature. The classical work is given in units of $k_B T$ and the quantum work W_M and energy transfer $\Delta \bar{H}_M$ are given in units of $\frac{\hbar^2 g_V^2}{m\omega_M^2}$. In this plot $\lambda/\omega_M = 2$, $g_V/g_H = 6$, $\omega = 10\omega_M$. 88

3.10 **HOM effect in optomechanical setting.** Elementary processes of the Hong-Ou-Mandel effect in the present optomechanical setup. In (a) the photon from the left is reflected and the photon from the right is transmitted and vice versa in (b). In (c) both photons are transmitted and in (d) both photons are reflected. When the photons are perfectly distinguishable, i.e. $j = H$ and $k = V$ or $j = V$ and $k = H$, then all four outcomes (a - d) are equally probable. When the photons are perfectly indistinguishable, *i.e.* $j = H$ and $k = H$ or $j = V$ and $k = V$, then the amplitudes for outcomes (c) and (d) destructively interfere and the outcomes (a) and (b) are equally probable. 92

3.11 **Correlation functions for BS membrane.** In (a) we plot the $\mathcal{g}_{\text{L,R}}(t)$ correlation function as a function of time and in (b) we plot 1 minus the time average of the $\mathcal{g}_{\text{L,R}}(t)$ correlation function as a function of the distinguishability of the two photon gases θ. In both figures we plot the data for when the photons are initially in a Fock state with $n = 1$ photons per cavity (light blue squares) and $n = 100$ photons per cavity (dark blue circles) and for when the photons are initially in a thermal state at temperature $k_BT = 5\omega_L$ (peach diamonds) and $k_BT = 100\omega_L$ (red triangles). . 94

3.12 **Correlation functions for PBS membrane.** In (a) we plot $\mathcal{g}_{\text{L,R}}(t)$ as a function of time for perfectly distinguishable photons ($\theta = \pi/2$, solid), partially distinguishable photons ($\theta = \pi/4$, dashed) and perfectly indistinguishable photons ($\theta = 0$, dotted). In (b) we plot 1 minus the time average of the $\mathcal{g}_{\text{L,R}}(t)$ dips shown in (a) as a function of distinguishability. The photons are initially in a Fock state and we plot data for a PBS membrane with $n = 1$ photons per cavity (red) and $n = 100$ photons per cavity (dark blue) and for a BS membrane with $n = 1$ photons per cavity (orange) and $n = 100$ photons per cavity (light blue). 95

3.13 **Displacement of PBS membrane under proposed implementation.** The left hand figure plots the average displacement of the membrane as a function of time when the left cavity is driven by photons that are polarised at angle θ and the right cavity is driven by horizontally polarised photons. Polarisation angles $\theta = \pi/2$, $\theta = \pi/4$ and $\theta = 0$ are shown in blue, purple and red respectively. On the right, we plot our estimate for the steady state displacement of the membrane, Eq. (3.87), as a function of distinguishability. This confirms our estimate is accurate since the steady state displacements in the left hand plot for $\theta = 0$, $\theta = \pi/4$ and $\theta = \pi/2$ align well with the predicted displacements from the right hand plot. In both plots the parameters are taken from Table 3.9.1. 97

3.14 **Energy transfer to BS membrane in presence of damping.** We plot the average energy of the membrane as a function of time when the photons in the left cavity are vertically polarised and the photons in the right hand cavity are polarised at angle θ such that when $\theta = 0$ (blue) the photons are perfectly indistinguishable, when $\theta = \pi/2$ (red) the photons are perfectly distinguishable and when $\theta = \pi/4$ (purple) the photons are partially distinguishable. We suppose that the light in both cavities is in a coherent state containing 10^6 photons and use the parameters in Table 3.9.1. 101

3.15 **Symmetric superposition state of photons and membrane.** The membrane is always in a symmetric superposition of different displacements. It is in a superposition of there being more photons on the right with the membrane displaced to the left and there being more photons on the left with the membrane displaced to the right. This symmetry is enforced by the mirror symmetry of the Hamiltonian which is invariant under a swap of the right and left modes combined with a change of sign of the displacement of the membrane. Thus, while the average displacement of the membrane vanishes, the variance to its displacement does not. Moreover, if we measure the number of photons in each cavity, the symmetric superposition will collapse leading to a well defined displacement and potential energy of the membrane. 105

A.1 **Quotes on quantum thermodynamics community.** These are a selection of quotes from physicists working in Quantum Thermodynamics on current tensions within the community. The facebook posts from Oppenheim, Goold and Campisi are taken from the COST network 2017 Quantum Thermodynamics conference page. The quote from Hänggi is taken from the a review of this conference that was published in Nature News. 121

B.1 **Enlarged system setup.** The total setup consists of a system, heat bath, work store, and control system (small circles). We can reduce this to a bipartite system (large circles) by using a single hybrid work store and control system, that we will call a 'battery' B and by viewing the system and heat bath as a composite enlarged system S. The arrows denote the systems which exchange energy. 123

C.1 **Time averaged displacement of PBS membrane.** Plot of $\langle X_M \rangle$ (directly related to the work output via (3.54)) normalised by the mean number of photons $\langle N \rangle$ per gas as a function of the distinguishability θ of the photon gases. a) Photons are initially in a Fock state with $n = 1$ photons per cavity (light blue squares) and $n = 100$ photons per cavity (dark blue circles). b) Photons are initially in a thermal state at temperature $T = \hbar\omega/k_B$ (peach diamonds) and $T = 100\hbar\omega/k_B$ (red triangles). For all four cases (light blue squares, dark blue circles, red triangles, peach diamonds) the displacement per photon is the same function over the distinguishability parameter θ. The shaded region shows the normalised standard deviation of the displacement. Parameters in both figures: $g_V x_{\text{zpf}} = 6 g_H x_{\text{zpf}} = 600\text{kHz}$, $\lambda = 10\text{GHz}$, $\omega = 1\text{THz}$, $\omega_M = 1\text{MHz}$, $m = 10\text{ng}$ and the membrane is at temperature $T_M = 5\hbar\omega_M/k_B$. All distances are given in units of $\frac{\hbar g_V}{m\omega_M^2}$. 130

C.2 **Second order contribution to energy transfer.** We plot the first and second order contributions to the time averaged energy transfer to a beamsplitter membrane as a function of the distinguishability of the photons in the cavity in the absence of damping effects ($\kappa = \kappa_C = 0$). Once the energy transfer to the membrane is averaged over fast oscillations the first order contribution to the energy transfer is constant in time, while the second order contribution has an amplitude that grows quadratically in time. Here we plot the second order correction up to $10\mu s$ (the cavity lifetime in the experimental setup of Ref[23]). The membrane is prepared in a thermal state containing on average $\bar{n}_{th}$ phonons, where $\bar{n}_{th} = 10$, $\bar{n}_{th} = 100$ and $\bar{n}_{th} = 1000$ in the left, centre and right plots respectively and the light field in both halves of the cavity is initially in a coherent state containing on average 10^6 photons. We utilise the following parameters from the experimental settings in [2,3]: $\omega_M = 350$kHz, $\omega = 20$THz, $\lambda = 34$GHz, $m = 45$ng and $gx_{\text{zpf}} = 3.3$kHz, with similar behaviour expected for a range of parameters. 131

Chapter 1

Introduction

It all began with a desire to improve the efficiency of steam engines. Carnot apparently thought ultra efficient steam engines would help France win the Napoleonic war. However, not long after its original development, Clausius recognised the applicability of thermodynamics to the study chemical compounds and chemical reactions. Since then the theory has gone from strength to strength. In contrast to many of its contemporaries, thermodynamics survived the revolutions of quantum mechanics and relativity. The breadth of the theory continues to grow and has now been successfully applied to a diverse range of systems from galactic gases to biological materials. Moreover, despite thermodynamics' distinctly industrial origins, it has shown itself well suited to answering fundamental theoretical questions on irreversibility and the direction of time.

Classical thermodynamics is complemented by kinetic theory and statistical mechanics. These two fields of research tackle similar questions concerning heat and temperature and their relationship to work; however, they do so from a different perspective. Einstein's distinction between principle theories and constructive theories is helpful here to understand how these approaches fit together.

A principle theory takes empirically discovered phenomena and raises them to the status of fundamental principles. These fundamental principles then form the foundation of the theory and are used as the starting point to study other physical phenomena. Thermodynamics is the paradigm example of a principle theory. Its starting points are the observations that energy cannot be created or destroyed only transformed and that perpetual motion machines are impossible. These empirical observations become the first and second laws of thermodynamics from which much of the rest of thermodynamics is derived. Thermodynamics' robustness and generality stems from its principle theory status. In being formulated in terms of general empirical laws, rather than being built from a picture of the underlying nature of things, thermodynamics can survive paradigm shifts to our ontological understanding while also being applicable to a broad spectrum of systems.

Constructive theories take a theoretical model of the underlying constituents of nature as their starting point and use the laws governing their microscopic behaviour to deduce the behaviour of more complex composite systems. The paradigm example of a constructive theory is kinetic theory. Kinetic theory treats atoms and molecules as tiny classical billiard balls which obey the laws of classical mechanics. The macroscopic properties of classical gases can then be deduced by modelling classical gases as containing a large number of such particles undergoing elastic collisions between themselves and the walls of the container. Statistical mechanics is also a constructivist theory but its starting point is a picture of ensembles of systems each represented by a point in



Figure 1.1: **Coarse-grained photo of city.** When the exposure time of a photo is long as compared to the dynamics captured, the resulting image is coarse-grained and captures the average behaviour of the system. In this long exposure photo of a city at night we can tell that the road on the right (left) contains cars moving away from (towards) us and get a sense of the average occupancy of the buildings in the background. An understanding of the precise microscopic dynamics of every subcomponent, in this case each car and each person in the city, is unnecessary to understand this average behaviour. Image is taken from [1].

phase space.

Constructive theories and principle theories complement each another. In broad terms, while constructive theories provide causal explanations for the founding principles of principle theories, principle theories can provide a robust unifying picture with which to understand the diverse phenomena that emerge from constructive theories. Thus thermodynamics takes its laws as given without attempting to provide an explanation for them, whereas kinetic theory and statistical mechanics explain how these laws emerge from a picture of the microscopic constituents of physical systems. Conversely, thermodynamics provides an account of why galactic gases and biological materials, in spite of their different underlying natures, display the same general thermodynamical phenomena. Note, this does not exclude constructive theories from also being unifying. Statistical mechanics' account of the structure of phase space, irrespective of the precise nature of the system represented by a point in phase space, can also be argued to provide a unifying framework. However, there is always a causal element to the unifying story told by constructive theories that complements the simple and resilient picture provided by principle theories.

Thermodynamics, statistical mechanics and kinetic theory fundamentally provide a coarse-grained picture of macroscopic systems. An underlying principle of the approaches is that the microscopic degrees of freedom of a macroscopic system become effectively irrelevant as long as any measurements are made on a time scale that is long compared to that of the microscopic dynamics. For such measurements we obtain a coarse-grained picture of the system's dynamics which can be well described by a small number of thermodynamic variables that capture the average properties of the system.

More pictorially, thermodynamics' description of nature is analogous to the blurred photo taken with a slow shutter speed. In Fig. 1.1 you can tell that the road on the right contains cars moving away from us, that the road on the left contains cars moving towards us and get a sense of the average occupancy of the buildings in the background. Details such as the precise location of each car or the rooms occupied at any moment in time are unnecessary to understand the behaviour

captured by the photo.

For an explicitly thermodynamic example consider the work done slowly compressing a volume of gas. The exact work done depends on the precise location and velocity of the particles in the box. However, with standard measurements we only have access to the average pressure of the gas where this average can be measured on a time scale that is long as compared to the molecular dynamics but short compared to the compression process. The average work done during the compression is calculated from this average pressure and fluctuations away from the average work are expected to be so small as to be unmeasurable.

When we could only study *macroscopic classical* systems on *'slow'* time scales this picture of the average behaviour of systems was highly effective. However, we are increasingly capable of controlling microscopic and even nanoscopic systems, including those which manifest quantum phenomena. This opens up the study of new regimes of thermodynamic behaviour. The coarse-grained picture of classical thermodynamics, statistical mechanics and kinetic theory is insufficient to quantify such regimes for the following four reasons.

Firstly, on the nano-scale fluctuations away from the average behaviour of a system become significant. For example, there is a finite probability for nanoscale systems to locally violate the second law of thermodynamics, a feature which is not captured through the study of average properties such as average entropy or heat production. Furthermore, with rapid progress in ultra-fast control and measurement protocols, we can now study and manipulate such fluctuations. This motivates the extension of thermodynamics to quantify higher order statistical properties of thermodynamic systems.

Secondly, on the nano-scale thermodynamic assumptions which hold for macroscopic systems cease to hold. For example, in classical thermodynamics it is implicitly assumed that the coupling between a system and its thermal environment is very weak. This is reasonable for macroscopic systems since interactions between the system and the environment will take place at the boundary of the system, which for large systems is a small proportion of their total volume. However, for nano-scale objects, consisting of only a handful of particles, the weak coupling assumption may break down.

Thirdly, while these theories are routinely applied to quantum systems; they lack the tools to explicitly study the thermodynamic role of quantum phenomena such as coherence, entanglement and contextuality. Such phenomena have proven advantageous in a wide range of areas including computation, cryptography and metrology. It is thus natural to ask they too can be harnessed to the advantage of thermodynamical machines, such as fridges or thermometers.

Finally, traditional classical thermodynamics and statistical mechanics concern the properties of systems at *equilibrium*, that is a system within which there are no net flows of energy or matter. However, in many cases we are interested in the work required or heat flows generated when a system is driven from equilibrium. This is true in general, not just in the context of nano-scale systems, and 'non-equilibrium thermodynamics' is a field of research in and of itself that is almost as old as conventional thermodynamics. However, the limitation is heightened in the context of quantum systems since states with interesting quantum properties such as energetic coherence and entanglement are generally non-equilibrium states.

Quantum thermodynamics is a new field of research that seeks to counter these limitations by extending the laws of thermodynamics to the study of *equilibrium* and *non-equilibrium* systems on the *nano-scale*. In particular, quantum thermodynamics probes whether quantum phenomena

such as coherence, entanglement or contextuality generate novel thermodynamical effects.

The extension of thermodynamics to the nanoscale has the potential to impact industries from pharmaceutical development to information technology. We can now build molecular motors and optical thermal engines that operate on the nanoscale [4] and study the role of quantum effects in the functioning of biological thermodynamical processes [5,6]. There is an increasing evidence that naturally occurring molecular motors, such as kinesin a protein which transport chemicals around cells, are substantially more efficient than our best macroscopic engines [7]. This suggests that we have a lot to learn from studying the thermodynamics of microscopic biological systems.

Moreover, resources are being poured into the development of hardware to realise quantum technologies for computing, communication and cryptography. However, as with all hardware, the efficiency of the new quantum technologies will be determined by the effectiveness of their energy supply and storage systems as well as heat management. Thus, an understanding of thermodynamics of quantum systems will be essential to the successful realisation of these new technologies.

While physicists have been discussing the thermodynamics of quantum systems for as long as the two theories have existed, over the last decade or so quantum thermodynamics has developed into a field of research in its own right. Under the umbrella of 'quantum thermodynamics' sit a range of approaches that generalise thermodynamics, statistical mechanics and kinetic theory to the quantum regime. The community has gathered researchers from a mix of different backgrounds and thus naturally breaks into distinct sub-communities characterised by the techniques used. Three dominant sub-communities are the quantum information theoretic community, the stochastic thermodynamics community and the open quantum systems community. Again, the principle-constructive theory distinction is useful to understand how these approaches complement one another.

Quantum Information. Quantum information theory is the study of the informational content of a quantum state, independently of the physical system that supports that information. Thus quantum information theory remains agnostic to the physical constitutes of nature and instead quantifies the cost and value of general transformations on quantum states. Quantum information theory was first used to design quantum algorithms and construct quantum communication and cryptography protocols. While the breadth of the theory is continually expanding, its primary aim, similarly to classical thermodynamics, remains to deduce strategies to exploit nature for technological purposes. This shared perspective makes quantum information theory well suited to the study of thermodynamics on the quantum scale.

In broad brush strokes the quantum information theoretic approach to quantum thermodynamics is a principle theory. Rather than starting from microscopic physical models, the quantum information theoretic approach starts from the principle that all fundamental operations are unitary and energy conserving and treats heat baths and work storing batteries as primitives. This approach is reminiscent of the rods and clocks of special relativity, another paradigm example of a principle theory. While more constructive approaches to quantum thermodynamics, such as the stochastic or open systems approaches detailed below, to varying degrees assume a pre-existing structure of what quantum thermodynamics should look like; the quantum information theoretic approach can be viewed as formulating desiderata for a new theory of quantum thermodynamics. This can be compared with Einstein's construction of special relativity, where there simply was no preexisting theory, but instead principles were formulated in order to pick out an essentially unique and sensible physical theory. In the case of special relativity the principle approach was effectively

forced on Einstein as classical mechanics was in crisis and so he had no underlying constructive theory to build from. Here we are not similarly stumbling in complete darkness and the stochastic and open quantum systems approach offer viable alternatives. Nonetheless the information theoretic approach can be viewed as seeking to establish the underlying structure of a new theory of quantum thermodynamics and thus provide a unifying framework to understand thermodynamics on the nanoscale.

A particularly successful technique, adopted from quantum information theory, is the establishment of the resource theory of thermodynamics. Resource theories take a property that is in some sense useful, but usually scarce, and attempt to precisely characterise it. One way of formally characterising a resource is by specifying a restricted set of operations, 'free operations', that cannot be used to create 'more' of a resource. Resources are then defined as the states that cannot be generated using solely free operations. Resource theories were originally developed to quantify entanglement [8] and proved a fruitful technique for quantifying the distillation and teleportation of entanglement. The resource theory of thermodynamics [9–13] treats thermal states as free states and all other states as resources. Specifically, in the 'thermal operations' framework [11, 12] (one of a number of closely related variations of the resource theory of thermodynamics) the free operations are energy conserving unitary operations, the introduction of a thermal state and the throwing away (that is tracing out) of a system. Such resource theoretic approaches have been used to help clarify the fundamental principles of thermodynamics.

More generally, the quantum information theoretic approach has been successfully used to incorporate quantum mechanical phenomena into thermal physics; for a general review see [14–16]. Much of this work was kick started by [17], which investigated the role of quantum entanglement for Landauer erasure (that is, the work cost of erasing information) and applied this to the thermodynamics of reversible computations. This paper was quickly followed by results on the consequences of entanglement for the thermodynamic arrow of time [18] and thermalisation [19]. Subsequent papers have established generalisations of the second law of thermodynamics [20, 21] and bounds on the efficiency of work extraction protocols [22–26] for quantum systems, including those with multiple non-commuting conserved quantities [27–29]. The resource theory framework, specifically the concept of thermal operations, proved a useful tool for much of this research [20–26].

Open quantum systems. An open quantum system is a quantum system that interacts with a quantum environment. This interaction typically results in dissipation, that is a heat flow into the environment, and therefore also alters the dynamics of the system. A vast tool kit of mathematical techniques have been developed to study such open quantum systems. One common approach is to model the environment as consisting of a large number of identical quantum particles, represented as spins or bosons, analogous to the kinetic theory picture of classical gases. More generally, and in contrast to the information theoretic approaches, the open quantum systems perspective depends on specific accounts of the nature of systems and their interactions with thermal environments and thus is more naturally considered a constructive theory.

Researchers are now adopting and adapting tools from the open quantum systems community to study questions of interest to the quantum thermodynamics community. A broad range of issues have been tackled including studying irreversibility [30], quantum friction [31, 32] and the operation of heat engines and pumps with coherent and squeezed baths [33–35]. While the majority of this work has utilised the Lindblad formalism [36] which maintains the classical assumption that systems interact weakly with thermal environments, more recently tools such as the reaction

coefficient formalism [37–40] or hierarchical equations of motion [41], have also been adopted to investigate the thermodynamic consequences for systems which are strongly correlated with their thermal environment.

Stochastic thermodynamics. Stochastic thermodynamics is another constructive approach to quantum thermodynamics which uses techniques from statistical physics and non-equilibrium thermodynamics to better understand non-equilibrium dynamics on the nano-scale. In particular, the field focuses on predicting distribution functions of thermodynamic quantities, such as fluctuating heat or work production, when a nanoscale system is driven from equilibrium.

One of the major successes of non-equilibrium thermodynamics is the development of fluctuation relations [42–44]. These are *equalities*, which generalise the second law of thermodynamics, an *inequality*, to non-equilibrium systems. In doing so, fluctuation relations reveal how equilibrium information, for example the free energy of a thermal system, is encoded in the response of a driven system.

Researchers from a non-equilibrium thermodynamics background have sought to generalise fluctuation relations to quantum systems [45–49]. The resulting relations have since been applied to study the work statistics of many body quantum systems [50] such as spin chains [51–53] and Fermionic [54, 55] and Bosonic [56, 57] systems. This research has lead to new results on topics including dynamical quantum criticality [58] and information scrambling [59].

More recently, the quantum trajectories framework [60], and the closely related measurement based approach[1] to quantum thermodynamics [61], has been developed. This crossover between open quantum systems and stochastic thermodynamics, which draws an analogy between the stochastic sequences of pure states followed by a system interacting with an environment and classical trajectories in phase space, has been used to investigate the role of decoherence in work and entropy production [62] and the thermodynamics consequences of measurement [61].

There is naturally some overlap between the work of the various communities both in terms of questions investigated and techniques used. Some topics, such as fluctuation relations or the performance of nano-scale engines, have been tackled from different perspectives by all communities leading to a rich spectrum of results.

However, in contrast to classical thermodynamics, statistical mechanics and kinetic theory which generally get along and complement each other nicely, not all is sweet and harmonious within the quantum thermodynamics community. Given the different assumptions and language used by the different sub-communities translating between their results can be tricky. Moreover, communication between the quantum information theoretic community and the rest of the quantum thermodynamics community can be fraught. Tensions were running especially high around the time I started my PhD (see Appendix A for more details). The research put out by quantum information

[1] This framework could be viewed as either a principle theory or a constructive theory depending on your perspective. On the one hand the approach shares many traits in common with a principle theory since it derives fundamental features of quantum mechanics from phenomenological postulates, in particular quantisation and contextuality, while drawing a fundamental distinction between systems and measurement devices which are treated effectively as black boxes. It is also explicitly non-reductionist in the sense that the approach actively avoids reducing classical phenomena to the complex dynamics of large numbers of microscopic quantum systems. However, not all constructive theories are built up from the dynamics of microscopic systems (for example the Minkowski spacetime approach to Special Relativity). Therefore one could perhaps alternatively try to argue that as the distinction between systems and measurement devices under this approach is objective, rather than operational, it presents a constructive account of nature in which systems and measurement devices are its 'building blocks'.

theoretic community is accused both of being too radical (that is too much of a departure from classical thermodynamics to be called thermodynamics) and for being overly abstract.

More generally, while a large body of theoretical results have been produced by the quantum thermodynamics community, far too few experiments are being done to verify their results. This is especially true of the quantum information theoretic approach [63], adding fuel to the accusation that the approach is overly abstract.

The broad aim of my PhD has been to try and improve communication between the various fields by proposing

Physical Realisations of Quantum Thermodynamics.

The hope was that by proposing physical realisations for the quantum information theoretic approach in particular, we would counter the criticism that the field is overly abstract while disseminating its results to a wider audience of researchers including experimentalists.

The quantum information theoretic approach, as a principle theory, is formulated in terms of a set of physical principles that thermodynamical systems are expected to obey rather than a picture of the underlying nature of physical systems. These principles are physically natural and thus the expectation is that a large number of systems will obey both them and any results which follow from them. However, little work has been done to concretely list such physical realisations. Moreover, as it turns out, constructing such realisations, by which I mean writing down the Hamiltonian for a known physical setup which obeys all the required assumptions, is a highly non-trivial task. It is this challenge that my PhD has focused on.

We further use these physical realisations to construct concrete experimental proposals, which we argue are implementable using state of the art techniques. Thus we hope they will be realised in the near future, addressing the objection that too few experiments are being conducted in quantum thermodynamics.

Chapter 2, tackles the central aim of my PhD head on by exploring physical realisations of a fluctuation relation, specifically a Crooks equality, developed from a quantum information theoretic perspective [64]. This relation in many ways embodies both the best and some of the most frustrating aspects of the information theoretic approach. The relation is formulated from a small number of physically natural assumptions and can incorporate a wide range of quantum phenomena including coherence and entanglement. However, the relation is rather abstract and intimidating. The original paper [64], which comes to 75 pages, is a rather intense read even for those with a quantum information theoretic background, let alone for someone outside of the community.

We have tried to make the results of the paper a little more physical and accessible in three key ways. Firstly, we digested the paper and presented an abridged and more accessible summary of it in a chapter for a Springer series textbook on quantum thermodynamics [65]. Secondly, we developed from the relation quantum Crooks equalities for the well known coherent, squeezed and cat states [66]. We use these relations to explore coherence induced corrections to the classical Crooks equality and discuss the consequences of coherence for irreversibility. Finally, we proposed an experimental scheme to test these equalities for a trapped ion system [66]. Our proposal uses a tapered laser beam to implement a position dependent AC Stark shift.

Chapter 3, continues on the theme of physical realisations of thermodynamics but deviates slightly from the original target of improving community cohesion. Here we explore a physical implementation of a quantum generalisation of Gibbs iconic thought experiment on the work

that can be extracted from mixing a pair of distinguishable or indistinguishable gases. We argue that optomechanical setups, in which a optical cavity is divided in two by a movable microscopic membrane, provide a platform to generalise such thought experiments to the quantum regime and explore quantum signatures of distinguishability in thermodynamics.

With this broad aim we start by investigating the work that can be extracted from the mixing of partially distinguishable photon gases. Here the semipermeable wall proposed by Gibbs for classical gases, is played by a polarising beamsplitter for the photonic gases in the optomechanical setup. We then show that, in contrast to classical thermodynamics where particles are always either perfectly distinguishable or indistinguishable, the extractable work increases continuously with the degree of distinguishability of the two photon gases.

We further present theoretical results showing that for an ordinary beamsplitter membrane (as opposed to a polarising beamsplitter membrane) the photon dynamics results in an energy transfer to the membrane that increases with the distinguishability of the photons in the cavity. We suggest that this phenomena can be understood as a realisation of the well known Hong-Ou-Mandel effect. We thus conclude that the bunching of photons, arising from their Bosonic character, generates an energetic footprint that does not exist in classical thermodynamics. We end by discussing strategies for observing these new phenomena in state of the art optomechanical systems.

Chapter 2

Coherent fluctuation relations: from the abstract to the concrete

2.1 Introduction

Quantum information theoretic approaches to thermodynamics, as argued in Chapter 1, have proven an effective means of probing the role of quantum phenomena, such as coherence, in thermodynamics. However, the field is sometimes criticised for being overly abstract and far too few experiments are being done to test its results. An alternative significant development, this one originating from the stochastic thermodynamics, is the field of fluctuation relations. Crucially, these generalisations of the second law of thermodynamics are, in contrast to quantum information theoretical approaches at least, well suited to experimentation.

Classical fluctuation theorems have been verified in classical systems such as stretched RNA molecules [67, 68], colloidal particles [69] and classical two-state systems [70]. Experimental implementations of fluctuation relations have also been performed in quantum systems including trapped ion [71, 72], NMR [73] and circuit QED systems [74]. However, while these experiments have been performed on quantum systems the fluctuation relations they probe utilise pairs of projective measurements or continual weak measurements to determine the work probability distribution. Such measurements attenuates the role of coherence plays and the resulting fluctuation relations do not deviate substantially if at all from the equivalent classical relation. Thus is it debatable whether these experiments, while performed on quantum systems, have truly tested a quantum fluctuation relation.

We chose to explore the intersection of these two fields and study a fluctuation relation that sits broadly within the quantum information theoretic approach to quantum thermodynamics. The purpose of doing so was two fold. Firstly, we hoped we could use the information theoretic approach to probe the extent to which coherence generates deviations from classical fluctuation relations. Secondly, we hoped fluctuation relations might provide a bridge from some of the more abstract ideas of the quantum information theoretic approach towards experiment.

Our starting point for the project was a fluctuation theorem derived Johan Åberg. This Crooks-like equality is framed as a relationship between a forwards and reverse quantum channel. It is widely applicable in the sense that it can incorporate both coherence and entanglement. However, the paper is pretty abstract and the channel equality it is so different from the classical Crooks equality that is can be hard to access the impact of the quantum phenomena.

We have made this result more concrete and hopefully comprehensible to those outside of the information theoretic quantum thermodynamics community by taking a two pronged approach. Firstly, we have reformulated the channel equality in terms of transition probabilities between certain easy to prepare quantum states, specifically coherent states, squeezed states and cat states. We use these equalities to discuss quantum deviations from the classical Crooks equality. Secondly, we have come up with a proposal to test this equality using trapped ions.

This chapter is structured as follows. In Section 2.2 we introduce classical and quantum fluctuation relations. In Section 2.3, we introduce our take on Johan Åberg's quantum Crooks equality. This is a heavily processed version of Åberg's work in which we try to present his main equality is a manner that is closer to the original classical Crooks equality. Section 2.4 presents a derivation of this relation to provide a better understanding of how it emerges. Section 2.5 introduces our coherent, squeezed and cat state equalities and uses these to discuss corrections to the classical Crooks equality due to coherence. Section 2.6, describes an autonomous variant of Åberg's relation, which we use to present our experimental proposal utilising trapped ions in Section 2.7. Section 2.8 contains our conclusions.

2.2 Background

2.2.1 Non equilibrium classical thermodynamics

Heat, Q, and work, W, are two types of thermodynamic energy exchanges with the difference between them lying in how useful the energy transfer is. While work is a useful directed energy exchange which can be controlled, heat is an uncontrolled wasteful energy exchange. The first law of thermodynamics states that the change in energy of any system, ΔH, is composed of the sum of these contributions

$$\langle \Delta H \rangle = \langle Q \rangle + \langle W \rangle \ . \tag{2.1}$$

Classical equilibrium thermodynamics quantifies average heat and work exchanges. However, for driven microscopic systems fluctuations away from the average heat and work exchanges become significant. To quantify these fluctuations we introduce the concepts of fluctuating heat and work as the heat and work done along an ensemble of trajectories in phase space.

More precisely, a system is assigned a trajectory in phase space $x(t) = x_t = (q_t, p_t)$ where q_t and p_t are the position and momentum respectively of the system at time t. An ensemble of systems is assigned a probability distribution of such trajectories in phase space $\mathcal{P}(x_t)$. This probability distribution can be understood as the probability to find any system in the ensemble at the point x at time t. The Hamiltonian of the system at time t can be written as $H(x_t, \lambda_t)$ where λ is some external controllable parameter that may be varied over time [14].

We are now in a position to make the notion of work and heat precise by defining them as the controlled and uncontrolled energy exchanges of the system as λ is varied. Specifically, fluctuating work

$$W(\lambda_t, x_t, t_i, t_f) := \int_{t_i}^{t_f} \frac{\partial H(x_t, \lambda_t)}{\partial \lambda_t} \dot{\lambda}_t dt \ , \tag{2.2}$$

is defined to be the change in energy of a single system due to the change in its Hamiltonian, within a time window, here t_i to t_f. Similarly, fluctuating heat

$$Q(\lambda_t, x_t, t_i, t_f) := \int_{t_i}^{t_f} \frac{\partial H(x_t, \lambda_t)}{\partial x_t} \dot{x}_t dt \ , \tag{2.3}$$

is taken to be the change in energy of a single system due to the response of the system, that is the changes to its trajectory, as its Hamiltonian is changed. Fluctuating heat and work are fluctuating in the sense that they are microscopic probabilistic quantities dependent on the initial location of the particle in phase space. The probability distributions for the work done on the system

$$\mathcal{P}(W) := \int \delta(W - W(\lambda_t, x_t, t_i, t_f))\mathcal{P}(x_{t_i})\, dx_{t_i}\,, \tag{2.4}$$

and heat flow into the system,

$$\mathcal{P}(Q) := \int \delta(Q - Q(\lambda_t, x_t, t_i, t_f))\mathcal{P}(x_{t_i})\, dx_{t_i}\,, \tag{2.5}$$

depend on the initial probability distribution over trajectories, $\mathcal{P}(x_{t_i})$, as well as the work performed or heat generated along each trajectory. Energy conservation ensures that the sum of heat and work equals the total change in energy of the system,

$$W(\lambda_t, x_t, t_i, t_f) + Q(\lambda_t, x_t, t_i, t_f) = H(x_{t_f}, \lambda_{t_f}) - H(x_{t_i}, \lambda_{t_f})\,, \tag{2.6}$$

thus extending the first law of thermodynamics to microscopic systems. Moreover, if we take the average of the above equality over all trajectories we regain the usual macroscopic first law, Eq. (2.1).

2.2.2 The classical Crooks equality

Fluctuation theorems are generalisations of the second law of thermodynamics which quantify fluctuating heat and work production. The second law, interpreted at its simplest, rules out certain thermodynamic processes from happening. For example, the second law of thermodynamics would say that 'anti-friction' [75] is impossible: a ball moving along a table is slowed as its kinetic energy is converted to heat but we do not see balls spontaneously absorb heat from the table and accelerate. Conversely, fluctuation theorems acknowledge that the processes ruled out by the second law can happen and that, while such thermal fluctuations are generally improbable, they become increasingly likely as the size of the system considered is reduced. We do see 'anti-friction' in microscopic systems: a teeny tiny particle can be kicked into motion by thermal fluctuations in its environment.

The Crooks equality [42] is part of a class of fluctuation theorems [43] that quantify the extent to which certain processes are more likely than others by quantifying the relative probabilities of particular pairs of processes. The Crooks equality for friction, for example, would state the ratio of the probability of friction to the probability of anti-friction. The larger the ratio of a process to its inverse, the smaller the relative probability for the reverse process and the more irreversible that process can be said to be. For macroscopic systems, a tennis ball say, the probability for anti-friction is negligible and therefore ratio of the probabilities of friction and anti-friction is large. However, for a single molecule the probability for anti-friction may be substantial and therefore the ratio will be smaller indicating that irreversibility is milder.

In particular, the Crooks equality quantifies the work produced or absorbed when an initially thermal system is driven by a change to its Hamiltonian. In the forwards process the Hamiltonian is changed from some initial Hamiltonian $H_i \equiv H(x_{t_i}, \lambda_{t_i})$, to some final Hamiltonian, $H_f \equiv H(x_{t_f}, \lambda_{t_f})$, with the manner in which the Hamiltonian changes over time, that is λ_t, defining the forwards protocol. In the reverse protocol the Hamiltonian is cranked from H_f back to H_i

following the forwards control protocol in reverse, that is varying the control parameter according to $\lambda_{t_f - t}$.

The change in Hamiltonian H_i to H_f, is associated with a change in free energy, ΔF. Crucially, ΔF can be written in terms of the partition function of the initial and final Hamiltonians, Z_i and Z_f respectively, and the temperature T of the driving process via

$$\Delta F = -k_B T \ln \left[\frac{Z_f}{Z_i} \right] \quad \text{where} \quad Z_k = \mathrm{Tr} \left[\exp \left(-\frac{H_k}{k_B T} \right) \right] \ . \tag{2.7}$$

Thus ΔF is a state function in the sense it only depends on the initial and final Hamiltonians and not on the trajectory of the driven system.

In both the forwards and reverse processes the system starts at equilibrium, that is in the forwards process the system is initially in a thermal state with respect to H_i and in the reverse the system is in a thermal state with respect to H_f. However, the change of Hamiltonian in general drives the system far from equilibrium producing or absorbing work in the process. The Crooks equality relates the ratio of probability distributions of the work done in the forwards process, $\mathcal{P}_+(W)$, and the work produced in the reverse process, $\mathcal{P}_-(-W)$, to the change in free energy, with

$$\frac{\mathcal{P}_+(W)}{\mathcal{P}_-(-W)} = \exp \left(\frac{1}{k_B T} (W - \Delta F) \right) \ . \tag{2.8}$$

Thus we learn from the classical Crooks equality that free energy increasing, work producing processes are exponentially suppressed. In this manner the Crooks equality quantifies how irreversible the process of driving a system from equilibrium is.

The Jarzynski equality [44],

$$\left\langle \exp \left(-\frac{W}{k_B T} \right) \right\rangle = \exp \left(-\frac{\Delta F}{k_B T} \right) \ , \tag{2.9}$$

which relates the average work output over all irreversible isothermal processes to the free energy difference of the process, emerges as the integral variant of the Crooks equality. By applying Jensen's inequality [76], which states that $f(\langle x \rangle) \leq \langle f(x) \rangle$ for any convex function f, we regain the second law of thermodynamics,

$$\langle W \rangle \geq \Delta F \ , \tag{2.10}$$

as the statement that the irreversible work required in any process is greater than the corresponding change in free energy. The Jarzynski equality strengthens the second law of thermodynamics in two key related ways. Firstly, we can expand the left hand side of Eq. (2.9) as

$$\left\langle \exp \left(-\frac{W}{k_B T} \right) \right\rangle = \sum_n \frac{1}{n!} \left\langle \left(-\frac{W}{k_B T} \right)^n \right\rangle \ . \tag{2.11}$$

The Jarzynski relation thus includes information about all moments of the work distribution, that is all n, as opposed to just the first moment. Secondly, in being an equality rather than an inequality the restrictions it places on systems are much greater than that of the second law. In this manner, under the shadow of the Jarzynski equality, the second law is reduced to an *inequality* concerning the *first moment* of the work distribution.

The Crooks and Jarzynski equalities relate the change in equilibrium free energy to the non-equilibrium work required for a driving process and thus provide a means of measuring free energies.

Of course, the second law of thermodynamics is saturated for quasi-static driving processes and thus can also provide a means of calculating free energy changes. However, quasi-static processes are at best impractically time consuming and at worse a theoretical idealisation. The crucial difference with the Crooks and Jarzynski equalities is that they hold for arbitrarily fast driving processes and therefore open up more practical avenues for measuring free energy. Indeed, the Jarzysnki equality was originally developed specifically as a tool for aiding numerical simulations for molecular free energy calculations [44, 77].

The relations have since been verified experimentally by stretching RNA molecules (a molecule which plays an important role in biochemical processes and can be pictured as a tiny elastic band) [67, 68]. In the forwards process one end of the RNA molecule is fixed and the other is stretched using a pair of optical tweezers. This in general requires work. In the reverse the RNA molecule is refolded by allowing the end to pull back, generally producing work. The work distributions can be approximated as the product of the pulling force and the displacement of the pulled end of the molecule. By repeating the experiment many times at different pulling speeds the forwards and reverse probability distributions can be obtained for the work done on or by the molecule. The Crooks equality states that

$$\mathcal{P}_+(W) = \mathcal{P}_-(-W) \quad \text{iff} \quad W = \Delta F \tag{2.12}$$

and therefore the value of work W at the crossing point of the forwards and reverse work distributions gives the change in free energy ΔF. Similar experiments have been conducted by studying the fluid dynamics of colloidal particles [69] and classical two-state systems [70].

2.2.3 Quantum fluctuation relations

The simplest derivation of a quantum Crooks equality considers the effect of driving a closed system with a unitary operation. In the forwards process the system is driven from equilibrium with respect to some initial Hamiltonian H_i by a unitary U. This is compared to a reverse process in which the system is initially at equilibrium with respect to some final Hamiltonian H_f and is driven by the inverse of the forwards unitary $U^\dagger$. The work done on the closed system during these driving processes is equal to the change in energy of the system. One way of determining the change in energy of the system is by performing projective measurements at the start and end of the process [45–49].

More concretely, if we consider the spectral decomposition of the initial and final Hamiltonians,

$$H_i = \sum_k E_k(t_i) \left|E_k(t_i)\right\rangle \left\langle E_k(t_i)\right| \quad \text{and} \quad H_f = \sum_k E_k(t_f) \left|E_k(t_f)\right\rangle \left\langle E_k(t_f)\right| \ , \tag{2.13}$$

the quantum work distribution for the forwards (+) and reverse (-) processes under this two-point projective measurement scheme,

$$\mathcal{P}_\pm(\pm W) = \sum_{nm} \mathcal{P}_\pm\big(E_m(t_f), E_n(t_i)\big)\, \delta\big(W - (E_m(t_f) - E_n(t_i))\big) \ , \tag{2.14}$$

is recreated from the joint probability distribution, $\mathcal{P}_\pm(E_m(t_f), E_n(t_i))$, to find the system in the pair of energy eigenstates $E_n(t_i)$ and $E_m(t_f)$. These joint probabilities can be broken into an initial probability and a transition probability, that is we can write

$$\mathcal{P}_+\big(E_m(t_f), E_n(t_i)\big) = \mathcal{P}\big(E_n(t_i)\big)\mathcal{P}_+\big(E_m(t_f)\big|E_n(t_i)\big) \tag{2.15}$$

$$\mathcal{P}_-\big(E_m(t_f), E_n(t_i)\big) = \mathcal{P}\big(E_m(t_f)\big)\mathcal{P}_-\big(E_n(t_i)\big|E_m(t_f)\big) \ . \tag{2.16}$$

As the system is initially prepared in a thermal state the initial probability to find the system with energy $E_n(t_k)$ is Boltzmann distributed, with

$$\mathcal{P}\big(E_n(t_k)\big) = \frac{\exp(-E_n(t_k))}{Z_k} \tag{2.17}$$

for all n and for $k = i$ and $k = f$. For the simple unitary protocol discussed above, the transition probabilities take the form

$$\mathcal{P}_+\big(E_m(t_f)\big|E_n(t_i)\big) = \mathcal{P}_-\big(E_n(t_i)\big|E_m(t_f)\big) = ||\left\langle E_m(t_f)\right| U \left|E_n(t_i)\right\rangle||^2 . \tag{2.18}$$

On substituting the explicit expression for joint measurement probabilities, Eq. (2.18), Eq. (2.17) and Eq. (2.15), into the definition of the work probability distribution, Eq. (2.14), one finds that

$$\begin{aligned}\mathcal{P}_+(W) &= \sum_{nm} \frac{\exp(-E_n(t_i))}{Z_i} ||\left\langle E_m(t_f)\right| U \left|E_n(t_i)\right\rangle||^2 \delta\big(W - (E_m(t_f) - E_n(t_i))\big) \\ &= \frac{Z_f}{Z_i} \sum_{nm} \exp\left(\frac{E_m(t_f) - E_n(t_i)}{k_B T}\right) \mathcal{P}_-\big(E_m(t_f), E_n(t_i)\big)\, \delta\big(W - (E_m(t_f) - E_n(t_i))\big) ,\end{aligned} \tag{2.19}$$

which, making use of the definition of free energy, Eq. (2.7), evaluates to

$$\mathcal{P}_+(W) = \exp\left(\frac{1}{k_B T}(W - \Delta F)\right) \mathcal{P}_-(-W) . \tag{2.20}$$

Thus under this definition of quantum work, the classical Crooks equality, Eq. (2.8), and therefore also the Jarzyski relation, Eq. (2.9), hold unaltered [45–49].

While the above two point projective measurement scheme Crooks and Jarzysnki equalities may be applied to quantum systems, and indeed have been verified in trapped ions [72] and NMR systems [73], the use of projective measurement destroys any coherence generated by the dynamics. As a result the initial and final states of the system are devoid of coherence[1] and therefore these relations cannot be considered *fully* quantum mechanical.

Countless quantum Crooks and Jarzynski equalities have been proposed in recent years. Generalisations of the two-point projective measurement protocol include extensions to open quantum systems [79, 80], driving protocols formulated in terms of quantum channels [81–83] as well as the construction and motivation of new definitions of fluctuating quantum work [84–86]. Examples of such definitions include those which utilise quasi-probabilities [87, 88], the quantum jump approach [61, 62, 89] and the consistent histories framework [90]. While such extensions do lead to some quantum deviations being observed, they are to varying degrees limited by what Hänggi and Talkner, in their review of quantum fluctuation theorems [48], call 'the unavoidable impact that any measurement has on a quantum system'. By defining quantum work in terms of pairs of projective measurements or continual weak measurements, coherence with respect to the energy eigenbasis is attenuated and so is prevented from contributing significantly to the fluctuation theorem.

The challenges encountered by these previous attempts suggest that there are three main obstacles to be overcome should one wish to derive a quantum fluctuation relation. Firstly, it is not clear how work should be defined in the quantum regime (for a review see [84, 91]). Since quantum particles do not have well defined trajectories, the classical definition of fluctuating work [14, 42, 44] is

[1] We use the term 'coherence' in the sense of a 'superposition of states belonging to different energy eigenspaces'. Such energetic coherences can be formally quantified by the thermal operations framework [11, 12] or by measures such as the l_1 norm of coherence [78], $C_{l_1}(\rho) := \sum_{j\neq k} |\left\langle E_j\right| \rho \left|E_k\right\rangle|$, the sum of the absolute value of the off diagonal elements of a state in the energy eigenbasis.

not well defined in the quantum regime. Moreover, it has recently been proven that certain natural features we might expect quantum fluctuating work to possess are incompatible [86][2]. The second challenge stems from the fact that the system in the standard Crooks equality starts in a thermal state, a diagonal state in the energy eigenbasis [92]. As such, if the evolution is to involve quantum mechanical phenomena there needs, implicitly or explicitly, to be a source of coherence. Thirdly, measurements are required to obtain the probability of some process; however, if not careful these measurements kill off the quantum mechanical phenomena to be investigated.

The purpose of the next section is to explicate a quantum information theoretic approach which tries to surmount these challenges by introducing a quantum work store and using non-projective measurements to probe the dissipation of coherence in a thermal environment. We focus on the "fully quantum Crooks equality" (FQC); a Crooks equality derived by Åberg [64] in which coherence plays a non-trivial role. A similar approach was independently used in [93] to incorporate the concept of fluctuating work into the resource theory framework [10] and to generalise the Jarzynski equality [44].

The following section aims to provide non-technical overview of the FQC, with more technical details provided in subsequent sections. The section is developed from a chapter [65], which I wrote for a new Springer Series textbook on quantum thermodynamics [16].

2.3 The fully quantum Crooks equality

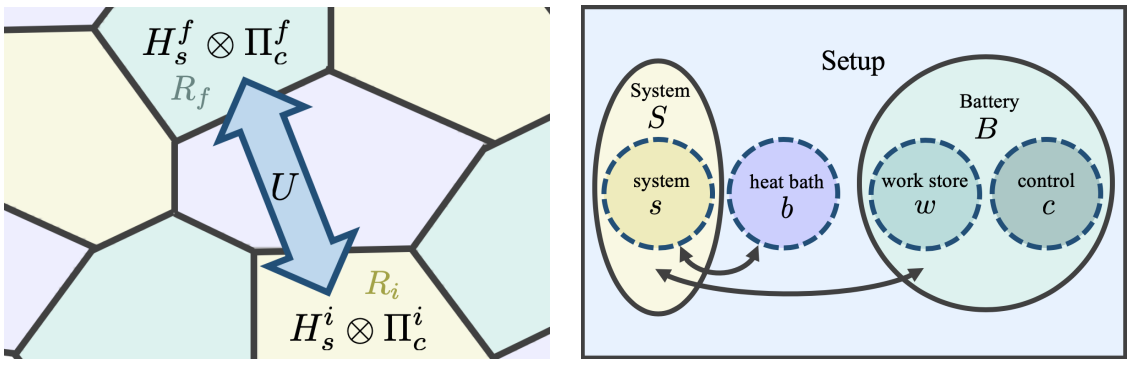
The FQC is derived by making explicit all the systems that are involved in the process of changing the Hamiltonian of some system of interest. The total setup involved in the Crooks equality can be taken to consist of a:

- System of interest.
- Control system: a state of affairs or variable that when changed enables the system's Hamiltonian to be changed.
- Work store: this is the system that provides or absorbs the energy required to drive the system with a change of Hamiltonian.
- Thermal bath: this both allows the system to be prepared in a thermal state and for it to re-equilibriate after the driving process.

The decision to explicitly model enables many of the challenges met in deriving a quantum Crooks equality to be countered. Firstly, the equality is formulated as a relation between work store state transition probabilities, thus sidestepping the question of how to define 'quantum work'. Secondly, the work store may be prepared in superposition of energy states and therefore provides a means of injecting coherence. Thirdly, transition probabilities between superpositions of energy states are considered and therefore the measurements do not destroy *all* energetic coherences. The net result is a general Crooks-like equality in which coherence plays a non-trivial role.

To facilitate a more careful analysis of the energy and coherence changes of the system, the total setup is taken to have a time-independent Hamiltonian. This is in marked contrast to the classical setup, as well as most previous quantum fluctuation theorems [45–47, 61, 62, 79, 80, 87, 90],

[2]Namely, fluctuating quantum work cannot both correspond to the change in average internal energy of a closed quantum system *and* recover the results of classical non-equilibrium thermodynamics for states with no coherence.



(a) (b)

Figure 2.1: **Full quantum fluctuation relation setup.** (a). Here we sketch the Hilbert space of a system with a Hamiltonian that varies between regions. By evolving the support of the control between regions, a change in system Hamiltonian is induced. In the forwards driving process, the setup is evolved from region i to f and vice versa for the reverse. (b). The total setup consists of a system, heat bath, work store, and control system (dashed circles). We can reduce this to a bipartite system (solid ovals) by using a single hybrid work store and control system, that we will call a 'battery' B and by setting aside the thermal bath and viewing it rather as an implicit means of preparing a thermal state. The arrows denote the systems which exchange energy.

which utilise explicitly time dependent Hamiltonians. The disadvantage of such approaches, which we will call the *exclusionary* picture, is they implicitly depend on external classical systems both to induce the time dependent Hamiltonian and to supply or absorb the energy required to do so. This dependence on external classical systems is undesirable in a *fully quantum* approach. Moreover, it inhibits that careful tracking of energy and coherence exchanges.

The *inclusive* picture adopted here, characterised by explicitly modelling all necessary systems with a time independent Hamiltonian, is not inherently quantum mechanical but rather was first introduced classically by Deffner and Jarzynski in [94]. Nonetheless, this approach really took off within resource theoretic approaches to quantum thermodynamics [10,11,13] where the picture proved an effective means of accounting for the role of coherence in thermodynamics. It is therefore also natural to adopt here to study coherent fluctuation relations[3].

Without an explicitly time dependent Hamiltonian, a more subtle means of inducing the change in the system Hamiltonian is required. For this reason, a control (or 'switch' [93]) system is modelled. The Hamiltonian is designed such that a change to the state of the control can be used to induce an effective change in the system Hamiltonian.

To make the role of the control system more concrete let us consider the example of a spin $\frac{1}{2}$ particle in a position dependent magnetic field. The spin degree of freedom experiences an effectively time dependent Hamiltonian, a time-dependent energy level splitting, by varying the location of the particle's wavepacket in the magnetic field over time. In this case, the position of the particle acts as the control.

More abstractly, a change in system Hamiltonian can be induced by evolving the state of the control between different regions of the Hilbert space associated with different effective system

[3]We use the term 'coherent fluctuation relations' as a shorthand for fluctuation relations in which energetic coherences play a non-trivial role. That is, we are not explicitly quantifying fluctuations of coherence as considered in [95].

Hamiltonians. Consider a Hamiltonian of the form

$$H_{sc} = H_s^i \otimes \Pi_c^i + H_s^f \otimes \Pi_c^f + V_{sc}^{\perp} \tag{2.21}$$

where Π_c^i and Π_c^f are projectors onto different subregions, R_i and R_f respectively, of the control. $V_{sc}^{\perp}$ has support only outside those two subspaces, *i.e.* $(Q_s \otimes \Pi_c^i)V_{sc}^{\perp} = (Q_s \otimes \Pi_c^f)V_{sc}^{\perp} = 0$ for any system operator Q_s. When the control is prepared in a state with support in region R_i, the initial effective system Hamiltonian is H_s^i. If the control evolves to a state with support in the region of R_f, the effective system Hamiltonian evolves to H_s^f. This is sketched in Fig. 2.1a.

For the spin example above Π_c^i and Π_c^f correspond to projectors onto different regions of physical space with different magnetic field strengths. To take a simple scenario, imagine a spin $\frac{1}{2}$ particle confined to travel in 1D in a magnetic field of strength B_i in the region $x < x_i$ and B_f in the region $x > x_f$. Assuming the magnetic field points in the z direction, the corresponding Hamiltonian can be written as

$$H_{sc} = E_i \sigma_s^z \otimes \sum_{x<x_i} |x\rangle \langle x|_c + E_f \sigma_s^z \otimes \sum_{x>x_f} |x\rangle \langle x|_c + V_{sc}^{\perp} \tag{2.22}$$

where $\sigma_s^z = |e_s\rangle \langle e_s| - |g_s\rangle \langle g_s|$ with $|e_s\rangle$ and $|g_s\rangle$ the excited and ground states of the two level system respectively and where $E_{i,f} = \frac{\mu B_{i,f}}{2}$, with μ the Bohr magneton. Similarly to classical fluctuation relations which hold for arbitrary driving processes, the FQC is independent of the manner in which the Hamiltonian changes from H_S^i to H_S^f. It thus follows that the choice of $V_{sc}^{\perp}$, the Hamiltonian in the region $x_i \leq x \leq x_f$, and therefore the choice of form of the magnetic field in the region $x_i \leq x \leq x_f$, is arbitrary.

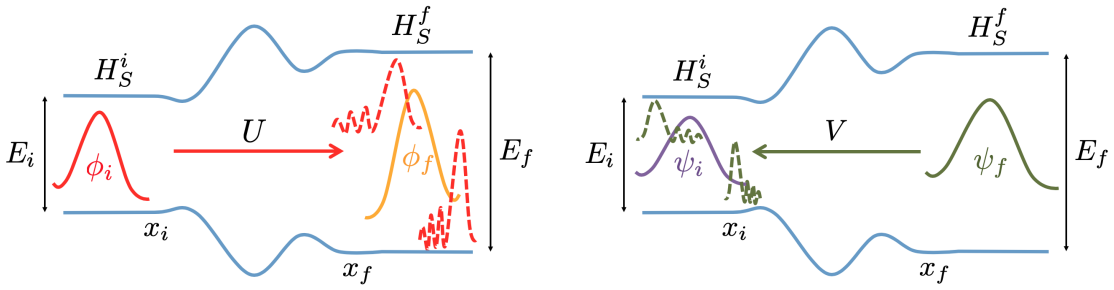
There are two versions of the FQC which correspond to two different manners in which the evolution of the control system can be induced. In the first an energy conserving unitary operation, U, is applied to move the setup between the two regions of the Hilbert space. In the second, the setup evolves *autonomously* under its Hamiltonian. In the case of the spin example, the applied unitary operation is a translation operation; where as, under the autonomous variant, that total Hamiltonian contains kinetic and potential energy terms to drive the translation process. The autonomous variant is easier to physically implement but, as we will discuss in detail in Section 2.6, comes at the cost of not being exact.

The total setup can be simplified to that of a bipartite system. This is done by first using a single system, a *battery* B, that acts as both the control system and work store. The battery both drives the change in system Hamiltonian and provides or absorbs the energy required to do so. The fluctuation relation is formulated in terms of battery state transition probabilities. For example, for the case of a spin in a magnetic field the motional state of the spin can act as a battery with its position the control, its total energy the work store, and the fluctuation relation formulated in terms of transition probabilities between the spin's motional states. Secondly, rather than explicitly modelling the bath we can view it instead implicitly as a means of defining the temperature of the isothermal process and of preparing the system in a thermal state. For a more rigorous discussion of the role of the bath see Appendix B.1. The full setup and this bipartite variant are sketched in 2.1.

Henceforth we will consider the simplified bipartite setup. The bipartite setup has the time-independent Hamiltonian,

$$H_{SB} = H_S^i \otimes \Pi_B^i + H_S^f \otimes \Pi_B^f + V_{SB}^{\perp} + \mathbb{1}_S \otimes H_B \ , \tag{2.23}$$

where, similarly to Eq. (2.21), Π_B^i and Π_B^f are projectors onto different subregions, R_i and R_f respectively, of the battery and $V_{SB}^{\perp}$ has support only outside those two subspaces. When the



(a) Forwards Process

(b) Reverse Process

Figure 2.2: **Sketch of forwards and reverse dynamics.** The blue lines represent the energy level splitting of the two level system as a function of position x. The battery states that are prepared at the start of the protocols (red/green) and the measurements that are performed at the end of the protocols (yellow/purple) are indicated by solid lines. The evolved states of the battery at the end of the driving process as sketched as dashed lines.

battery, which has the constant Hamiltonian H_B, is initialised in a state in subspace R_i only and evolves to a final state in subspace R_f only, the system Hamiltonian evolves from H_S^i to H_S^f and vice versa for the reverse process. For the spin in a magnetic field example, the first three terms of Eq. (2.23) can be written as

$$H_{SB}^{\text{int}} = \sigma_S^z \otimes E(x_B) \tag{2.24}$$

where $E(x_B) \propto B(x_B)$ is an energetic level-shift that depends on the position, x_B, of the battery in the magnetic field B. For the initial and final Hamiltonians of battery to be well defined we require $E(x < x_i) = E_i$ and $E(x > x_f) = E_f$. While we explicitly state the interaction Hamiltonian for the spin example here, this is only for pedagogical purposes, and the relation also holds for more general choices in H_S^i, H_S^f and $V_{SB}^{\perp}$. The battery Hamiltonian may be chosen freely but, as will become clear, a natural choice is a quantum harmonic oscillator Hamiltonian.

The aim now is to use this inclusive bipartite framework to quantify the energetic fluctuations of a system driven by a coherent energy supply. To do so, we consider a protocol that broadly replicates the standard Crooks scenario; however, one in which the battery may occupy a superposition of energy states. Specifically, the forwards protocol (sketched in Fig. 2.2) consists of the following steps:

Preparation The battery is prepared in a state $|\phi_i\rangle$ with support in region R_i such that the effective Hamiltonian of the system is H_S^i. Other than this constraint, the state $|\phi_i\rangle$ may be chosen freely and in general can occupy a superposition of energy states. Similarly to the classical case, the system is prepared in a thermal state, at temperature T, with respect to its initial Hamiltonian,

$$\gamma_i \propto \exp\left(-\frac{H_S^i}{k_B T}\right) . \tag{2.25}$$

Evolution The system and battery propagate under an energy conserving unitary U which evolves the battery such that a change in the effective system Hamiltonian from H_S^i to H_S^f is induced. This change in Hamiltonian drives the system from equilibrium with the energy required or produced as a result of the driving process supplied by the battery. The unitary driving process thus couples the system and the battery such that their evolved state, $U(\gamma_i \otimes |\phi_i\rangle\langle\phi_i|)U^\dagger$,

is correlated.

Measurement To quantify the energy changes of the driven system, a measurement with POVM elements

$$\{|\phi_f\rangle\langle\phi_f|, \mathbb{1} - |\phi_f\rangle\langle\phi_f|\} \tag{2.26}$$

is performed on the evolved state to answer the binary question "is the battery in the state $|\phi_f\rangle$?". Similarly to the prepared state, $|\phi_f\rangle$ must have support in region R_f but otherwise can be chosen freely. When $|\phi_f\rangle$ is a superposition of energy states, this measurement probes the coherent properties of the battery, and therefore also the system.

The transition probability for the forwards protocol,

$$\mathcal{P}(\phi_f|\phi_i,\gamma_i) = \langle\phi_f|\,\mathrm{Tr}_S[U(\gamma_i\otimes|\phi_i\rangle\langle\phi_i|)U^\dagger]\,|\phi_f\rangle \ , \tag{2.27}$$

is the probability for the battery to be found in $|\phi_f\rangle$ having been prepared in $|\phi_i\rangle$.

The FQC, similarly to the classical Crooks equality, purports to quantify the irreversibility of non-equilibrium processes. For this reason, the transition probability for the forwards process, Eq. (2.27), is compared to one for its reverse. The time-reversal could be implemented by an application of the inverse unitary $U^\dagger$ as in the two-point measurement fluctuation relation set out in Section 2.2.3. However, this requires implementing the inverse unitary on the *entire* setup, which in the general case also includes the thermal bath. Such an operation would require an unrealistic level of experimental control. Instead, the time reversal operation $\mathcal{T}$ is introduced so that the reverse operation does not require reversing the unitary on the bath. In broad terms, $\mathcal{T}$ is defined such that if the dynamics are time reversal invariant, then if the battery is prepared in the state $\mathcal{T}|\phi_f\rangle$ its evolution under U drives a change in Hamiltonian from H_S^f back to H_S^i. We formally define the time reversal operation in Section 2.4.

The reverse protocol is analogous to the forwards protocol. The battery is prepared in some state $|\psi_f\rangle$ in region R_f corresponding to the Hamiltonian of the system H_S^f. The system is prepared in a thermal state γ_f with respect to H_S^f. The transition probability for the reverse process, $\mathcal{P}(\psi_i|\psi_f,\gamma_f)$, quantifies the probability for the battery to collapse to $|\psi_i\rangle$ having prepared it in $|\psi_f\rangle$.

A Crooks-like equality is derived for the ratio of the forwards, $\mathcal{P}(\phi_f|\phi_i,\gamma_i)$, and reverse, $\mathcal{P}(\psi_i|\psi_f,\gamma_f)$, transition probabilities. As we will show explicitly in Section 2.4, it is found that this ratio reduces to a natural Crooks-like form for pairs of states related by the following temperature dependent mapping

$$\begin{aligned} |\phi_i\rangle &\propto \mathcal{T}\exp\left(-\frac{H_B}{2k_BT}\right)|\psi_i\rangle \quad \text{and} \\ |\psi_f\rangle &\propto \mathcal{T}\exp\left(-\frac{H_B}{2k_BT}\right)|\phi_f\rangle \ . \end{aligned} \tag{2.28}$$

For energy eigenstates, the pairs of states in the forwards and reverse processes are related solely by a time reversal, that is $|\phi_i\rangle = \mathcal{T}|\psi_i\rangle$ and $|\phi_f\rangle = \mathcal{T}|\psi_f\rangle$. However, more generally the action of the mapping is non-trivial. As will be explained further in Section 2.4, this mapping emerges from a conceptually natural map, called the Gibbs map. We summarise the relationship between the four states quantified by the FQC in Fig. 2.3.

Having parameterised the relevant battery states in this way, the ratio of the transition probabilities is calculable and the FQC is found,

$$\frac{\mathcal{P}(\phi_f|\phi_i,\gamma_i)}{\mathcal{P}(\psi_i|\psi_f,\gamma_f)} = \exp\left(-\frac{\Delta F}{k_BT}\right)\exp\left(\frac{\Delta\tilde{E}}{k_BT}\right) . \tag{2.29}$$

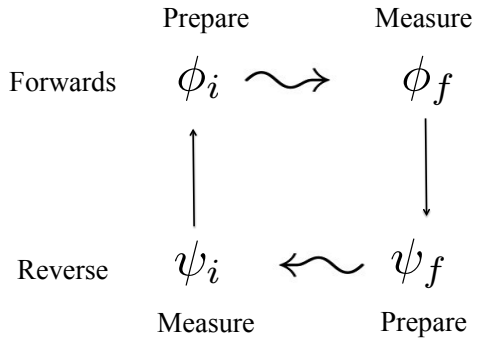


Figure 2.3: **Relation between states.** In the forwards process, the state $|\phi_i\rangle$ is prepared, evolves (indicated by the wiggly arrow) and the state $|\phi_f\rangle$ is measured. In the reverse process, the state $|\phi_i\rangle$ is prepared, evolves and the state $|\psi_f\rangle$ is measured. As indicated by the solid lines, the state $|\psi_i\rangle$ ($|\phi_f\rangle$) is related to the state $|\phi_i\rangle$ ($|\psi_f\rangle$) by the mapping specified in Eq. (2.28).

The dependence on the change in equilibrium free energy ΔF carries over from the classical Crooks equality [42]. However, the classical work term is replaced with a quantum generalisation of the energy supplied to, or absorbed from, the system, $\Delta\tilde{E} := \tilde{E}_{\psi_i}(H_B) - \tilde{E}_{\phi_f}(H_B)$. The function $\tilde{E}_\psi$, which is defined as

$$\tilde{E}_\psi(H) := -k_B T \ln\left(\langle\psi| \exp\left(-\frac{H}{k_B T}\right)|\psi\rangle\right) , \tag{2.30}$$

is an effective potential that specifies the relevant energy value within the fluctuation theorem context. When the battery is prepared in an energy eigenstate $\Delta\tilde{E}$ corresponds to the energy supplied to the system from the battery. More generally, as we will discuss in Section 2.5, $\Delta\tilde{E}$ quantifies coherence induced corrections to the classical Crooks equality $\tilde{E}$.

In the classical limit of a battery which is prepared and measured in an energy eigenstates $\{|E_k\rangle\}$, the FQC reduces to

$$\frac{\mathcal{P}(E_f|E_i,\gamma_i)}{\mathcal{P}(E_i|E_f,\gamma_f)} = \exp\left(-\frac{\Delta F}{k_B T}\right)\exp\left(\frac{W}{k_B T}\right) . \tag{2.31}$$

where $W := E_i - E_f$ is the decrease in the energy of the battery and thus, due to global energy conservation, equivalent to the work done on the system. If we then additionally assume that the evolution of the setup does not depend on the initial energy of the battery, the above relation is equivalent to the usual classical Crooks equality. It is primarily in virtue of this that the FQC can be seen as a genuine quantum generalisation of the Crooks equality. However, in general, the temperature dependent parameterisation of the relevant quantum states and the generalised energy flow term are essential to capture the impact of coherence.

The FQC earns the badge 'fully quantum' in virtue of its ability to incorporate a full spectrum of quantum phenomena including coherence and entanglement. Thus we stress that the equality presented is not the most general but rather a simplified variant that captures the most important features of the equality. There are variants of Eq. (2.29) in which (to name just a few): (i) the control and work store are separate systems; (ii) the work store is prepared in a mixed state and correspondingly a non-projective POVM is performed at the end of the protocol. (iii) the system is prepared in a non thermal state. (iv) entanglement between the system and the battery or thermal

bath is incorporated. Moreover, in [64] the quantum crooks equality is initially formulated in terms of the forwards and reverse quantum channels induced on the work store. This is perhaps more in the spirit of a fully quantum, information theoretic, Crooks equality. For these general cases and others see [64].

We chose to present its reformulation in terms of transition probabilities in order to maintain a closer resemblance to the classical Crooks equality. The advantage of this transition probability formalism are two-fold. Firstly, it is clearer how one might go about experimentally testing the FQC. The example of the two level system that experiences a position dependent splitting is not just a pedagogical example but the basis of an experimental proposal utilising trapped ions and the AC Stark shift that is presented in Section 2.7. Secondly, the similarities with the classical formulation of the Crooks equality makes it easier to tease out the conceptual implications of coherence on irreversibly, as discussed in Section 2.5.

Before we proceed with showing how the FQC can be made more concrete, we temporarily dive into some more abstract material and show how the FQC is derived in order to place the equality on firmer foundations. This material is rather technical and can be skipped.

2.4 Derivation

The FQC is derived in [64] by combining two properties known as 'Global Invariance' and 'factorisability'. Global Invariance is a quantum analogue of the detailed balance condition for energy conserving and time reversal invariant unitary evolutions. Factorisability is a property that quantifies the extent to which two sub-components of a global system are well defined subsystems. The prepared and measured states quantified by the FQC are interrelated by a temperature dependent map called the Gibbs map. Therefore to derive the FQC we first explicate these four concepts: the Gibbs map, the quantum time reversal operation, Global Invariance and factorisability.

2.4.1 Gibbs map

The Gibbs map arises when considering the time reversal of a general quantum process and provides a natural way of parameterising the battery states. It is defined as follows.

Definition 1. Gibbs map.
Given a system with Hamiltonian H at temperature T, the action of the Gibbs map, G_H, on a state ρ is

$$G_H(\rho) := \frac{\exp\left(-\frac{H}{2k_BT}\right)\rho\exp\left(-\frac{H}{2k_BT}\right)}{\tilde{Z}_H(\rho)} \quad \text{with} \quad \tilde{Z}_H(\rho) := \mathrm{Tr}\left[\exp\left(-\frac{H}{k_BT}\right)\rho\right]. \tag{2.32}$$

The Gibbs map is closely linked with the Petz recovery map [96, 97] for general quantum processes and has a range of physically natural properties. When the input state is an energy eigenstate $|E_k\rangle$, and as such its energy is well defined, the Gibbs map has no effect and

$$G_H\left(|E_k\rangle\langle E_k|\right) = |E_k\rangle\langle E_k|. \tag{2.33}$$

Conversely, when the input state's energy is completely unknown the output state has thermally distributed populations. For example, the maximally mixed state, $\rho_{\mathbb{1}} \propto \mathbb{1}$, is mapped to the thermal state,

$$G_H(\rho_{\mathbb{1}}) = \gamma(H) := \frac{1}{Z_H}\exp\left(-\frac{H}{k_BT}\right) \quad \text{with} \quad Z_H := \mathrm{Tr}\left[\exp\left(-\frac{H}{k_BT}\right)\right], \tag{2.34}$$

and an equal superposition of energy states, $|\psi_+\rangle \propto \sum_k |E_k\rangle$, is mapped to the coherent thermal state

$$|\psi^\gamma\rangle = \frac{1}{\sqrt{Z_H}} \sum_k \exp\left(-\frac{E_k}{2k_B T}\right) |E_k\rangle \ , \tag{2.35}$$

that is a pure state the energy populations of a thermal state. In this manner, the Gibbs map can roughly be thought of a making the output state 'as thermal as possible' subject to the constraints imposed by the input state. However, this intuitive explanation is not intended to be taken too literally but rather as hinting at the Gibbs map's deeper conceptual role.

2.4.2 Time reversal

Imagine taking a video of a process and then running it backwards. In broad terms taking the time reverse of a process is the mathematical equivalent to pressing rewind. In classical physics, the time reversal operation can be implemented by replacing t by $-t$ in all variables describing a dynamical process.

In quantum mechanics time is a parameter rather than observable and therefore cannot be implemented directly by replacing t by $-t$. Instead, the quantum time reversal operation acts indirectly via its action on the position and momentum operators. To agree with our intuitive notion of time reversal and align with the classical case, the time reversal operation reverses the sign of the momentum operator p and leaves the position operator x invariant. Thus, taking $\mathfrak{T}(Q)$ to denote the time-reversal of any quantum operator Q, we require $\mathfrak{T}(x) = x$ and $\mathfrak{T}(p) = -p$. Additionally the time reversal operation is a length preserving symmetry operation. Therefore the trace of a quantum state is invariant under $\mathfrak{T}$, that is $\mathrm{Tr}[|\psi\rangle\langle\psi|] = \mathrm{Tr}[\mathfrak{T}(|\psi\rangle\langle\psi|)]$ for any state $|\psi\rangle$.

The requirements of length preservation and the action of $\mathfrak{T}$ on x and p, entail that $\mathfrak{T}$ is an anti-unitary operator [98]. To see why, first note that the Wigner theorem states that all length preserving operations are either unitary or anti-unitary [99]. Then, if we look at the action of the time reversal operation on the canonical commutation relation we see that as

$$\mathfrak{T}([x,p]) = -[x,p] \quad \text{we have that} \quad \mathfrak{T}(i) = -i \ . \tag{2.36}$$

As such, the time reversal operation is non-linear and therefore not a unitary operation. Thus it follows, as claimed, that $\mathfrak{T}$ is an anti-unitary operation.

The usual textbook [98] anti-unitary operation to represent $\mathfrak{T}$ is complex conjugation. However, the fact that complex conjugation is anti-unitary makes it a little awkward to calculate with. Conveniently, when acting on Hermitian operators the transpose operation and complex conjugation are equivalent. Since the FQC quantifies transition probabilities between quantum states (which are by definition Hermitian), we utilise this equivalence and choose to implement $\mathfrak{T}$ via the transpose.

Definition 2. Quantum time reversal.
The quantum time reversal operation $\mathfrak{T}$ on any quantum operator X is defined as

$$\mathfrak{T}(X) := X^T \, , \tag{2.37}$$

where ^{T} is the transpose operation. It follows that the time reversal operation $\mathcal{T}$ on any pure state $|\psi\rangle$ is given by

$$\mathcal{T}\,|\psi\rangle = |\psi^*\rangle \ , \tag{2.38}$$

where * denotes complex conjugation.

The transpose operation is basis dependent and therefore so too are $\mathfrak{T}$ and $\mathcal{T}$. The appropriate basis is dictated by physical context. Since here we seek to implement the reverse driving process within the inclusive framework, the basis is chosen to ensure:

1. The total Hamiltonian and the evolution operator are time reversal invariant, i.e. $\mathfrak{T}(H) = H$ and $\mathfrak{T}(U) = U$.

2. The evolution of time reversed battery states under U generates the reverse change in Hamiltonian H_S^f to H_S^i.

For the spin system example, with say an osccilator battery, we can take the time reversal of the system and battery with respect to the energy eigenbasis. The thermal system then remains unchanged under the time reversal operation. However, the time reversal reverses the momentum of any battery oscillator state, while leaving its position unchanged, and so the evolution of the battery states will be in the opposite direction to the forwards process undoing the change in Hamiltonian.

2.4.3 Global Invariance

Global Invariance relates the transition probabilities of a forwards process and the transition probability for a reverse process for a *single* system. The condition applies to all energy conserving and time reversal invariant unitary evolutions of systems with time reversal invariant Hamiltonians. Since most Hamiltonians are time reversal invariant and all dynamics are unitary and energy conserving as long as setup considered is sufficiently enlarged, Global Invariance is widely applicable. Global Invariance plays a role similar to detailed balance for classical fluctuation theorems, providing a basis from which to derive a myriad of interrelated quantum fluctuation theorems.

To ensure energy is strictly conserved we require the unitary propagator to commute with the system Hamiltonian, that is $[U, H] = 0$. This not only ensures the average energy of the system is conserved by the dynamics but also prevents the creation of superpositions of energy states from energy eigenstates, thus enabling the careful accounting of coherence [25].

Theorem 1. *Global Invariance.*
Consider a Hamiltonian H and evolution U such that: $\mathfrak{T}(H) = H$, $\mathfrak{T}(U) = U$ and $[U, H] = 0$. Global Invariance relates a forwards and reverse transition probability for such a system. In the forwards process, the system is prepared in a state $G_H(\rho_i)$, evolves under U and a binary POVM measurement is performed with POVM elements $\{\rho_f, \mathbb{1} - \rho_f\}$. The evolved state, $UG_H(\rho_i)U^\dagger$, collapses onto ρ_f with the probability

$$P(\rho_f|G_H(\rho_i)) := \mathrm{Tr}[\rho_f U G_H(\rho_i) U^\dagger] \ . \tag{2.39}$$

In the reverse process the state $G_H(\mathfrak{T}(\rho_f))$ evolves under U and on measurement collapses onto $\mathfrak{T}(\rho_i)$ with the probability

$$P(\mathfrak{T}(\rho_i)|G_H(\mathfrak{T}(\rho_f))) := \mathrm{Tr}[\mathfrak{T}(\rho_i) U G_H(\mathfrak{T}(\rho_f)) U^\dagger] \ . \tag{2.40}$$

The ratio of these transition probabilities is,

$$\frac{P(\rho_f|G_H(\rho_i))}{P(\mathfrak{T}(\rho_i)|G_H(\mathfrak{T}(\rho_f)))} = \frac{\tilde{Z}_H(\mathfrak{T}(\rho_f))}{\tilde{Z}_H(\rho_i)} \ . \tag{2.41}$$

To prove Global Invariance we begin with the definition of the forwards transition probability, and utilise the invariance of probabilities (as scalars) under time reversals, $P(\rho_f|G_H(\rho_i)) = \mathfrak{T}(P(\rho_f|G_H(\rho_i)))$, in combination with $\mathfrak{T}(H) = H$ and $\mathfrak{T}(U) = U$,

$$P(\rho_f|G_H(\rho_i)) := \mathrm{Tr}[\rho_f U G_H(\rho_i) U^\dagger] = \mathrm{Tr}[\mathfrak{T}\left(\rho_f U G_H(\rho_i) U^\dagger\right)] = \mathrm{Tr}[U^\dagger G_H(\mathfrak{T}(\rho_i)) U \mathfrak{T}(\rho_f)] \,. \tag{2.42}$$

Substituting in the definition of the Gibbs map, Eq. (2.32), we obtain

$$P(\rho_f|G_H(\rho_i)) = \frac{1}{\tilde{Z}_H(\rho_i)} \mathrm{Tr}\left[U^\dagger \exp\left(-\frac{H}{2k_BT}\right) \mathfrak{T}(\rho_i) \exp\left(-\frac{H}{2k_BT}\right) U \mathfrak{T}(\rho_f)\right] . \tag{2.43}$$

The above expression can be reordered using the cyclic nature of the trace operation combined with $[U, H] = 0$,

$$\begin{aligned} P(\rho_f|G_H(\rho_i)) &= \frac{1}{\tilde{Z}_H(\rho_i)} \mathrm{Tr}\left[\mathfrak{T}(\rho_i) \exp\left(-\frac{H}{2k_BT}\right) U \mathfrak{T}(\rho_f) U^\dagger \exp\left(-\frac{H}{2k_BT}\right)\right] \\ &= \frac{1}{\tilde{Z}_H(\rho_i)} \mathrm{Tr}\left[\mathfrak{T}(\rho_i) U \exp\left(-\frac{H}{2k_BT}\right) \mathfrak{T}(\rho_f) \exp\left(-\frac{H}{2k_BT}\right) U^\dagger\right] . \end{aligned} \tag{2.44}$$

The proof is completed by again using the definition of the Gibbs map and then the definition of the reverse transition probability,

$$\begin{aligned} P(\rho_f|G_H(\rho_i)) &= \frac{\tilde{Z}_H(\mathfrak{T}(\rho_f))}{\tilde{Z}_H(\rho_i)} \mathrm{Tr}\left[\mathfrak{T}(\rho_i) U G_H(\mathfrak{T}(\rho_f)) U^\dagger\right] \\ &= \frac{\tilde{Z}_H(\mathfrak{T}(\rho_f))}{\tilde{Z}_H(\rho_i)} P(\mathfrak{T}(\rho_i)|G_H(\mathfrak{T}(\rho_f))) \,. \end{aligned} \tag{2.45}$$

The FQC is derived for a bipartite setup composed of a *battery* and *system* which obeys Global Invariance. By carefully choosing the Hamiltonian H and states ρ_i and ρ_f, the transition probabilities $P(\rho_f|G_H(\rho_i))$ and $P(\mathfrak{T}(\rho_i)|G_H(\mathfrak{T}(\rho_f)))$, can quantify a Crooks-like scenario where a thermal system is driven by a change in Hamiltonian with the work required to do so supplied by a quantum battery. However, for the system to be a well defined system with concrete initial and final Hamiltonians, the system and battery must be, at least effectively, non-interacting at the start and end of the driving process. This is captured by an additional requirement that we call the 'factorisability' of the system and battery.

2.4.4 Factorisability

Factorisability characterises the extent to which a pair of systems can be considered effectively non-interacting subsystems. It is defined in terms of the unnormalised version of the Gibbs map, that is the map

$$J_H(\rho) := \exp\left(-\frac{H}{2k_BT}\right) \rho \exp\left(-\frac{H}{2k_BT}\right) , \tag{2.46}$$

which is defined for any state ρ and where $J_H(\rho) = \tilde{Z}_H(\rho)\, G_H(\rho)$. Armed with this map, factorisability can be defined as follows:

Definition 3. Factorisability.
A composite system with a Hamiltonian H_{AB} in the state $\rho_A \otimes \rho_B$ is factorisable if

$$J_{H_{AB}}(\rho_A \otimes \rho_B) = J_{H_A}(\rho_A) \otimes J_{H_B}(\rho_B) \tag{2.47}$$

for a pair of Hamiltonians H_A and H_B of subsystems A and B respectively.

Given the close relationship between the map J and the Gibbs map, Eq. (2.32), it follows that if a composite system is factorisable, then the Gibbs map also decomposes into terms acting on the separate subsystems. That is, for a factorisable composite system with a Hamiltonian H_{AB} in the state $\rho_A \otimes \rho_B$ we have that

$$G_{H_{AB}}(\rho_A \otimes \rho_B) = G_{H_A}(\rho_A) \otimes G_{H_B}(\rho_B) \quad \text{and} \quad \tilde{Z}_{H_{AB}}(\rho_A \otimes \rho_B) = \tilde{Z}_{H_A}(\rho_A) \otimes \tilde{Z}_{H_B}(\rho_B) \ . \tag{2.48}$$

To derive a Crooks-like equality we require the system and battery to be effectively non-interacting at the start of the forwards and reverse non-equilibrium driving processes. This requirement can be formalised by demanding that the system and battery Hamiltonian, H_{SB}, factorises into an initial or final system Hamiltonian, H_S^i or H_S^f, and battery Hamiltonian, H_B, when the battery states are chosen appropriately. That is, we assume that the following factorisability condition holds:

Assumption 1. *Factorisability of the system and battery.*
There exists a pair of pure battery states, $|\Psi_i\rangle$ and $|\Psi_f\rangle$, such that the system and battery Hamiltonian H_{SB} factorises as

$$\begin{aligned} J_{H_{SB}}\left(\rho_{\mathbb{1}} \otimes |\Psi_i\rangle\langle\Psi_i|\right) &= J_{H_S^i}(\rho_{\mathbb{1}}) \otimes J_{H_B}(|\Psi_i\rangle\langle\Psi_i|) \quad \textit{and} \\ J_{H_{SB}}\left(\rho_{\mathbb{1}} \otimes |\Psi_f\rangle\langle\Psi_f|\right) &= J_{H_S^f}(\rho_{\mathbb{1}}) \otimes J_{H_B}(|\Psi_f\rangle\langle\Psi_f|) \end{aligned} \tag{2.49}$$

where H_S^i and H_S^f are Hamiltonians of the system, H_B is a Hamiltonian of the battery and $\rho_{\mathbb{1}} \propto \mathbb{1}$.

This factorisability condition can be read as encoding that the system is a genuine system with well defined initial and final Hamiltonians. We are now in a position to derive the FQC by combining Global Invariance, Eq. (2.41), with the factorisability condition, Eq. (2.49).

2.4.5 Main derivation

To demonstrate that the FQC follows from Global Invariance and the factorisability of the system and battery, we set $|\Psi_i\rangle\langle\Psi_i| = \mathfrak{T}(|\psi_i\rangle\langle\psi_i|)$ and $|\Psi_f\rangle\langle\Psi_f| = \mathfrak{T}(|\phi_f\rangle\langle\phi_f|)$ and for convenience define

$$\sigma_i = \rho_{\mathbb{1}} \otimes \mathfrak{T}\left(|\psi_i\rangle\langle\psi_i|\right) \quad \text{and} \quad \mathfrak{T}(\sigma_f) = \rho_{\mathbb{1}} \otimes \mathfrak{T}(|\phi_f\rangle\langle\phi_f|) \ . \tag{2.50}$$

At first glance the reason for considering these states is perhaps not transparent; however, they enable us to make a connection with notation used earlier to frame the FQC. Namely, the factorisability condition, Eq. (2.49), entails that the Gibbs map as applied to σ_i and $\mathfrak{T}(\sigma_f)$, Eq. (2.50), decomposes as

$$G_{H_{SB}}(\sigma_i) = \gamma_i \otimes |\phi_i\rangle\langle\phi_i| \quad \text{and} \quad G_{H_{SB}}(\mathfrak{T}(\sigma_f)) = \gamma_f \otimes |\psi_f\rangle\langle\psi_f| \tag{2.51}$$

where we have used the shorthand $\gamma_k \equiv \gamma(H_S^k)$ for $k = i, f$ for the initial and final thermal states, Eq. (2.34), and with

$$\begin{aligned} |\phi_i\rangle &\propto \mathcal{T} \exp\left(-\frac{H_B}{2k_BT}\right)|\psi_i\rangle \\ |\psi_f\rangle &\propto \mathcal{T} \exp\left(-\frac{H_B}{2k_BT}\right)|\phi_f\rangle \end{aligned} \tag{2.52}$$

as in Eq. (2.28). Consequently, we see that the factorised Gibbs map gives rise to both the thermal states of the system, Eq. (2.25), and the temperature dependent mapping that parameterises the battery states, Eq. (2.52), in the FQC.

Furthermore, we can use the decomposition of the Gibbs map, Eq (2.51), to obtain a transition probability of the battery *alone* from a transition probability of both the system *and* battery. In particular, the forwards transition probability $P(\sigma_f|G_H(\sigma_i))$, Eq (2.39), of the system and battery reduces to $\mathcal{P}(\phi_f|\phi_i,\gamma_i)$, the transition probability of the battery from $|\phi_i\rangle$ to $|\phi_f\rangle$ for a system prepared in the thermal state γ_i. That is we find that

$$\begin{aligned} P\left(\sigma_f \,|\, G_{H_{SB}}\left(\sigma_i\right)\right) &= \mathrm{Tr}\left[\left(\rho_{\mathbb{1}} \otimes |\phi_f\rangle\langle\phi_f|\right) U \, G_{H_{SB}}\left(\rho_{\mathbb{1}} \otimes \mathfrak{T}(|\psi_i\rangle\langle\psi_i|)\right) U^\dagger\right] \\ &= \frac{1}{N}\langle\phi_f|\,\mathrm{Tr}_S\left[U(\gamma_i \otimes |\phi_i\rangle\langle\phi_i|)U^\dagger\right]|\phi_f\rangle \\ &:= \frac{1}{N}\mathcal{P}(\phi_f|\phi_i,\gamma_i)\ . \end{aligned} \tag{2.53}$$

where the factor $\frac{1}{N}$ is a normalisation term from the maximally mixed system state $\rho_{\mathbb{1}}$ and cancels out in the final fluctuation theorem. Likewise, the global transition probability for the reverse process $P\left(\mathfrak{T}(\sigma_i) \,|\, G_{H_{SB}}(\mathfrak{T}(\sigma_f))\right.$ evaluates to the transition probability of the battery for the reverse process $\mathcal{P}(\psi_i|\psi_f,\gamma_f)$, where the system is prepared in the thermal state γ_f,

$$\begin{aligned} P\left(\mathfrak{T}(\sigma_i) \,|\, G_{H_{SB}}(\mathfrak{T}(\sigma_f))\right. &= \mathrm{Tr}\left[\left(\rho_{\mathbb{1}} \otimes |\psi_i\rangle\langle\psi_i|\right) U \, G_{H_{SB}}\left(\rho_{\mathbb{1}} \otimes \mathfrak{T}(|\phi_f\rangle\langle\phi_f|)\right) U^\dagger\right] \\ &= \frac{1}{N}\langle\psi_i|\,\mathrm{Tr}_S\left[U(\gamma_f \otimes |\psi_f\rangle\langle\psi_f|)U^\dagger\right]|\psi_i\rangle \\ &:= \frac{1}{N}\mathcal{P}(\psi_i|\psi_f,\gamma_f)\ . \end{aligned} \tag{2.54}$$

Finally, since the system and battery factorise, the Gibbs map normalisation terms also decompose as

$$\tilde{Z}_{H_{SB}}\left(\sigma_f\right) = \frac{1}{N} Z_f \times \tilde{Z}_{\phi_f} \quad \text{and} \quad \tilde{Z}_{H_{SB}}\left(\sigma_i\right) = \frac{1}{N} Z_i \times \tilde{Z}_{\psi_i}\,. \tag{2.55}$$

Here we abbreviate $Z_k \equiv Z_{H_S^k}$ for $k = i, f$ for the partition functions of the system and we abbreviate $\tilde{Z}_{\phi_f} \equiv \tilde{Z}_{H_B}(|\phi_f\rangle\langle\phi_f|)$ and $\tilde{Z}_{\psi_i} \equiv \tilde{Z}_{H_B}(\mathfrak{T}(|\psi_i\rangle\langle\psi_i|)) = \tilde{Z}_{H_B}(|\psi_i\rangle\langle\psi_i|)$ for the Gibbs map normalisation terms of the battery.

We obtain the FQC by substituting the factorised global transition probabilities, Eq. (2.53) and Eq. (2.54), and the factorised Gibbs map normalisation terms, Eq. (2.55), into Global Invariance, Eq. (2.41),

$$\frac{\mathcal{P}(\phi_f|\phi_i,\gamma_i)}{\mathcal{P}(\psi_i|\psi_f,\gamma_f)} = \frac{Z_f}{Z_i}\frac{\tilde{Z}_{\phi_f}}{\tilde{Z}_{\psi_i}}\ . \tag{2.56}$$

We can rewrite the above expression in a more physical form by substituting in the change in free energy for the ratio of the partition functions,

$$\exp\left(-\frac{\Delta F}{k_B T}\right) = \frac{Z_f}{Z_i}\ , \tag{2.57}$$

and by similarly introducing the generalised energy flow in terms of the ratio of Gibbs map normalisation terms,

$$\exp\left(\frac{\Delta \tilde{E}}{k_B T}\right) = \frac{\tilde{Z}_{\phi_f}}{\tilde{Z}_{\psi_i}}\ . \tag{2.58}$$

This implicit definition of the generalised energy flow is entirely equivalent to the explicit definition given in Eq. (2.30). Thus we obtain the FQC in the form stated in section 2.3

$$\frac{\mathcal{P}(\phi_f|\phi_i,\gamma_i)}{\mathcal{P}(\psi_i|\psi_f,\gamma_f)} = \exp\left(-\frac{\Delta F}{k_B T}\right)\exp\left(\frac{\Delta \tilde{E}}{k_B T}\right)\ . \tag{2.59}$$

2.4.6 General comments on structure of the FQC

Before proceeding the study specific physical examples of the FQC; here we briefly comment on three conceptual aspects of the general structure of the relation.

Thermal operations link. The FQC sits naturally within the resource theoretic approach to quantum thermodynamics which formally characterises the manner in which states out of thermal equilibrium can be viewed of resources in virtue of their use in performing work. Specifically, the quantum channel induced on the battery in the FQC is a thermal operation and as such previous results within the thermal operations framework [10, 11, 13, 20, 21, 23–26] are applicable. Thermal operations, consist of the following three operations: firstly, performing a global unitary, U, that strictly conserves total energy, H, in the sense that $[H, U] = 0$; secondly, adding a system at thermal equilibrium; and thirdly, disregarding (tracing out) any system. The quantum channel on the battery is precisely of this form. For the forwards process we have,

$$\mathcal{E}(\rho_B) = \mathrm{Tr}_S \left[U(\gamma_i \otimes \rho_B) U^\dagger \right] \ , \tag{2.60}$$

and the reverse process channel is identical except the system is prepared in a thermal state with respect to its final Hamiltonian. The resource states of the thermal operations framework are states with coherence with respect to the energy eigenbasis or non-thermally distributed populations. Correspondingly, the battery states are resources in virtue of being prepared in a pure state. For further discussion on incorporating fluctuating work into the thermal operations framework see [93].

Off-diagonal Crooks relations The form of the FQC can be better understood by studying its action on off-diagonal elements of the battery state. Specifically, if instead of studying the transition probability between battery states we study the transition amplitude between a pair of battery elements $Q_i^\delta = |E_i\rangle \langle E_{i+\delta}|$ and $Q_f^\delta = |E_f\rangle \langle E_{f+\delta}|$ we find that similarly to the diagonal elements in Eq. (2.31), the ratio of the transition amplitudes obeys

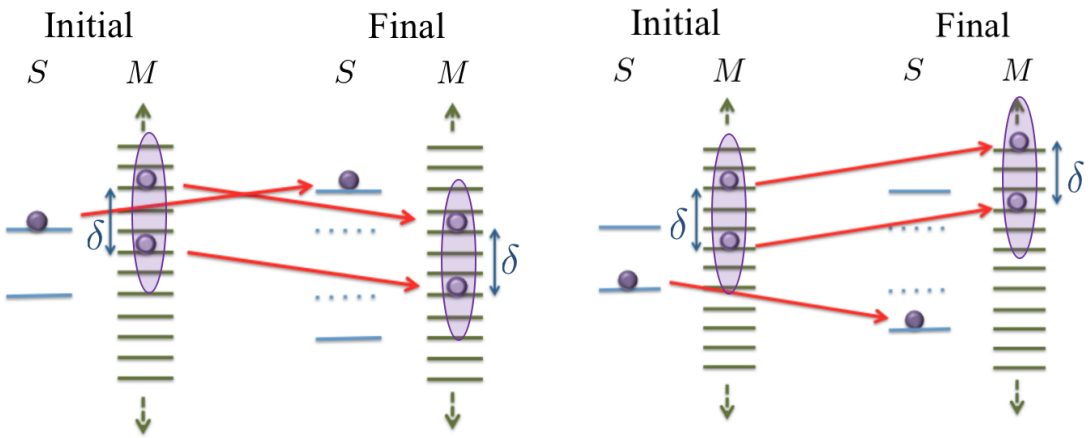
$$\frac{\mathcal{P}(Q_f^\delta | Q_i^\delta, \gamma_i)}{\mathcal{P}(\mathfrak{T}(Q_i^\delta) | \mathfrak{T}(Q_f^\delta), \gamma_f)} = \exp\left(-\frac{\Delta F}{k_B T}\right) \exp\left(\frac{W}{k_B T}\right) \ . \tag{2.61}$$

where $W := E_i - E_f$ is the negative change in energy of the battery and therefore the work done on the system. Thus we see that the evolution of the energy coherences of the battery (the off-diagonal elements of battery density operator with respect to the energy eigenbasis), evolve in the same way as the populations (the diagonal elements).

The off-diagonal Crooks equality can be seen as emerging from the non-trivial constraints imposed by thermal operations. That the coherences are constrained to evolve in the same way as the populations is a result of strict energy conservation and the fact the system is initially thermally distributed. Pictorially, as sketched in Fig. 2.4, energy conservation enforces a see-saw operation that maps changes in the system energy onto that of the battery. The strict conservation of energy then further ensures that a superposition of battery states is raised or lowered 'as one' and as such the coherences evolve in the same manner as the populations. Note, these constraints imposed by energy conservation can also be seen as resulting from time translation symmetry [100–102].

Significance of non-projective measurements In section 2.2.3 we presented a simple (non-fully) quantum Crooks equality using pairs of projective measurements to infer the work done on the driven system. Here we generalise this two-point measurement scheme to the case where a POVM measurement is performed on the system. The resulting Crooks relation provides a stepping stone between the standard TPM Crooks equality and the FQC, highlighting the significance of the non-projective measurements at the heart of the FQC.

Specifically, we consider the following protocol for the forwards process.



(a) Forwards Process

(b) Reverse Process

Figure 2.4: **Understanding the off-diagonal Crooks equality.** The process of increasing the splitting of a two level system in the presence of a harmonic oscillator battery. The left and right figures cover the cases when the two level system starts in the excited (a) and ground (b) states respectively. The see-saw like mechanism, highlighted by the red arrows, ensures energy conservation and maps changes in the system energy onto that of the battery. A superposition of battery states is raised or lowered 'as one' and as such the coherences evolve in the same manner as the populations.

1. The system is prepared in a thermal state γ_i.
2. A POVM measurement Q_i is performed on the system.
3. The system is driven by a unitary U.
4. A final POVM measurement Q_f is performed.

The probability of measuring Q_i and then Q_f is given by

$$\mathcal{P}^+ := \mathcal{P}_U(Q_f|Q_i)\mathcal{P}(Q_i|\gamma_i) = \mathrm{Tr}[Q_f U Q_i U^\dagger]\,\mathrm{Tr}[Q_i\gamma_i] \tag{2.62}$$

This transition probability for the forward process is compared to an analogous transition probability for the reverse process[4] which consists of the following steps:

1. The system is prepared in a thermal state γ_f.
2. A POVM measurement Q_f is performed.
3. The system is driven by the unitary $U^\dagger$.
4. A final POVM measurement Q_i is performed.

The probability of measuring Q_f and then Q_i is given by

$$\mathcal{P}^- := \mathcal{P}_{U^\dagger}(Q_i|Q_f)\mathcal{P}(Q_f|\gamma_f) = \mathrm{Tr}[Q_i U^\dagger Q_f U]\,\mathrm{Tr}[Q_f\gamma_f] \tag{2.63}$$

[4]One could derive an entirely analogous relation taking an approach closer to that used to derive the FQC by supposing that the dynamics are time reversal invariant, $\mathfrak{T}(U) = U$, $\mathfrak{T}(\gamma_i) = \gamma_i$ and $\mathfrak{T}(\gamma_f) = \gamma_f$ and quantifying the transition probability between $\mathfrak{T}(Q_f)$ and $\mathfrak{T}(Q_i)$.

From the cyclicity of the trace operation we have that $\mathcal{P}_U(Q_f|Q_i) = \mathcal{P}_{U^\dagger}(Q_i|Q_f)$ and therefore the ratio of the forwards and reverse transition probabilities is given by

$$\frac{\mathcal{P}^+}{\mathcal{P}^-} = \frac{Z_f}{Z_i} \frac{\mathrm{Tr}\left[Q_i \exp\left(-\frac{H_S^i}{k_B T}\right)\right]}{\mathrm{Tr}\left[Q_f \exp\left(-\frac{H_S^f}{k_B T}\right)\right]}. \tag{2.64}$$

In analogy with the FQC we define the generalised energy flow into the system as $\Delta\tilde{E}_S := \tilde{E}_S^f - \tilde{E}_S^i$ where

$$\tilde{E}_S^k := -k_B T \ln\left(\mathrm{Tr}\left[Q_k \exp\left(-\frac{H_S^k}{k_B T}\right)\right]\right) . \tag{2.65}$$

Note, that for $Q_i = |\psi_i\rangle\langle\psi_i|$ and $Q_f = |\psi_f\rangle\langle\psi_f|$ this expression for $\Delta\tilde{E}_S$ is entirely equivalent to the generalised energy flow between the system and battery as stated in Eq. (2.30). The final Crooks relation can be written as

$$\frac{\mathcal{P}^+}{\mathcal{P}^-} = \exp\left(\frac{\Delta\tilde{E}_S - \Delta F}{k_B T}\right) . \tag{2.66}$$

Thus, even in the absence of a quantum battery, the use of POVM measurements rather than projections onto energy states, results in a Crooks equality of the same form as the FQC, Eq. (2.59).

This observation highlights the power of non-projective measurements to introduce irreversibility. The WAY theorem from the 1950s tells us that the only observables that can be measured while conserving energy are those that commute with the Hamiltonian [103–105]. It follows that there is an unavoidable irreversibility for the measurement of quantum observables not in the energy eigenbasis. In broad terms, the generalised energy flow captures this type of irreversibility in a thermodynamic context.

Properties of generalised energy flow As shown above, the generalised energy flow term $\Delta\tilde{E}$ arises naturally when using non-projective measurements to compare a forwards and reverse process. We suggest $\tilde{E}$ should be interpreted as a statistical measure of the energy of a state in a superposition of energy eigenstates. An analysis of the properties of $\tilde{E}$ lends plausibility to this interpretation. In particular, treating the Hamiltonian H and temperature T as variables,

$$\tilde{E}(\psi, H, T) := -k_B T \ln\left(\langle\psi| \exp\left(-\frac{H}{k_B T}\right) |\psi\rangle\right) , \tag{2.67}$$

the following characteristics hold:

1. $\tilde{E}(\psi, H+\delta, T) = \tilde{E}(\psi, H, T) + \delta$.
2. $\tilde{E}(\psi, \lambda H, T) = \lambda\tilde{E}(\psi, H, \lambda T)$.
3. For an energy eigenstate, $|E_k\rangle$, $\tilde{E}$ is simply the associated eigenstate energy: $\tilde{E}(E_k, H, T) = E_k$.
4. In the high temperature limit $\tilde{E}$ tends to the average energy of the state: $\lim_{T\to\infty} \tilde{E}(\psi, H, T) = \langle\psi| H |\psi\rangle$.
5. In the general case $\tilde{E}$ is less than the average energy: $\tilde{E}(\psi, H, T) \leq \langle\psi| H |\psi\rangle$.
6. $\tilde{E}$ is independent of the the phase of the state: $\tilde{E}(\psi, H, T) = \tilde{E}\left(\psi e^{i\phi}, H, T\right)\ \forall\ \phi \in \Re$.

The scaling properties, captured by characteristics 1 and 2, verify that $\tilde{E}$ scales as one would expect an energy measure to scale. Property 3 captures the intuition that for a state with a known energy there is no need to statistically estimate its energy. Moreover, property 3 enables us to derive the classical Crooks equality when considering a two point projective measurement scheme. Property 6 ensures that in the absence of interactions $\tilde{E}$ is time independent, which is clearly a desirable condition for a statistical estimate of the energy of a quantum state.

Subsequent research has identified $\tilde{E}$ as the cumulant generating function [106, 107] for the measurement statistics of energy in a quantum state. This observation has been used to develop an account of $\Delta\tilde{E}$ in which $\tilde{E}$ is interpreted as 'an effective potential with both energetic and coherent contributions' [107]. For more details on this interpretation see Ref. [107] and Ref. [108].

This latter interpretation was inspired by our original approach which we move onto now. We clarify the empirical content of the generalised energy flow term $\Delta\tilde{E}$ by comparing it to the equivalent work term of the classical Crooks equality for specific choices in battery states.

2.5 Quantum corrections to the classical Crooks equality

To compare the FQC to the classical Crooks equality, it is instructive to compare the generalised energy flow term, $\Delta\tilde{E}$, to the equivalent energy flows in the classical relation. Specifically, we express $\Delta\tilde{E}$ in terms of the difference between the average change in the energy of the battery in the forwards process,

$$\Delta E_+ := \langle\phi_i| H_B |\phi_i\rangle - \langle\phi_f| H_B |\phi_f\rangle \ , \tag{2.68}$$

and the average change in the energy of the battery in the reverse process,

$$\Delta E_- := \langle\psi_f| H_B |\psi_f\rangle - \langle\psi_i| H_B |\psi_i\rangle \ , \tag{2.69}$$

by introducing the quantity

$$W_q := \frac{1}{2}(\Delta E_+ - \Delta E_-) \ . \tag{2.70}$$

Since the unitary evolution is energy conserving, in the sense that $[U, H] = 0$, it follows that $-W_q$ is also the difference between the average energy change of the *system* in the forwards and reverse processes.

If the battery is prepared and measured in energy eigenstates, then W_q reduces to the usual work term of the classical Crooks relation. Specifically, if $|\phi_i\rangle = |E_i\rangle$ and $|\phi_f\rangle = |E_f\rangle$ then it follows from Eq. (2.28) that $|\psi_i\rangle = |E_i\rangle$ and $|\psi_f\rangle = |E_f\rangle$ and therefore

$$W_q = \frac{1}{2}\left((E_i - E_f) - -(E_i - E_f)\right) \equiv \frac{1}{2}\left(W - (-W)\right) = W \ , \tag{2.71}$$

where we have identified $(E_i - E_f)$, the energy lost by the battery, as the work W done on the system.

For more general quantum battery states, W_q generalises W to the quantum regime in two key ways. Firstly, W_q accounts for coherence by quantifying the battery's *average* energy change rather than a well defined but stochastic energy change. Secondly, the definition of W_q ccounts for the fact that the magnitude of the energy flows between the system and the battery quantified by the FQC differ in the forwards and reverse processes, that is in general $\Delta E_+ \neq -\Delta E_-$.

The difference between the FQC and classical Crooks equality can in this manner be captured by the ratio of $\Delta\tilde{E}$ to W_q,

$$q := \frac{\Delta\tilde{E}}{W_q} \, . \tag{2.72}$$

We will call this quantity the quantum prefactor and since it enables the FQC to be written as

$$\frac{\mathcal{P}(\phi_f|\phi_i,\gamma_i)}{\mathcal{P}(\psi_i|\psi_f,\gamma_f)} = \exp\left(-\frac{\Delta F}{k_B T}\right) \exp\left(q\frac{W_q}{k_B T}\right) . \tag{2.73}$$

Since W_q can be explicitly calculated from the choice in initial and final battery states (ϕ_i, ϕ_f, ψ_i and ψ_f) it follows that the quantum deviation prefactor q (and the generalised energy flow $\Delta\tilde{E}$) can be experimentally deduced, via Eq. (2.73), from measuring the forwards and reverse transition probabilities.

The quantum prefactor q depends on both the Hamiltonian of the battery and the states the battery is prepared and measured in. Therefore, to allow us to concretely discuss the quantum corrections to the classical Crooks equality we henceforth focus on a quantum harmonic oscillator battery with the Hamiltonian,

$$H_B = \hbar\omega\left(N + \frac{1}{2}\right) \quad \text{with} \quad N := \sum_n n\,|n\rangle\langle n| . \tag{2.74}$$

An oscillator Hamiltonian corresponds to an infinite ladder with constant spacings between each energy level, thus naturally generalising an infinitely large classical battery to a discrete quantum system. Moreover, the Hamiltonian is practical since it may be realised by a large number of physical systems. We do not need to make any specific assumptions on the system Hamiltonian to calculate q and therefore H_S^i, H_S^f and $V_{SB}^{\perp}$ may still be chosen freely in what follows. In Section 2.7 the nature of the system Hamiltonians and the interaction between the system and the harmonic osccilator battery will be specified when we develop the results presented here into a more concrete experimental proposal.

Having chosen to focus on an oscillator battery, we derive specific FQCs for common harmonic oscillator states, namely coherent states, squeezed states and cat states [109]. To do so we calculate q as well as the specific relation between the initial and final states of the forward and reversed process, Eq. (2.28). The resulting coherent, squeezed and cat state Crooks equalities can be viewed as setting out quantum corrections to the classical Crooks equality.

2.5.1 Coherent state Crooks equality

Coherent states are commonly described as the most classical of the motional states of a quantum harmonic oscillator. Thus the coherent state Crooks equality, which we present in this section, can be seen as the lowest order extension of the Crooks equality to quantum states.

Before proceeding to derive the coherent Crooks equality let us first recap some of the features of coherent states. Coherent states are viewed as semi-classical due to their status as the minimal uncertainty quantum states. The standard deviation in the position and momentum of a coherent state are given by

$$\sigma_x = \sqrt{\frac{\hbar}{2m\omega}} \quad \text{and} \quad \sigma_p = \sqrt{\frac{\hbar m\omega}{2}} , \tag{2.75}$$

where m is the mass of the oscillator, and therefore coherent states saturate the uncertainty principle with $\sigma_x\sigma_p = \frac{\hbar}{2}$. Coherent states are also known as displaced states since they correspond to a vacuum state which has been displaced by amount α in phase space. Thus formally the coherent state can be defined as $|\alpha\rangle := D(\alpha)\,|0\rangle$ where

$$D(\alpha) := \exp\left(\alpha a^\dagger - \alpha^* a\right) \tag{2.76}$$

is the displacement operator with $a^\dagger$ and a the creation and annihilation operators of the oscillator. The displacement operator leaves the position and momentum fluctuations of the vacuum state unchanged, hence Eq. (2.75) holds as claimed, but displaces the mean position and momentum of the oscillator to

$$\langle x\rangle = x_0 = \Re(\alpha)\sqrt{\frac{2\hbar}{m\omega}} \quad \text{and} \quad \langle p\rangle = p_0 = \Im(\alpha)\sqrt{2\hbar m\omega}\,. \tag{2.77}$$

In the absence of interactions, a coherent state remains a coherent state with its position and momentum freely evolving according to

$$\langle x(t)\rangle_\alpha = \sqrt{x_0^2 + \left(\frac{p_0}{m\omega}\right)^2}\,\cos(\phi - \omega t) \quad \text{and} \quad \langle p(t)\rangle_\alpha = \sqrt{(m\omega x_0)^2 + p_0^2}\,\sin(\phi - \omega t)\,. \tag{2.78}$$

where $\tan(\phi) = p_0/x_0$. Thus the dynamics of a coherent state in a harmonic potential closely resembles that of a classical oscillator.

While coherent states are the most classical of the motional quantum states, crucially a coherent state consists of a superposition of energy eigenstates and thus fundamentally a battery prepared in a coherent state is non-classical. In the number basis, the coherent state can be written as

$$|\alpha\rangle = \exp\left(-\frac{|\alpha|^2}{2}\right)\sum_{n=0}^{\infty}\frac{\alpha^n}{\sqrt{n!}}\,|n\rangle \tag{2.79}$$

such that the probability to find the oscillator in the n_{th} Fock state is Poisson distributed. Moreover, the average and standard deviation of the energy of a coherent state are given by

$$\langle E\rangle = \langle H_B\rangle_\alpha = \hbar\omega\left(|\alpha|^2 + \frac{1}{2}\right) \quad \text{and} \quad \sigma_E = \sqrt{\hbar\omega}|\alpha|\,. \tag{2.80}$$

respectively. Consequently, in the classical limit of states with large displacements α, the ratio between the standard deviation and average energy of a coherent state, $\frac{\sigma_E}{E}$, vanishes and the uncertainty in the energy of the battery is increasingly insignificant. However, for small displacements the relative spread in the energy of a coherent state battery due to vacuum fluctuations may be substantial.

The coherent state Crooks equality is derived by considering transition probabilities between coherent states of an oscillator battery. We set the measured states $|\phi_f\rangle$ and $|\psi_i\rangle$ to the coherent states $|\alpha_f\rangle$ and $|\alpha_i^*\rangle$ respectively,

$$|\phi_f\rangle = |\alpha_f\rangle \quad \text{and} \quad |\psi_i\rangle = |\alpha_i^*\rangle \tag{2.81}$$

and calculate the prepared states $|\phi_i\rangle$ and $|\psi_f\rangle$ using the mapping specified by Eq. (2.28). This step involves calculating the effect of applying the operator $\exp\left(-\frac{H_B}{2k_BT}\right)$ to coherent state. We find that

$$\exp\left(-\frac{H_B}{2k_BT}\right)|\alpha\rangle \propto \exp\left(-\chi\left(N+\frac{1}{2}\right)\right)\sum_{n=0}^{\infty}\frac{\alpha^n}{\sqrt{n!}}\,|n\rangle \propto \sum_{n=0}^{\infty}\frac{(\alpha\exp(-\chi))^n}{\sqrt{n!}}\,|n\rangle \propto |\alpha\exp(-\chi)\rangle\ , \tag{2.82}$$

where the dimensionless parameter

$$\chi := \frac{\hbar\omega}{2k_BT}\,. \tag{2.83}$$

is the ratio of vacuum fluctuations of the battery, $\frac{\hbar\omega}{2}$ to thermal fluctuations of the system, k_BT, a measure which delineates between quantum and thermodynamic regimes. The prepared states are therefore given by

$$|\phi_i\rangle = |\alpha_i\exp(-\chi)\rangle \quad \text{and} \quad |\psi_f\rangle = |\alpha_f^*\exp(-\chi)\rangle\ . \tag{2.84}$$

We thus find that the pairs of states considered in the forwards and reverse process disagree by a factor of $\exp(-\chi)$. In the classical limit in which thermal fluctuations dominate and vacuum fluctuations are negligible, χ vanishes and $\exp(-\chi)$ tends to 1, and therefore the reverse process is the exact time-reversed process. However, in general the factor of $\exp(-\chi)$ is essential to capture the quantum uncertainty in the energy of a coherent state.

The next step to deriving the coherent state Crooks equality is to calculate the prefactor q. To do so, we first evaluate $\tilde{E}$, Eq. (2.30), for an oscillator battery in a coherent state and find that

$$\begin{aligned}\tilde{E}_\alpha\left(\hbar\omega\left(N+\frac{1}{2}\right)\right) &= -k_BT\,\ln\left(\langle\alpha|\exp\left(-2\chi\left(N+\frac{1}{2}\right)\right)|\alpha\rangle\right)\\ &= -k_BT\ln\left(\exp\left(-|\alpha|^2\right)\sum_n\frac{|\alpha|^{2n}}{n!}\exp\left(-2\chi\right)^n\exp\left(-\chi\right)\right)\\ &= -k_BT|\alpha|^2\left(\exp(-2\chi)-1\right)+\chi k_BT\ .\end{aligned} \tag{2.85}$$

From this it follows that the energy flow term, $\Delta\tilde{E} := \tilde{E}_{\alpha_i}(H_B) - \tilde{E}_{\alpha_f}(H_B)$, takes the form

$$\Delta\tilde{E} = k_BT(|\alpha_f|^2-|\alpha_i|^2)(\exp(-2\chi)-1)\ . \tag{2.86}$$

The energy flows ΔE_+ and ΔE_- evaluate to

$$\Delta E_+ := \langle\alpha_i\exp(-\chi)|\,\hbar\omega\left(N+\frac{1}{2}\right)|\alpha_i\exp(-\chi)\rangle - \langle\alpha_f|\,\hbar\omega\left(N+\frac{1}{2}\right)|\alpha_f\rangle \tag{2.87}$$

$$= (\exp(-2\chi)|\alpha_i|^2-|\alpha_f|^2)\hbar\omega \tag{2.88}$$

$$\Delta E_- := \langle\alpha_f^*\exp(-\chi)|\,\hbar\omega\left(N+\frac{1}{2}\right)|\alpha_f^*\exp(-\chi)\rangle - \langle\alpha_i^*|\,\hbar\omega\left(N+\frac{1}{2}\right)|\alpha_i^*\rangle \tag{2.89}$$

$$= (\exp(-2\chi)|\alpha_f|^2-|\alpha_i|^2)\hbar\omega\,. \tag{2.90}$$

from which it follows that the actual energy flow term, $W_q := (\Delta E_+ - \Delta E_-)/2$, is given by

$$W_q = \frac{\hbar\omega}{2}(|\alpha_i|^2-|\alpha_f|^2)(\exp(-2\chi)+1) \tag{2.91}$$

Thus for the coherent state Crooks equality the quantum prefactor q, the ratio of the generalised energy flow $\Delta\tilde{E}$ to the actual energy flow W_q, evaluates to

$$q\left(\chi\right) = \frac{1}{\chi}\frac{1-\exp(-2\chi)}{1+\exp(-2\chi)} = \frac{1}{\chi}\tanh(\chi)\ . \tag{2.92}$$

The quantum prefactor, Eq. (2.92), can be written in a more natural and instructive form by relating it to the average energy of a thermal oscillator battery. Specifically, we can calculate the average energy of a harmonic oscillator as follows

$$\mathrm{Tr}[H_B\gamma(H_B)] = \sum_n\hbar\omega(n+1/2)\frac{\exp\left(-\frac{\hbar\omega(n+\frac{1}{2})}{k_BT}\right)}{Z_{H_B}} = \frac{1}{2}\hbar\omega\left(\frac{1+\exp(-2\chi)}{1-\exp(-2\chi)}\right) = \frac{k_BT}{q(\chi)}\ . \tag{2.93}$$

On rearranging the above expression, we find that the quantum prefactor can be written as

$$q\left(\chi\right) = \frac{k_BT}{\mathrm{Tr}[H_B\gamma(H_B)]} := \frac{k_BT}{\hbar\omega_T}\ , \tag{2.94}$$

where we have implicitly defined the 'thermal frequency' ω_T as the average frequency of a harmonic oscillator in a thermal state. The coherent state Crooks equality therefore reads

$$\frac{\mathcal{P}\left(\alpha_f|\alpha_i\exp(-\chi),\gamma_i\right)}{\mathcal{P}\left(\alpha_i^*|\alpha_f^*\exp(-\chi),\gamma_f\right)} = \exp\left(-\frac{\Delta F}{k_BT}\right)\exp\left(\frac{W_q}{\hbar\omega_T}\right)\ . \tag{2.95}$$

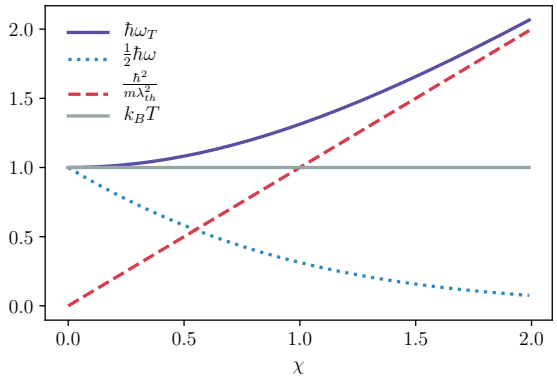


Figure 2.5: **Coherent state Crooks equality deviations.** The purple line indicates the average energy, $\hbar\omega_T$, of a quantum harmonic oscillator in a thermal state at temperature T. The grey line shows the classical limit in which $\hbar\omega_T$ tends to k_BT. The blue dotted line and red dashed line indicate the thermal and quantum contributions to $\hbar\omega_T$ respectively, as specified by Eq. (2.98). These energies are given in units of k_BT and are plotted as a function of χ, Eq. (2.83).

We thus find that the difference between the coherent state and the classical Crooks equalities is encoded in the thermal frequency, which acts as an effective temperature. Intriguingly, $\hbar\omega_T$ was also identified as an effective temperature in the context of an oscillator Szilard engine [110], suggesting it is a physically natural quantity.

A better handle on the role of the thermal frequency ω_T factor in inducing corrections to the classical Crooks relation can be obtained by splitting the factor into its thermal and quantum contributions. The average energy of a quantum harmonic oscillator is comprised of kinetic, potential, and vacuum fluctuation terms,

$$\hbar\omega_T = E_{\text{kin}} + E_{\text{pot}} + E_{\text{vac}}\,. \tag{2.96}$$

This expression can be simplified first by noting that for an oscillator in a thermal state it follows from the quantum Virial theorem [111] that the kinetic and potential energies are equal. Additionally, the expression can be written in a more instructive form by writing the kinetic energy in terms of the thermal De Broglie wavelength $\lambda_{th} := \frac{h}{p}$ [112] where p is the momentum of the oscillator. Combining these two observations we have that

$$E_{\text{pot}} = E_{\text{kin}} = \frac{p^2}{2m} = \frac{h^2}{2m\lambda_{th}^2}\,, \tag{2.97}$$

and therefore the thermal frequency can be written as

$$\hbar\omega_T = \frac{h^2}{m\lambda_{th}^2} + \frac{1}{2}\hbar\omega\,. \tag{2.98}$$

Thus we see that the the thermal frequency can be decomposed into a thermal contribution of the form $\frac{h^2}{m\lambda_{th}^2}$ and quantum contribution $\frac{1}{2}\hbar\omega$ given by the vacuum fluctuations. This lends support to our interpretation of $\hbar\omega_T$ as an effective temperature that incorporates quantum fluctuations as well as thermal fluctuations.

The thermal De Broglie wavelength sets the spatial scale on which a thermal system can be viewed as classical or quantum. In general, if λ_{th} is small the system is reasonably well localised and can effectively be considered classical. In this classical limit the dominant contribution to

the thermal frequency is thermal and $\hbar\omega_T$ tends to k_BT in agreement with the classical Crooks equality and the equipartition theorem. Conversely, for delocalised quantum systems, in which quantum effects are substantial, λ_{th} is large. In this quantum limit, the thermal contribution to $\hbar\omega_T$ vanishes and therefore the expression is dominated by vacuum fluctuations.

As shown in Fig. 2.5, $\hbar\omega_T$ increases monotonically with χ. As a result, the exponential dependence of the ratio of the forwards and reverse transition probabilities on the difference in the energy flows of the forwards and reverse processes, W_q, is suppressed. Consequently, in the general quantum limit the probability for the reverse process is larger than expected classically and therefore irreversibility is in a sense milder. We can attribute this to the presence of quantum coherence as it is the contribution from vacuum fluctuations that makes the thermal frequency $\hbar\omega_T$ larger than the temperature k_BT outside of the classical limit. Since the dynamics of the system and battery are unitary and so fully reversible, this heightened irreversibility arises from the choice in prepared and measured states in the forwards and reverse processes [113].

2.5.2 Squeezed state Crooks equality

Squeezed displaced states also saturate the uncertainty principle but, in contrast to coherent states, the variance in the position and momentum of a squeezed state are unequal. Specifically, the variance of the oscillator's position and momentum are rescaled as

$$\Delta x = \exp(-r)\sqrt{\frac{\hbar}{2m\omega}} \quad \text{and} \quad \Delta p = \exp(+r)\sqrt{\frac{\hbar m\omega}{2}}\,, \tag{2.99}$$

where the parameter r quantifies the magnitude of the squeezing. The squeezed state Crooks equality, which quantifies transition probabilities between squeezed battery states, can thus be seen as setting out higher order quantum corrections to the coherent state and classical Crooks equalities. Analogously to the coherent state, the squeezed displaced state is formally defined as the state generated by squeezing and then displacing the vacuum state, that is $|\alpha, r\rangle = D(\alpha)S(r)\,|0\rangle$, where

$$S(r) = \exp\left(\frac{r^2}{2}\left(a^2 - a^{\dagger 2}\right)\right) \tag{2.100}$$

is the squeezing operator.

To derive a squeezed state Crooks equality the measured states $|\phi_f\rangle$ and $|\psi_i\rangle$ are set to the squeezed displaced states $|\alpha_f, r_f\rangle$ and $|\alpha_i^*, r_i\rangle$ respectively, that is

$$|\phi_f\rangle = |\alpha_f, r_f\rangle \quad \text{and} \quad |\psi_i\rangle = |\alpha_i^*, r_i\rangle\ . \tag{2.101}$$

Similarly to the coherent state Crooks equality, to derive a squeezed state relation we need to calculate the prepared states $|\phi_i\rangle$ and $|\psi_f\rangle$ using Eq. (2.28), as well as $\Delta\tilde{E}$, Eq. (2.30). These calculations utilise standard techniques in operator algebra but are rather involved and so we leave them to the Appendix B.2. We find that the prepared states are given by the squeezed states $|\psi_f\rangle = |s_f, \mu_f^*\rangle$ and $|\phi_i\rangle = |s_i, \mu_i\rangle$ with

$$s := \tanh^{-1}\left(\exp(-2\chi)\tanh(r)\right) \quad \text{and} \quad \mu := \frac{\exp(-\chi)\left(1+\tanh(r)\right)}{1+\exp(-2\chi)\tanh(r)}\,. \tag{2.102}$$

We further find that for real α (we include the general expression for complex α in Appendix B.2) that $\Delta\tilde{E} = \tilde{E}_{\alpha_i,r_i} - \tilde{E}_{\alpha_f,r_f}$ where $\tilde{E}_{\alpha,r} = -k_BT\ln(\tilde{Z}_{\alpha,r})$ with

$$\tilde{Z}_{\alpha,r} := \frac{\exp\left(-|\alpha|^2(1-\tanh(r)\right)}{\cosh(r)\sqrt{1-\tanh(r)^2\exp\left(-4\chi\right)}} \quad \exp\left(|\alpha|^2\frac{\left(1+\tanh(r)\right)^2\left(1-\tanh(r)\exp\left(-2\chi\right)\right)\exp\left(-2\chi\right)}{1-\tanh(r)^2\exp\left(-4\chi\right)}\right)\,. \tag{2.103}$$

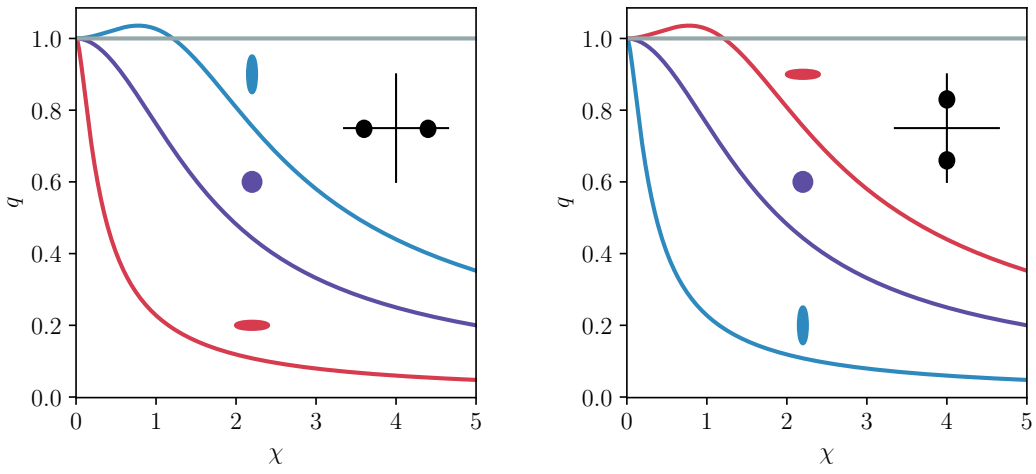


Figure 2.6: **Squeezed state Crooks equality deviations.** We plot the prefactor q, Eq. (2.127), as a function of χ for coherent states and squeezed displaced states. The red, purple and blue lines plot $r = 1$, $r = 0$ (i.e. the coherent state case) and $r = -1$ respectively. The grey line indicates the classical limit in which $q = 1$. As indicated by the black Wigner plot insets, in a) the prepared and measured squeezed displaced battery state are displaced with respect to position only, that is the displacement is real $\alpha_{i,f} = \Re(\alpha_{i,f})$ and $\mu_{i,f} = \Re(\mu_{i,f})$; whereas in b) the state is displaced with respect to momentum only, that is the displacement is purely imaginary $\alpha_{i,f} = \Im(\alpha_{i,f})$ and $\mu_{i,f} = \Im(\mu_{i,f})$.

While the precise form of the above expression is not especially insightful we can use it to plot the quantum prefactor $q(\chi)$, Eq. (2.72), for squeezed states.

In Fig. 2.6, we compare the effect of using a battery that is prepared in a squeezed or coherent state with the effect of using a classical battery by plotting $q(\chi)$ for these three cases[5]. In the classical limit, where thermal fluctuations dominate over vacuum fluctuations, χ tends to 0 and q tends to 1 for both coherent and squeezed states. Thus, in this classical limit we regain the classical dependence on work despite the uncertainty in the energy of the coherent and squeezed state batteries. Conversely, in the low temperature quantum limit where the contribution from vacuum fluctuations becomes substantial and χ tends to ∞, we see that q vanishes for both coherent and squeezed states.

While the predictions of the squeezed and coherent state relations, as quantified by the prefactor q, qualitatively agree in the high and low temperature limits; beyond these extremes we find that squeezing can generate deviations from the coherent state case. In Fig. 2.6(a) we suppose that the battery is prepared and measured in states which are displaced with respect to position only. In this case we see that for prepared and measured states that are squeezed with respect to momentum, that is for negative r, the behaviour of q is qualitatively similar to the coherent state case but decreases more rapidly. Conversely, if the battery is squeezed with respect to position, that is for positive r, then the behaviour is again similar to the coherent state case in the quantum limit of large χ, but intriguingly there is now an intermediary regime in which q is greater than the classical value of 1. In Fig. 2.6(b) the prepared and measured states are displaced with respect to

[5]The coherent state case, shown in purple, is equivalent to the inverse of the thermal frequency $\hbar\omega_T$ which is plotted in purple in Fig. 2.5.

Table 2.1: Forwards Process

	Preparation	Measurement
Coherent	$\|\alpha_i e^{-\chi}\rangle$	$\|\alpha_f\rangle$
Squeezed	$\|s_i, \mu_i\rangle$	$\|r_f, \alpha_f\rangle$
Cat	$\eta_\chi^{\|\alpha_i\|^2} \|\alpha_i e^{-\chi}\rangle + \eta_\chi^{\|\beta_i\|^2} \|\beta_i e^{-\chi}\rangle$	$\|\alpha_f\rangle + \|\beta_f\rangle$

Table 2.2: Reverse Process

	Preparation	Measurement
Coherent	$\|\alpha_f^* e^{-\chi}\rangle$	$\|\alpha_i^*\rangle$
Squeezed	$\|s_f, \mu_f^*\rangle$	$\|r_i, \alpha_i^*\rangle$
Cat	$\eta_\chi^{\|\alpha_f\|^2} \|\alpha_f^* e^{-\chi}\rangle + \eta_\chi^{\|\beta_f\|^2} \|\beta_f^* e^{-\chi}\rangle$	$\|\alpha_i^*\rangle + \|\beta_i^*\rangle$

Table 2.3: **Summary of prepared and measured states.** The coherent, squeezed, and cat state equalities are characterised by the preparation and measurement states of the battery. This table lists the form of these battery states respectively for the forwards ($|\phi_{i/f}\rangle$) and reverse ($|\psi_{i/f}\rangle$) processes. In the above we have defined $\eta_\chi := \exp\left(-\frac{1}{2}\left(1-\exp(-2\chi)\right)\right)$, $s := \tanh^{-1}\left(\exp(-2\chi)\tanh(r)\right)$ and $\mu := \frac{\exp(-\chi)(1+\tanh(r))}{1+\exp(-2\chi)\tanh(r)}$ and the cat states are unnormalized for brevity.

momentum only. In this regime, we see the same behaviour as for displacements with respect to position but with the roles of squeezing with respect to position and momentum reversed.

We therefore observe that for a squeezed battery the ratio of the probabilities for the forwards and reverse processes is again smaller than predicted by the classical Crooks equality in the quantum limit of large χ. However, there is now an intermediary regime, where this ratio is larger than the classical limit of 1. Thus, while in the deep quantum limit we see that squeezing again leads to milder irreversibility than expected classically, before this limit is reached irreversibility can be strengthened.

2.5.3 Cat state Crooks equality

Cat states, like Schrödinger's illustrious feline, are inherently quantum mechanical. In the context of quantum optics cat states are usually defined to be superpositions of two coherent states of opposite phases, $|\alpha\rangle$ and $|-\alpha\rangle$, and thus in a sense captures a superposition of two contrary properties (comparable to a dead and alive cat). For the purpose of this section we consider a more general variant of this defintion and consider superpositions of two general coherent states $|\alpha\rangle$ and $|\beta\rangle$

$$|\text{Cat}\rangle \propto |\alpha\rangle + |\beta\rangle \ . \tag{2.104}$$

Such states are highly non-classical whenever $|\alpha - \beta| \gg 0$ and thus the cat state Crooks equality is also highly non-classical.

To derive a cat state Crooks equality the measured states $|\phi_f\rangle$ and $|\psi_i\rangle$ are set to

$$|\phi_f\rangle = |\text{Cat}_f\rangle \propto |\alpha_f\rangle + |\beta_f\rangle \quad \text{and} \quad |\psi_i\rangle \quad = |\text{Cat}_i^*\rangle \propto |\alpha_i^*\rangle + |\beta_i^*\rangle \ . \tag{2.105}$$

The prepared states $|\phi_i\rangle$ and $|\psi_f\rangle$ are calculated using the relation between the prepared and measured states as specified in Eq. (2.28). As shown in Appendix B.3, the prepared states evaluate

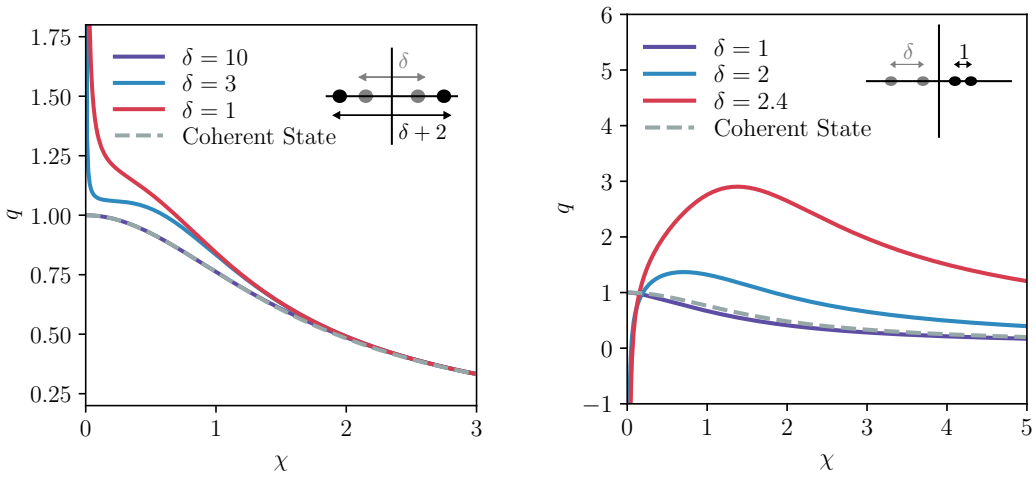


Figure 2.7: **Cat state Crooks equality deviations.** We plot $q := \frac{\Delta\tilde{E}}{W_q}$ as a function of χ for cat states. As indicated by the insets, in a) the prepared and measured battery states consist of superpositions of coherent states with opposite phase, specifically $|\phi_i\rangle = |\text{Cat}_i\rangle \propto |\delta/2\rangle + |-\delta/2\rangle$ and $|\phi_f\rangle = |\text{Cat}_f\rangle \propto |\delta/2+1\rangle + |-\delta/2-1\rangle$. In b) the prepared and measured states consist of superpositions of different displacements with the same phase, specifically $|\phi_i\rangle = |\text{Cat}_i\rangle \propto |-2\rangle + |-2-\delta\rangle$ and $|\phi_f\rangle = |\text{Cat}_f\rangle \propto |2\rangle + |3\rangle$. In both figures the dark blue line indicates $q(\chi)$ for coherent states.

to the following weighted superpositions of coherent states

$$\begin{aligned} |\phi_i\rangle &\propto \eta_\chi^{|\alpha_i|^2} |\exp(-\chi)\alpha_i\rangle + \eta_\chi^{|\beta_i|^2} |\exp(-\chi)\beta_i\rangle \quad \text{and} \\ |\psi_f\rangle &\propto \eta_\chi^{|\alpha_f|^2} |\exp(-\chi)\alpha_f^*\rangle + \eta_\chi^{|\beta_f|^2} |\exp(-\chi)\beta_f^*\rangle \end{aligned} \tag{2.106}$$

where we have defined

$$\eta_\chi := \exp\left(-\frac{1}{2}\left(1-\exp(-2\chi)\right)\right) . \tag{2.107}$$

In Table 3.9.1 we summarise the states prepared and measured in the forwards and reverse protocols for cat state equality as well as the coherent and squeezed state equalities. We further find that the generalised energy flow term is given by $\Delta\tilde{E} = \tilde{E}_{\text{Cat}_i} - \tilde{E}_{\text{Cat}_f}$ where $\tilde{E}_{\text{Cat}_k} = -k_B T \ln(\tilde{Z}_{\text{Cat}_k})$ with

$$\tilde{Z}_{\text{Cat}_k} = \frac{\eta_\chi^{2|\alpha_k|^2} + \eta_\chi^{2|\beta_k|^2} + \eta_\chi^{|\alpha_k|^2+|\beta_k|^2} 2\Re\left(\exp\left(-\frac{1}{2}\exp(-2\chi)(|\beta_k|^2+|\alpha_k|^2-2\beta_k^*\alpha_k)\right)\right)}{2+2\Re(\exp(-\frac{1}{2}(|\alpha_k|^2+|\beta_k|^2-2\beta_k^*\alpha_k)))} \tag{2.108}$$

for $k = i$ and $k = f$.

Since cat states are inherently quantum mechanical, the limit of low χ ceases to correspond to the classical limit of the cat state Crooks equality. As a result, the plots of $q(\chi)$ for cat states, shown in Fig. 2.7, are rather uninstructive. The closest we get to a classical limit for cat states is when the distance between the two coherent states in the superposition vanishes and a cat state tends to a coherent state. In this limit, as one would expect, $q(\chi)$ for the cat and coherent state Crooks equalities agree as shown in purple in Fig. 2.7. More generally, as previously observed for coherent states and squeezed state batteries, in the quantum limit of large χ, the prefactor q tends to zero. However, outside of these two limits, the behaviour of $q(\chi)$ is hard to analyse.

While in this section we have focused on the quantum corrections to the classical Crooks equality induced by preparing the battery in coherent, squeezed and Schrödinger cat states, these results have recently been extended in [114]. There we firstly study the corrections resulting from preparing the battery in binomial states, which can be viewed as analogues of coherent states for finite dimensional systems rather than infinite dimensional oscillators [115, 116], leading to highly non-classical properties [117, 118]. We additionally explore the effect of preparing the system in a non-equilibrium state rather than a perfectly thermal state. In particular, we have developed Crooks equalities for a system that is prepared in photon added and photon subtracted thermal states. These states have received interest in quantum optics owing to their non-Gaussian and negative Wigner functions [119–121] and unusual thermodynamic properties [122, 123]. We do not discuss these new results here as they do not fit with the experimental proposal that we now proceed to discuss; however, for a complete discussion on these new equalities, along with proposals on how they could be implemented, see [114].

2.6 Autonomous quantum Crooks equality

In the next section we will develop the spin example considered earlier into an experimental proposal to test the coherent, squeezed and cat state Crooks equalities. To do so, we consider the autonomous variant of the FQC (the AQC) whereby the system and battery evolve autonomously under their joint Hamiltonian, as compared to the non-autonomous variant in which a unitary operation is applied to induce the evolution. Our reasons for considering this autonomous variant are twofold. Firstly, the non-autonomous variant implicitly depends on an external classical observer to apply the unitary which is undesirable in a fully quantum equality. Secondly, and more honestly, it is surprisingly hard to think of non-autonomous implementations whereby a physically implementable unitary both induces a change in Hamiltonian and transfers energy between the system and battery such that energy is globally conserved.

However, crucially, the FQC only holds approximately for autonomous evolutions. In this section we explain why this is the case and establish error bounds to quantify the degree to which the FQC approximately holds. We further demonstrate there there are regimes in which the equality, while strictly approximate, can be treated as exact for all practical purposes. Again, this material is reasonably technical and can be skipped.

2.6.1 Autonomy and approximate factorisability

The reason that the FQC does not hold exactly for autonomous evolutions boils down to the fact that the factorisability condition, Eq. (2.49), can not hold exactly in this case. To see why, we start by recalling that to realise an effectively time dependent system Hamiltonian, while considering a globally time independent Hamiltonian, we consider a Hamiltonian of the general form

$$H_{SB} = H_S^i \otimes \Pi_B^i + H_S^f \otimes \Pi_B^f + V_{SB}^{\perp} + \mathbb{1}_S \otimes H_B \ , \tag{2.109}$$

such that if the battery is initialised in a state in subspace R_i and evolves to a final state in subspace R_f, the system Hamiltonian evolves from H_S^i to H_S^f. For the autonomous variant of the FQC the evolution is induced by evolution under this Hamiltonian $U = \exp(-iH_{SB}t)$; where as for the non-autonomous variant the evolution is induced by the application of some unitary $U \neq \exp(-iH_{SB}t)$.

The factorisability condition holds exactly for this Hamiltonian, Eq. (2.109), and the battery states

$$\sigma_i = \rho_{\mathbb{1}} \otimes \mathfrak{T}\left(|\psi_i\rangle\langle\psi_i|\right) \quad \text{and} \quad \mathfrak{T}(\sigma_f) = \rho_{\mathbb{1}} \otimes \mathfrak{T}(|\phi_f\rangle\langle\phi_f|) \tag{2.110}$$

when the following two conditions hold:

1. The battery state $\mathcal{T}|\psi_i\rangle$ has support solely in R_i and the battery state $\mathcal{T}|\phi_f\rangle$ has support solely in R_f.

2. The battery Hamiltonian does not induce evolution between subregions R_i and R_f, that is if $(\mathbb{1}_B - \Pi_B^i)H_B\Pi_B^i = 0$ and $(\mathbb{1}_B - \Pi_B^f)H_B\Pi_B^f = 0$.

If we make these two assumptions it follows that

$$\begin{aligned} J_{H_{SB}}(\sigma_i) &= \exp\left(-\frac{H_S^i \otimes \Pi_B^i + \mathbb{1}_S \otimes H_B}{2k_BT}\right)(\rho_{\mathbb{1}} \otimes \mathfrak{T}(|\phi_f\rangle\langle\phi_f|))\exp\left(-\frac{H_S^i \otimes \Pi_B^i + \mathbb{1}_S \otimes H_B}{2k_BT}\right) \\ &= J_{H_S^i}(\rho_{\mathbb{1}}) \otimes J_{H_B}(\mathfrak{T}(|\phi_f\rangle\langle\phi_f|)) \end{aligned} \tag{2.111}$$

and similarly for $J_{H_{SB}}(\mathfrak{T}(\sigma_f))$. Thus the factorisability assumption holds exactly in this limit and therefore so do does the FQC.

However, to implement an *autonomous* change in the effective Hamiltonian of the system, the evolution of the battery between subspaces R_i and R_f must be generated by the autonomous evolution of the battery under H_{SB}, that is by the propagator $U = \exp(-iH_{SB}t/\hbar)$. Therefore the battery Hamiltonian H_B is required to induce evolution between the subregions R_i and R_f and so the second condition stated above does not hold. Consequently, the factorisability condition cannot hold exactly for non trivial autonomous dynamics meaning the FQC is strictly only ever approximate.

The approximate nature of the FQC for autonomous dynamics can be attributed to the fact that since the system must interact with the battery, the system's local Hamiltonian is strictly never perfectly well-defined. Thus, at its core, the approximate nature here stems from the impossibility of perfectly delineating the individual energies of interacting systems. While usually implicit, this tension in fact holds for all fluctuation theorems since all systems evolve autonomously under time independent Hamiltonians once all control mechanics and energy sources are explicitly modelled. Nonetheless, this tension can be, and usually is, set aside because generally it is possible to identify subsystems and Hamiltonians that are sufficiently well defined for all practical purposes.

The FQC holds to a high degree of approximation when the system and battery can be considered effectively non-interacting at the start and end of the forwards and reverse protocols. This idea is captured by the claim that with an appropriate choice in the battery states the factorisability condition approximately holds, that is

$$\begin{aligned} &J_{H_{SB}}(\sigma_i) \simeq J_{H_S^i}(\rho_{\mathbb{1}}) \otimes J_{H_B}(\mathfrak{T}(|\psi_i\rangle\langle\psi_i|)) \quad \text{and} \\ &J_{H_{SB}}(\mathfrak{T}(\sigma_f)) \simeq J_{H_S^f}(\rho_{\mathbb{1}}) \otimes J_{H_B}(\mathfrak{T}(|\phi_f\rangle\langle\phi_f|)) \ . \end{aligned} \tag{2.112}$$

In this limit the FQC also approximately holds,

$$\frac{\mathcal{P}(\phi_f|\phi_i,\gamma_i)}{\mathcal{P}(\psi_i|\psi_f,\gamma_f)} \simeq \exp\left(-\frac{\Delta F}{k_BT}\right)\exp\left(\frac{\Delta\tilde{E}}{k_BT}\right) \ , \tag{2.113}$$

with the degree of approximation depending directly on the degree to which factorisability holds.

2.6.2 Error bounds

We can quantify the approximate nature of the FQC for autonomous evolutions by establishing error measures. In this section we establish three such error measures: an analytic upper bound on the error, ϵ, and the actual errors calculated from the difference between, D, and ratio of, $1-R$, the predicted forwards and reverse transition probabilities.

Following the approach first used in [64], to derive the measures D and ϵ, we first note that the FQC can be rewritten as

$$Z_i \langle\psi_i| \exp\left(-\frac{H_B}{k_B T}\right) |\psi_i\rangle \mathcal{P}(\phi_f|\phi_i,\gamma_i) - Z_f \langle\phi_f| \exp\left(-\frac{H_B}{k_B T}\right) |\phi_f\rangle \mathcal{P}(\psi_i|\psi_f,\gamma_f) \approx 0 \tag{2.114}$$

using the definition of the generalised energy flow, Eq. (2.30), and the definition of the system's free energy in terms of the initial and final partition functions, $\exp(-\Delta F/k_B T) = Z_f/Z_i$. The degree of approximation can then be quantified by switching from the claim that the left hand side of Eq.(2.114) is approximately zero, to a statement that it is bounded by the error measure ϵ,

$$D := |Z_i \langle\psi_i| \exp\left(-\frac{H_B}{k_B T}\right) |\psi_i\rangle \mathcal{P}(\phi_f|\phi_i,\gamma_i) - Z_f \langle\phi_f| \exp\left(-\frac{H_B}{k_B T}\right) |\phi_f\rangle \mathcal{P}(\psi_f|\psi_f,\gamma_f)| \leq \epsilon. \tag{2.115}$$

D can be calculated analytically for the coherent, squeezed and cat state Crooks equalities since it is possible to infer the terms $\langle\psi_i| \exp\left(-\frac{H_B}{k_B T}\right) |\psi_i\rangle$ and $\langle\psi_f| \exp\left(-\frac{H_B}{k_B T}\right) |\psi_f\rangle$ simply by rearranging their expressions.

The error bound, ϵ, consists of the sum of the initial and final factorisation errors,

$$\epsilon = ||\epsilon^i_{SB}||_1 + ||\epsilon^f_{SB}||_1 \tag{2.116}$$

where $||\epsilon||_1 = \mathrm{Tr}\left[\sqrt{\epsilon^\dagger \epsilon}\right]$ denotes the trace norm of the operator ϵ. The initial and final factorisation errors, ϵ^i_{SB} and ϵ^f_{SB},

$$\begin{aligned} \epsilon^i_{SB} &:= J_{H_{SB}}(\mathbb{1}_S \otimes |\psi_i\rangle\langle\psi_i|) - J_{H^i_S}(\mathbb{1}_S) \otimes J_{H_B}(|\psi_i\rangle\langle\psi_i|) \quad \text{and} \\ \epsilon^f_{SB} &:= J_{H_{SB}}(\mathbb{1}_S \otimes |\phi_f\rangle\langle\phi_f|) - J_{H^f_S}(\mathbb{1}_S) \otimes J_{H_B}(|\phi_f\rangle\langle\phi_f|). \end{aligned} \tag{2.117}$$

capture the degree to which the exponential of the total Hamiltonian, H_{SB}, can be split into the product of the exponential of a battery Hamiltonian, H_B, and the initial or final system Hamiltonian, H^i_S or H^f_S, when applied to the battery states $|\psi_f\rangle$ or $|\phi_f\rangle$ respectively. These errors typically can only be calculated numerically as they require exponentiating H_{SB} which in general will involve non-trivial interactions between the system and battery.

The form of the above error bounds is obtained by rerunning the proof of the FQC while tracking the error induced from approximate factorisability. As before, the Global Invariance condition for the states σ_i and σ_f, Eq. (2.110), reads

$$\begin{aligned} &\tilde{Z}_{H_{SB}}(\rho_{\mathbb{1}} \otimes |\psi_i\rangle\langle\psi_i|)\, P(\rho_{\mathbb{1}} \otimes |\phi_f\rangle\langle\phi_f|\, |G_{H_{SB}}(\rho_{\mathbb{1}} \otimes \mathfrak{T}(|\psi_i\rangle\langle\psi_i|))) \\ &= \tilde{Z}_{H_{SB}}(\rho_{\mathbb{1}} \otimes |\phi_f\rangle\langle\phi_f|)\, P(\rho_{\mathbb{1}} \otimes |\psi_i\rangle\langle\psi_i|\, |G_{H_{SB}}(\rho_{\mathbb{1}} \otimes \mathfrak{T}(|\phi_f\rangle\langle\phi_f|)))\,. \end{aligned} \tag{2.118}$$

Substituting in the definition of the factorisability errors ϵ^i_{SB} and ϵ^f_{SB}, Eq. 2.117, gives

$$\begin{aligned} &Z_i\, \tilde{Z}_{\psi_i}\, \mathcal{P}(\phi_f|\phi_i,\gamma_i) + \mathrm{Tr}[(\mathbb{1}_S \otimes |\phi_f\rangle\langle\phi_f|) U \mathfrak{T}(\epsilon^i_{SB}) U^\dagger] \\ &= Z_f\, \tilde{Z}_{\phi_f}\, \mathcal{P}(\psi_i|\psi_f,\gamma_f) + \mathrm{Tr}[(\mathbb{1}_S \otimes |\psi_i\rangle\langle\psi_i|) U \mathfrak{T}(\epsilon^f_{SB}) U^\dagger]\,, \end{aligned} \tag{2.119}$$

which can be rearranged and combined with the triangle inequality to give

$$\begin{aligned}&|Z_i\,\tilde{Z}_{\psi_i}\,\mathcal{P}(\phi_f|\phi_i,\gamma_i) - Z_f\,\tilde{Z}_{\phi_f}\,\mathcal{P}(\psi_i|\psi_f,\gamma_f)| \\ &\leq |\operatorname{Tr}[(\mathbb{1}_S\otimes|\phi_f\rangle\langle\phi_f|)U\mathfrak{T}(\epsilon^i_{SB})U^\dagger]| + |\operatorname{Tr}[(\mathbb{1}_S\otimes|\psi_i\rangle\langle\psi_i|)U\mathfrak{T}(\epsilon^f_{SB})U^\dagger]|\,.\end{aligned} \tag{2.120}$$

The Cauchy Schwartz identity entails that

$$\begin{aligned}&\operatorname{Tr}[(U^\dagger(\mathbb{1}_S\otimes|\phi_f\rangle\langle\phi_f|)U)\,\epsilon^i_{SB}] \leq ||\mathfrak{T}(\epsilon^i_{SB})||_1 = ||\epsilon^i_{SB}||_1 \quad \text{and} \\ &\operatorname{Tr}[(U^\dagger(\mathbb{1}_S\otimes|\psi_i\rangle\langle\psi_i|)U)\,\epsilon^f_{SB}] \leq ||\mathfrak{T}(\epsilon^f_{SB})||_1 = ||\epsilon^f_{SB}||_1\,.\end{aligned} \tag{2.121}$$

Thus, combining Eq. (2.120) and Eq. (2.121) gives the *error bounded* FQC

$$|Z_i\,\tilde{Z}_{\psi_i}\,\mathcal{P}(\phi_f|\phi_i,\gamma_i) - Z_f\,\tilde{Z}_{\phi_f}\,\mathcal{P}(\psi_i|\psi_f,\gamma_f)| \leq ||\epsilon^f_{SB}||_1 + ||\epsilon^i_{SB}||_1\,. \tag{2.122}$$

While the error bounded FQC enables the FQC to be tested for autonomous evolutions, in some regimes the error measures D and ϵ cease to be reliable indicators of the accuracy of the FQC. For example, D is small when the transition probabilities $\mathcal{P}$ are small even if the FQC could not reasonably be considered to hold accurately. Therefore, we also consider R the ratio of the left and right hand sides of the FQC,

$$R := \frac{\mathcal{P}(\phi_f|\phi_i,\gamma_i)}{\mathcal{P}(\psi_i|\psi_f,\gamma_f)}\left(\exp\left(\frac{\Delta\tilde{E}-\Delta F}{k_BT}\right)\right)^{-1}\,. \tag{2.123}$$

The quantity $1-R$ vanishes when the FQC holds exactly, irrespective of the magnitude of the transition probabilities, and thus is a better measure of the accuracy of the FQC in regimes where the transition probabilities are small.

2.6.3 Verification of bounds

Here we consider an autonomous variant of the spin example from earlier and show that there are regimes in which the coherent, squeezed and cat states Crooks equalities are exact for all practical purposes.

As a reminder, the Hamiltonian for the spin example is of the form

$$H_{SB} = \mathbb{1}_S\otimes H_B + \sigma^z_S\otimes E(x_B)\,. \tag{2.124}$$

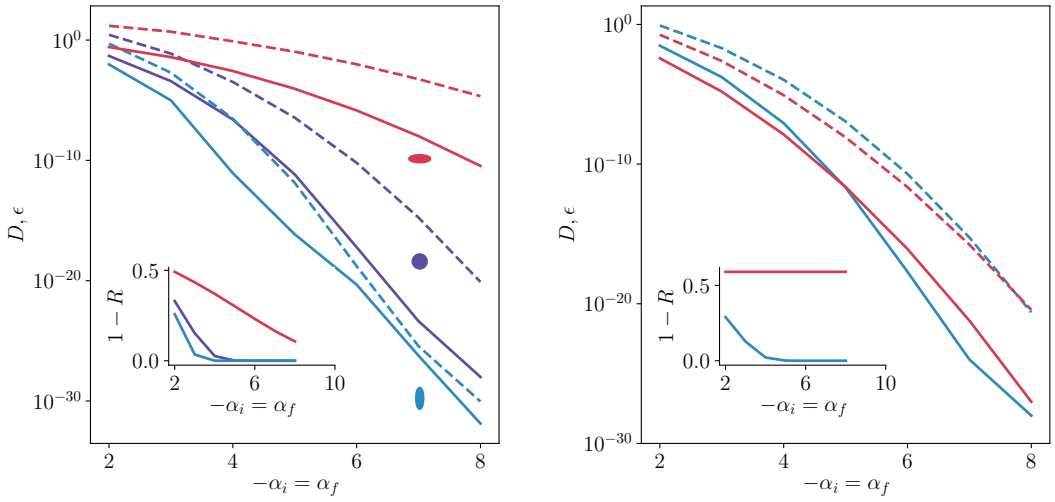
For now we assume that the battery is a harmonic oscillator, Eq. (2.74), and we take the level splitting $E(x)$ to linearly increase from some initial value E_i to some final value E_f with

$$E(x) = \begin{cases} E_i & x \leq x_i \\ \frac{E_f-E_i}{x_f-x_i}(x-x_i)+E_i & x_i < x < x_f \\ E_f & x \geq x_f \quad . \end{cases} \tag{2.125}$$

Without loss of generality, we chose to centre the interaction region around $x=0$ such that $|x_i| = |x_f|$.

We numerically simulated the full quantum state evolution of the two level system and harmonic oscillator battery for this choice in Hamiltonian to obtain the error measures D and R, as defined in Eq. (2.115) and Eq. (2.123). We further numerically calculated the error bound ϵ, defined in Eq. (2.116). As shown in Fig. 2.8, we find that D is less than ϵ, for a wide range of simulated parameters.

For the coherent states and squeezed states the inset of Fig. 2.8a shows that $1-R$ tends to 0 as $|\alpha_i|$ is increased. As is shown in blue and red respectively, for a given $|\alpha_i|$ squeezing the momentum



(a) (b)

Figure 2.8: **Verification of error bounds.** We plot the error measures for evolution under the total Hamiltonian with the position dependent level splitting interaction and a harmonic oscillator battery. In the main figures, the solid (dashed) lines plot D (ϵ) and the insets plot $1-R$. In (a) the coherent state Crooks equality data is shown in purple and squeezed state Crooks equality data shown in red ($r = -1$) and blue ($r = 1$). In (b) the data for cat states prepared and measured either side of the interaction, $|\psi_i\rangle = |\phi_f\rangle \propto |\alpha\rangle + |-\alpha\rangle$, is shown in red and the data for cat states prepared and measured on a single side of the interaction region, $|\psi_i\rangle \propto |-\alpha\rangle + |-(\alpha+1)\rangle$ and $|\phi_f\rangle \propto |\alpha\rangle + |\alpha+1\rangle$, is shown in blue. In this simulation we have used the following parameters: $x_i = -4$, $x_f = 4$, $\hbar\omega = 1$, $E_i = 1$, $E_f = 2$ and $k_B T = 1$. Both plots are a function of $-\alpha_i = \alpha_f$ the displacement of the prepared/measured state. The displacement parameters, $\alpha_{i,f}$, and the positions x_i and x_f, are given in units of dimensionless position $X = \sqrt{\frac{2m\omega}{\hbar}}x$.

variance of the prepared and measured states increases $1-R$; while, squeezing the position variance decreases $1-R$. For simplicity, in these plots we present data for real displacements. However, we have additionally observed similar behaviour for coherent and squeezed states with a complex displacement α, and therefore a finite momentum.

For the cat state equality, we firstly consider measured states involving superpositions of coherent states solely within the region $x < x_i$ or solely within the region $x > x_f$, that is states of the form $|\psi_i\rangle \propto |-\alpha\rangle + |-(\alpha+1)\rangle$ and $|\phi_f\rangle \propto |\alpha\rangle + |\alpha+1\rangle$. On doing so, as is shown by the red line in the inset of Fig. 2.8b, we see that similarly to the coherent state case $1-R$ tends to 0 for large α. However, for the cat states which straddle both the regions $x < x_i$ and $x > x_f$, that is states of the form $\propto |\alpha\rangle + |-\alpha\rangle$, we observe, as shown by blue line, that $1-R \approx 0.6$ for all α.

We thus see that the accuracy of the FQC is increased by minisiming the overlap of the prepared and measured battery states with the interaction region. Moreover, the equality is effectively exact for sufficiently displaced states. For example, for coherent states with $|\alpha_i| = |\alpha_f| \geq 6$ the error measures D, ϵ, $(1-R)$ are less than 10^{-6}. Consequently, states that are prepared comfortably outside of the interaction region experience errors lower than experimental error margins and therefore for such states the approximate nature of the FQC can be disregarded.

The behaviour of the error bounds make physical and conceptual sense. For autonomous evolutions under a time-independent interacting Hamiltonian, the system and battery are technically

interacting at all times and thus the system never strictly has a well-defined local Hamiltonian. However, when the battery is initially prepared with support far from the interaction region, the system's Hamiltonian is approximately well defined. In this limit, the system can properly thermalise with respect to its initial Hamiltonian and therefore the initial thermal states of the forwards and reverse processes are effectively well defined. Therefore, in this limit, the autonomous FQC quantifies precisely the usual Crooks-like scenario in which an initially thermal system is driven by a change in Hamiltonian and thus may hold exactly.

2.7 Experimental proposal

To make the spin proposal more concrete in this section we will discuss how it could be experimentally implemented utilising an ion confined to a linear Paul trap. We propose using an elongated axial mode of a trapped ion to represent the oscillator battery and use a pair of internal electronic levels to represent the system. We assume that the radial confinement is sufficiently large that all radial motion is frozen out and we can disregard this degree of freedom. To practically and convincingly verify the FQC the following six conditions must hold of the experimental setup.

1. For the forwards and reverse transition probabilities to be measurable they need to be an experimentally accessible order of magnitude. That is they cannot be vanishingly small or too close to 1,
$$\begin{aligned} 10^{-2} &\lesssim \mathcal{P}(\phi_f|\phi_i,\gamma_i) \lesssim 1-10^{-2} \\ 10^{-2} &\lesssim \mathcal{P}(\psi_i|\psi_f,\gamma_f) \lesssim 1-10^{-2} \ . \end{aligned}$$

2. To simulate a non-trivial thermal system state with a practical number of experimental runs we need there to be non-negligible populations in both the ground and excited states. This is realised as long as the initial and final splitting between the two system energy levels, $2E_i$ and $2E_f$ respectively, are a similar order of magnitude to the temperature the experiment is conducted at, that is
$$2E_i \approx k_B T \approx 2E_f \ .$$

3. For the experimental implementation to probe the FQC in a regime in which the system is substantially driven from equilibrium we require a moderately strong system-battery interaction. We therefore require the increase in the splitting of the system energy levels to be reasonably large, that is at least as large as the trap frequency,
$$|2E_f - 2E_i| \gtrsim \hbar\omega \ .$$

4. In modelling the interaction between the system and the battery as a unitary operation, we have assumed that decoherence and heating can be neglected on the timescale of the interaction. Therefore, to test the FQC, we require the decoherence and heating rates of the battery to be considerably lower than the trap frequency. The heating of the two level system can be made negligible by using long-lived internal levels. The primary constraint is thus the heating rate of the phonon mode battery, ν_{therm}, and we require
$$\nu_{\text{therm}} \ll \omega.$$

5. For the FQC to hold to a high degree of approximation, the interaction needs to be designed in such a way, such that the initial overlap between the phonon wavepacket and the interaction

region, $x_i < x < x_f$ is negligible. That is, the interaction needs to be designed such that the ion can be prepared in a state that sits comfortably within the regions $x < x_i$ or $x > x_f$.

6. Finally, we need the temperature to be reasonably low compared to the trapping frequency, $k_B T \lesssim \hbar\omega$, if we wish to test the FQC in the regime of larger χ in which quantum deviations are predicted.

We observed in Section 2.5.1 that coherent states with smaller displacements are 'more quantum' in the sense that the relative uncertainty in their energy compared to their mean energy is larger, Eq. (2.80). Thus performing the experiment on a smaller spatial scale allows deeper quantum regimes to be probed.

More concretely, the requirements for measurable transition probabilities (requirement 1) and manageable heating rates (requirement 4) combined with the desire to probe low temperature regimes as compared to the trapping frequency (requirement 6) sets the spatial scale on which the experiment would need to be conducted. Firstly, the heating rate sets the minimum trap frequency. Linear Paul traps typically have heating rates of around 40 phonons per second [124] and therefore to ensure negligible heating of the ion within half an oscillation, the axial trap frequency must be at least of the order of MHz. The trap frequency then determines the spread of the wavefunction for the ion in a coherent state. The standard deviation of a coherent state ion in a MHz trap, by Eq. (2.75), is on the order of tens of nanometers. Finally the spread of the ion, combined with the temperature and the spatial scale of the trap, sets the typical magnitude of the transition probabilities. In general terms the smaller the spatial scale on which the ion oscillates the larger its position variance is as compared to its displacement and the easier it is to ensure a substantial overlap between the evolved and measured states. However, for lower temperatures regimes it can be hard to ensure a significant overlap because the pairs of prepared and measured states differ substantially due to the temperature dependent parameterisation of the measured states specified by Eq. (2.28). Therefore, to ensure substantial overlap between the evolved and measured states for both the forwards and reverse processes, even in the low temperature regimes, the oscillation amplitude must be at least on the μm scale, ideally smaller.

The simplest means of inducing our proposed Hamiltonian with the position dependent level splitting specified by Eq. (2.125) would be to use a position dependent magnetic field. When an ion is placed in a static magnetic field, the interaction between the magnetic dipole of the ion and the magnetic field perturbs the electronic energy level structure of the ion. The splitting of an energy level into several components due to a magnetic field is known as the Zeeman effect and is proportional to the applied magnetic field. Thus by taking the system to be a pair of Zeeman levels and applying a magnetic field with $B(x) \propto \Delta E(x)$ we can realise any splitting of our choice. Specifically, realising the level splitting specified by Eq. (2.125) would require a weak constant magnetic field in the region $x < x_i$, followed by a linearly increasing magnetic field in the region $x_i < x < x_f$ and then a constant larger magnetic field in the region $x > x_f$.

However, realising this magnetic field geometry on a μm scale would be a formidable engineering challenge. Moreover, even if successful, it would likely require conducting wires in close proximity to the ion, which would cause substantial heating of the ion making requirement 4 harder to satisfy.

Therefore, rather than using the Zeeman shift, we advocate using the AC Stark shift to implement the position dependent level splitting. The AC shift is a splitting to an atom or ion's energy levels due to the interaction between an ion's electric dipole and an oscillating electric field. It can be generated by an off resonance laser field.

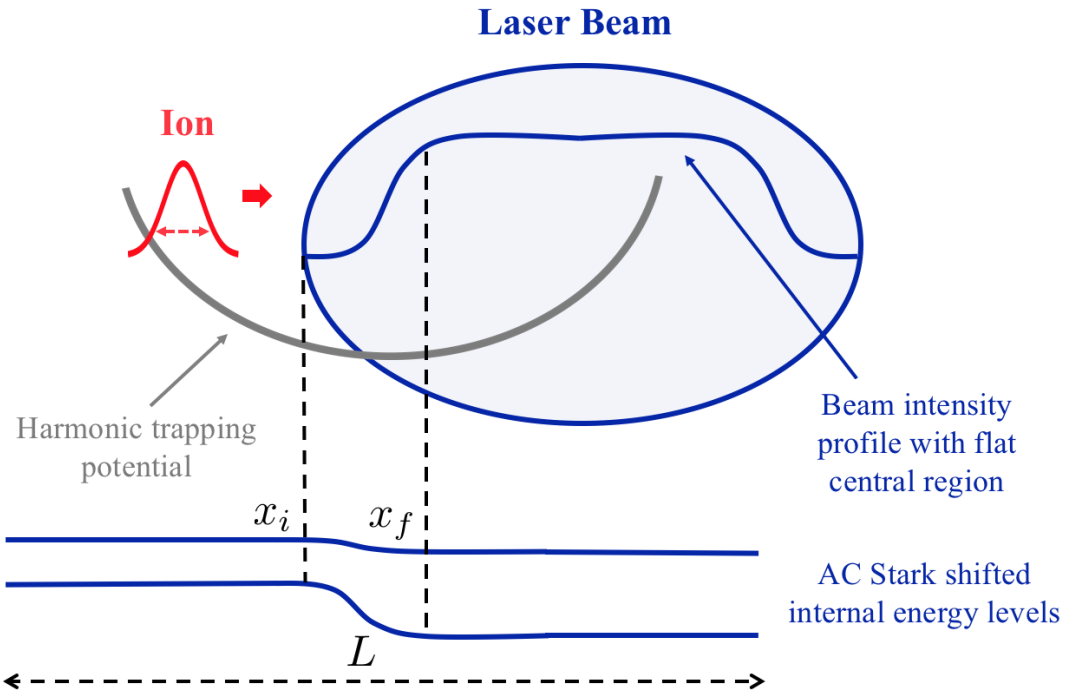


Figure 2.9: **Sketch of trapped ion proposed implementation.** An ion (red wavepacket) is trapped in an elongated trap (grey line) which drives its evolution through the trap (indicated by red arrow). An off-resonance laser is applied perpendicularly across one half of the trap (blue oval). The laser beam has an intensity profile with a flat central region (blue line in oval). The trapped ion experiences a position dependent AC Stark shift (pair of blue lines) as it travels autonomously through the laser beam. The red dashed line indicates the spread of the ion and the black dashed line the width of the elongated trap. Here we show the ion at the start of the autonomous evolution stage of the protocol. The preparation and measurement stages of the protocol are sketched in Fig. 2.10.

Similarly to the magnetic field implementation, the energy level splitting specified by Eq. (2.125) can be realised by using a sculptured laser beam profile. As sketched in Fig. 2.9, to replicate Eq. (2.125) as closely as possible we suggest using a laser beam with a flat central region corresponding to $x > x_f$. Outside of the laser beam corresponds to the region $x < x_i$ and there is a constant initial splitting to the energy levels corresponding to the initial Hamiltonian H_S^i. The flat central region of the beam corresponds to the region $x > x_f$. Here the laser induces a constant AC Stark shift realising H_S^f. The tail of the laser beam corresponds to the region $x_i < x < x_f$ in which the Hamiltonian evolves from H_S^i to H_S^f. Fig. 2.9 sketches this arrangement for a smoothed top hat potential beam profile; however, there are no constraints on the interaction in the region x_i and x_f and therefore the tails of the beam need not be smoothed.

The AC Stark shift in general changes the average energy of the system as well as the splitting between the energy levels. This change in average energy and the non-linear change in gradient in the interaction region between x_i and x_f (sketched in Fig. 2.9) requires a minor change to V_{SB} as specified in Eq. (2.125). However, the underlying thermal physics probed with the adjusted Hamiltonian remains unchanged.

While the Zeeman shift implementation is perfectly autonomous, strictly speaking the Stark shift implementation involves an exchange of energy between the ion and the light field. Thus

this realisation is not *strictly* entirely autonomous. However, for large, experimentally realisable, detunings this energy exchange can be made negligible and in such regimes the ion's dynamics are nonetheless effectively autonomous for all practical purposes.

2.7.1 Experimental parameters

In this section we present a set of experimentally realisable parameters for the Stark shift implementation that satisfy the requirements listed in the previous section.

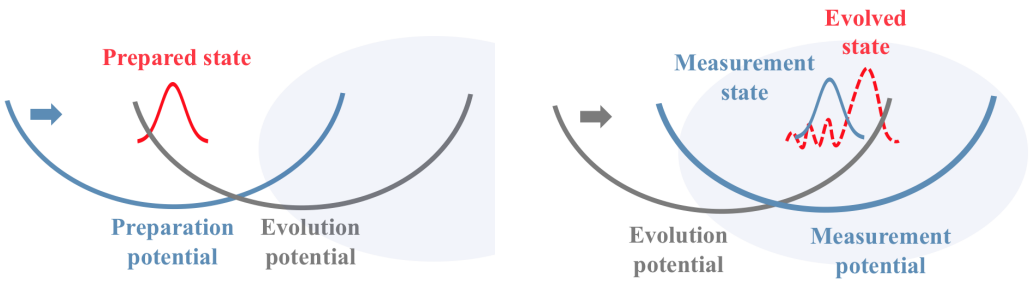
We propose using a single $^{171}Yb^{+}$ ion trapped in a linear Paul trap with an axial trapping frequency of 0.3 MHz [125]. As discussed above, a frequency of the order of MHz is compatible with typical heat rates of linear Paul traps. The magnetic component of the laser will generate a small radial force on the ion [126] and therefore the radial trapping strength needs to be large enough counter act this. Radial trapping forces of the order of GHz can be readily applied and this should be more than adequate.

To probe the lower temperature regime for the case of an axial trap frequency of the order of 0.3MHz, the temperature of the setup must also be of the order of MHz. Therefore, for the thermal states to be preparable (requirement 2), the initial and final energy level splittings must also be of the order of MHz. We are therefore constrained to using hyperfine levels. For concreteness, we suggest using the F = 1, $M_F = 1$ and $M_F = -1$ levels of the $^2S_{1/2}$ ground state. In the absence of a magnetic field these energy levels are degenerate. To lift this degeneracy a magnetic field may be applied and the splitting E_i can then be chosen at will within an approximate range from 0.5 MHz to 10 MHz.

To ensure that the change to the energy levels of the system are large enough for the system to be genuinely driven from equilibrium (requirement 3), the AC Stark shift induced by the laser beam should be of the order of MHz. To induce these shifts we suggest using a laser field with an intensity of 4.5 Wmm^{-2} that is red detuned from the 369nm $^2S_{1/2}$ - $^2P_{1/2}$ transition by 0.1×10^{14}Hz. This is expected to induce an AC Stark shift on the $M_F = 1$ and $M_F = -1$ states of -0.2 MHz and -1.2 MHz respectively [127, 128].

The parameters of the beam profile are set by the requirement for it to be possible to prepare the system comfortably in the region $x > x_f$ (requirement 5) and the fact that, as discussed previously, the smaller the displacement of the prepared and measured the more quantum regimes can be probed. The position variance of a coherent state of $^{171}Yb^{+}$ for an axial frequency of 0.3 MHz is 0.01 μm [109]. Therefore, to prepare the system comfortably in the region $x > x_f$, the flat region of the laser beam profile must be at least 0.05 μm. The minimum distance the ion must travel to realise the change in Hamiltonian H_S^i to H_S^f is $x_f - x_i$ and therefore this sets the minimum possible displacement of the initial and final states. Our simulations indicate that the $k_B T \approx 25\,\hbar\omega$ regime can be probed with $x_f - x_i = 1\mu$m. A beam with a tail on the order of $0.1\mu m$, would allow lower temperature regimes to be probed; however, beam shaping on the sub-μm scale becomes increasingly challenging. There is thus a trade off between the spatial scale on which the beam can be engineered and the temperature regime that can be probed.

There is some flexibility in how accurately the beam profile needs to be shaped. Numerical simulations indicate that the accuracy with which the FQC holds, as quantified by $1 - R$, scales linearly with an undesired gradient across the ideally flat region of the beam. The exact constant of proportionality of this linear scaling depends on the magnitude of the Stark shift, the temperature as well as the displacement of the battery. The gradient broadly scales as $1 - R \approx \frac{\delta I}{I}$ where δI



(a) (b)

Figure 2.10: **Preparation and measurement techniques**. Here we sketch, for the forwards protocol, the preparation (a) and measurement (b) stages of the coherent state trapped ion implementation. (a) To prepare the ion in a coherent state the ion is first cooled to the motional ground state with respect to an initial harmonic trapping potential, shown here in blue. The center of the trapping potential is then shifted non-adiabatically. The new trapping potential after the shift is shown in grey. The ion will remain in the ground state with respect to the old potential but will be in a coherent state with respect to the new trapping potential. (b) The measurement to find the overlap between some test coherent state (the blue Gaussian) and the evolved state of the ion (the dashed red wavepacket) effectively runs the preparation process in reverse. First, the trap potential is shifted such that were the evolved state equal to the test state then after the shift the evolved state would be in the ground state with respect to the new trapping potential. The old potential from the evolution process is shown in grey and the new shifted potential is shown in blue. Secondly, a projective measurement is made to find the overlap between the evolved state and the ground state of the new trapping potential. The laser beam that induces the AC Stark shift is indicated in both figures by the blue oval.

is the change in laser intensity over a distance of $0.1\,\mu$m and I is the maximum laser intensity in that region. The sensitivity of the accuracy of the FQC to an intensity gradient in the ideally flat region is higher for lower temperatures, larger Stark shifts and battery states that are prepared close to the interaction region.

2.7.2 Experimental techniques

To test the coherent, squeezed and cat state FQCs in this trapped ion setting we need to be able to prepare the internal energy levels in a two level thermal state, prepare the phonon modes in coherent, squeezed and cat states and perform measurements to find the overlap between the evolved ion state and a coherent, squeezed or cat state. These procedures are realisable using the following experimental techniques.

Preparation of two-level system. A thermal state of the internal energy levels can be simulated by pre-processing the prepared states [129]. Specifically, by preparing an ion in the ground state N_g times and preparing the ion in an excited state N_e times where the ratio N_e/N_g is a Boltzmann factor, $N_e/N_g = \exp(-2E_i/k_BT)$, an ensemble of $N = N_g + N_e$ ions in a thermal state can be simulated. Laser control techniques for preparing an ion in the ground state or excited state are well established. Using this method to model the thermal state makes it straightforward to simulate any temperature state.

Preparation of oscillator states. To generate coherent, squeezed and cat states the ion must first be cooled to the motional ground state using sideband cooling [130]. As sketched in Fig. 2.10, the ion can be effectively displaced into a coherent state by shifting the trap centre non-adiabatically. After the trap has been shifted, the ion remains in the ground state with respect to the old potential but will be in a coherent state with respect to the new trapping potential [109].

A squeezed displaced state can similarly be prepared from the motional ground state by rapidly changing the frequency of trap such that the state remains in the ground state with respect to the old potential but is in a squeezed vacuum state with respect to the new potential [109]. A squeezed *displaced* state is then generated using an additional non-adiabatic shift of the trap centre as used for coherent state preparation.

Cat states can be generated using laser pulses that entangle the internal energy levels and the motional states of the ion [109]. The current record for the largest cat state, i.e. largest displacement between the pair of superposed coherent states, is 259nm [131]. The experimentalists who achieved this argue their apparatus could be used to generate states separate μm. Thus we are rapidly reaching the stage at which the cat state Crooks equality could be tested in the regime of cats straddling the interaction region as in Fig. 2.7(a).

Measurement of oscillator states. To measure the overlap between the evolved state of the phonon modes, $|\psi_{\text{final}}\rangle$, and some test state, $|\psi_{\text{test}}\rangle$, we can use the fact that the overlap takes the form

$$\langle\psi_{\text{test}}|\psi_{\text{final}}\rangle = \langle 0|\, U_B^{\text{test}\dagger}\, |\psi_{\text{final}}\rangle \tag{2.126}$$

where U_B^{test} is the unitary to generate the state $|\psi_{\text{test}}\rangle$ from the motional ground state. Thus, to test whether the evolved state is in $|\psi_{\text{test}}\rangle$ we can simply apply the inverse of the relevant preparation procedure, $U_B^{\text{test}\dagger}$, to the evolved state, and then measure to see whether the battery is in the ground state. For example, to determine the overlap of the evolved state with some coherent state $|\alpha_{\text{test}}\rangle$, the inverse preparation unitary is a displacement by $-\alpha_{\text{test}}$, i.e. $U_B^{\text{test}\dagger} = D(\alpha_{\text{test}})^\dagger = D(-\alpha_{\text{test}})$ (this is sketched in Fig. 2.10).

A 'filtering' protocol for testing whether an ion is in a certain vibrational Fock state, $|m_{\text{test}}\rangle$, was introduced in [71], an and can be used to determine whether the ion is in the ground state by picking $m_{\text{test}} = 0$. The protocol uses the dependence of the Rabi frequency of the red and blue sidebands on phonon number, to determine a pulse sequence that excites the ion deterministically to the excited internal state if the initial phonon state is $|0\rangle$. For initial states other than $|0\rangle$, the ion evolves into a superposition of the excited and ground electronic states. The internal state of the ion is then measured using the electron shelving techniques. If the ion was initially in $|0\rangle$ no fluorescence is observed. However, if the ion was not initially in $|0\rangle$, there is a finite probability of observing fluorescence. The probability to observe florescence if the ion was not in $|0\rangle$, which can be made arbitrarily close to one by repeating the protocol, sets the measurement fidelity

2.7.3 Experimental outlook

The tapered beam experimental proposal detailed above is limited by the spatial scale on which it is possible to engineer a beam shape. As discussed in the previous section, the shorter the spatial scale of the experiment, the lower the temperature regime can practically be probed, and the larger the χ induced quantum corrections can be detected. In this section, we sketch a couple of alternative proposals, utilising difference choices in the energy level splittings $E(x)$, which could

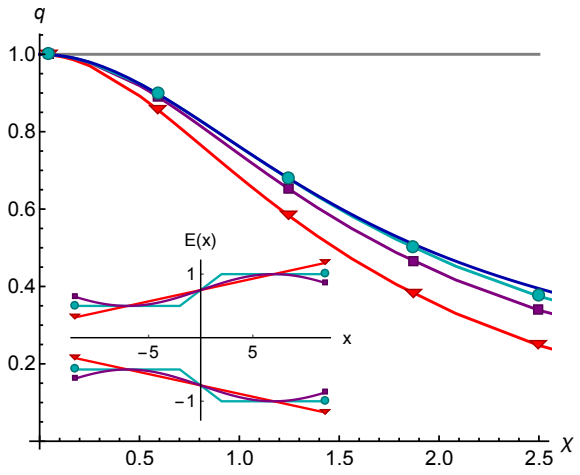


Figure 2.11: **Alternative position dependent potentials**. We plot the predicted quantum deviation q deduced from the transition probabilities between coherent states, using Eq.(2.127), for different choices of $E(x)$ which we plot in the inset. The turquoise circles indicate q for the usual 'flat ends' potential, the purple squares q for a $\sin(x)^2$ potential, and the red triangles q for a purely linear potential. The predicted analytical form of $q = \frac{\tanh(\chi)}{\chi}$ (also sketched in Fig. 2.6) is plotted in blue and the classical limit in which $q = 1$ is plotted in grey. In this simulation we have chosen the following physically plausible parameters, $x_i = -2$, $x_f = 2$, $E_i = 1$MHz, $E_f = 2$MHz, $\alpha_i = -5$ and $\alpha_f = 4$. The displacement parameters $\alpha_{i,f}$ and the positions, x_i and x_f, are given in units of dimensionless position.

be used to test the FQC on shorter spatial scales thus enabling larger quantum deviations to be explored.

In Eq. (2.125) we took $E(x)$ to be constant in the regions in which the system and battery are prepared and measured to ensure that the initial and final Hamiltonians are well-defined. This maintains a closer resemblance to the classical Crooks equality setup and ensures the FQC holds to a high degree of approximation. However, if instead of directly aiming to verify the FQC, we instead focus on the less demanding task of detecting the quantum deviation predicted by the FQC, then there is more flexibility regarding the form of $E(x)$.

The difference between the FQC and the classical Crooks equality is captured by the quantum prefactor q. The prefactor q can always be inferred from the transition probabilities by rearranging Eq. (2.73), that is

$$q = \frac{k_B T}{W_q} \ln\left(\frac{\mathcal{P}(\phi_f|\phi_i,\gamma_i)}{\mathcal{P}(\psi_i|\psi_f,\gamma_f)} \exp\left(\frac{\Delta F}{k_B T}\right)\right) . \tag{2.127}$$

However, in regimes in which the FQC does not hold exactly, this expression will deviate slightly from the analytical expression for q, that is deviate from $\Delta\tilde{E}/W_q$.

The key prediction of the FQC is that for quantum systems outside of the classical limit of high temperatures, q will deviate from the classical value of 1. We suggest that even though the FQC may not hold to a high degree of accuracy when the system's initial and final Hamiltonians are not well defined, as is the case for energy level splittings which vary in the the regions in which the system and battery is prepared and measured, it might nonetheless be possible to detect deviations of q from 1 in these regions.

To investigate the viability of this hypothesis we numerically simulated the evolution of a coherent state for different choices of $E(x)$ and used the resultant transition probabilities to infer

q as per Eq. (2.127). In Fig. 2.11 we compare $q(\chi)$ for three possible choices in the splittings which are sketched in the inset.

Firstly, as a point of comparison we consider again the usual 'flat ends' splitting, Eq. (2.125). We find that in this case the functional form for $q(\chi)$ as found from the transition probabilities (shown in turquoise) closely replicates the analytic form (dark blue). This is to be expected since we have already shown in Fig. 2.8 that the FQC holds accurately for this splitting.

Secondly, we consider a sinosoidal splitting. The change in effective Hamiltonian from $E_i\sigma_S^z$ to $E_f\sigma_S^z$ can be approximately replicated by using a $\sin(x)^2$ function and choosing α_i and α_f to sit in the troughs and peaks of the potential where the effective Hamiltonian is approximately constant. As shown in purple, for this sinosoidal splitting the form of $q(\chi)$ replicates the analytic expression reasonably closely.

Finally, we get rid of the flat ends completely and consider a change in effective Hamiltonian which is implement using a solely linearly increasing splitting. In this case, as shown in red, we find that while $q(\chi)$ deviates more substantially from the predicted analytic form, it is still of broadly the same functional form.

These results suggest that it would be possible to detect quantum deviations from the classical Crooks equality using sinusoidal potentials, linear potentials and perhaps other potentials that we are yet to conceive of and investigate. This flexibility in the energy level splitting of the system opens up many possible realisations to probe the FQC. The sinosoidal splitting could be realised using the AC Stark shift induced by a standing wave generated by two counter propagating lasers [132, 133]. The linearly increasing splitting could be implemented via a linearly increasing Zeeman shift induced by a magnetic field strength $B(x) \propto x$ [134–136]. Crucially, standing waves and linear magnetic field gradients can be realised on the scale of $10^{-2}\mu m$ [132, 136]. The small spatial scales of these alternative approaches would thus enable deeper quantum regimes to be explored.

2.8 Conclusions

Have we achieved our aim of making information theoretic approaches to quantum thermodynamics slightly more physical? An honest answer would be both yes and no.

On the one hand we have made the FQC more concrete by deriving the coherent, squeezed and cat state Crooks equalities which enable us to discuss quantum corrections to the classical Crooks equality. The compact form we found for the coherent state Crooks equality, Eq. (2.95), with its dependence on an effective temperature that incorporates both vacuum fluctuations and thermal fluctuations, is especially satisfying. It would be interesting to investigate whether the squeezed state Crooks equality, or even the cat state equality, can similarly be written in a more compact form by introducing appropriate effective temperatures and thermal wavelengths.

Additionally, the introduction of the quantum prefactor q allows the consequences of quantum coherence for irreversibility to be read off the FQC. In the low temperature deep quantum regime we found that whether the battery is prepared in a coherent, squeezed or cat state, the probability for the reverse process is greater than expected classically and correspondingly irreversibility is softened. Conversely in the intermediary regime, for squeezed state and cat state batteries there are regimes in which irreversibility is apparently strengthened.

The second sense in which we have made the FQC more physical is that we have constructed a realisation which obeys the assumptions that go into deriving the FQC and used this to develop an

experimental proposal to test the relation. Moreover, our proposal can be seen to provide a means to experimentally investigate resource theories for quantum thermodynamics. Since the system starts in a thermal state and energy is globally conserved, the operation on the battery is a thermal operation for a system with a changing Hamiltonian [93]. Consequently, the proposed experiment implements a thermal operation and more broadly verifies a result that sits naturally within the thermal operations framework. This is significant since for the large part these frameworks [11, 12, 26] have, with the exception of a few recent developments [137, 138], been considered abstract and unamendable to experimental realisations.

On the other hand, we freely admit that the implementation we propose, whereby the change of Hamiltonian is implemented by the physical movement of a system between different locations of physical space to enact a change in Hamiltonian, is rather niche. While it is interesting to note that a number of other groups have utilised similar approaches [133, 139, 140] when constructing experimental implementations to explore thermodynamics on the quantum scale, this "change in Hamiltonian over space" implementation is certainly pretty different to classical implementations, such as the stretched RNA molecule experiment [67, 68] described in Section 2.2.2, as well as previous quantum experimental implementations [71–74].

Proponents of information theoretic and resource theoretic approaches to quantum thermodynamics claim that the set of assumptions which they use are natural and can capture the usual setting quantified by fluctuation relations. It is indeed true that all Hamiltonians are time independent once the control mechanism is incorporated and energy is globally conserved as long as the setting includes all energy supplies and sinks. However, if the FQC really is so natural and widely applicable then it ought to be able to capture more typical driving processes and not only the proposal involving a change in Hamiltonian over space that we have developed.

To convincingly demonstrate that the resource theoretic approach really is applicable to the usual setting quantified by fluctuation relations one could perhaps take a series of experimental proposals to test classical fluctuation relation, as well as previous more conventional quantum fluctuation relations, and show that with minor modifications that these settings can be used to test the FQC. Such work would truly make the resource theoretic approach more concrete. However, although we have tried to do this, we have had little luck. One can easily imagine variants of the experiment being done which again utilise a change in Hamiltonian implemented over physical space. However, it is substantially harder to think of experimental implementations closer to the spirit of previous fluctuation relations which implicitly utilise classical control systems to realise more conventional looking time dependent Hamiltonians.

Thus, there is a disconnect. This setting ought to be able to capture more typical looking fluctuation relation experiments, taking the fields proponents at face value and glancing over the set of assumptions. Yet at the same time, actually trying to construct a physical scenario obeying these assumptions it is frustratingly hard. This prompts the question, are we simply lacking imagination here or is there a more fundamental problem?

The sticking point is realising the change in Hamiltonian *while* ensuring energy is conserved. Realising an energy conserving operation for a fixed Hamiltonian between a pair of microscopic systems is straightforward using an unitary operation which exchanges energy between a pair of systems. Similarly, implementing a change in Hamiltonian on a microscopic system could be done using a range of electronic or laser protocols. However, ensuring the energy required to do so is provided or absorbed by quantum battery or work store, that is a controllable quantum system, is considerably harder. Ultimately it all boils down to the fact that real experimental setups are

messily complex and thus hard to split into well defined system, bath, control and work store subsystems.

Faced with these challenges, one might alternatively argue that seeking to experimentally ground the inclusive approach is unnecessary and rather its results should be seen as setting out an idealised theoretical framework to understand thermodynamics in the quantum regime. That is the FQC would be viewed as establishing the structural relations between work fluctuations and coherence, independently of its implementability. An analogy here would be the Carnot cycle which provides the upper limit on the efficiency of any classical thermodynamic engine. The Carnot cycle is a theoretic construct, rather than a physically realisable thermodynamic process, and the same could perhaps be argued of the setting here in the general case.

Thus the nature of the relationship of inclusive fluctuation relations, and the resource theoretic approach to quantum thermodynamics more generally, to physical realisations remains an open question. We hope that others might succeed, where we have failed, at showing that the framework is widely physically implementable. However, even if this does not come to fruition, the approach might still be understood as establishing the underlying structure of thermodynamics in the quantum regime.

In this chapter we investigated the role of coherence for work fluctuations by studying physical realisations of quantum fluctuation relations. In the next chapter we switch our attention from coherence to the study of quantum signatures of distinguishability. While we no longer explicitly focus on fluctuation relations, we still are interested in the work and work fluctuations produced by thermodynamic phenomena, this time from the mixing of quantum gases. We continue the theme of physical realisations of quantum thermodynamics but now use an optomechanical setup as a platform to explore these topics.

Chapter 3

An optomechanical piston setup to probe thermodynamic signatures of distinguishability

3.1 Introduction

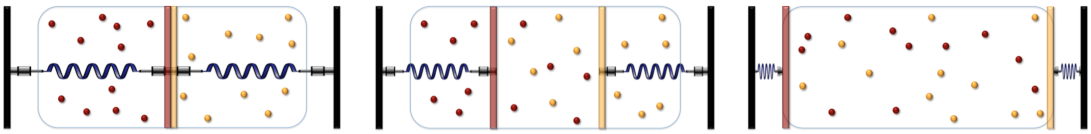
As Hermann Weyl remarked in 1950, one cannot 'even in principle... demand an alibi from an electron' [141]. That the elementary physical particles of the universe, Fermions and Bosons, are fundamentally entirely indiscernible, in the sense that their states are symmetric up to a global phase under a permutation of particle indices, is one of the remarkable ontological lessons from quantum mechanics and one that has profound consequences throughout modern physics.

While quantum mechanics elevated particle indistinguishably to the status of a fundamental principle; the concept predates its development. Indeed it was Planck's attempts to reconcile Wien's Law and the Rayleigh-Jeans limit of black body radiation, utilising the indistinguishability of energy quanta, which eventually lead to the birth of quantum mechanics. Arguably the first time the importance of the concept was appreciated, at least in modern physics, was in the 19th century when Gibbs realised that the particles that make up a gas must be indistinguishable in order for entropy to be an extensive function [142].

With the recent explosion of research into thermodynamics in the quantum regime, the role of particle indistinguishability in thermodynamics has been partially reconsidered. The dependence of the Szilard engine on quantum particle statistics has been explored in several works with [143] finding that in general the work that can be extracted from information is independent of whether the working substance is Bosonic or Fermionic and [144] arguing that in certain circumstances Bosonic bunching can enhance the conversion of information and work.

In this chapter we argue that optomechanical setups, involving an optical cavity in which a microscopic membrane is inserted, provide a suitable platform to explore thermodynamic signatures of distinguishability in the quantum regime. Here we primarily present these proposals as thought experiments but hopefully, in the not so distant future, they might be realised as experiments.

This chapter is structured chronologically in the sense that it follows our original line of thought when conducting this research. We start in Section 3.2 by recapping classical Gibbs mixing and the Gibbs paradox. We then in Section 3.3 review quantum generalisations of Gibbs mixing from



(a) Initial state. (b) Mixing Process. (c) Final state.

Figure 3.1: **Gibbs mixing.** (a) Two types of gas, a 'red' gas and a 'yellow' gas, are initially confined to two halves of a box of volume $2V$. To draw work from the mixing of the two gases, a pair of semi permeable membranes is inserted, with red (yellow) particles passing through the red (yellow) membrane while being confined by the yellow (red) membrane. (b) The membranes are held in place with two springs, allowing them to move. Since each membrane confines one gas, which exerts a pressure on it, the gases compress the springs, performing work and mixing in the volume between the springs. (c) Eventually the membranes are pushed to the far edges of the vessel and the two gases are fully mixed. The expansion of each of the two ideal gases from V to $2V$, while in thermal contact with a heat bath at temperature T, can be used to draw work.

which we identify a number of unanswered questions and highlight the lack of research into how one might physically implement the theoretical processes being discussed. In Section 3.4 we introduce an optomechanical implementation of quantum mixing and in Section 3.5 we analyse the dynamics of this setup [145]. In Section 3.7 we abstract further away from the quantum Gibbs mixing scenario to probe more general quantum thermodynamic signatures of distinguishability [146] by drawing links with the Hong-Ou-Mandel effect [147] which we discuss in Section 3.8. Finally, in Section 3.9 we discuss how our proposals could be experimentally implemented. Section 3.10 contains our conclusions and a discussion of answered questions.

3.2 Classical Gibbs mixing

The first time the importance of the concept of distinguishability was appreciated in modern physics was when Gibbs considered the thermodynamic consequences of mixing gases. Gibbs realised that mixing two gases of different types, that is different isotopes or elementary or molecular compositions, can be used to extract work, while no work can be extracted mixing gases of the same type [142].

A protocol for extracting this work is sketched in Fig. 3.1. Initially, there are N particles of an ideal gas of type 1 and N particles of another non-interacting ideal gas of type 2, confined in two volumes V separated by a pair of membranes. One of these membranes is permeable to type 1 particles while impermeable to type 2 particles, and vice versa for the second membrane. Both gases are in thermal equilibrium at temperature T and each gas exerts a force on its confining membrane, while exerting no force on the other membrane. By allowing the membranes to move under the force of the gases, the two gases can isothermally expand resulting in them mixing in the space between the membranes as shown in Fig. 3.1. At the end of the protocol the two gases occupy the full volume $2V$ and are fully mixed.

By standard thermodynamics, the work done by an ideal gas isothermally expanding from volume V to $2V$ at temperature T is found by integrating the pressure p exerted on the membrane with respect to the change in volume and then rewriting the pressure in terms of temperature using



(a) Initial state. (b) Final state.

Figure 3.2: **Gibbs mixing generalisation to gases containing uneven particle numbers.** (a) Two types of gas, a 'red' gas containing $2Nx$ particles and a 'yellow' gas containing $2N(1-x)$ particles, are initially confined to volumes $2Vx$ and $2V(1-x)$ respectively. The two gases are at the same temperature and pressure. To draw work from the mixing of the two gases, a pair of semi permeable membranes is inserted, with red (yellow) particles passing through the red (yellow) membrane while being confined by the yellow (red) membrane. (c) Eventually the membranes are pushed to the far edges of the vessel and the two gases are fully mixed. The expansion of each gas while in thermal contact with a heat bath at temperature T, can be used to draw work.

the ideal gas equation, that is

$$W = \int_V^{2V} p\, dV = \int_V^{2V} \frac{Nk_BT}{V}\, dV = Nk_BT \ln 2\,. \tag{3.1}$$

Thus the maximal work that can be extracted by mixing the *two* distinguishable gases is

$$W_{\text{dist}} = 2Nk_BT \ln 2\,. \tag{3.2}$$

The protocol to extract work from mixing that is sketched in Fig. 3.1 is fully reversible and therefore the work *cost* of *separating* a pair of perfectly distinguishable gases containing equal numbers of particles is also given by $2Nk_BT \ln 2$.

This protocol is only possible if two suitable semi-permeable membranes can be found. Clearly, if the gases are in fact identical then no such membranes are available. Thus no work can be drawn from the 'mixing' of two identical gases,

$$W_{\text{indist}} = 0\,. \tag{3.3}$$

Indeed, were it possible to extract work by 'mixing' identical gases then, since it is also possible to redivide the identical gases by simply reinserting the barrier, this would allow an unlimited amount of heat to be extracted from a single heat bath and converted into work thereby violating the Second Law of Thermodynamics.

If we consider only homogeneous gases, that is gases consisting of only particles of the same type, and assume, at least in principle, the existence of semi-permeable membranes that can perfectly differentiate any two distinguishable particle types, then as the degree of similarity between a pair of gases is varied, the work that can be drawn jumps discontinuously from 0 for two indistinguishable gases to $2Nk_BT \ln 2$ for two distinguishable gases.

The protocol discussed above can be generalised to calculate the work that can be extracted from mixing two gases which contain unequal numbers of particles. Let us consider the mixing of two types of gases, both at temperature T, where type 1 contains $2Nx$ particles and type 2 contains $2N(1-x)$ particles. If work is to be extracted from the mixing process *alone*, the two gases must initially be in thermal equilibrium and therefore the two gases must be of the same temperature and pressure. Consequently, if we suppose as before that the total volume occupied by the two

gases is $2V$, then the type 1 gas must occupy volume $2Vx$ and type 2 the volume $2V(1-x)$, as sketched in Fig. 3.2. The work extraction protocol utilising the pair of semipermeable membranes sketched in Fig. 3.1 can then be rerun as before. Gas 1 isothermally expands from volume $2Vx$ to $2V$ and Gas 2 expands from $2V(1-x)$ to $2V$ with the gases mixing in the process. The total work that can be extracted as a result of these expansions is given by

$$W = 2Nxk_BT\ln\left(\frac{1}{x}\right) + 2N(1-x)k_BT\ln\left(\frac{1}{1-x}\right) , \tag{3.4}$$

which is equivalent to

$$W = 2Nk_BTS_B(x) , \tag{3.5}$$

where the binary Shannon entropy is defined as

$$S_B(x) = -x\ln(x) - (1-x)\ln(1-x) . \tag{3.6}$$

As before, this protocol can be run in reverse and therefore Eq. (3.5) is also the work cost of separating two distinguishable gases containing an unequal number of particles.

The mixing of distinguishable and indistinguishable gases is the foundations of the famous Gibbs' paradox. There are two formulations of this paradox; a purely thermodynamical one and a statistical mechanical one. The statistical mechanical formulation is a disagreement between Boltzmann entropy and the thermodynamic entropy when two identical gases mix. While this component to the paradox is genuinely paradoxical, and a number of different solutions have been proposed [148–150], we will not discuss it here.

The thermodynamic formulation, which is more of a tension than a paradox, leads nicely onto the quantum generalisation of the Gibbs mixing that we will consider. It has been argued [151,152] that the discontinuous jump in the extractable work is at odds with the fact that the similarity of any two gases may be varied continuously. There is a growing consensus [148–150] that this tension is not especially mysterious in that it is distinguishability of two gases rather than their similarity that matters. While similarity may vary continuously, the question of whether or not we can distinguish a pair of gases is an operational question which classically has a 'yes' or 'no' answer. Fundamentally, any two classical gases can either be distinguished or they can not and any difficulty doing so is an epistemic limitation due to lack of knowledge on the part of the experimentalist. It is thus unsurprising that the work that can be extracted from homogeneous gases varies discontinuously: either 'yes' we can distinguish the gases, in which case we can extract the work W_{Dist}, or 'no' we cannot in which case we can extract no work.

However, for quantum systems this does not hold true. Due to the possibility of non-orthogonal quantum states, quantum systems can fundamentally be neither perfectly distinguishable nor perfectly indistinguishable. This idea underlies the quantum generalisation of Gibbs mixing that we consider.

3.3 Quantum Gibbs mixing

Before we proceed to set out the quantum version of Gibbs mixing, for clarity let us briefly draw a distinction between two different types of distinguishability that can be considered in the quantum setting. Two particles are *intrinsically identical* if they share exactly the same intrinsic properties, that is the same mass, electric charge, spin and so forth. Any two intrinsically identical quantum particles are subject to the symmetrisation postulate which states that their combined state must

either be symmetric (in which case the particles are known as Bosons) or antisymmetric (known as Fermions) with respect to a permutation of particle labels. The concept of intrinsic identity, like classical distinguishability, is binary. Either two particles are intrinsically identical or they are not.

While the majority of fundamental quantum particles (electrons, protons, photons, hydrogen atoms, quarks, etc.) are identical in this sense, in many instances it is nonetheless possible to distinguish them via their internal states [153]. As pointed out in [151], this occurs in nuclear physics, where the neutron and proton are considered as identical particles (nucleons) but are distinguished by their isotropic spin states. When two intrinsically identical particles can be perfectly distinguished by their internal state, then their internal state may be used to label the particles, in which case the symmetrisation postulate ceases to apply.

In contrast to intrinsic identity and classical distinguishability, this *operational distinguishability* admits degrees because quantum mechanics allows for superposition states and therefore the overlap between any pair of quantum states may vary continuously. It follows that, a pair of quantum particles may be fundamentally neither perfectly distinguishable nor perfectly indistinguishable, despite the best efforts of an omniscient experimentalist, in virtue of occupying non-orthogonal quantum states. Thus, in contrast to the classical mixing scenario considered by Gibbs, in the quantum regime we can consider the effect of mixing partially distinguishable quantum gases.

The significance of partially distinguishable quantum gases for Gibbs mixing was explored by early researchers in quantum mechanics [152, 154–158], who argued that the work which can be drawn from mixing two quantum gases increases *continuously* with the distinguishability of the two gases' internal states. More specifically, suppose that we are given a box of volume $2V$ that is in thermal contact with a heat bath at temperature T. The box is split in half by a barrier with one half containing N particles of an ideal gas in state ρ_1 and the other N particles of an ideal gas in state ρ_2. After mixing the two gases there will be $2N$ particles in the mixed state

$$\rho_{\text{mix}} := \frac{1}{2}\left(\rho_1 + \rho_2\right) \ . \tag{3.7}$$

From the second law of thermodynamics, the change in von Neumann entropy provides an upper bound on the work that can be extracted from the quantum gases in the thermodynamic limit of large numbers of particles[1]. Therefore the maximum amount of work that can be extracted is given by

$$W_{\text{VN}} = k_B T \left(2N S_{\text{VN}}(\rho_{\text{mix}}) - N S_{\text{VN}}(\rho_1) - N S_{\text{VN}}(\rho_2)\right) \tag{3.8}$$

where $S_{\text{VN}}(\rho) = -\operatorname{Tr}[\rho \ln(\rho)]$ is the von Neumann entropy of the state ρ. The work cost of separating a gas containing $2N$ particles in the state ρ_{mix} into two equally sized gases in states ρ_1 and ρ_2 is also given by Eq. (3.8). If, in analogy with the classical case, we limit ourselves to considering homogeneous gases and suppose ρ_1 and ρ_2 are the pure states $|\psi_1\rangle$ and $|\psi_2\rangle$ respectively, then $S_{\text{VN}}(\rho_1)$ and $S_{\text{VN}}(\rho_2)$ vanish and the extracted work reduces to

$$W_{\text{VN}} = 2N k_B T S_{\text{VN}}(\rho_{\text{mix}}) = 2N k_B T S_B\left(\frac{1 - |\langle\psi_1|\psi_2\rangle|}{2}\right) \tag{3.9}$$

where S_B is the binary Shannon entropy defined in Eq. (3.6). For perfectly indistinguishable gases where the overlap between the gas particles internal states $\langle\psi_1|\psi_2\rangle$ equals 1, this expression

[1]This statement effectively assumes that the change in von Neumann entropy of a system is equivalent to the change in thermodynamic entropy. This was simply assumed by early practitioners, and has been questioned by some [151], in recent years more rigorous arguments for this equivalence, at least in the thermodynamic limit of large numbers of particles, have been established from a resource theoretic perspective [20].

reduces to 0 and so no work can be extracted in agreement with the classical case. Similarly, for perfectly distinguishable gases, with orthogonal internal states, we regain the classical value of $2Nk_BT\ln(2)$. However, in contrast to the classical case which only describes these two extremes, Eq. (3.9) increases continuously and monotonically between these two limiting cases.

The 'standard' [2] quantum protocol to extract W_{VN} by mixing partially distinguishable gases, or equivalently separating a mixed gas at work cost W_{VN}, is sketched in Fig. 3.3. For simplicity we consider the case in which ρ_1 and ρ_2 are the pure states $|\uparrow\rangle$ and $|\theta\rangle = \cos(\theta)\,|{\rightarrow}\rangle + \sin(\theta)\,|\uparrow\rangle$, where the states $|{\rightarrow}\rangle$ and $|\uparrow\rangle$ are orthogonal. The structure of the protocol is more intuitive when run 'backwards' to separate the state ρ_{mix} and so let us start by describing it in that direction. Initially a box of volume $2V$ contains $2N$ particles in the state

$$\rho_{\text{mix}} = \left(\frac{1}{2}\,|\uparrow\rangle\langle\uparrow| + \frac{1}{2}\,|\theta\rangle\langle\theta|\right) . \tag{3.10}$$

This state can be written as a mixture of orthogonal states given by its eigen-decomposition

$$\rho_{\text{mix}} = \left(\lambda\,|\psi\rangle\langle\psi| + (1-\lambda)\,|\psi_\perp\rangle\langle\psi_\perp|\right) \quad \text{where} \quad \lambda = \frac{1}{2}\left(1 - \langle\uparrow|\theta\rangle\right) . \tag{3.11}$$

Having established the basis of this eigen-decomposition we obtain a pair of semipermeable membranes that can perfectly distinguish the gas particles in their orthogonal ψ and $\psi_\perp$ basis. As sketched in Fig. 3.3(b), the mixed gas can then be divided into its ψ and $\psi_\perp$ components using this pair of membranes by running the general classical mixing protocol, sketched in Fig. 3.2, in reverse. The work cost of this separation from Eq. (3.5) is

$$W_{\text{cost}} = 2Nk_BTS_B\left(\lambda\right) . \tag{3.12}$$

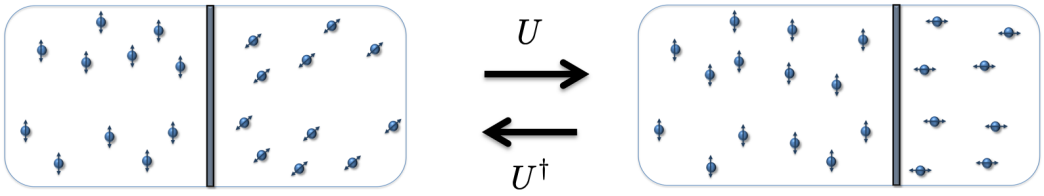
Finally, as sketched in Fig. 3.3(a) the separated state is unitarily rotated back to two equal sized gases in states $|\uparrow\rangle$ and $|\theta\rangle$ respectively. Since this is an isentropic transformation, this step requires no work or heat exchanges. The total work cost of separation is therefore $2Nk_BTS_B\left(\lambda\right)$ in agreement with Eq. (3.9). The protocol is perfectly reversible and therefore can be run in the opposite direction to extract the work $2Nk_BTS_B\left(\lambda\right)$ by mixing a pair of $|\uparrow\rangle$ and $|\theta\rangle$ gases each containing N particles.

The above protocol was turned on its head by Peres [159] who warned it would be foolish invest in a shrewd inventor who claims to have created a pair of semipermeable membranes that can perfectly distinguish partially distinguishable quantum states. His argument, which we sketch in Fig. 3.4, is effectively a generalisation of the observation that if it were it possible to extract work mixing indistinguishable classical gases then this would allow heat from a single heat bath to be perfectly converted into work.

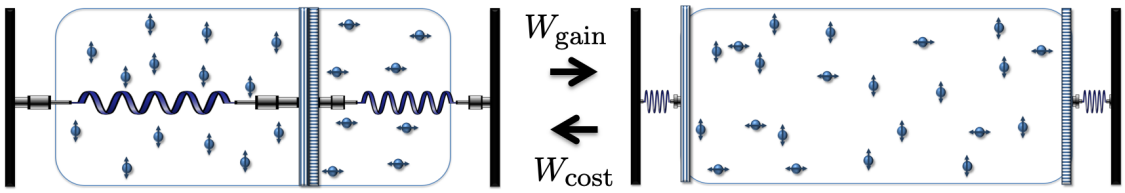
The argument, which we summarise in Fig. 3.4, runs as follows. As above, there are initially N particles of a gas in state $|\uparrow\rangle$ and N particles of a gas in state $|\theta\rangle$ confined in two volumes V separated by a pair of membranes. In order to set up a proof by contradiction, let us suppose that these membranes can perfectly distinguish $|\uparrow\rangle$ and $|\theta\rangle$ particles, with $|\uparrow\rangle$ particles passing through the the first membrane while being confined by the second membrane and vice versa for $|\theta\rangle$ particles. With such hypothetical membranes we can perform classical Gibbs mixing protocol sketched in Fig. 3.1 to extract the work

$$W_{\text{gain}} = 2Nk_BT\ln 2 . \tag{3.13}$$

[2] The term 'standard' is used here generously. This protocol is referenced in [159] and [160] but we have yet to see it elsewhere.



(a) Unitary transformation with no work cost



(b) Mixing or separation using semi-permeable membranes

Figure 3.3: **Quantum Gibbs mixing.** a) Initially (left) there are N particles of an ideal gas in state $|\uparrow\rangle$ and N particles of another non-interacting ideal gas in state $|\theta\rangle$, confined in two volumes V separated by a solid barrier. Let λ, $|\psi\rangle$ and $|\psi_\perp\rangle$ denote the eigenvalue and eigenstates of $\frac{1}{2}|\uparrow\rangle\langle\uparrow| + \frac{1}{2}|\theta\rangle\langle\theta|$. The initial state (left) can be unitarily rotated to the state (right) in which there are $2N\lambda$ particles of an ideal gas in state $|\psi\rangle$ occupying volume $2V\lambda$ and $2N(1-\lambda)$ particles of a gas in state $|\psi_\perp\rangle$ occupying volume $2V(1-\lambda)$ separated by a barrier. The inverse unitary transforms this final state (right) back into the initial state (left). Both processes are isentropic and so the transformations require no work or heat exchanges. b) A gas containing $2N$ particles in the state ρ_{mix} can be divided into two gases containing N particles in state the $|\psi\rangle$ and N particles in the state $|\psi_\perp\rangle$ using a pair of semi-permeable membranes that can perfectly distinguish $|\psi\rangle$ and $|\psi_\perp\rangle$ particles. This separation process requires work and the converse mixing process produces work as shown in Fig. 3.2.

After mixing, the gas in the vessel is in the state ρ_{mix}, Eq. (3.10), which can be rewritten in terms of its eigen-decomposition as per Eq. (3.11). To complete the thermodynamic cycle the gas is re-separated into its $|\uparrow\rangle$ and $|\theta\rangle$ components using the protocol for separating partially distinguishable gases in Fig. 3.3. As per Eq. (3.12), this incurs a work cost of

$$W_{\text{cost}} = 2Nk_BTS_B(\lambda) \ . \tag{3.14}$$

The binary entropy $S_B(\lambda)$ is always less than $\ln 2$ as long as $\lambda \neq \frac{1}{2}$, that is as long as the gases are not perfectly distinguishable. Consequently, the difference between the work gain and the work costs in the cycle is always a positive quantity for partially distinguishable gases. Therefore running this cycle repeatedly would allow an unlimited amount of heat to be converted into work using a single heat bath, in violation of the second law. On this basis Peres concludes that membranes which can perfectly distinguish partially distinguishable quantum states cannot exist.

Quantum thermodynamics has progressed substantially over the last decade but interestingly Gibbs mixing and its quantum variants have only been revisited by a handful of authors in the light of recent developments.

In [88] the mixing work for finite sized systems is investigated. The authors take the extractable work to be given by the change in 'ergotropy' [161] during the mixing process, that is the difference between the maximal work that can be extracted using a cyclic process from the initial separated

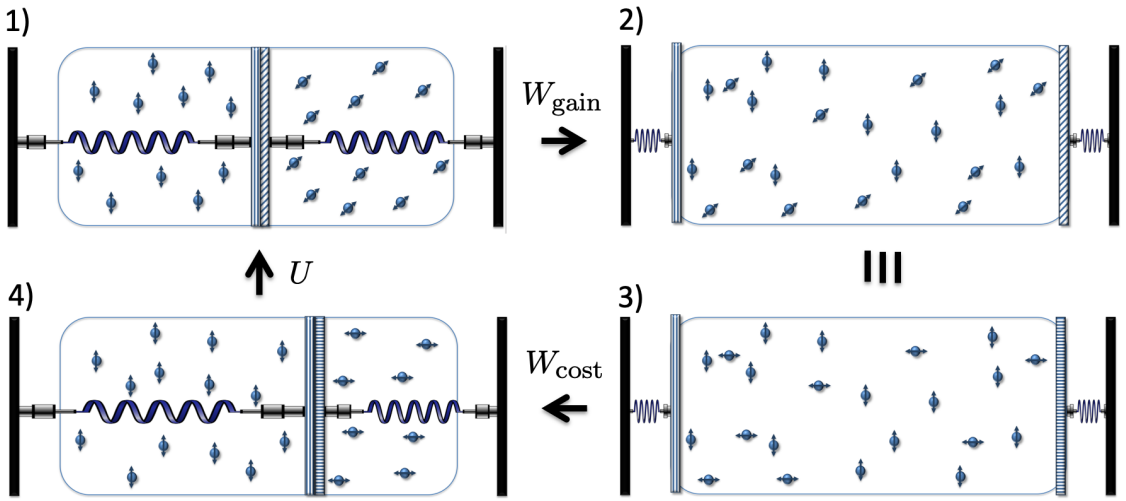


Figure 3.4: **Peres' argument against magic membranes.** 1) Two gases in non-orthognal states $|\uparrow\rangle$ and $|\theta\rangle$ (indicated by the vertical arrows and diagonal arrows) are initially confined to two halves of a box of volume $2V$. To set up a proof by contradiction we suppose have a pair of *fictional* membranes that can perfectly distinguish between these non-orthogonal states, with vertical (diagonal) particles passing through the vertical (diagonal) membrane while being confined by the diagonal (vertical) membrane. 1) to 2) Following the same protocol as in Fig. 3.1 we can extract the work by mixing the gases with these fictional membranes. 2) to 3) The fully mixed state can written as a mixture of orthogonal states given by its eigen-decomposition. Having established the basis of this eigen-decomposition, which we sketch with horizontal and vertical arrows respectively, we switch the original membranes for a pair of physically realisable semipermeable membranes that can perfectly distinguish the the gas particles in this orthogonal basis (again sketched by horizontal and vertical dashes). 3) to 4) Work is done on the gas to divide it into its orthogonal components. 4) to 1) Finally, to complete the cycle the newly separated state is transformed back to the initial state. Since these states have the same entropy this step can be performed using a unitary operation requiring no work or heat exchanges. The net extracted work in the cycle is given by $W_{\text{gain}} - W_{\text{cost}}$.

state and the maximal work that can be extracted using a cyclic process from the final mixed state. The authors show that for pure states, that is homogeneous gases, the extractable work does indeed increase smoothly with distinguishability. However, for mixed states they find that the story is more complex with the work at times even decreasing with distinguishability. The change in ergotropy reduces to the change in von Neumann entropy in the thermodynamic limit of large numbers of particles [161] and thus these results can be seen as quantifying the deviations from W_{vN}, Eq. (3.8), due to finite size effects.

In [160], the authors consider a semi classical protocol to extract work from mixing two partially distinguishable states and use this to relate the work that can be extracted from mixing to the Holevo bound [162, 163]. This semi-classical perspective assumes that the pair of semipermeable membranes measure the quantum gases in an orthogonal basis, thereby collapsing the gases into mixtures of perfectly distinguishable quantum states. It is further assumed that these measurements incur no work costs.

The work that can be extracted from a pair of partially distinguishable quantum gases using

this semi-classical protocol can be calculated as follows. Let us suppose initially there are $p(\psi_1)2N$ particles of a gas in state $|\psi_1\rangle$ and $p(\psi_2)2N$ particles of a gas in state $|\psi_2\rangle$, confined in two volumes $p(\psi_1)2V$ and $p(\psi_2)2V$ separated by a pair of membranes which measure in the orthogonal basis $\{|m_1\rangle, |m_2\rangle\}$. To make a connection with the Holevo bound, let M be the random variable associated with the projective measurement outcomes m_1 and m_2 and P be the random variable of associated with the preparation label ψ_p. That is $\mathcal{P}_M = \{p(m_1), p(m_2)\}$ is the probability distribution that any gas particle in the box collapses onto the state $|m_1\rangle$ or $|m_2\rangle$ on measurement and $\mathcal{P}_P = \{p(\psi_1), p(\psi_2)\}$ is the probability distribution that any gas particle in the box is prepared in that state $|\psi_1\rangle$ or $|\psi_2\rangle$ respectively. The protocol[3], sketched in Fig. 3.5, to extract work mixing the ψ_1 and ψ_2 gases consists of the following three steps.

Firstly, the ψ_1 and ψ_2 gases are each separated into their orthogonal m_1 and m_2 components using the inverse of the classical Gibbs mixing protocol (Fig. 3.2). These separation protocols require the work

$$W_{\text{cost k}} = -2Nk_BT \sum_{i=1,2} p(m_i|\psi_k) \log(p(m_i|\psi_k)) \quad \text{for} \quad k = 1, 2 \tag{3.15}$$

where $p(m_j|\psi_k) = |\langle m_j|\psi_k\rangle|^2$ is the probability that the state ψ_k is collapsed by the semipermeable membrane into state the m_j. The total work cost of the two separations therefore evaluates to

$$W_{\text{cost}} = W_{\text{cost 1}} + W_{\text{cost 2}} = -2Nk_BT \sum_{i=1,2;k=1,2} p(m_i|\psi_k) \log(p(m_i|\psi_k)) = 2Nk_BTH(M|P) \tag{3.16}$$

where $H(M|P)$ is the conditional entropy between the distributions M and P.

Secondly, having separated the ψ_1 and ψ_2 gases individually into m_1 and m_2 components the pairs of vessels containing gases in states m_1 and m_2 are recombined to give one box containing

$$p(m_1)2N = \left(p(m_1|\psi_1)p(\psi_1) + p(m_1|\psi_2)p(\psi_2)\right) 2N \tag{3.17}$$

particles in state $|m_1\rangle$ and another box containing

$$p(m_2)2N = \left(p(m_2|\psi_1)p(\psi_1) + p(m_2|\psi_2)p(\psi_2)\right) 2N \tag{3.18}$$

particles in state $|m_2\rangle$. Since this step involves mixing identical gases it incurs no work cost.

Finally, the two vessels, one containing gas particles in the state m_1 and the other containing gas particles in the state m_2, are mixed using the classical Gibbs mixing protocol (Fig. 3.2). The work gained is given by

$$W^{\text{gain}} = -2Nk_BT \sum_{i=1,2} p(m_i) \log(p(m_i)) = 2Nk_BTS_B(p(m_1)) = 2Nk_BTH(M) \tag{3.19}$$

where $H(M)$ is the Shannon entropy associated with the measurement performed by the semipermeable membranes, that is $H(M) \equiv S_B(p(m_1)) = S_B(p(m_2))$.

The net extractable work from the two stage protocol is given by the difference between the work cost of the first separation stage and the work gained mixing the perfectly distinguishable gases, that is

$$W_{\text{SC}} = W^{\text{gain}} - W^{\text{cost}} = 2Nk_BT \left(H(M) - H(M|P)\right) = 2Nk_BT\, H(M:P)\,, \tag{3.20}$$

[3]Note the protocol and argument presented here differs slightly from that given in [160] because we suspect that the analysis in [160] smuggles in an unwelcome and unaccounted for Maxwell demon.

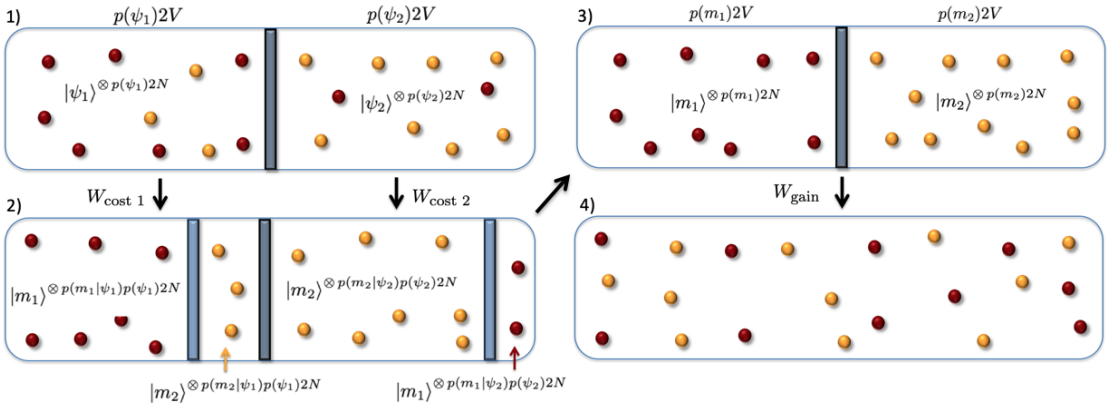


Figure 3.5: **Semi-classical work extraction protocol.** 1) We start with $p(\psi_1)2N$ particles of a gas in state $|\psi_1\rangle$ and $p(\psi_2)2N$ particles of a gas in state $|\psi_2\rangle$, confined in two volumes $p(\psi_1)2V$ and $p(\psi_2)2V$ separated by a pair of membranes which measure in the orthogonal basis $\{|m_1\rangle, |m_2\rangle\}$. 1) to 2) The ψ_1 and ψ_2 gases are each separated into their orthogonal m_1 (red) and m_2 (yellow) components using the inverse of the classical Gibbs mixing protocol (Fig. 3.2) incurring work costs $W_{\text{cost 1}}$ and $W_{\text{cost 2}}$ respectively. 2) to 3) The pairs of vessels containing gases in states m_1 and m_2 are combined at no work cost. 3) to 4) The two vessels, one containing gas particles in the state m_1 and the other containing gas particles in the state m_2, are mixed using the classical Gibbs mixing protocol and allowing work to be extracted.

which is equivalent to the classical mutual information, $H(M:P)$, between the projective measurement performed by the membranes M and the preparation P.

One thing to notice immediately about the above expression for the extractable work using the semi-classical protocol is that the same amount of work can be extracted from mixing two gases in pure states and from mixing their corresponding mixtures. That is, the work that can be extracted from mixing say a gas where all particles are in state $|\uparrow\rangle$ and a gas where all particles are in the state $|\theta\rangle$ is equal to that from mixing a gas with all particles in the state $|\uparrow\rangle$ and a gas containing particles in the mixture $\cos(\theta)^2 |\uparrow\rangle\langle\uparrow| + \sin(\theta)^2 |\rightarrow\rangle\langle\rightarrow|$. This arises from the fact that we are assuming that the membrane measures the state of the gas particles, which kills off coherence and prevents it playing a role in the extractable work. However, if the maximum extractable work is given by the change in von Neumann entropy, W_{VN}, then it should be possible to extract more work from pure states than mixtures. This is also what one would expect intuitively since pure states are zero entropy states and thus are further from thermal equilibrium.

An alternative perspective on the difference between the semi-classical protocol and the 'standard' quantum Gibbs mixing protocol can be gained by reference to the Holevo bound. This is a bound from quantum information theory on the amount of information that can be known about a quantum state, i.e. the mutual information $H(M:P)$ between a measurement and a prepared state. The Holevo bound can be stated as follows. Consider a set of mixed states $\{\rho_1, \rho_2, ..., \rho_n\}$ where any state ρ_P is prepared with probability distribution $\{p_1, p_2, ..., p_n\}$. Then for any POVM measurement M, the amount of information available about the preparation P from obtaining the outcome M of the measurement is bounded by

$$H(M:P) \leq S_{\text{VN}}\left(\sum_i p_i \rho_i\right) - \sum_i p_i S_{\text{VN}}(\rho_i)\ . \tag{3.21}$$

In the context of the mixing protocol the states ρ_1 and ρ_2 are the pure states ψ_1 and ψ_2 and therefore their entropy vanishes and we are left with the bound

$$H(M:P) \leq S_{\text{VN}}(\rho_{\text{mix}}) \quad \text{where} \quad \rho_{\text{mix}} = \frac{1}{2}\left|\psi_1\right\rangle\left\langle\psi_1\right| + \frac{1}{2}\left|\psi_2\right\rangle\left\langle\psi_2\right| \ . \tag{3.22}$$

Thus the work that can be extracted by this semi-classical protocol is upper bounded by the change in von Neumann entropy and we have that

$$W_{\text{SC}} \leq W_{\text{VN}} \ . \tag{3.23}$$

However, crucially, the Holevo bound applies to both projective measurements and non projective measurements and if we limit ourselves to only projective measurements the above bound, Eq. (3.23), is only saturated if $|\psi_1\rangle$ and $|\psi_2\rangle$ are either identical or orthogonal, that is in the classical limit in which the gases are either perfectly distinguishable or indistinguishable. Therefore, the work that can be extracted using the semi-classical work extraction scheme sketched above for partially distinguishable quantum gases is always less than the limit set by the change in von Neumann entropy. This prompts an interesting question: *could more work be extracted from coherence, using a pair of semi-permeable membranes, if the membranes do not perform projective measurements on the gases?*

In summary, there is a reasonably large body of theoretical results on the work that can be extracted by mixing partially distinguishable quantum gases. Using the 'standard' quantum Gibbs mixing protocol, the work that can be extracted from mixing is equal to the change in von Neumann entropy which for mixing pure state gases is equal to the binary entropy $2Nk_BTS_B(\lambda)$. However, this protocol with its unitary rotations of the internal state of individual gas particles seemingly requires challenging levels of external experimental control and somewhat deviates in spirit from the original classical work extraction protocol. In contract, the semi-classical protocol, with its use of semi-permeable membranes is closer to the original classical protocol. The main disadvantage of the semi-classical protocol is that it seemingly does not allow the full amount of work to be extracted from mixing because it does not extract any of the work originating from the coherence of the quantum gases. Moreover, both of these approaches, and the cyclic driving approach [151] that we briefly touched on, consider generic mixing processes without reference to specific physical systems or operations.

Thus we decided to take a different perspective and explore a specific physical realisation of the quantum gases and semi-permeable membranes. In particular, by choosing the membrane to be a *quantum* system, which evolves unitarily and therefore *does not perform projective measurements* on the gases, we hoped to clarify how to utilise coherence when extracting work from mixing. Spoiler alert: we have yet to succeed at this final task and thus how to practically extract work from mixing, utilising coherence, remains an open questions. However despite this, as will become clear, we stumbled upon an alternative phenomena which generates a quantum advantage from Gibbs mixing.

3.4 Optomechanical piston setup

The first step to constructing a physical realisation for quantum Gibbs mixing is to conceive of realistic membranes that can differentiate between different internal states of a quantum system. Such membranes are hard to think up for the internal states of an atom or molecule; however, if

we instead consider photons of different polarisations then a polarising beamsplitter (PBS) does the job [145]. A PBS membrane can act as a mirror for vertically polarised (V) photons, while acting as standard beamsplitter for horizontally polarised (H) photons [164]. Thus similarly to a classical semi-permeable membrane the PBS is permeable to one gas (H) and impermeable to the other (V). However, unlike a classical semi-permeable membrane, a PBS acts coherently on the H gas, generating superpositions of the left and right H modes, thus generalising the semi-permeable membrane to the quantum realm.

One could conceive of generalising the classical Gibbs mixing protocol, sketched in Fig. 3.1, by simply replacing the classical gases with photonic gases and the semi-permeable membranes with a PBS; however, in that case the pistons are implicitly macroscopic and therefore the work output would remain entirely classical. Instead, we will here model the PBS membrane as a microscopic system such that the pistons, as well as the gases, are quantum mechanical. We further simplify the setting and consider a single piston membrane, as shown in Fig. 3.6, rather than the pair considered in the original classical protocol, Fig. 3.1. This reduces the number of light and mechanical modes required, making both the calculations more tractable and the experimental setting more feasible, while leaving the core physics of the thought experiment unchanged.

The interaction between light and microscopic membranes has been explored in the field of optomechanics [165, 166]. In the 'membrane-in-the-middle' optomechanical setup, a photonic cavity is divided into two by a membrane, which acts as a beamsplitter (BS). The membrane is attached to a microscopic cantilever and is allowed to oscillate. Quantum regimes for such optomechanical setups have been realised experimentally by a number of groups [2,3,167–171]. Here we extend the 'membrane-in-the-middle' setup by replacing the standard beamsplitter with a *polarising* beamsplitter, as sketched in Fig. 3.6 and model the ensuing dynamics between photons in the cavity and the PBS membrane. We argue here that this multi-mode optomechanical setup goes beyond previous proposals to study the quantum thermodynamics of the interaction of gases and *pistons* in single-mode systems [172–175], by providing a platform both for studying quantum signatures of distinguishability and, more broadly, realising thermodynamic thought experiments involving the interaction of gases with *membranes*.

We use this 'PBS-in-the-middle' setting to investigate the work that can be extracted from mixing two homogeneous photon gases as a function of their distinguishability[4]. Gas 1 consists of horizontally polarised photons and gas 2 consists of photons each polarised in a superposition state

$$|\theta\rangle = \cos(\theta)\,|H\rangle + \sin(\theta)\,|V\rangle\,, \tag{3.24}$$

where $|H\rangle$ ($|V\rangle$) is the horizontally (vertically) polarised state and $\theta \in [0, \pi/2]$ determines the degree of distinguishability of gas 2 from photon gas 1. When the two gases are perfectly distinguishable, i.e. $\theta = \pi/2$, the radiation pressure exerted by the vertically polarised photons, which are reflected by the PBS, generates a net force on the PBS membrane and this displaces the membrane. Conversely, when the two gases are indistinguishable, i.e. $\theta = 0$, both gases are horizontally

[4]One could also investigate the work required to separate a mixture of two quantum gases. In theory, for perfectly unitary dynamics (as will be considered here) this would simply be the strict inverse of the forwards protocol (i.e. evolution from the final state back to the initial state under the inverse unitary $U^\dagger$). In practice, however, this would be utterly infeasible to implement. Alternatively, one could instead implement a variant of the classical protocol for separating a mixture of gases (i.e. the protocol shown in Fig. 3.1 run backwards) using a PBS as a semi-permeable membrane. However, it is hard to conceive of how this might be done using a microscopic quantum PBS membrane and thus it is hard to picture how the quantum properties of the protocol might be studied. We therefore leave this question for future studies and focus on the work that can be extracted from mixing.

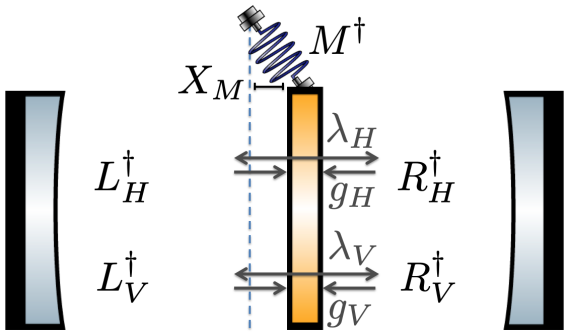


Figure 3.6: **Optomechanical setup.** A microscopic membrane is inserted into a cavity and allowed to oscillate. The displacement of the membrane from the mid-point of the cavity is denoted by X_M and the creation operator for this mechanical mode is $M^\dagger$. The transmission rate between the horizontally (vertically) polarised photon modes on the left hand side of the membrane, $L_H^\dagger$ ($L_V^\dagger$), and horizontally (vertically) polarised modes on the right, $R_H^\dagger$ ($R_V^\dagger$), is determined by the constant λ_H (λ_V). The force exerted per horizontally (vertically) polarised photon on the membrane is given by g_H (g_V). When the membrane is a perfect BS it interacts identically with horizontally and vertically polarised modes and thus $\lambda_H = \lambda_V$ and $g_H = g_V$. When the membrane is a perfect PBS, the membrane reflects all vertically polarised photons and thus $\lambda_V = 0$. It follows that for a PBS membrane the vertically polarised photons exert a greater force on the membrane than the horizontally polarised photons and therefore $g_V > g_H$.

polarised and so there is no net force on the membrane and thus no displacement. It is possible to smoothly vary between these two cases by considering *partially distinguishable* photons such that $0 < \theta < \pi/2$. In analogy to the classical mixing scenario, we associate the motion of the membrane with a work output. In contrast to the mixing of classical homogeneous gases, this work output is now expected to be a smooth function of the distinguishability of the two photon gases.

3.4.1 Hamiltonian

The 'PBS-in-the-middle' optomechanical setup is composed of a cavity with a PBS membrane, which is allowed to oscillate, inserted at the cavity half length. The cavity is capped with two perfectly reflecting mirrors and the membrane is assumed to absorb no photons and thus the number of photons in the cavity is conserved. The Hamiltonian,

$$H_{\text{Total}} = H_0 + H_{\text{LR}}(\lambda_H, \lambda_V) + H_{\text{OptMech}}(g_H, g_V)\,, \tag{3.25}$$

describing the photons and membrane in the cavity is comprised of the non-interacting Hamiltonians of the photons and membrane, H_0, the polarisation dependent beamsplitter interaction between the photons in the left and right cavities, H_{LR}, and the optomechanical interaction between the photons and the membrane, H_{OptMech} [168]. The Hamiltonian for the independent optical and mechanical modes can be written explicitly as

$$H_0 = \hbar\omega\left(R_H^\dagger R_H + L_H^\dagger L_H\right) + \hbar\omega\left(R_V^\dagger R_V + L_V^\dagger L_V\right) + \hbar\omega_M M^\dagger M\,, \tag{3.26}$$

where ω_M is the mechanical frequency of the membrane, ω is the light frequency, $M^\dagger$ is the creation operator for the phonon membrane mode and $L_H^\dagger$ ($R_H^\dagger$) and $L_V^\dagger$ ($R_V^\dagger$) are the creation operators for horizontally and vertically polarised photons respectively in the left (right) cavity.

To allow us to model imperfect as well as perfect semipermeable membranes, we consider a general polarisation dependent beamsplitter interaction between the modes in the left and right cavities of the form

$$H_{\text{LR}}(\lambda_H, \lambda_V) = \frac{\hbar\lambda_H}{2}\left(R_H^\dagger L_H + L_H^\dagger R_H\right) + \frac{\hbar\lambda_V}{2}\left(R_V^\dagger L_V + L_V^\dagger R_V\right) . \tag{3.27}$$

The coefficient λ_H (λ_V) determines the reflection r_H (r_V) and transmission t_H (t_V) coefficients of the horizontally (vertically) polarised photons at time t, with $r_k = \cos^2\left(\frac{\lambda_k t}{2}\right)$ and $t_k = \sin^2\left(\frac{\lambda_k t}{2}\right)$ for $k = H$ and $k = V$ [164]. A perfect polarising beamsplitter is modelled by setting $\lambda_V = 0$,

$$H_{\text{PBS}} = H_{\text{LR}}(\lambda_H, 0) , \tag{3.28}$$

such that the membrane acts as a mirror for the vertical modes ($r_V = 1$ and $t_V = 0$ for all times) but acts as a beamsplitter for the horizontal modes. A standard beamsplitter is captured by setting $\lambda_H = \lambda_V = \lambda$ such that the membrane reflects and transmits horizontally and vertically polarised photons at the same rate,

$$H_{\text{BS}} = H_{\text{LR}}(\lambda, \lambda) . \tag{3.29}$$

By choosing λ_V such that $0 \leq \lambda_V \leq \lambda_H$, we can smoothly interpolate between these two limits to model a membrane that imperfectly distinguishes between horizontally and vertically polarised photons.

Photons in the cavity will collide and exchange momentum with the membrane and as a result exert a pressure (radiation pressure) on the surface of the membrane [176]. The total force exerted by photons on the membrane,

$$F(g_H, g_V) = \hbar g_H \Delta N_H + \hbar g_V \Delta N_V , \tag{3.30}$$

is equal to the product of the force exerted per photon, $\hbar g_H$ and $\hbar g_V$ respectively for horizontally and vertically polarised photons respectively, and the difference in the number of horizontal and vertical photons in the left and right cavities,

$$\Delta N_H := (L_H^\dagger L_H - R_H^\dagger R_H) \quad \text{and} \quad \Delta N_V := (L_V^\dagger L_V - R_V^\dagger R_V) . \tag{3.31}$$

Radiation pressure thus gives rise to an interaction energy of the form

$$H_{\text{OptMech}}(g_H, g_V) = -F(g_H, g_V) X_M , \tag{3.32}$$

where X_M is the displacement of the membrane from the centre of the cavity. When the membrane is a perfect PBS, all vertical photons are reflected but horizontal photons are both reflected and transmitted and therefore the force exerted by vertical photons on the membrane is greater than that of horizontal photons which implies choosing $g_V > g_H$.

For future convenience we note that the optomechanical interaction Hamiltonian can alternatively be written explicitly in terms of the membrane creation and annihilation operators as

$$H_{\text{OptMech}}(g_H, g_V) = -\left(\hbar\tilde{g}_H \Delta N_H + \hbar\tilde{g}_V \Delta N_V\right)\left(M + M^\dagger\right) , \tag{3.33}$$

where $\tilde{g}_H$ and $\tilde{g}_V$ are the single photon coupling strengths of the horizontally and vertically polarised photons respectively, in the units of frequency. That is, $\tilde{g}_p = g_p\, x_{\text{zpf}}$, for $p = H$ and $p = V$, where x_{zpf} is the mechanical oscillators zero point uncertainty $x_{\text{zpf}} = \sqrt{\frac{\hbar}{2m\omega_M}}$ with m the effective mass of the mechanical oscillator.

3.4.2 Calculation of the dynamics

To calculate the dynamics of the light field and mechanical degree of freedom we work in the Heisenberg picture as this enables us to obtain general results for the evolution of the relevant observables, i.e. the membrane's displacement and energy, for a general initial state.

To maintain an analogy with classical Gibbs mixing where the number of gas molecules is fixed and the motion of the pistons are assumed to be frictionless we will consider for now an idealised cavity and membrane which experience no dissipative effects. We relax this assumption in Section 3.9 where we discuss more realistic experimental implementations.

Using Heisenberg's equation of motion for a system with the Hamiltonian H and an operator Q,

$$\frac{dQ}{dt} = \frac{i}{\hbar}[H, Q] \ , \tag{3.34}$$

one finds that the evolution of the position operator of the membrane reads

$$\frac{dX_M}{dt} = \frac{P_M}{m} \tag{3.35}$$

and the evolution of the momentum operator of the membrane is given by

$$\frac{dP_M}{dt} = -m\omega_M^2 X_M + F(g_H, g_V) \ , \tag{3.36}$$

where $F(g_H, g_V)$ is the total force exerted by the photons on the membrane defined in Eq. (3.30). The coupled differential equations, Eq. (3.35) and Eq. (3.36) reduce to the second order differential equation,

$$\frac{d^2X_M}{dt^2} + \omega_M^2 X_M = \frac{F(g_H, g_V)}{m} \ . \tag{3.37}$$

Thus the membrane evolves as a quantum harmonic oscillator driven by the radiation pressure from the photons in the cavity.

To determine the time dependent driving force $F(g_H, g_V)$ we similarly derive Heisenberg's equations of motion for ΔN_H and ΔN_V, the imbalance in the number of horizontally and vertically polarised photons between the two cavities. We find that horizontally and vertically photons oscillate between the two cavities at the rates λ_H and λ_V respectively, with their motion coupled to the position of the membrane via

$$\frac{d^2\Delta N_p}{dt^2} = -\lambda_p^2 \Delta N_p - 2g_p\lambda_p X_M(L_p^\dagger R_p + L_p R_p^\dagger) \ \text{ for } \ p = H, V \ . \tag{3.38}$$

Thus for a complete description of the exact dynamics of the photons and membrane, we would need to solve the highly non-linear coupled differential equations Eq. (3.37) and Eq. (3.38).

While the exact solution is prohibitively difficult, a perturbative solution that describes the dynamics of selected observables for any given initial state can be constructed. Given that the force exerted by a single photon on the massive membrane is weak[5], the single photon coupling strengths, g_H and g_V, are small compared to the PBS coupling rate, λ (see Table 3.9.1). It is therefore appropriate to solve the dynamics perturbatively in $\tilde{g}_H$ and $\tilde{g}_V$. With the membrane cooled to cryogenic temperatures (mean phonon occupation number $\bar{n}_{th}$ of the order of 10) [177], the higher order contributions are negligible, as discussed in Appendix C.2.

Studying the motion of the membrane to first order in $\tilde{g}_H$ and $\tilde{g}_V$ amounts to disregarding the back action that the motion of the membrane has on the dynamics of the photons and simply

[5]Note, we are implicitly still considering what is usually called the strong coupling regime here in that we have assumed that the cavity damping rate κ is sufficiently small that we can disregard it and therefore $g_H > \kappa$ and $g_V > \kappa$.

solving the dynamics of the photons to 0th order in $\tilde{g}_H$ and $\tilde{g}_V$. On dropping the $\tilde{g}_H$ and $\tilde{g}_V$ dependent term of Eq. (3.38), we find that the horizontally (vertically) polarised photons oscillate at a rate $2\lambda_H$ ($2\lambda_V$) between the two halves of the cavity according to

$$\Delta N_p(t) = \Delta N_p(0)\cos(\lambda_p t) + \Delta K_p(0)\sin(\lambda_p t) \ , \tag{3.39}$$

where we have defined

$$\Delta K_p := i(R_p^\dagger L_p - R_p L_p^\dagger) \quad \text{for} \quad p = H, V \ . \tag{3.40}$$

Substituting the first order solution for the evolution of the photons, Eq. (3.39), into the expression for the total force on the membrane, Eq.(3.30), we find that the membrane is driven by the force

$$F(g_H, g_V) = \hbar \sum_{p=H,V} g_p \, \Delta N_p(0)\cos(2\lambda_p t) + g_p \, \Delta K_p(0)\sin(2\lambda_p t) \ . \tag{3.41}$$

The solution to the equation of motion of the membrane, Eq. (3.37), for this first order driving force, is simply the classical solution for a harmonic oscillator that is driven by a sinusoidal force but with the classical variables promoted to operators,

$$\begin{aligned} X_M(t) \ = & \sum_{p=H,V} a_p \Delta N_p(0)\left(\cos(\lambda_p t) - \cos(\omega_M t)\right) \\ & + \sum_{p=H,V} a_p \Delta K_p(0)\left(\sin(\lambda_p t) - \frac{\lambda_p}{\omega_M}\sin(\omega_M t)\right) \\ & + X_M(0) + \frac{P_M(0)}{m\omega_M} \ , \end{aligned} \tag{3.42}$$

where to simplify the notation we have introduced the shorthand

$$a_p := \frac{\hbar g_p}{m(\omega_M^2 - \lambda_p^2)} \ . \tag{3.43}$$

This expression is our starting point to study the thermodynamics of mixing within the present optomechanical setting. We use it in Section 3.5 to calculate the energetic properties of the membrane. Before we proceed to do so, let us first clarify the initial states of the photons and membrane that we will focus on.

3.4.3 Initial states

To replicate the mixing of *homogeneous* gases considered by Gibbs, we suppose *all* photons in the left hand side of the cavity to be polarised at angle $\theta_L = \theta$ and *all* photons in the right part to be polarised at $\theta_R = 0$. This allows us to explore the transition between distinguishable and indistinguishable gases by varying θ. Apart from the different polarization, we assume the state, in particular the number distribution, of the photons in the left part of the cavity to be the same as the state of the light in the right part in order to avoid a displacement of the piston membrane due to an initial photon imbalance. That is we assume that

$$\langle f(N_L(0))\rangle = \langle f(N_R(0))\rangle \tag{3.44}$$

for any function f and where $N_L = L_H^\dagger L_H + L_V^\dagger L_V$ and $N_R = R_H^\dagger R_H + R_V^\dagger R_V$ are the total number of photons in the left and right hand cavities respectively. For simplicity we take the photons and piston membrane states to be initially uncorrelated. We further assume that the initial average momentum and displacement of the membrane vanishes, as would be true, for example, were the membrane to be prepared in its ground state or a thermal state.

The above skeleton set of initial conditions suffices to obtain highly general results for the dynamics of the setup which are independent of the specific choice in the number distribution of the photon gases and specific state of the membrane. However, to make a closer connection with the original Gibbs mixing scenario we will also hone in on pertinent choices for the photon number distribution.

A photon gas in a thermal state has a well defined temperature but does not have a well defined number of photons and conversely a photon gas in a Fock state has a well defined number of particles but not temperature. Therefore, we cannot capture the classical case of thermal gases with a well defined number of particles. Instead, we consider the two cases separately. More specifically, we compare a *Fock state configuration* in which there are precisely n photons per cavity and thus the initial state of the photons can be written as

$$\begin{aligned} &\rho_{\text{F}} := |\psi_L(n,\theta)\rangle\langle\psi_L(n,\theta)| \otimes |\psi_R(n,0)\rangle\langle\psi_R(n,0)| \quad \text{with} \\ &|\psi_C(n,\theta)\rangle \propto \left(\cos(\theta)C_H^\dagger + \sin(\theta)C_V^\dagger\right)^n |0\rangle \quad \text{for} \quad C = R, L \,, \end{aligned} \tag{3.45}$$

to a *thermal configuration*,

$$\begin{aligned} &\rho_{\text{T}} := \gamma_L(\theta) \otimes \gamma_R(0) \quad \text{with} \\ &\gamma_C(\theta) \propto \sum_{n=0}^{\infty} e^{-\frac{n\hbar\omega}{k_B T}} |\psi_C(n,\theta)\rangle\langle\psi_C(n,\theta)| \quad \text{for} \quad C = R, L \,, \end{aligned} \tag{3.46}$$

in which the photons in each cavity are in a thermal state at temperature T. While the thermal configuration perhaps allows us to make better contact with the thermodynamics which is central to the original Gibbs mixing thought experiment; the Fock state configuration is conceptually interesting in virtue of the fact that the Fock state is a genuinely quantum mechanical state of light.

Both configurations have experimental limitations. As the frequency of the cavity is typically of the order of THz [178], in order to have a non-negligible number of photons in each gas the temperature of that gas would have to be of order 10^3K (roughly the temperature of the sun). This is not only experimentally impractical, but also would necessitate a temperature gradient between the photons and membrane. One way around this problem would be to use pseudo-thermal states of light [179]. Fock states of high $n \gtrsim 50$ are experimentally challenging; however, the regime of low photon number optomechanics is increasingly achievable [180]. We therefore consider the Fock and thermal configurations initially to maintain a continuity with the classical Gibbs mixing setting; however, in Section 3.9 we will present a more realistic experimental proposal to test some of these ideas.

3.4.4 Work output

When the photons and membrane are left to evolve the two gases will mix in the right cavity and this drives the membrane. To compare the work drawn in this mixing process to the work that can be extracted mixing classical gases, we need to specify the work done on the membrane by the mixing of the photon gases. As touched on in Chapter 2, the question of how to define work in the quantum regime has been discussed substantially elsewhere [84–86, 181–183] and is far from resolved. Here we simply suggest a natural candidate that could be associated with work in this setting.

In Fig. 3.1, one could imagine the work done by the expanding gases is stored by a pair of springs that are compressed during the mixing process. By analogy, we will consider the work done on

the membrane to be the potential energy associated with the displacement of the membrane that results from the mixing of the photon gases. While in the protocol for mixing classical gases the final displacement of the membrane is constant and well defined, here the membrane oscillates about a new displaced origin and there will be some spread to its wave function. We therefore consider the potential energy associated with the oscillator's new displaced origin, that is

$$W_M := \frac{1}{2} m\omega_M^2 \langle X_M \rangle^2 \,, \tag{3.47}$$

where

$$\langle X_M \rangle := \frac{1}{\tau} \int_0^\tau \mathrm{Tr}[X_M(t)\rho]\, dt \,, \tag{3.48}$$

is the displacement of the membrane averaged over both the state of the membrane and an oscillation cycle τ.

Another relevant thermodynamic quantity is the total change in the energy of the membrane. In general the energy of the membrane is a quantum variable and oscillates in time and so to have a well defined quantity we again consider the average change in energy of the membrane,

$$\Delta H_M := \langle H_M(t) - H_M(0) \rangle = \frac{1}{\tau} \int_0^\tau \mathrm{Tr}[(H_M(t) - H_M(0))\rho]\, dt \,, \tag{3.49}$$

where the average is taken over the membrane's quantum state and over an oscillation cycle, as in Eq. (3.48). Since, as will become clear, this energy is stored in the fluctuations and oscillatory motion of the membrane, the change in energy of the membrane has a substantial heat-like component.

3.5 Optomechanical Gibbs mixing analysis

In this section we investigate the work output, W_M, and the change in energy of membrane, ΔH_M, from the mixing of partially distinguishable photon gases using a polarising beamsplitter membrane. The starting point for all these calculations is the general expression for the evolution of the displacement of the mechanical degree of freedom specified by Eq.(3.42).

Work output. As argued above, we take the work done on the membrane to be the potential energy of the membrane associated with the membrane's new displaced origin. For a perfect polarising beamsplitter membrane, it follows from Eq. (3.42) that the displacement of the membrane is of the form

$$X_M(t) = X_M^{\mathrm{osc}}(t) + \frac{\hbar g_V \Delta N_V(0)}{m\omega_M^2} \,, \tag{3.50}$$

where $X_M^{\mathrm{osc}}(t)$ is an oscillatory term, which vanishes when we consider the average the displacement of the membrane over its state and a complete oscillation cycle, leaving

$$\langle X_M \rangle = \frac{\hbar g_V}{m\omega_M^2} \langle \Delta N_V(0) \rangle \,. \tag{3.51}$$

For horizontally polarised photons in the right cavity and photons polarised at an angle θ in the left cavity, the time averaged displacement of the membrane is therefore given by

$$\langle X_M \rangle = \frac{\hbar g_V \langle N \rangle}{\omega_M^2 m} \sin^2(\theta) \,. \tag{3.52}$$

where $\langle N \rangle$ is shorthand for the average number of photons per gas

$$\langle N \rangle := \langle N_L(0) \rangle \equiv \langle N_R(0) \rangle \,. \tag{3.53}$$

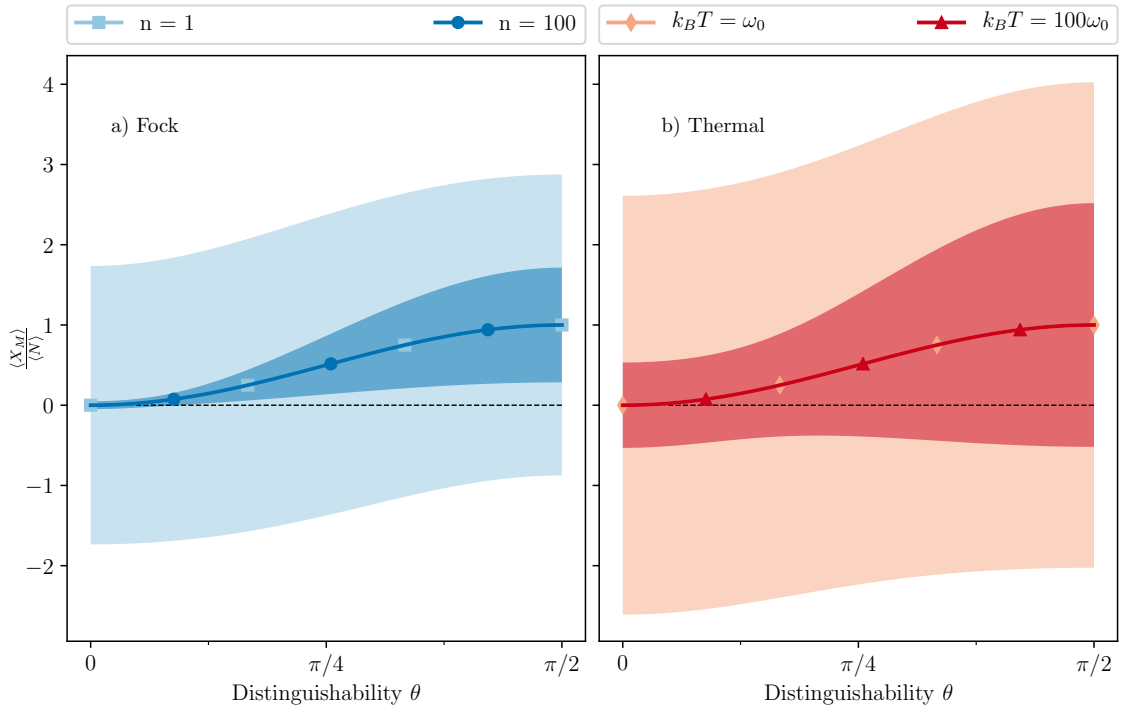


Figure 3.7: **Time averaged displacement of PBS membrane.** We plot the time averaged displacement of the PBS membrane normalised by the mean number of photons per gas, $\frac{\langle X_M \rangle}{\langle N \rangle}$, and shade the normalised standard deviation of this displacement, $\frac{\sqrt{\langle X_M^2 \rangle - \langle X_M \rangle^2}}{\langle N \rangle}$, as a function of the distinguishability θ of the photons in the left cavity from the photons in the right cavity. In a) the photons are initially in a Fock state with $n = 1$ photons per cavity (light blue squares) and $n = 100$ photons per cavity (dark blue circles) and the membrane is in a thermal state at temperature $k_BT = \omega_M$. In b) both the photons and the membrane are initially in a thermal state at the same temperature $k_BT = \omega$ (peach diamonds) and $k_BT = 100\omega$ (red triangles), to ensure there is no temperature gradient such that the work output and fluctuations can be attributed solely to mixing. In both plots the following parameters were chosen to illustrate the thought experiment: $\lambda/\omega_M = 2$, $g_V/g_H = 6$ and $\omega = 10\omega_M$. All distances are given in units of $\frac{\hbar g_V}{m\omega_M^2}$.

It thus follows that the potential energy associated with the average displacement of the membrane is

$$W_M = \frac{\hbar^2 g_V^2 \langle N \rangle^2}{2\omega_M^2 m} \sin^4(\theta) \ . \tag{3.54}$$

This expression for the work output is highly general in the sense that it holds for any photon number distribution as long as the initial distribution is the same in the two cavities and the optomechanical setup is in the regime where the back action of the membrane on the dynamics of the photons is negligible. Thus, in this setting, the work output vanishes for perfectly indistinguishable gases and is maximised for perfectly distinguishable gases, in agreement with the classical case as one would expect. However, crucially, in contrast to classical Gibbs mixing, the work now smoothly increases between these two extremes. That is, in this setting, we see precisely the continuous increase in the work output with distinguishability that we set out to demonstrate.

A key distinction between Gibbs mixing in the optomechanical setting compared to prior studies

concerns the fluctuations in the work output. When the pistons are assumed to be macroscopic classical systems, as in Gibbs' classical analysis [142] and in quantum analyses based on entropic arguments [152, 154–156], the fluctuations in the work output from mixing are negligible. Here, however, as shown in Fig. C.1, the standard deviation of the displacement of the membrane is large as compared to the membrane's average displacement which implies that there are large fluctuations in W_M^{mix}.

These substantial fluctuations in the work output are a feature arising from using a microscopic quantum piston membrane that is sensitive to the microscopic dynamics of the photon gases. The fluctuations capture both the motion of the mechanical degree of freedom due to the oscillatory force exerted by the photons as well as its quantum uncertainty. This quantum component to the uncertainty stems from the initial vacuum fluctuations of the photonic and phononic modes and the coherent nature of the dynamics. In particular, the PBS interaction gives the photons access to coherent superpositions between the two halves of the cavity and the optomechanical interaction entangles the photonic modes and the microscopic piston generating quantum fluctuations in the membrane's position. As shown in light blue and peach in Fig. C.1, the fluctuations per photon are largest for low photon numbers and low temperatures. This can be attributed to the increased relative significance of vacuum fluctuations when the number of photons in the cavity is small.

3.6 Optomechanical Gibbs mixing analysis

Here we provide a more detailed account of the thermodynamic properties of Gibbs mixing in this optomechanical setting.

Role of coherence for work output. The work extracted from mixing the photon gases, Eq. (3.54), depends only on the difference in the number of vertically polarised photons in the two cavities and therefore is independent of the purity of the two gases. It follows that the same amount of work can be extracted mixing two homogeneous partially distinguishable quantum gases, where the internal state of the photons in the left and right cavities are given by $\rho_L = |\theta\rangle\langle\theta|$ and $\rho_R = |H\rangle\langle H|$ respectively, and mixing the equivalent classical mixture, that is mixing a homogeneous classical gas consisting of horizontally polarised photons and a non-homogeneous classical gas consisting of a mix of $\langle N\rangle\cos^2(\theta)$ horizontally polarised photons and $\langle N\rangle\sin^2(\theta)$ vertically polarised photons. In the latter case the internal state of the photons in the inhomogeneous gas in the left hand cavity is described by the density matrix $\rho_L = \mathcal{D}(|\theta\rangle\langle\theta|)$ where $\mathcal{D}$ is the depolarising operation such that $\mathcal{D}(|\theta\rangle\langle\theta|) = \cos^2(\theta)|H\rangle\langle H| + \sin^2(\theta)|V\rangle\langle V|$. In this sense, the work output is independent of the coherence of the internal state of the gases. This is a feature of the optomechanical setting that deviates from the previous entropic analyses [152, 154–156] discussed in Section 3.3. As summarised in Table 3.9.1, while the work output from mixing W_M agrees for both pure and mixed photonic gases, W_{vN} differs.

This distinction between the current optomechanical analysis and previous entropic analyses is perhaps unsurprising given the fundamental differences between the settings. The prior entropic analyses aim to quantify the work output in an optimum protocol, assuming the thermodynamic limit of quantum gases containing large numbers of particles which completely mix while interacting continually with classical pistons and a classical thermal bath. In contrast, here we consider an autonomous, non-optimal, protocol involving (possibly finite sized) quantum gases and a quantum piston, where the gases partially rather than fully mix.

	ρ_L	ρ_R	W_M	W_{VN}
Pure	$\|\theta\rangle\langle\theta\|$	$\|H\rangle\langle H\|$	W_M^{mix}	$2Nk_BTS(\rho_{\text{mix}})$
Mixed	$\mathcal{D}(\|\theta\rangle\langle\theta\|)$	$\|H\rangle\langle H\|$	W_M^{mix}	$2Nk_BTS(\mathcal{D}(\rho_{\text{mix}})) - Nk_BTS(\mathcal{D}(\|\theta\rangle\langle\theta\|))$

Table 3.1: **Comparison of optomechanical and entropic analyses for gases prepared in pure and mixed states.** Here ρ_L and ρ_R are the states of the polarisation degree of freedom of a single photon in the left and right cavities initially, W_M is the measure of the work output in the optomechanical setting, Eq. (3.47), W_M^{mix} is the calculated work output from mixing, Eq. (3.54), and W_{VN} is the equivalent work output given by analogous entropic analyses, Eq. (3.8). The internal state of a photon after mixing is denoted $\rho_{\text{mix}} = \frac{1}{2}|\theta\rangle\langle\theta| + \frac{1}{2}|H\rangle\langle H|$ and $\mathcal{D}$ denotes the dephasing operation.

Energy change. The total energy of the PBS membrane is composed of a contribution from the driving force provided by the oscillating horizontal photons and a contribution from the constant force exerted by the vertically polarised photons. The average energy of the membrane rapidly oscillates; however, taking its time average to remove fast oscillating terms we find that the time averaged change in energy of the membrane obeys

$$\Delta H_M = \alpha\langle\Delta N_V^2(0)\rangle + \beta\langle\Delta N_H(0)\Delta N_V(0)\rangle + \mu\langle\Delta K_H^2(0)\rangle + \eta\langle\Delta N_H^2(0)\rangle \,, \tag{3.55}$$

where the prefactors $\alpha = \frac{\hbar^2 g_V^2}{m\omega_M^2}$, $\beta = \frac{\hbar^2 g_H g_V}{m(\omega_M^2-\lambda_H^2)}$, $\mu = \frac{\hbar^2 g_H^2(3\lambda_H^2+\omega_M^2)}{4m(\lambda_H^2-\omega_M^2)^2}$ and $\eta = \frac{\hbar^2 g_H^2(\lambda_H^2+3\omega_M^2)}{4m(\lambda_H^2-\omega_M^2)^2}$ depend only on system parameters but not on the initial state.

Since the radiation pressure exerted by the vertically polarised photons is greater than that exerted by the horizontally polarised photons, $g_V > g_H$, the first term of Eq. (3.55) dominates the expression and the time averaged change in energy of the membrane can be approximated as

$$\Delta H_M \approx \frac{\hbar^2 g_V^2}{m\omega_M^2}\langle\Delta N_V(0)^2\rangle \,. \tag{3.56}$$

For horizontally polarised photons in the right cavity and photons polarised at angle θ in the left cavity, the expected squared difference in the number of vertically polarised photons in the left and right cavities initially is

$$\langle\Delta N_V(0)^2\rangle = \langle N^2\rangle\sin^4(\theta) + \langle N\rangle(\sin^2(\theta) - \sin^4(\theta)) \,, \tag{3.57}$$

where

$$\langle N^2\rangle := \langle N_L(0)^2\rangle \equiv \langle N_R(0)^2\rangle \,, \tag{3.58}$$

is the average number of photons squared per gas. Thus, similarly to the work output, W_M, the change in energy of the membrane again increases monotonically with the distinguishability of the photons. Indeed, as shown in Fig. 3.8, for photon gases containing large numbers of photons, the dependence of ΔH_M on distinguishability tends to $\sin^4(\theta)$ coinciding with the θ-dependence of W_M.

While the above approximation for the change in energy of the membrane, Eq. (3.56), is generally accurate; it implies that the change in energy of the membrane vanishes for indistinguishable photons which is not strictly true. Certainly, for perfectly indistinguishable gases, $\theta = 0$, both gases are horizontally polarised and therefore the first term of Eq. (3.55) vanishes. However, the other terms in Eq. (3.55) still contribute to the change in the energy of the membrane. Consequently, in contrast to the work output from mixing, Eq. (3.54), which in agreement with classical

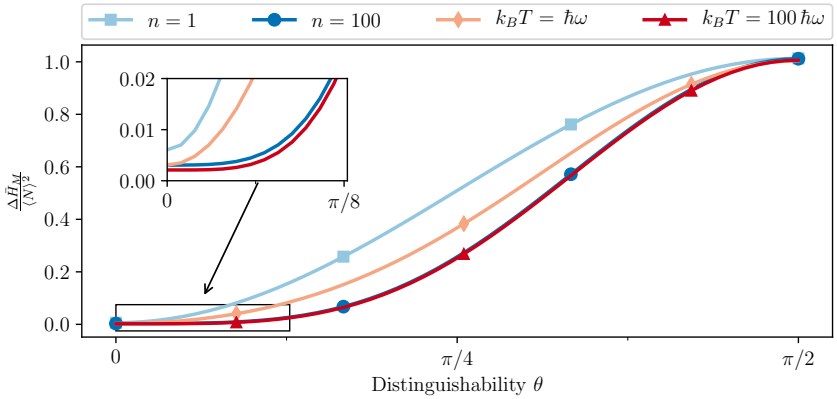


Figure 3.8: **Change in energy of PBS membrane.** We plot the time averaged change in energy of the PBS membrane to first order in g_H and g_V, normalised by the expected number of photons per gas squared, as a function of the distinguishability of the photons in the left cavity from the photons in the right cavity. We plot the data for when the photons are initially in a Fock state with $n = 1$ photons per cavity (light blue squares) and $n = 100$ photons per cavity (dark blue circles) and for when the photons are initially in a thermal state at temperature $k_BT = \omega$ (peach diamonds) and $k_BT = 100\omega$ (red triangles). The inset magnifies the data for $\theta \leq \pi/8$ to highlight that the energy transfer does not vanish as $\theta \to 0$. All energies are given in units of $\frac{\hbar^2 g_V^2}{m\omega_M^2}$. In this plot $\lambda/\omega_M = 2$, $g_V/g_H = 6$, $\omega = 10\omega_M$.

Gibbs mixing vanishes for perfectly distinguishable gases; the energy transfer to the membrane is strictly non-zero even for the 'mixing' of indistinguishable gases. This arises from the fact that the PBS membrane is a microscopic quantum system and thus experiences heating from the radiation pressure exerted by the photons in the cavity irrespective of their polarisation. Nonetheless, as is clear from Fig. 3.8, the contribution of these terms are very small compared to the energy transfer for distinguishable gases.

Thus far we have focused on the distinguishability dependence of the work output and energy transfer to the membrane that results from the photon dynamics. However, classically, the work output is expected to also depend on the temperature of the heat bath used for the mixing protocol. It is therefore natural to also discuss this dependence in the current setting.

Temperature dependence. In the limit in which the back action of the membrane on the photon dynamics can be neglected and damping effects are assumed negligible, any temperature dependence of the work measures W_M and ΔH_M enters through the initial state of the photons. Thus these measures do not depend on temperature if the number of photons in each gas is temperature independent, as in the Fock state configuration. However, in the thermal configuration the number of photons per gas is thermally distributed with

$$\begin{aligned} \langle N\rangle &= \frac{\exp(-\hbar\omega/k_BT)}{1-\exp(-\hbar\omega/k_BT)} \quad \text{and} \\ \langle N^2\rangle &= \frac{\exp(-\hbar\hbar\omega/k_BT)(1+\exp(-\hbar\omega/k_BT)}{(1-\exp(-\hbar\omega/k_BT))^2}\,. \end{aligned} \tag{3.59}$$

The resulting temperature dependence of the work output and energy transfer to the membrane in the thermal configuration is shown in Fig. 3.9. To aid comparison with classical Gibbs mixing, Eq. (3.2), we choose to plot the work done and energy change *per photon*, that is $\frac{W}{\langle N\rangle}$ and $\frac{\Delta H_M}{\langle N\rangle}$,

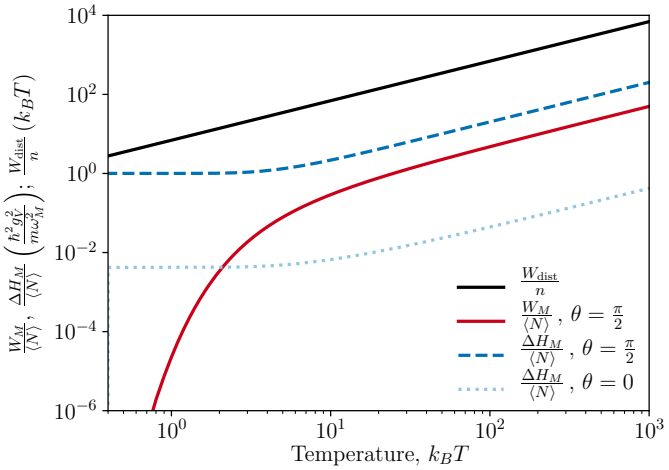


Figure 3.9: **Temperature dependence.** The mixing work $W_M/\langle N\rangle$, Eq. (3.54), to first order in g_H and normalised by the average photon gas number $\langle N\rangle$. For perfectly distinguishable gases ($\theta = \pi/2$, solid red) $W_M/\langle N\rangle$ grows as a function of the photon state temperature T, Eq. (3.46), and is zero for indistinguishable gases ($\theta = 0$, not shown). For higher temperatures the slope becomes the same as that of the classical Gibbs mixing work per particle $W_{\rm dist}/n$, Eq. (3.2), for distinguishable gases (solid black). Also shown is the full energy transfer to the membrane given by $\Delta\bar{H}_M$ in Eq. (3.55) for perfectly distinguishable gases (dark blue dashed) and for perfectly indistinguishable gases (light blue dotted). Again in the high temperature regime, both slopes become the same as the classical mixing work (solid black) and hence the energy transfers to the membrane grows linearly with the photon gas thermal state temperature. The classical work is given in units of k_BT and the quantum work W_M and energy transfer $\Delta\bar{H}_M$ are given in units of $\frac{\hbar^2 g_V^2}{m\omega_M^2}$. In this plot $\lambda/\omega_M = 2$, $g_V/g_H = 6$, $\omega = 10\omega_M$.

to compensate for the fact that classically the number of particles in the gas is assumed to be constant; whereas, for thermal photon gases the particle number is temperature dependent.

As shown in Fig. 3.9, we find that in the high temperature limit both the work output and the change in energy, for both distinguishable and indistinguishable gases, is proportional to the initial temperature of the thermal state. Thus in the high temperature limit, we regain the linear temperature dependence of the mixing work that is observed both in the classical case, Eq. (3.2). However, for low temperatures W_M tends to zero at a super-linear rate and ΔH_M tends sub-linearly to

$$\frac{\Delta H_M}{\langle N\rangle} \approx \frac{\hbar^2 g_V^2}{m\omega_M^2}\sin^2(\theta) \tag{3.60}$$

before dropping discontinuously to 0 at $k_BT = 0$. These low temperature deviations are perhaps unsurprising since classical thermodynamics is formulated for the asymptotic limit of large numbers of particles; however, in the low temperature limit here, the gases consist of only a handful of photons.

The work that can be extracted in this optomechanical setting is expected to be generally less than can be extracted classically since $\frac{\hbar^2 g_V^2}{m\omega_M^2} < k_BT$ for typical experimental parameters (see Table 3.9.1). This is because, in contrast to the classical analysis (and previous entropic analyses), we have investigated a particular work extraction protocol which we have no reason to expect is optimal. Now one could view this as a criticism of our approach. Certainly, from a purely theo-

retical perspective our predicted work output perhaps lacks the aesthetic appeal of a clean upper bound. However, from a more practical perspective in general even specifying, let alone implementing, an *optimal* experimental protocol is a daunting task. Therefore, turning the argument around, we suggest it is noteworthy that we have found a scheme whereby an experimentalist could observe the same qualitative behaviour as predicted by these bounds, a work output that increases monotonically with distinguishability, without needing to perform an optimal protocol.

Nonetheless, it could be valuable in the future to investigate whether a more efficient work extraction scheme is possible within the 'PBS-in-the-middle' optomechanical setting. One could, for example, consider variants of the setup utilising multiple PBS membranes to enable the two photon gases to mix fully rather than partially as currently. Or, more fundamentally, the work extracted with the current scheme is independent of the purity of the internal state of the quantum gases, leaving open the question of whether/how the coherence of the polarisation of the photons could be utilised to extract additional work from mixing.

3.7 Bunching enhanced energy transfer

In this section, we share some intriguing results concerning the membrane dynamics when we abstract further away from the standard Gibbs mixing scenario and consider the effect of replacing the polarising beamsplitter with a standard beamsplitter. While this setting is no longer a direct analogue of classical Gibbs mixing, it exposes a novel quantum signature of distinguishability in thermodynamics [146].

With a BS membrane the photon gases in the two cavities will fully mix in both the left and right hand cavities, rather than just the right hand cavity as with a PBS membrane. By analogy with the protocol for extracting work from mixing classical photon gases, Fig 3.1, we expect there to be no work output when this mixing occurs because a beamsplitter is a fully permeable rather than semipermeable membrane and thus photon gases of different polarisations do not exert partial pressures on it. Indeed, we find from Eq. (3.42) that the average displacement of a BS membrane, and therefore W_M, vanishes for all times and choice in physical parameters.

The vanishing average displacement of the BS membrane can be seen as direct consequence of the system's mirror symmetry. The Hamiltonian is invariant under the exchange of L_p and R_p and simultaneous replacement of X_M with $-X_M$. Therefore, given a symmetric initial state, this symmetry is preserved during the dynamics and necessarily needs to be satisfied in the final state. As a result, since we assume both that the average displacement of the membrane initially vanishes and that there are initially equal numbers of photons in the two cavities, the average displacement of the membrane vanishes at all times.

However, the energy transfer to the membrane does not vanish and, as it turns out, its dependence on distinguishability is rather curious. Using the general expression for the evolution of the membrane's displacement operator $X_M(t)$, Eq. (3.42), we find that the time averaged change in energy of the membrane is given by

$$\Delta H_M = \frac{\mu}{2}\langle(\Delta N(0))^2\rangle + \frac{\eta}{2}\langle(\Delta K(0))^2\rangle \,, \tag{3.61a}$$

where $\mu = \frac{2\hbar^2 g^2(\lambda^2+3\omega_M^2)}{m(\lambda^2-\omega_M^2)^2}$ and $\eta = \frac{\hbar^2 g^2(3\lambda^2+\omega_M^2)}{m(\lambda^2-\omega_M^2)^2}$ depend only on system parameters but not on the initial state.

The distinguishability and photon number dependence of the energy of the membrane enters through the evaluation of the $\langle\Delta N(0)^2\rangle$ and $\langle\Delta K(0)^2\rangle$ terms. The $\langle\Delta N(0)^2\rangle$ term is calculated as

follows

$$\begin{aligned}\langle \Delta N(0)^2 \rangle &= \langle (N_L(0) - N_R(0))^2 \rangle \\ &= \langle N_L(0)^2 + N_R(0)^2 - 2N_L(0)N_R(0) \rangle \\ &= 2\langle N^2 \rangle - 2\langle N \rangle^2 \ ,\end{aligned} \tag{3.62}$$

where the final line follows from the fact that we assume the photon number distribution in the two halves of the cavity are equal and therefore we can write $\langle N_L \rangle = \langle N_R \rangle = \langle N \rangle$ and $\langle N_L^2 \rangle = \langle N_R^2 \rangle = \langle N^2 \rangle$. Thus $\langle \Delta N(0)^2 \rangle$ is distinguishability independent and equal to the variance in photon number in either cavity,

$$\langle \Delta N(0)^2 \rangle = \delta N \tag{3.63}$$

where $\delta N = \langle N^2 \rangle - \langle N \rangle^2$. Similarly, for the $\langle \Delta K(0)^2 \rangle$ term we have that

$$\begin{aligned}\langle \Delta K(0)^2 \rangle &= \langle (\Delta K_H(0) + \Delta K_V(0))^2 \rangle \\ &= \langle \Delta K_H(0)^2 + \Delta K_V(0))^2 + 2K_H(0)K_V(0) \rangle \ .\end{aligned} \tag{3.64}$$

The cross term vanishes since all photons in the right cavity are horizontally polarised and remaining two terms evaluate to

$$\begin{aligned}\langle \Delta K(0)^2 \rangle &= \langle \Delta K_H(0)^2 + \Delta K_V(0))^2 \rangle \\ &= \langle L_H^\dagger L_H \rangle + \langle R_H^\dagger R_H \rangle + 2\langle L_H^\dagger L_H \rangle \langle R_H^\dagger R_H \rangle + \langle L_V^\dagger L_V \rangle + \langle R_V^\dagger R_V \rangle + 2\langle L_V^\dagger L_V \rangle \langle R_V^\dagger R_V \rangle \\ &= 2\langle N \rangle + 2\langle N \rangle^2 \cos(\theta)^2 \ .\end{aligned} \tag{3.65}$$

Substituting these expressions into the equation for the total energy of the membrane, the change in energy of the membrane reads

$$\Delta H_M = \mu \delta N + \eta \left(\langle N \rangle + \langle N \rangle^2 \cos(\theta)^2 \right) \ . \tag{3.66}$$

This expression for the energy transfer to the membrane is again highly general in the sense that it holds for any photon number distribution as long as the initial distribution is the same in the two cavities and the optomechanical setup is in the weak coupling regime where the backaction of the membrane's motion on the photon's dynamics may be neglected.

For high temperature thermal gases the initial fluctuations in photon number $\delta N(0)$ will be substantial and so there is a large contribution to ΔH_M that is independent of θ, softening the distinguishability dependence of the energy transfer. However, for special non-classical initial states such as Fock states, the variance in photon number, $\delta N(0)$, may be negligible as compared to the average number of photons in each gas, $\langle N(0) \rangle$. In such quantum regimes, the energy transfer ΔH_M is proportional to $\langle N(0) \rangle$ for distinguishable gases since the cos-term in Eq. (3.66) vanishes. However, for indistinguishable gases the energy transfer is quadratically enhanced, scaling as $\langle N(0) \rangle^2$ in the limit of large photon numbers. This dependence of the energy transfer to the piston membrane on distinguishability is precisely the opposite to Gibbs mixing where work extraction is possible for distinguishable gases but not for indistinguishable gases. The difference in behaviour is perhaps unsurprising as the present mechanism does not rely on mixing but rather, as we explain in the following section, is a direct consequence of photon bunching as observed in the Hong-Ou-Mandel effect.

3.8 The role of photonic bunching

The photons in the cavity are subject to the well known Hong-Ou-Mandel (HOM) effect [147], a distinguishability dependent interference effect between two photons. Here we argue that the

HOM effect can explain the indistinguishability enhanced energy transfer to a BS membrane and further investigate the contribution of the HOM effect to the photon dynamics by calculating the correlation function, $\mathfrak{g}_{\mathrm{L,R}}$.

The Hong-Ou-Mandel (HOM) effect is maximised for perfectly indistinguishable photons and vanishes for perfectly distinguishable photons. When two perfectly distinguishable photons impinge on opposite sides of a beamsplitter simultaneously, there are four equally probable outcomes:

(a) the photon from the right is transmitted and the photon from the left is reflected,

(b) the photon from the left is transmitted and the photon from the right is reflected.

(c) both photons are transmitted,

(d) both photons are reflected,

However, when the two photons are indistinguishable, the amplitude for both photons to be reflected by the BS and the amplitude for both photons to be transmitted through the BS destructively interfere, and thus the probability for the photons to exit the beamsplitter through opposite sides vanishes. Indistinguishable photons are therefore guaranteed to leave a beamsplitter in the same mode, a phenomena known as 'bunching'.

To understand heuristically how this bunching affects the membrane dynamics, it is instructive to consider the initial state with one photon in each part of the cavity. When the two photons impinge on the beamsplitter, there are four equally likely outcomes, each of which generates a different effect on the motion of the membrane as sketched in Fig. 3.10. When the two photons leave the beamsplitter to different parts of the cavity there will be no net displacement to the membrane. However, when the two photons leave the beamsplitter to the left part of the cavity, the beamsplitter will be displaced to the right, and vice versa when the two photons leave the BS to the right part of the cavity. For both distinguishable and indistinguishable photons the average displacement of the membrane will be zero. However, the fluctuations in the position of the membrane will be greater for the case of indistinguishable photons because the probability for the membrane to be displaced to the left or right is double that for distinguishable photons. By the same argument, the time dependent bunching of indistinguishable photons will increase the effective driving force on the membrane and thereby increase its energy.

The degree of bunching of the photons in the cavity is quantifiable by the second order coherence correlation function $\mathfrak{g}$. The second-order correlation function between any two modes a and b is given by

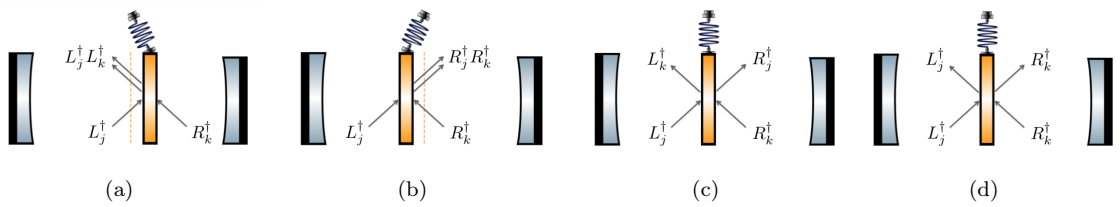
$$\mathfrak{g}_{a,b}(t) := \frac{\langle a^\dagger(t)b^\dagger(t)b(t)a(t)\rangle}{N_a(t)N_b(t)} \,, \tag{3.67}$$

where $\langle a^\dagger(t)b^\dagger(t)b(t)a(t)\rangle$ is the probability of measuring a photon in mode a and a photon in mode b at time t, and the product of

$$N_a(t) = \langle a^\dagger(t)a(t)\rangle \quad \text{and} \quad N_b(t) = \langle b^\dagger(t)b(t)\rangle \tag{3.68}$$

is a normalisation factor.

The second order correlation function is most often used to quantify the spacing of photons within a *single* mode, i.e. where $a = b$. A coherent light beam has randomly spaced photons and therefore a $\mathfrak{g}_{a,a}$ value of 1. If $\mathfrak{g}_{a,a}$ is greater than 1 the probability of measuring two photons simultaneously is greater than expected for a random beam of photons and in this sense the



(a) (b) (c) (d)

Figure 3.10: **HOM effect in optomechanical setting.** Elementary processes of the Hong-Ou-Mandel effect in the present optomechanical setup. In (a) the photon from the left is reflected and the photon from the right is transmitted and vice versa in (b). In (c) both photons are transmitted and in (d) both photons are reflected. When the photons are perfectly distinguishable, i.e. $j = H$ and $k = V$ or $j = V$ and $k = H$, then all four outcomes (a - d) are equally probable. When the photons are perfectly indistinguishable, *i.e.* $j = H$ and $k = H$ or $j = V$ and $k = V$, then the amplitudes for outcomes (c) and (d) destructively interfere and the outcomes (a) and (b) are equally probable.

photons are 'bunched' together. Thermal light with super-Poissonian statistics and a $\mathfrak{g}_{a,a}$ value of 2 is therefore bunched. In contrast, if $\mathfrak{g}_{a,a}$ is less than 1 then the probability of measuring two photons simultaneously is greater than expected for a random beam of photons and the photons are said to be 'antibunched'. The correlation function corresponding to an n photon Fock state scales as $1 - \frac{1}{n}$. Therefore a single Fock state photon is maximally antibunched with a $\mathfrak{g}_{a,a}$ of 0 but the degree of antibunching decreases as the number of photons is increased [184, 185].

We are primarily interested in the correlations between the *between* the left and right modes, rather than within a mode, that is $\mathfrak{g}_{L,R}(t)$ which can be written as

$$\mathfrak{g}_{L,R}(t) = \frac{\langle N_L(t) N_R(t) \rangle}{\langle N_L(t) \rangle \langle N_R(t) \rangle} \ . \tag{3.69}$$

A $\mathfrak{g}_{L,R}$ value of 0 entails that if we simultaneously measure the number of photons in the left and right cavities, we are certain to find at least one photon in the left cavity and zero photons in the right cavity, or vice versa, despite on average there being photons in both cavities. Thus, in contrast to the single mode correlation function, a $\mathfrak{g}_{\mathrm{L,R}}$ value of 0 indicates that the correlations between the photons in the cavities are such that the photons are bunched in a single cavity. Conversely, a $\mathfrak{g}_{\mathrm{L,R}}$ of 1 indicates that whenever a photon is measured in the one cavity, it is certain that at least one photon will be measured in the other cavity, indicating that the photons are evenly spread between the two cavities. In this way, we can use $\mathfrak{g}_{\mathrm{L,R}}$ to quantify the degree to which on measurement the photons bunch in one half of the optical cavity.

To verify that bunching is playing an active role in the dynamics we calculate the correlation function $\mathfrak{g}_{\mathrm{L,R}}(t)$ for cavities containing a BS and a PBS membrane. To do so, we use the expressions for the evolution of the creation and annihilation operators of the cavity modes on disregarding the back-action of the membrane on the photon dynamics,

$$\begin{aligned} L_p^\dagger &= \exp(-i\omega t) \left(L_p^\dagger(0) \cos\left(\frac{\lambda_p}{2} t\right) - i R_p^\dagger(0) \sin\left(\frac{\lambda_p}{2} t\right) \right) \quad \text{and} \\ R_p^\dagger &= \exp(-i\omega t) \left(R_p^\dagger(0) \cos\left(\frac{\lambda_p}{2} t\right) - i L_p^\dagger(0) \sin\left(\frac{\lambda_p}{2} t\right) \right) \quad \text{for} \quad j = H \text{ and } V \ . \end{aligned} \tag{3.70}$$

In what follows we describe for completeness the explicit time dependent behaviour of the correlation function, for perfectly distinguishable and perfectly indistinguishable photon gases, depending

on whether the photons in the gases are initially prepared in the thermal or Fock state configuration. However, if so wished, one can skip this detailed description and go straight to the punchline at Eq. (3.80).

Beamsplitter Membrane ($\lambda_H = \lambda_V = \lambda$): For indistinguishable photons, the correlation function can be written as

$$\mathfrak{g}_{\mathrm{L,R}}(t) = \frac{1}{4}\left(\left(1-\cos\left(2\lambda t\right)\right)\mathfrak{g}_{\mathrm{L,L}}(0) + 2 + 2\cos\left(2\lambda t\right)\right) \tag{3.71}$$

where $\mathfrak{g}_{\mathrm{L,L}}(0)$ denotes the initial correlation function within the left cavity, which is equal to the correlation function in the right cavity, $\mathfrak{g}_{\mathrm{R,R}}(0)$, since we assume the number distribution of the two photon gases are equal. When there is initially one precisely photon per cavity $\mathfrak{g}_{\mathrm{L,L}}$ vanishes and therefore $\mathfrak{g}_{\mathrm{L,R}}(t)$ evaluates to

$$\mathfrak{g}_{\mathrm{L,R}}(t) = \frac{1}{2}\left(1+\cos\left(2\lambda t\right)\right) \ . \tag{3.72}$$

As indicated by the light blue line in Fig. 3.11(a) the correlation function $\mathfrak{g}_{\mathrm{L,R}}(t)$ equals zero, and therefore the two photons are perfectly bunched, at intervals of

$$t = \lambda^{-1}\left(\frac{\pi}{4} + k\frac{\pi}{2}\right) \quad \forall k \quad \in \mathbb{N} \ . \tag{3.73}$$

For large Fock states $\mathfrak{g}_{\mathrm{L,L}}$ tends to 1 and therefore,

$$\mathfrak{g}_{\mathrm{L,R}}(t) = \frac{1}{4}\left(3+\cos\left(2\lambda t\right)\right) \ . \tag{3.74}$$

As shown by the solid dark blue line in Fig. 3.11(a), $\mathfrak{g}_{\mathrm{L,R}}(t)$ oscillates at the same frequency but the minimum value of $\mathfrak{g}_{\mathrm{L,R}}(t)$ is now 1/2 and therefore bunching is still occurring but to a lesser degree than the single photon gases. For thermal photons $\mathfrak{g}_{\mathrm{L,L}}(0)$ evaluates to 2 for all temperatures and therefore the correlation function is temperature independent and equal to

$$\mathfrak{g}_{\mathrm{L,R}}(t) = 1 \quad \forall t \ , \tag{3.75}$$

as indicated by the dotted red and orange lines.

For perfectly distinguishable photons, the correlation function can be written as

$$\mathfrak{g}_{\mathrm{L,R}}(t) = \frac{1}{4}\left(\left(1-\cos\left(2\lambda t\right)\right)\mathfrak{g}_{\mathrm{L,L}}(0) + 3 + \cos\left(2\lambda t\right)\right) \tag{3.76}$$

which reduces to

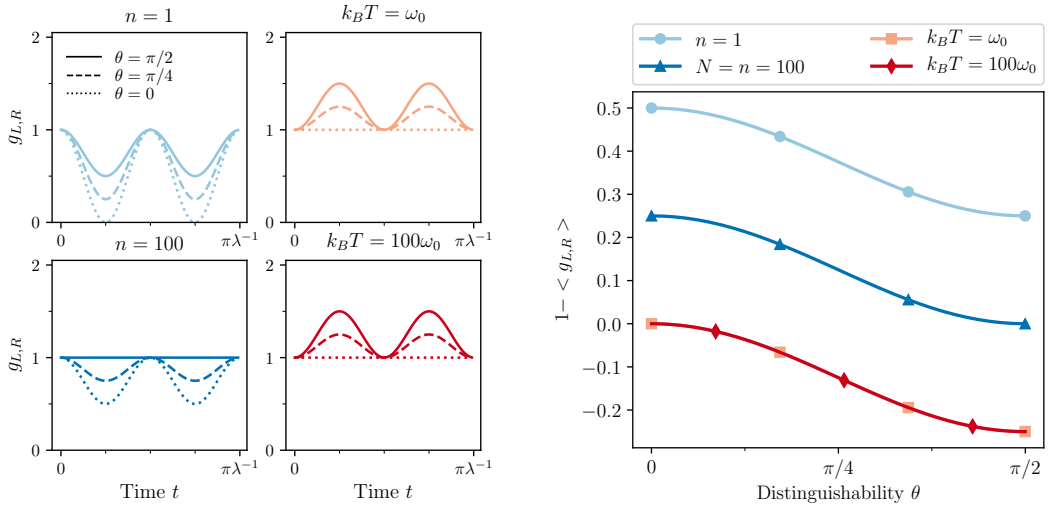
$$\mathfrak{g}_{\mathrm{L,R}}(t) = \frac{1}{4}\left(3+\cos\left(2\lambda t\right)\right) \tag{3.77}$$

for the Fock state configuration in which there is one photon per cavity and to

$$\mathfrak{g}_{\mathrm{L,R}}(t) = 1 \tag{3.78}$$

as the number of photons per cavity tends to infinity. These two cases are plotted by the solid light and dark blue lines in Fig. 3.11(a). Note that when there is one horizontal photon and one vertical photon per cavity there can be no interference effect and thus the dip in that case derives from the regular oscillation of the single horizontal photon between the two cavities rather than bosonic bunching. For thermal photons the correlation function takes the form

$$\mathfrak{g}_{\mathrm{L,R}}(t) = \frac{1}{4}\left(5-\cos\left(2\lambda t\right)\right) \tag{3.79}$$



(a) Initial state.

(b) Final state.

Figure 3.11: **Correlation functions for BS membrane.** In (a) we plot the $\mathfrak{g}_{\mathrm{L,R}}(t)$ correlation function as a function of time and in (b) we plot 1 minus the time average of the $\mathfrak{g}_{\mathrm{L,R}}(t)$ correlation function as a function of the distinguishability of the two photon gases θ. In both figures we plot the data for when the photons are initially in a Fock state with $n = 1$ photons per cavity (light blue squares) and $n = 100$ photons per cavity (dark blue circles) and for when the photons are initially in a thermal state at temperature $k_BT = 5\omega_L$ (peach diamonds) and $k_BT = 100\omega_L$ (red triangles).

for all temperatures. Thus for thermal photons, as indicated by the solid orange and red lines in Fig. 3.11(a), the photons $\mathfrak{g}_{\mathrm{L,R}}(t)$ takes a maximum value of $\frac{1}{2}$ indicating antibunching between the two cavities.

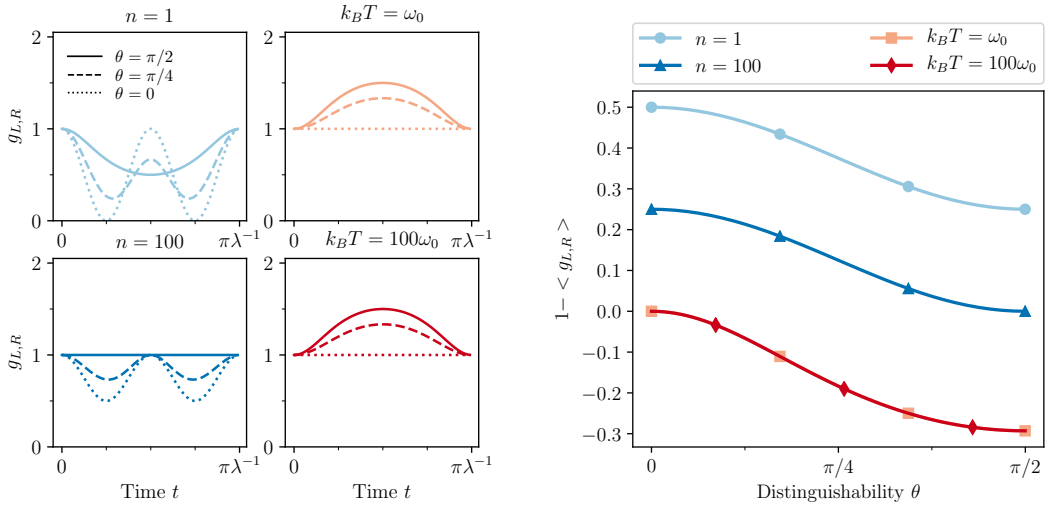
Above we have described the detailed time dependent behaviour of the second order correlation function for Fock state and thermal photon gases. However, we are primarily interested in the dependence of $\mathfrak{g}_{L,R}$ on distinguishability. To highlight this dependence and amalgamate the results above, it is insightful to consider the quantity

$$1 - \langle \mathfrak{g}_{\mathrm{L,R}}(t) \rangle = \frac{1}{4} \left(1 + \cos(\theta)^2 - \mathfrak{g}_{\mathrm{L,L}}(0) \right) \ . \tag{3.80}$$

where $\langle \mathfrak{g}_{\mathrm{L,R}}(t) \rangle$ denotes the time average of $\mathfrak{g}_{\mathrm{L,R}}(t)$. This quantity is a measure of the degree of bunching in the cavity. More precisely, it equals 0 when the photons are evenly spread between the two cavities but is positive for light bunched in a single cavity and negative for light that is antibunched between the two cavities.

As shown in Fig. 3.11(b), we find that, for all possible photon number distributions of the initial gases, the bunching within one half of the cavity decreases with the distinguishability of the photons. That is, bunching is most pronounced for indistinguishable gases, which is perfectly consistent with the Hong-Ou-Mandel effect. Indeed, the degree of bunching, as measured by Eq. (3.80), even has the same $\cos(\theta)^2$ dependence on distinguishability as the energy transfer to the membrane, Eq. (3.66). This further supports the argument that the enhanced energy transfer to the membrane for indistinguishable photons arises from photonic bunching.

Polarising beamsplitter membrane ($\lambda_H = \lambda$ and $\lambda_V = 0$): While the effect of photonic bunching is not as pronounced when the membrane is a polarising beamsplitter, it nonetheless



(a) Initial state.

(b) Final state.

Figure 3.12: **Correlation functions for PBS membrane.** In (a) we plot $\mathfrak{g}_{\mathrm{L,R}}(t)$ as a function of time for perfectly distinguishable photons ($\theta = \pi/2$, solid), partially distinguishable photons ($\theta = \pi/4$, dashed) and perfectly indistinguishable photons ($\theta = 0$, dotted). In (b) we plot 1 minus the time average of the $\mathfrak{g}_{\mathrm{L,R}}(t)$ dips shown in (a) as a function of distinguishability. The photons are initially in a Fock state and we plot data for a PBS membrane with $n = 1$ photons per cavity (red) and $n = 100$ photons per cavity (dark blue) and for a BS membrane with $n = 1$ photons per cavity (orange) and $n = 100$ photons per cavity (light blue).

plays a role in the dynamics. Of course, if both photon gases are horizontally polarised then the dynamics are the same whether there is a beamsplitter or a polarising beamsplitter in the cavity and therefore in this limit Eq. (3.71) holds unaltered for a PBS membrane. For the case of perfectly distinguishable photons interacting with a PBS membrane, that is $\theta = \pi/2$, the $\mathfrak{g}_{\mathrm{L,R}}(t)$ correlation function can be written as

$$\mathfrak{g}_{\mathrm{L,R}}(t) := \mathfrak{g}_{\mathrm{L,L}}(0) + (1 - \mathfrak{g}_{\mathrm{L,L}}(0))\frac{2}{3 - \cos(\lambda t)} \tag{3.81}$$

which is denoted by the solid lines in Fig. 3.12(a). Note that the frequency of the $\mathfrak{g}_{\mathrm{L,R}}$ dips is now half of that for indistinguishable photons or even distinguishable photons in the presence of a beamsplitter. This makes sense in the case of $n = 1$ because then there is one horizontal photon and one vertical photon per cavity and so there can be no interference effect rather the dip derives from the oscillation of the single horizontal photon between the two cavities. Nonetheless, the punchline is the same here as for a beamsplitter membrane. Specifically, as shown in Fig. 3.12(b), we find that the time average of the dips in $\mathfrak{g}_{\mathrm{L,R}}(t)$ increases, and therefore bunching decreases, with the distinguishability of the photons.

Thus bunching contributes to the dynamics of the PBS membrane piston for indistinguishable photons and therefore, as with the BS membrane, also contributes to the energy transfer to the membrane. We observed earlier that the energy transfer to the PBS membrane does not vanish for indistinguishable photons. At the time we attributed this to the fact that the the membrane is a microscopic quantum system that will experience heating from the membrane. The results in this section demonstrate that there is a quantum component to that heating effect, namely that the energy transfer partially arises from fluctuations in the dynamics of the membrane resulting from the back action of photonic bunching. However, in contrast to a BS membrane, for a PBS

membrane the energy transfer to the membrane nonetheless increases with distinguishability. This is because for a PBS membrane the effect of bunching is drowned out by the substantially larger effect of quantum Gibbs mixing when the two photons gases are distinguishable.

3.9 Experimental outlook

In this section we discuss how the results observed in this chapter could be experimentally verified. In general preparing the light field in the cavity in a thermal photonic state or a Fock state containing sufficiently many photons to have a non-negligible effect on the membrane is experimentally challenging. Instead, in this section we will discuss more realistic strategies whereby the cavities are driven by lasers. Additionally, while thus far we have considered an idealised lossless cavity and a frictionless membrane, in practise the effect of the dissipation of photons from the cavity and damping of the mechanical oscillator cannot be disregarded entirely. Therefore, we now phenomenologically incorporate these effects into our calculations.

3.9.1 Quantum Gibbs mixing with PBS membrane

Let us start by discussing how one could experimentally implement quantum Gibbs mixing using a polarising beamsplitter membrane. The aim of the experiment is to observe a work output that increases continuously with the distinguishability of the photon gases.

Given that in practise no cavity is entirely lossless, all photons initially in the cavity will eventually escape. Similarly, realistically the mechanical oscillator will be subject to damping effects. Consequently, in practise, any energy transfer to the membrane due to the initial photonic state will only be transient. Therefore, to observe a substantial work transfer to the membrane that varies with distinguishability we propose continuously driving the two cavities.

Specifically, we propose simultaneously strongly driving the left cavity with photons polarised at an angle θ and driving the right cavity with horizontally polarised photons. We assume that this driving is performed on resonance with the cavity frequency and that the two driving processes are in phase. This can be modelled by adding the following driving term to the Hamiltonian,

$$H_D = \hbar\epsilon \left((L_\theta + R_H)\exp(i\omega t) + (L_\theta^\dagger + R_H^\dagger)\exp(-i\omega t) \right) \tag{3.82}$$

where $L_\theta = \cos(\theta)L_H + \sin(\theta)L_V$ and ϵ is the laser driving amplitude.

To solve for the dynamics of the membrane we first switch to a frame rotating at the driving frequency. In this rotating frame the equation of motion of the photonic modes take the form

$$\frac{dL_H}{dt} = -i\left(-(gX_M + i\kappa)L_H + \frac{\lambda_H}{2}R_H + \epsilon\cos(\theta) \right) \tag{3.83}$$

$$\frac{dL_V}{dt} = -i\left(-(gX_M + i\kappa)L_V + \frac{\lambda_V}{2}R_V + \epsilon\sin(\theta) \right) \tag{3.84}$$

$$\frac{dR_H}{dt} = -i\left((gX_M - i\kappa)R_H + \frac{\lambda_H}{2}L_H + \epsilon \right) , \tag{3.85}$$

where κ, the rate of cavity dissipation, has been incorporated phenomenologically. Similarly, the equation of motion of the membrane now reads

$$\frac{d^2X_M}{dt^2} + \kappa_M\frac{dX_M}{dt} + \omega_M^2 X_M = \frac{F(g_H, g_V)}{m} , \tag{3.86}$$

where we account for the damping of the mechanical mode at rate κ_M.

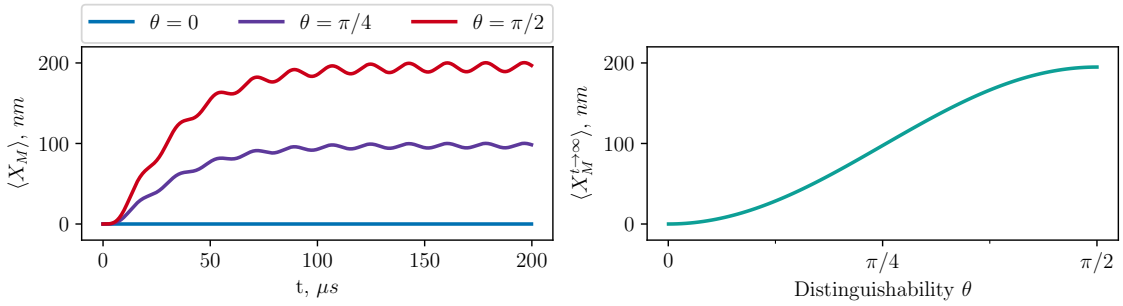


Figure 3.13: **Displacement of PBS membrane under proposed implementation.** The left hand figure plots the average displacement of the membrane as a function of time when the left cavity is driven by photons that are polarised at angle θ and the right cavity is driven by horizontally polarised photons. Polarisation angles $\theta = \pi/2$, $\theta = \pi/4$ and $\theta = 0$ are shown in blue, purple and red respectively. On the right, we plot our estimate for the steady state displacement of the membrane, Eq. (3.87), as a function of distinguishability. This confirms our estimate is accurate since the steady state displacements in the left hand plot for $\theta = 0$, $\theta = \pi/4$ and $\theta = \pi/2$ align well with the predicted displacements from the right hand plot. In both plots the parameters are taken from Table 3.9.1.

These coupled differential equations can be solved in the limit that the back-action of the photons on the membrane is negligible; however, in general the time dependent expressions are rather messy and uninsightful. In Fig. 3.13, we plot the average displacement of the membrane as a function of time assuming that the left and right cavities are initially in the vacuum state. The displacement of the membrane is largest for the mixing of perfectly distinguishable photon gases (red), vanishes for perfectly indistinguishable gases (blue) with the displacement for partially distinguishable gases with $\theta = \pi/4$ sitting between these two extremes.

In the limit[6] in which the cavity damping rate κ is substantially faster than the membrane damping rate κ_M, the displacement of the membrane increases initially before reaching a steady oscillatory state about a new displaced origin on the time scale $\kappa^{-1} \ll t \ll \kappa_M^{-1}$. To calculate this displaced origin we can disregard the membrane damping, that is set $\kappa_M = 0$, and evaluate the time averaged change in energy of the membrane in the limit of large t by dropping exponentially vanishing terms and averaging over the remaining sinusoidal terms. On doing so we obtain

$$\lim_{t\to\infty} \langle X_M(t) \rangle = \frac{4\epsilon^2 \hbar g_V}{m\kappa^2 \omega_M^2} \sin(\theta)^2 \tag{3.87}$$

in the limit that $g_V \gg g_H$ (as considered previously in Section 3.5). As shown by the right hand plot in Fig. 3.13, the above expression provides an accurate estimate of the position of the displaced origin of the membrane on the scale $\kappa^{-1} \ll t \ll \kappa_M^{-1}$. The displacement for this driven damped implementation is directly proportional to the displacement observed previously for the un-damped and un-driven case, Eq. (3.52). Thus we find again that the displacement of the membrane is expected to increase continuously with the distinguishability of the photon gases. Moreover, as argued previously, the potential energy associated with the new displaced origin of the membrane can be associated with a work output. Thus this driven implementation could be

[6]This limit is experimentally realisable for *beamsplitter* membranes as shown in Table 3.9.1. The data is currently unavailable for *polarising beamsplitter membranes*.

used to observe a continuous increase in the work output with distinguishability.

One might worry that since we are no longer considering a closed system, the work output can no longer be solely attributed to a mixing process and therefore this driven experimental implementation deviates from the original spirit of Gibbs' mixing experiment. This worry is, however, largely misplaced. The time averaged displacement of the membrane vanishes for indistinguishable gases and therefore any displacement to the membrane stems from the distinguishability of the photon gases. In this sense it would seem that the work output can, despite the driving, be solely attributed to mixing. The driving proposed here is primarily intended to compensate for the loss of the gases from the cavity due to damping. One could similarly imagine a variant of the classical Gibbs mixing setting where the box in which the gases are held is lossy and the gases are continually pumped into the box to compensate. In this setting, as in ours, the spirit of the experiment, a demonstration that the work output from mixing gases depends on their distinguishability, remains unchanged.

Experimental prospects. There does however remain one pretty fundamental sticking point. Fig. 3.13 is plotted using a set of typical experimental parameters for the standard BS 'membrane-in-the-middle' setup which we list in Table 3.9.1. We use this data, despite considering a PBS membrane here because, while the beamsplitter membranes used for standard 'membrane-in-the-middle' experiments are readily available, polarising beamsplitter membranes are not. The smallest polarising beamsplitters that are currently engineered are still several orders of magnitude thicker and heavier than the membranes that are typically used in 'membrane-in-the-middle' experiments [3, 186, 187]. Therefore current PBS membranes are too massive to experience a substantial impact from the photons in the cavity and furthermore cannot be considered quantum mechanical. Thus our proposed experiment is not viable in the short term; however, since the task of miniaturising membranes is an active field of research [186, 187] we hope that in the not too distant future the ultra-thin polarising beamsplitters which are required for our proposal will become available.

3.9.2 Indistinguishability enhanced energy transfer to BS membrane

Having discussed the outlook for an experimental implementation of Gibbs mixing using a PBS membrane, we proceed to discussing how one could experimentally observe the enhanced energy transfer to a BS membrane for indistinguishable photons that we found in Section 3.7. Since preparing the light field in the cavity in a thermal photonic state or large Fock states is experimentally challenging, we again consider driving strategies.

Intriguingly, the continuous driving strategy we used to implement quantum Gibbs mixing with the PBS membrane does not seem to generate a distinguishability dependent energy transfer here. That is, on re-running the calculation set out in the previous section, but this time for the case in which $\lambda_H = \lambda$ but $\lambda_V = 0$ and $g_V > g_H$, we find that the energy transfer to the membrane is independent of the distinguishability of the two photon gases. Interestingly, both the driving force exerted by the photons on the membrane and the energy transfer to the membrane is also substantially reduced in this case as compared to the PBS membrane. We therefore suggest that the lack of distinguishability dependence in the energy transfer for continuous driving stems from an interference effect akin to electromagnetic transparency induced effects observed elsewhere [2]. However, in all honesty, as of yet we are not entirely sure how to explain this phenomenon.

Parameter	Value
Membrane frequency ω_M	350kHz
Cavity frequency ω	20THz
Tunnelling rate λ	34GHz
Length of cavity L	93mm
Radiation pressure $\tilde{g}$	3.3kHz
Cavity decay rate κ	85kHz
Membrane quality factor Q	122000
Membrane damping rate $\kappa_M = \frac{\omega_M}{Q}$	1Hz
Membrane mass m	45ng
Laser power P	$25\mu W$
Driving Amplitude $\epsilon = \sqrt{\frac{P\kappa}{\hbar\omega}}$	39GHz

Table 3.2: **Experimental parameters.** Here we provide list of typical experimental parameters for 'membrane-in-the-middle' optomechanical setups to use to get a handle on the viability of our experimental proposals. All parameters are taken from [2], except for the tunnelling rate λ which is taken from [3] because [2] did not provide a value for the tunnelling rate. While these parameters are for a beamsplitter membrane, we also use them to discuss the experiment involving a polarising beamsplitter membrane because 'PBS-in-the-middle' setups are yet to be implemented and so the data is unavailable. For horizontal photons a PBS membrane acts as a perfect beamsplitter and so we expect g_H to be equal to g for a beamsplitter membrane. Conversely, for vertically polarised photons a PBS membrane acts as a mirror and so we expect g_V to be larger than g_H but we have been unable to find precise prediction for g_V in this case. Therefore, some what arbitrarily, we set $g_V = 6g_H$ for our calculations in Fig. 3.13.

Nonetheless, the enhanced energy transfer for indistinguishable photons observed in Eq. (3.66) applies to any initial state in the cavity, including coherent states, which can be generated by driving a cavity with a laser. This suggests that a pulsed driving strategy might be appropriate. If the cavities were driven with a pulse that is shorter than the tunnelling time of the membrane then the photons do not have time to tunnel between the two cavities during the driving processes. This removes the possibility of an unintended interference effect between the two pulses and, since they occur on separate time scales, we can consider the driving processes and tunnelling processes independently. As a consequence, during the driving process we are simply driving a single cavity mode with a coherent light source and it is well known that this generates a coherent state with respect to the driven mode.

We therefore propose driving the left modes of the cavity with an ultra short laser pulse of θ polarised photons and the right modes with an ultrashort pulse of horizontally polarised photons. This will generate a coherent state with polarisation θ in the left cavity and a coherent state of horizontally polarised photons in the right. If the photons are then left to oscillate between the two cavities, this will, as per Eq. (3.66), generate an enhanced energy transfer to the membrane for indistinguishable photons. More specifically, since both the mean and variance of the number for photons in a coherent state $|\alpha\rangle$ is $|\alpha|^2$, the change in energy of the membrane after the application of a single pair of pulses of light into the left and right cavities, each containing on average $|\alpha|^2$ photons, is given by

$$\Delta H_M = \mu|\alpha|^2 + \eta\left(|\alpha|^2 + |\alpha|^4\cos(\theta)^2\right) \ . \tag{3.88}$$

We therefore expect a significant distinguishability dependent contribution to the change in energy of the membrane under this proposed pulsed implementation.

The above expression calculated from Eq. (3.66) does not incorporate the effect of cavity and mechanical damping. Once these effects are incorporated we obtain a modified version of Eq. (3.88) with the same distinguishability and α dependence but new parameters μ and η which are reduced by the damping rates κ and κ_M. The equations of motion of the membrane and photons in the presence of damping but not driving read

$$\frac{d^2X_M}{dt^2} + \kappa_M\frac{dX_M}{dt} + \omega_M^2 X_M = \frac{\hbar g}{m}\left(\Delta N_H + \Delta N_V\right) \tag{3.89}$$

$$\frac{dL_p}{dt} = -i\left((\omega - gX_M - i\kappa)L_p + \frac{\lambda_p}{2}R_p\right) \tag{3.90}$$

$$\frac{dR_p}{dt} = -i\left((\omega + gX_M - i\kappa)R_p + \frac{\lambda_p}{2}L_p\right) \ , \tag{3.91}$$

On solving this set of coupled differential equations in the limit that the effect of the back-action of the photons on the membrane can be disregarded, we find that the change in energy of the membrane is given by

$$\langle H_M(t) - H_M(0)\rangle = u(t)\delta N + v(t)\left(\langle N\rangle + \langle N\rangle^2\cos(\theta)^2\right) \tag{3.92}$$

where $u(t)$ and $v(t)$ are oscillatory functions depending on the system parameters but not the initial state.

Similarly to the PBS implementation, and as shown in Fig. 3.14, in the experimentally realisable limit in which the cavity damping κ is much faster than the membrane damping κ_M, the energy of the membrane tends to an approximately constant value on the time scale $\kappa^{-1} \ll t \ll \kappa_M^{-1}$. In this limit, the long time averaged change in energy of the membrane,

$$\Delta H_M^{t\to\infty} = \lim_{t\to\infty}\langle H_M(t) - H_M(0)\rangle \ , \tag{3.93}$$

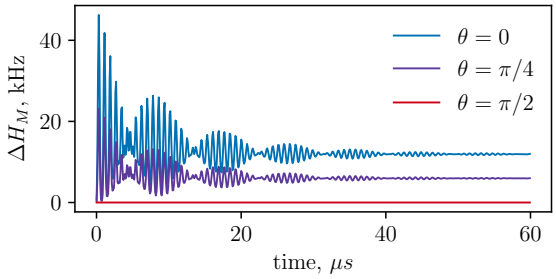


Figure 3.14: **Energy transfer to BS membrane in presence of damping.** We plot the average energy of the membrane as a function of time when the photons in the left cavity are vertically polarised and the photons in the right hand cavity are polarised at angle θ such that when $\theta = 0$ (blue) the photons are perfectly indistinguishable, when $\theta = \pi/2$ (red) the photons are perfectly distinguishable and when $\theta = \pi/4$ (purple) the photons are partially distinguishable. We suppose that the light in both cavities is in a coherent state containing 10^6 photons and use the parameters in Table 3.9.1.

is found by disregarding any terms that exponentially vanish in the limit of large t and averaging over remaining sinusoidal terms. On doing so we obtain,

$$\Delta H_M^{t\to\infty} = \mu\delta N + \eta\left(\langle N\rangle + \langle N\rangle^2\cos(\theta)^2\right) \tag{3.94}$$

where

$$\mu = \frac{2g^2}{m}\frac{2(4\kappa^2+\omega_M^2)+(\lambda^2+\omega_M^2)\delta_{\kappa,0}}{(4\kappa^2+(\lambda-\omega_M)^2)(4\kappa^2+(\lambda+\omega_M)^2)} \tag{3.95}$$

$$\eta = \frac{g^2}{m}\frac{2\lambda^2+(\lambda^2+\omega_M^2)\delta_{\kappa,0}}{(4\kappa^2+(\lambda-\omega_M)^2)(4\kappa^2+(\lambda+\omega_M)^2)}\,. \tag{3.96}$$

In the presence of cavity damping, that is for $\kappa \neq 0$, these expressions reduce to

$$\mu = \frac{2g^2}{m}\frac{2(4\kappa^2+\omega_M^2)}{(4\kappa^2+(\lambda-\omega_M)^2)(4\kappa^2+(\lambda+\omega_M)^2)} \tag{3.97}$$

$$\eta = \frac{2g^2}{m}\frac{\lambda^2}{(4\kappa^2+(\lambda-\omega_M)^2)(4\kappa^2+(\lambda+\omega_M)^2)}\,, \tag{3.98}$$

with the ratio of the prefactors given by

$$\frac{\eta}{\mu} = \frac{\lambda^2}{2(4\kappa^2+\omega_M^2)}\,. \tag{3.99}$$

Since κ and ω_M are typically several orders of magnitude smaller than λ, it follows that $\eta \gg \mu$ and therefore the distinguishability dependent term in Eq. 3.92 dominates over the fluctuation dependent term. The final expression for the energy transfer to the membrane after a single pair of pulses have dissipated from the cavity is given by Eq. (3.88) with the prefactors μ and η as defined by Eq. (3.95).

Experimental prospects. Pulsed optomechanical schemes have been both proposed [188, 189] and implemented [190] in the context of 'single mode' optomechanical setups where there is a single photonic mode and the mechanical mode is a movable cavity mirror. In this setting, the pulse length is required to be short compared to the mechanical frequency, ω_M. Using short pulses in single mode optomechanical systems enables one to probe the regime in which the back action of

the membrane's motion on the photons can be ignored. As far as we are aware, no pulsed schemes have yet been proposed or implemented in the context of 'membrane-in-the-middle' two mode optomechanical systems. However, as we will now discuss, the required experimental parameters do not sound insurmountably challenging.

To prepare a pulse that is sufficiently short that we can consider the driving processes and tunnelling processes independently, we require the length of the pulse, $\Delta\tau$, to be less than the tunnelling time, λ^{-1}, that is

$$\Delta\tau \ll \lambda^{-1} \, . \tag{3.100}$$

Since λ is usually on the order of GHZs [3,167,191], we require a laser pulse on the sub-nanosecond scale. This is readily achievable experimentally. Indeed the shortest pulses currently generated are on the attosecond scale [192]. Nonetheless, it does mean that the pulses required for the proposal here are several orders of magnitude shorter than those used for short pulse implementations in single mode optomechanical schemes [188–190].

While we require the pulse to be shorter than the tunnelling time, there are also constraints on quite how short the pulse can be. This is because, to ensure the photons in the cavity are only distinguishable via their polarisation, all the photons in the cavity are required to be of the same frequency. Therefore, we need to ensure that only a single frequency cavity mode of either polarisation in the two halves of the cavity is driven. Since the spacing between the cavity modes is on the order of the cavity frequency, we therefore require that the pulse bandwidth, $\Delta\omega_D$, is substantially less than the cavity frequency

$$\Delta\omega_D \ll \omega \, . \tag{3.101}$$

However, ultra-short laser pulses necessarily have a large bandwidth. This is forced by the pulse length and bandwidth product. For example, for a Gaussian shaped pulse this product cannot be smaller than 0.44, that is $\Delta\tau\Delta\omega_D > 0.44$ [192]. More generally, for most pulse shapes the pulse length bandwidth product is of the order of 1 thus we have roughly that

$$\Delta\omega_D \geq \Delta\tau^{-1} \, . \tag{3.102}$$

Combining the above three bounds, Eq. (3.100), Eq. (3.102) and Eq. (3.101), we obtain the following bound on the pulse length

$$\omega^{-1} \ll \Delta\tau \ll \lambda^{-1} \tag{3.103}$$

Since the cavity frequency is typically on the order of 10^{13}Hz [2, 167] or 10^{14}Hz [169] and the tunnelling rate is on the order of 10^{9}Hz [191] to 10^{10}Hz [3,167], we advocate using picosecond laser pulses.

For a fixed number of photons in a pulse, the length and intensity of a pulse are inversely correlated. We therefore need to be careful that the ultrashort laser pulses are not so intense that they damage the membrane while also ensuring that there are sufficiently many photons in the cavity to have a non-negligible effect on the energy of the membrane. Reference [190] uses a laser pulse of length 10^{-6}s that contains 10^{7} photons. Other implementations [189] have proposed using pulses containing between 10^{6} and 10^{9} photons and pulses on the order of 10^{-9}s. Assuming a 10^{-9}s pulse containing of the order of 10^{9} photons is of a manageable intensity, then a pulse of 10^{-12}s containing of the order of 10^{6} photons, should also be of an unproblematic intensity. However, this loose argument is not intended to be taken too literally. The number of photons a cavity can support and intensity a membrane can withstand is hardware specific and a more detailed analysis is required for any concrete proposed implementation.

We are now in a position to calculate the predicted energy transfer to the membrane. Specifically, using the parameters from Table 3.9.1, the prefactors μ and η in Eq. (3.94) evaluate to

$$\eta = 12 \times 10^{-9}\text{Hz} \quad \text{and} \quad \mu = 1.3 \times 10^{-18}\text{Hz} \, . \tag{3.104}$$

Therefore, it follows from Eq. (3.94), that the energy transfer to the membrane $\Delta H_M^{t\to\infty}$ for a pulse containing 6×10^6 indistinguishable photons is 430kHz, which would be sufficient to increase the energy of the membrane by a single phonon. Therefore we find that the effect of photonic bunching on the energy transfer to the membrane is small, a fact which is perhaps unsurprising, but perhaps not so small as to be beyond experimental detection.

The energy transfer to the membrane could be amplified by applying a train of laser pulses instead of a single laser pulse. For a train of n pulses that arrive before substantial membrane damping, that is on the time scale $t \ll \kappa_M^{-1}$, the cumulative change in energy of the membrane is equal to $n\,\Delta H_M^{t\to\infty}$. Since the damping rate of the cavity is typically several orders of magnitude greater than the membrane damping, this suggests that a train of a hundred pulses could raise the energy of the membrane substantially, increasing the viability of experimentally observing this effect.

3.10 Discussion and outlook

We started this chapter by remarking that while classically the work that can be extract from mixing two gases jumps discontinuously as their similarity is varied, the work that can be extracted from quantum gases is expected to vary smoothly with their distinguishability due to the impossibility of perfectly distinguishing non-orthogonal quantum states. To make this phenomena a little more concrete and provide a framework to investigate it further, we introduced the 'PBS-in-the-middle' optomechanical setting as a platform to study the mixing of photonic gases. Our study of the dynamics of this setting confirmed that the work output, as measured by the potential energy of the displaced PBS membrane, increases continuously with the angle of polarisation between the photon gases, in agreement with our expectations and in contrast with the classical case.

However, we were also hoping to gain a clearer understanding of how work could be extracted from the coherence of a quantum gas. As noted earlier, comparing the change in von Neumann entropy associated with mixing two homogeneous partially distinguishable gases, $|H\rangle$ and $|\theta\rangle$, with the change in von Neumann entropy associated with mixing the equivalent mixture, that is $|H\rangle$ and $\cos^2(\theta)\,|H\rangle\langle H| + \sin^2(\theta)\,|V\rangle\langle V|$, one would expect to be able to extract more work from mixing homogeneous gases than the mixtures. This, however, is not captured by our study thus far. The mixing work W_M depends only on the difference in the number of vertically polarised photons in the two cavities and thus is independent of the purity of the two gases. It therefore remains an open question whether this optomechanical setting can capture this feature of quantum Gibbs mixing.

Nonetheless, the beamsplitter interaction gives the photons access to coherent superpositions between the two halves of the cavity and the optomechanical interaction entangles the photons and the membrane. As a result, coherence and entanglement play an active role in the dynamics and thus the implementation is a genuinely quantum mechanical variant to Gibbs mixing.

The role of these quantum effects was brought into sharp relief by considering the thermodynamic consequences of mixing distinguishable and indistinguishable photons using a standard BS membrane (as opposed to a PBS membrane). Since a BS is a quantum mechanical analogue

of a fully permeable membrane, the work output from mixing vanishes as expected. Somewhat surprisingly, however, we found that the total energy transfer to the membrane does not vanish but rather, in a reversal of the usual Gibbs mixing distinguishability dependence, increases with indistinguishability. We attribute this effect, which to the best of our knowledge is a novel observation, to photonic bunching. While the phenomena is highlighted when the membrane is a perfect BS, a PBS acts as a BS for horizontally polarised photons and thus photonic bunching also contributes to the energy transfer to the PBS membrane when the photon gases are indistinguishable.

A natural question is whether this energy transfer should be interpreted as heat or work. While the question of how to define work [85, 86, 182] and heat [61, 193] in the quantum regime has been discussed extensively, in essence the distinction reduces to the extent to which the energy is 'useful' energy as opposed to un-directed fluctuating energy.

Since the mean position and momentum of the BS membrane vanishes at every instance in time, the average energy of the BS membrane can be written in terms of its position and momentum variances, with

$$\langle H_M(t)\rangle = \frac{m\omega^2\delta X(t)}{2} + \frac{\delta P(t)}{2m} \ . \tag{3.105}$$

Here $\delta Q = \langle Q(t)^2\rangle - \langle Q(t)\rangle^2$ is the variance of observable Q at time t for $Q = X_M$ and $Q = P_M$. The energy transfer ΔH_M is thus entirely given in terms of fluctuations in the position and momentum of the membrane, resulting from the entanglement between light field and mechanical degree of freedom. In this vein [194], it seems natural to classify the enhanced energy transfer to the BS membrane as heat rather than work.

For the case of the PBS membrane, the situation is more complex since the average position of the membrane only vanishes when the two photon gases are indistinguishable, while the momentum of the membrane only vanishes when taking its average over a complete oscillation cycle as well as the state of the setup. Nonetheless, we can split the change in the energy of the membrane into contributions from fluctuations and average behaviour

$$\langle H_M(t)\rangle = \frac{m\omega^2\langle X_M(t)\rangle^2}{2} + \frac{\langle P_M(t)\rangle^2}{2m} + \frac{m\omega^2\delta X_M(t)}{2} + \frac{\delta P_M(t)}{2m} \ . \tag{3.106}$$

It then follows that the time averaged change in energy of the membrane, ΔH_M, can be split into a work-like and a heat-like contribution

$$\Delta H_M = W_M + Q_M \ , \tag{3.107}$$

where the work term, W_M, is equal to the potential energy increase of the membrane associated with the displaced membrane defined in Eq. (3.47), and the heat flow, Q_M quantifies the increase in the membrane's fluctuations. More precisely, we define the heat flow as

$$Q_M := \frac{m\omega^2}{2}\langle \delta X_M(t) - \delta X_M(0)\rangle + \frac{1}{2m}\langle \delta P_M(t) - \delta P_M(0)\rangle \ , \tag{3.108}$$

where $\langle \delta X_M(t) - \delta X_M(0)\rangle$ and $\langle \delta P_M(t) - \delta P_M(0)\rangle$ are the time averaged change in the fluctuations in the displacement and momentum of the membrane respectively. For indistinguishable gases W_M vanishes and therefore the energy transfer to the PBS membrane is, similarly to the case of a BS membrane, purely heat-like. However, for distinguishable photons with a PBS membrane, W_M is large and therefore dominates the energy transfer to the membrane.

In this sense, it seems that for both a BS and PBS membrane there is a substantial heat-like component to the energy transfer to the membrane which is associated with the growth in the

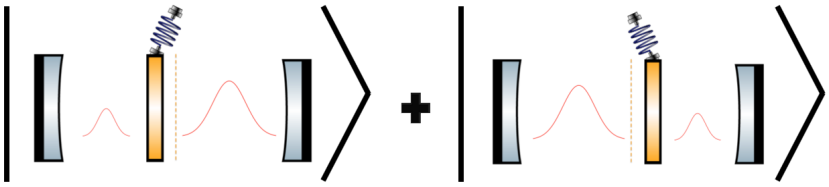


Figure 3.15: **Symmetric superposition state of photons and membrane.** The membrane is always in a symmetric superposition of different displacements. It is in a superposition of there being more photons on the right with the membrane displaced to the left and there being more photons on the left with the membrane displaced to the right. This symmetry is enforced by the mirror symmetry of the Hamiltonian which is invariant under a swap of the right and left modes combined with a change of sign of the displacement of the membrane. Thus, while the average displacement of the membrane vanishes, the variance to its displacement does not. Moreover, if we measure the number of photons in each cavity, the symmetric superposition will collapse leading to a well defined displacement and potential energy of the membrane.

membrane's fluctuations. Elsewhere energetic fluctuations induced by quantum measurement have been interpreted as a purely quantum component to heat exchange [61]. Here the bunching induced growth in the fluctuations and energy of the beamsplitter membrane might similarly be viewed as a quantum heat exchange but one due to quantum particle statistics. For both distinguishable and indistinguishable photons the optomechanical coupling entangles the photons and the membrane and as a consequence the oscillatory dynamics of the photons between the two cavities heats the membrane. However, when the photons are perfectly indistinguishable the resultant bunching of the photons increases this drive and thereby increasing the effective heating of the membrane. This additional heating component can be considered 'quantum' in virtue of originating from the permutation symmetry of Bosonic quantum states.

The role of quantum particle statistics in quantum thermodynamics is thus ripe for further investigation. It would be interesting to explore whether photonic bunching induces distinguishability dependent heating effects in other thermodynamical processes, or, indeed, to seek analogous signatures in Fermionic systems.

Although the energy transfer for indistinguishable gases to the PBS membrane and for all gases to the BS membrane is seemingly purely heat-like, it could plausibly be converted into work using a Szilard type protocol. The system's mirror symmetry could be broken with a measurement of the photon number in the left or right part of the cavity. As sketched in Fig. 3.15, the membrane is always in a superposition of there being more photons on the right with the membrane displaced to the left and there being more photons on the left with the membrane displaced to the right. However, a suitable measurement is likely to find a pronounced misbalance of photons between left and right, which corresponds to a substantial displacement, and thus potential energy, of the membrane. Indeed, the correlation function between the photon number difference and the displacement of the membrane,

$$\langle (N_L(t) - N_R(t)) X_M(t) \rangle = \nu(t)\delta N + \zeta(t) \left(\langle N \rangle + \langle N \rangle^2 \cos(\theta)^2 \right) \tag{3.109}$$

with $\nu(t)$ and $\zeta(t)$ oscillatory prefactors depending only the system parameters, features the same quadratic enhancement for indistinguishable photons as found in Eq. (3.66). This suggests that a reasonably simple Szilard-type extraction protocol [144], using auxiliary measurements on the

light field, would allow one to find a predictable displacement, and thus potential energy, of the membrane that increases with the indistinguishability of the photons in the cavity. It would be interesting to investigate whether such an approach could be used to develop a viable new strategy to exploit the bunching enhanced energy transfer for thermodynamic purposes such as thermal power generation or information-to-work conversion.

As well as the coherence of the polarisation and spatial degrees of freedom, there are a number of other pertinent differences between the current optomechanical setting and the classical thought experiment. While temperature enters the present analysis through the initial state of the photons and membrane, in the original analysis the gases continually thermalise with a heat bath. This feature of classical Gibbs mixing could be studied in the current setting either through a more detailed analysis of the dissipative coupling of the cavity and mechanical modes to their surrounding thermal environments or by using dye-molecules to actively mediate effective interactions between photons resulting in thermalisation [195, 196]. Since the mechanical and light modes interact with reservoirs of different natures, in practise there may exist a temperature gradient between the gases and the piston leading to additional thermodynamic effects.

An additional key difference between the current setting and the original analysis is the dependence of the pressure exerted on the membrane on the volume occupied by the photon gases. Classically, the pressure exerted depends inversely on the volume occupied by the photons, whereas here the pressure depends solely on the difference in the number of vertically and horizontally polarised photons on either side of the membrane, independently of the location of the membrane. Such effects could perhaps be investigated by studying higher order coupling regimes between the photonic and mechanical modes, leading to a rich spectrum of (thought) experiments on the quantum thermodynamics of mixing.

More generally, these results provide a perspective into the quantum mechanical generalisations of iconic thermodynamical experiments that can be discussed as thought-experiments or even, as we have argued, in the hopefully not so distant future might be realised as experiments. In addition to the continuous variation of distinguishability [152, 154] of the two photons gases, the present analysis gives a flavor of the rich physics that can be explored in terms of variations of properties of the membrane. One can imagine variants of the 'membrane-in-the-middle' optomechanical setting utilising alternative types of membranes. In addition to the semi-permeable membrane used in Gibbs mixing, many of the pioneering thought experiments in thermodynamics can be framed in terms of gases performing work on a membrane attached to a movable piston. For example, the Szilard-experiment [197] effectively uses a uni-directionally transmissive membrane and a Maxwell demon [198] could take the form of a fictitious semi-permeable membrane that separates fast and slow moving particles. This suggests that 'membrane-in-the-middle' optomechanics has wide ranging potential, not just as a platform to study the role of distinguishability and mixing in thermodynamics, but also for probing the fundamental relationships between information, heat and work.

Closing remarks

A fair question, and one which I have often been asked when presenting the material in this thesis, is *why construct physical realisations?* My default answer has been that if the assumptions that go into deriving a theoretical result do not hold for any real physical situation then we are not discussing physics but mathematics. Thus the aim of proposing physical realisations for quantum thermodynamics is to demonstrate that we are doing thermodynamics.

However, as I have written this thesis my answer has evolved. The process of proposing physical realisations can provide a new perspective on a topic and thus aid the teasing out of new conceptual insights and physical phenomena. This was observed in both projects. In the coherent fluctuation relations project, our coherent, squeezed and cat state relations were in fact originally derived so that we could test the FQC within the trapped ion implementation. However, it turned out that their specific form enabled us to discuss the extent to which coherence generates deviations from the classical Crooks relation. Similarly, in the optomechanical Gibbs mixing project, we set out to find a platform to study quantum Gibbs mixing and ended up discovering that the HOM effect can generate a quadratically enhanced energy transfer to the membrane for indistinguishable photons. These are both novel phenomena that were only brought to our attention by writing down a specific Hamiltonian and studying its behaviour.

I also increasingly believe that its overly harsh to claim that a theory which is unamendable to physical implementation is 'only mathematics' and not physics. We found when studying the information theoretic approach to quantum thermodynamics that what seemed at first a highly natural set of physical assumptions were surprisingly hard to satisfy when constructing physical implementations. However, rather than arguing that this demotes the results to status of mathematics, we suggested that these results could instead be understood as providing a conceptual framework for the study of quantum fluctuation relations.

Einstein's principle theory-constructive theory distinction is perhaps helpful again here. The QI approach is a principle theory which provides a unifying framework within which to understand the core content of quantum thermodynamics. However, principle theories are well complemented by constructive approaches. The process of proposing physical realisations forces you to engage with constructive theories and their concrete account of the microscopic constituents of physical systems. Moreover, the process of doing so may well shed fresh light on a topic and help tease out new results.

Bibliography

[1] Slow shutter speed photography: https://skylum.com/blog/an-introduction-to-slow-shutter-speed.

[2] M. Karuza, C. Biancofiore, M. Bawaj, C. Molinelli, M. Galassi, R. Natali, P. Tombesi, G. Di Giuseppe, and D. Vitali. Optomechanically induced transparency in a membrane-in-the-middle setup at room temperature. *Phys. Rev. A*, 88:013804, Jul 2013.

[3] M Karuza, M Galassi, C Biancofiore, C Molinelli, R Natali, P Tombesi, G Di Giuseppe, and D Vitali. Tunable linear and quadratic optomechanical coupling for a tilted membrane within an optical cavity: theory and experiment. *Journal of Optics*, 15(2):025704, dec 2012.

[4] Anatoly B. Kolomeisky and Michael E. Fisher. Molecular motors: A theorist's perspective. *Annual Review of Physical Chemistry*, 58(1):675–695, 2007. PMID: 17163836.

[5] Gregory S. Engel, Tessa R. Calhoun, Elizabeth L. Read, Tae-Kyu Ahn, Tomá*s* Man*c*al, Yuan-Chung Cheng, Robert E. Blankenship, and Graham R. Fleming. Evidence for wavelike energy transfer through quantum coherence in photosynthetic systems. *Nature*, 446(7137):782–786, 2007.

[6] Jennifer C. Brookes. Quantum effects in biology: golden rule in enzymes, olfaction, photosynthesis and magnetodetection. *Proceedings of the Royal Society A: Mathematical, Physical and Engineering Sciences*, 473(2201):20160822, 2017.

[7] R.A Cross. Molecular motors: The natural economy of kinesin. *Current Biology*, 7(10):R631 – R633, 1997.

[8] Ryszard Horodecki, Paweł Horodecki, Michał Horodecki, and Karol Horodecki. Quantum entanglement. *Rev. Mod. Phys.*, 81:865–942, Jun 2009.

[9] Nelly Huei Ying Ng and Mischa Prebin Woods. Resource theory of quantum thermodynamics: Thermal operations and second laws. In Felix Binder, Luis A. Correa, Christian Gogolin, Janet Anders, and Gerardo Adesso, editors, *Thermodynamics in the Quantum Regime: Fundamental Aspects and New Directions*, pages 625–650. Springer International Publishing, Cham, 2018.

[10] Fernando G. S. L. Brandão, Michał Horodecki, Jonathan Oppenheim, Joseph M. Renes, and Robert W. Spekkens. Resource theory of quantum states out of thermal equilibrium. *Phys. Rev. Lett.*, 111:250404, Dec 2013.

[11] D. Janzing, P. Wocjan, R. Zeier, R. Geiss, and Th. Beth. Thermodynamic cost of reliability and low temperatures: Tightening landauer's principle and the second law. *International Journal of Theoretical Physics*, 39(12):2717–2753, Dec 2000.

[12] Fernando G. S. L. Brandão, Michał Horodecki, Jonathan Oppenheim, Joseph M. Renes, and Robert W. Spekkens. Resource theory of quantum states out of thermal equilibrium. *Phys. Rev. Lett.*, 111:250404, Dec 2013.

[13] Michal Horodecki and Jonathan Oppenheim. Fundamental limitations for quantum and nanoscale thermodynamics. *Nature Communications*, 4:2059 EP –, Jun 2013.

[14] Sai Vinjanampathy and Janet Anders. Quantum thermodynamics. *Contemporary Physics*, 57(4):545–579, 2016.

[15] John Goold, Marcus Huber, Arnau Riera, Lídia del Rio, and Paul Skrzypczyk. The role of quantum information in thermodynamics—a topical review. *Journal of Physics A: Mathematical and Theoretical*, 49(14):143001, feb 2016.

[16] Felix Binder, Luis Correa, Christian Gogolin, Janet Anders, and Gerardo Adesso, editors. *Thermodynamics in the Quantum Regime*. Springer, 2019.

[17] Lídia del Rio, Johan Åberg, Renato Renner, Oscar Dahlsten, and Vlatko Vedral. The thermodynamic meaning of negative entropy. *Nature*, 474:61, Jun 2011.

[18] David Jennings and Terry Rudolph. Entanglement and the thermodynamic arrow of time. *Phys. Rev. E*, 81:061130, Jun 2010.

[19] Sandu Popescu, Anthony J. Short, and Andreas Winter. Entanglement and the foundations of statistical mechanics. *Nature Physics*, 2:754, Oct 2006.

[20] Fernando Brandão, Michał Horodecki, Nelly Ng, Jonathan Oppenheim, and Stephanie Wehner. The second laws of quantum thermodynamics. *Proceedings of the National Academy of Sciences*, 112(11):3275–3279, 2015.

[21] Matteo Lostaglio, David Jennings, and Terry Rudolph. Description of quantum coherence in thermodynamic processes requires constraints beyond free energy. *Nature Communications*, 6:6383, Mar 2015.

[22] Michał Horodecki and Jonathan Oppenheim. Fundamental limitations for quantum and nanoscale thermodynamics. *Nature Communications*, 4(1):2059, 2013.

[23] Johan Åberg. Truly work-like work extraction via a single-shot analysis. *Nature Communications*, 4:1925, Jun 2013.

[24] Johan Åberg. Catalytic coherence. *Phys. Rev. Lett.*, 113:150402, Oct 2014.

[25] Kamil Korzekwa, Matteo Lostaglio, Jonathan Oppenheim, and David Jennings. The extraction of work from quantum coherence. *New Journal of Physics*, 18(2):023045, 2016.

[26] Gilad Gour, David Jennings, Francesco Buscemi, Runyao Duan, and Iman Marvian. Quantum majorization and a complete set of entropic conditions for quantum thermodynamics. *Nature Communications*, 9(1):5352, 2018.

[27] Erick Hinds Mingo, Yelena Guryanova, Philippe Faist, and David Jennings. Quantum thermodynamics with multiple conserved quantities. In Felix Binder, Luis A. Correa, Christian Gogolin, Janet Anders, and Gerardo Adesso, editors, *Thermodynamics in the Quantum Regime: Fundamental Aspects and New Directions*, pages 751–771. Springer International Publishing, Cham, 2018.

[28] Yelena Guryanova, Sandu Popescu, Anthony J. Short, Ralph Silva, and Paul Skrzypczyk. Thermodynamics of quantum systems with multiple conserved quantities. *Nature Communications*, 7(1):12049, 2016.

[29] Matteo Lostaglio, David Jennings, and Terry Rudolph. Thermodynamic resource theories, non-commutativity and maximum entropy principles. *New Journal of Physics*, 19(4):043008, apr 2017.

[30] Tiago B. Batalhão, Stefano Gherardini, Jader P. Santos, Gabriel T. Landi, and Mauro Paternostro. Characterizing irreversibility in open quantum systems. In Felix Binder, Luis A. Correa, Christian Gogolin, Janet Anders, and Gerardo Adesso, editors, *Thermodynamics in the Quantum Regime: Fundamental Aspects and New Directions*, pages 395–410. Springer International Publishing, Cham, 2018.

[31] Tova Feldmann and Ronnie Kosloff. Performance of discrete heat engines and heat pumps in finite time. *Phys. Rev. E*, 61:4774–4790, May 2000.

[32] Ronnie Kosloff and Tova Feldmann. Discrete four-stroke quantum heat engine exploring the origin of friction. *Phys. Rev. E*, 65:055102, May 2002.

[33] Jan Klaers, Stefan Faelt, Atac Imamoglu, and Emre Togan. Squeezed thermal reservoirs as a resource for a nanomechanical engine beyond the carnot limit. *Phys. Rev. X*, 7:031044, Sep 2017.

[34] J. Roßnagel, O. Abah, F. Schmidt-Kaler, K. Singer, and E. Lutz. Nanoscale heat engine beyond the carnot limit. *Phys. Rev. Lett.*, 112:030602, Jan 2014.

[35] Gonzalo Manzano, Fernando Galve, Roberta Zambrini, and Juan M. R. Parrondo. Entropy production and thermodynamic power of the squeezed thermal reservoir. *Phys. Rev. E*, 93:052120, May 2016.

[36] Israel Reichental, Anat Klempner, Yariv Kafri, and Daniel Podolsky. Thermalization in open quantum systems. *Phys. Rev. B*, 97:134301, Apr 2018.

[37] Ahsan Nazir and Gernot Schaller. The reaction coordinate mapping in quantum thermodynamics. In Felix Binder, Luis A. Correa, Christian Gogolin, Janet Anders, and Gerardo Adesso, editors, *Thermodynamics in the Quantum Regime: Fundamental Aspects and New Directions*, pages 551–577. Springer International Publishing, Cham, 2018.

[38] Jake Iles-Smith, Neill Lambert, and Ahsan Nazir. Environmental dynamics, correlations, and the emergence of noncanonical equilibrium states in open quantum systems. *Phys. Rev. A*, 90:032114, Sep 2014.

[39] Philipp Strasberg, Gernot Schaller, Neill Lambert, and Tobias Brandes. Nonequilibrium thermodynamics in the strong coupling and non-markovian regime based on a reaction coordinate mapping. *New Journal of Physics*, 18(7):073007, Jul 2016.

[40] David Newman, Florian Mintert, and Ahsan Nazir. Performance of a quantum heat engine at strong reservoir coupling. *Phys. Rev. E*, 95:032139, Mar 2017.

[41] Akihito Kato and Yoshitaka Tanimura. Hierarchical equations of motion approach to quantum thermodynamics. In Felix Binder, Luis A. Correa, Christian Gogolin, Janet Anders, and Gerardo Adesso, editors, *Thermodynamics in the Quantum Regime: Fundamental Aspects and New Directions*, pages 579–595. Springer International Publishing, Cham, 2018.

[42] Gavin E. Crooks. Entropy production fluctuation theorem and the nonequilibrium work relation for free energy differences. *Phys. Rev. E*, 60:2721–2726, Sep 1999.

[43] Denis J. Evans and Debra J. Searles. Equilibrium microstates which generate second law violating steady states. *Phys. Rev. E*, 50:1645–1648, Aug 1994.

[44] C. Jarzynski. Nonequilibrium equality for free energy differences. *Phys. Rev. Lett.*, 78:2690–2693, Apr 1997.

[45] H. Tasaki. Jarzynski Relations for Quantum Systems and Some Applications. *eprint arXiv:cond-mat/0009244*, September 2000.

[46] J. Kurchan. A Quantum Fluctuation Theorem. *eprint arXiv:cond-mat/0007360*, July 2000.

[47] Peter Talkner and Peter Hänggi. The tasaki–crooks quantum fluctuation theorem. *Journal of Physics A: Mathematical and Theoretical*, 40(26):F569, 2007.

[48] Peter Hänggi and Peter Talkner. The other qft. *Nature Physics*, 11:108, Feb 2015.

[49] Michele Campisi, Peter Hänggi, and Peter Talkner. Colloquium: Quantum fluctuation relations: Foundations and applications. *Rev. Mod. Phys.*, 83:771–791, Jul 2011.

[50] John Goold, Francesco Plastina, Andrea Gambassi, and Alessandro Silva. The role of quantum work statistics in many-body physics. In Felix Binder, Luis A. Correa, Christian Gogolin, Janet Anders, and Gerardo Adesso, editors, *Thermodynamics in the Quantum Regime: Fundamental Aspects and New Directions*, pages 317–336. Springer International Publishing, Cham, 2018.

[51] F. Borgonovi, F.M. Izrailev, L.F. Santos, and V.G. Zelevinsky. Quantum chaos and thermalization in isolated systems of interacting particles. *Physics Reports*, 626:1 – 58, 2016. Quantum chaos and thermalization in isolated systems of interacting particles.

[52] Sven Dorosz, Thierry Platini, and Dragi Karevski. Work fluctuations in quantum spin chains. *Phys. Rev. E*, 77:051120, May 2008.

[53] L. Fusco, S. Pigeon, T. J. G. Apollaro, A. Xuereb, L. Mazzola, M. Campisi, A. Ferraro, M. Paternostro, and G. De Chiara. Assessing the nonequilibrium thermodynamics in a quenched quantum many-body system via single projective measurements. *Phys. Rev. X*, 4:031029, Aug 2014.

[54] Michael Knap, Aditya Shashi, Yusuke Nishida, Adilet Imambekov, Dmitry A. Abanin, and Eugene Demler. Time-dependent impurity in ultracold fermions: Orthogonality catastrophe and beyond. *Phys. Rev. X*, 2:041020, Dec 2012.

[55] Marco Schiró and Aditi Mitra. Transient orthogonality catastrophe in a time-dependent nonequilibrium environment. *Phys. Rev. Lett.*, 112:246401, Jun 2014.

[56] Guillaume Roux. Quenches in quantum many-body systems: One-dimensional bose-hubbard model reexamined. *Phys. Rev. A*, 79:021608, Feb 2009.

[57] Louis Villa and Gabriele De Chiara. Cavity assisted measurements of heat and work in optical lattices. *Quantum*, 2:42, Jan 2018.

[58] M. Heyl, A. Polkovnikov, and S. Kehrein. Dynamical quantum phase transitions in the transverse-field ising model. *Phys. Rev. Lett.*, 110:135704, Mar 2013.

[59] Michele Campisi and John Goold. Thermodynamics of quantum information scrambling. *Phys. Rev. E*, 95:062127, Jun 2017.

[60] Cyril Elouard and M. Hamed Mohammady. Work, heat and entropy production along quantum trajectories. In Felix Binder, Luis A. Correa, Christian Gogolin, Janet Anders, and Gerardo Adesso, editors, *Thermodynamics in the Quantum Regime: Fundamental Aspects and New Directions*, pages 363–393. Springer International Publishing, Cham, 2018.

[61] Cyril Elouard, David A. Herrera-Martí, Maxime Clusel, and Alexia Auffèves. The role of quantum measurement in stochastic thermodynamics. *npj Quantum Information*, 3(1):9, 2017.

[62] Jordan M. Horowitz. Quantum-trajectory approach to the stochastic thermodynamics of a forced harmonic oscillator. *Phys. Rev. E*, 85:031110, Mar 2012.

[63] Nicole Yunger Halpern. Toward physical realizations of thermodynamic resource theories. In Ian T. Durham and Dean Rickles, editors, *Information and Interaction: Eddington, Wheeler, and the Limits of Knowledge*, pages 135–166. Springer International Publishing, Cham, 2017.

[64] Johan Åberg. Fully quantum fluctuation theorems. *Phys. Rev. X*, 8:011019, Feb 2018.

[65] Zoe Holmes. The coherent crooks equality. In Felix Binder, Luis A. Correa, Christian Gogolin, Janet Anders, and Gerardo Adesso, editors, *Thermodynamics in the Quantum Regime: Fundamental Aspects and New Directions*, pages 301–316. Springer International Publishing, Cham, 2018.

[66] Zoë Holmes, Sebastian Weidt, David Jennings, Janet Anders, and Florian Mintert. Coherent fluctuation relations: from the abstract to the concrete. *Quantum*, 3:124, February 2019.

[67] Jan Liphardt, Sophie Dumont, Steven B. Smith, Ignacio Tinoco, and Carlos Bustamante. Equilibrium information from nonequilibrium measurements in an experimental test of jarzynski's equality. *Science*, 296(5574):1832–1835, 2002.

[68] D. Collin, F. Ritort, C. Jarzynski, S. B. Smith, I. Tinoco Jr, and C. Bustamante. Verification of the crooks fluctuation theorem and recovery of rna folding free energies. *Nature*, 437:231, Sep 2005.

[69] V. Blickle, T. Speck, L. Helden, U. Seifert, and C. Bechinger. Thermodynamics of a colloidal particle in a time-dependent nonharmonic potential. *Phys. Rev. Lett.*, 96:070603, Feb 2006.

[70] O.-P. Saira, Y. Yoon, T. Tanttu, M. Möttönen, D. V. Averin, and J. P. Pekola. Test of the jarzynski and crooks fluctuation relations in an electronic system. *Phys. Rev. Lett.*, 109:180601, Oct 2012.

[71] Gerhard Huber, Ferdinand Schmidt-Kaler, Sebastian Deffner, and Eric Lutz. Employing trapped cold ions to verify the quantum jarzynski equality. *Phys. Rev. Lett.*, 101:070403, Aug 2008.

[72] Shuoming An, Jing-Ning Zhang, Mark Um, Dingshun Lv, Yao Lu, Junhua Zhang, Zhang-Qi Yin, H. T. Quan, and Kihwan Kim. Experimental test of the quantum jarzynski equality with a trapped-ion system. *Nature Physics*, 11:193, Dec 2014.

[73] Tiago B. Batalhão, Alexandre M. Souza, Laura Mazzola, Ruben Auccaise, Roberto S. Sarthour, Ivan S. Oliveira, John Goold, Gabriele De Chiara, Mauro Paternostro, and Roberto M. Serra. Experimental reconstruction of work distribution and study of fluctuation relations in a closed quantum system. *Phys. Rev. Lett.*, 113:140601, Oct 2014.

[74] P. G. Di Stefano, J. J. Alonso, E. Lutz, G. Falci, and M. Paternostro. Nonequilibrium thermodynamics of continuously measured quantum systems: A circuit qed implementation. *Phys. Rev. B*, 98:144514, Oct 2018.

[75] Richard E. Spinney and Ian J. Ford. Fluctuation relations: A pedagogical overview. In Dr. Rainer Klages, Dr. Wolfram Just, and Prof. Christopher Jarzynski, editors, *Nonequilibrium Statistical Physics of Small Systems: Fluctuation Relations and Beyond*. Wiley-VCH, 2012.

[76] J. L. W. V. Jensen. Sur les fonctions convexes et les inégalités entre les valeurs moyennes. *Acta Math.*, 30:175–193, 1906.

[77] Félix Ritort. Work fluctuations, transient violations of the second law and free-energy recovery methods: Perspectives in theory and experiments. *Poincaré Seminar 2003*, page 193–226, 2004.

[78] T. Baumgratz, M. Cramer, and M. B. Plenio. Quantifying coherence. *Phys. Rev. Lett.*, 113:140401, Sep 2014.

[79] Michele Campisi, Peter Talkner, and Peter Hänggi. Fluctuation theorem for arbitrary open quantum systems. *Phys. Rev. Lett.*, 102:210401, May 2009.

[80] Chris Jarzynski. Nonequilibrium work theorem for a system strongly coupled to a thermal environment. *Journal of Statistical Mechanics: Theory and Experiment*, 2004(09):P09005, 2004.

[81] Tameem Albash, Daniel A. Lidar, Milad Marvian, and Paolo Zanardi. Fluctuation theorems for quantum processes. *Phys. Rev. E*, 88:032146, Sep 2013.

[82] Gonzalo Manzano, Jordan M. Horowitz, and Juan M. R. Parrondo. Nonequilibrium potential and fluctuation theorems for quantum maps. *Phys. Rev. E*, 92:032129, Sep 2015.

[83] Alexey E Rastegin. Non-equilibrium equalities with unital quantum channels. *Journal of Statistical Mechanics: Theory and Experiment*, 2013(06):P06016, 2013.

[84] A. E. Allahverdyan and Th. M. Nieuwenhuizen. Fluctuations of work from quantum subensembles: The case against quantum work-fluctuation theorems. *Phys. Rev. E*, 71:066102, Jun 2005.

[85] Peter Talkner, Eric Lutz, and Peter Hänggi. Fluctuation theorems: Work is not an observable. *Physical Review E*, 75:050102(R), May 2007.

[86] Peter Talkner and Peter Hänggi. Aspects of quantum work. *Phys. Rev. E*, 93:022131, Feb 2016.

[87] P. Solinas, H. J. D. Miller, and J. Anders. Measurement-dependent corrections to work distributions arising from quantum coherences. *Phys. Rev. A*, 96:052115, Nov 2017.

[88] A. E. Allahverdyan. Nonequilibrium quantum fluctuations of work. *Phys. Rev. E*, 90:032137, Sep 2014.

[89] Cyril Elouard and M. Hamed Mohammady. Work, heat and entropy production along quantum trajectories. In Felix Binder, Luis A. Correa, Christian Gogolin, Janet Anders, and Gerardo Adesso, editors, *Thermodynamics in the Quantum Regime: Fundamental Aspects and New Directions*, pages 363–393. Springer International Publishing, Cham, 2018.

[90] Harry J D Miller and Janet Anders. Time-reversal symmetric work distributions for closed quantum dynamics in the histories framework. *New Journal of Physics*, 19(6):062001, Jun 2017.

[91] Elisa Bäumer, Matteo Lostaglio, Martí Perarnau-Llobet, and Rui Sampaio. Fluctuating work in coherent quantum systems: Proposals and limitations. In Felix Binder, Luis A. Correa, Christian Gogolin, Janet Anders, and Gerardo Adesso, editors, *Thermodynamics in the Quantum Regime: Fundamental Aspects and New Directions*, pages 275–300. Springer International Publishing, Cham, 2018.

[92] Nikolaos Koukoulekidis, Rhea Alexander, Thomas Hebdige, and David Jennings. The geometry of passivity for quantum systems and a novel elementary derivation of the Gibbs state. *arXiv e-prints*, page arXiv:1912.07968, Dec 2019.

[93] Álvaro M. Alhambra, Lluis Masanes, Jonathan Oppenheim, and Christopher Perry. Fluctuating work: From quantum thermodynamical identities to a second law equality. *Phys. Rev. X*, 6:041017, Oct 2016.

[94] Sebastian Deffner and Christopher Jarzynski. Information processing and the second law of thermodynamics: An inclusive, hamiltonian approach. *Phys. Rev. X*, 3:041003, Oct 2013.

[95] Benjamin Morris and Gerardo Adesso. Quantum coherence fluctuation relations. *Journal of Physics A: Mathematical and Theoretical*, 51(41):414007, Sep 2018.

[96] Dénes Petz. Sufficient subalgebras and the relative entropy of states of a von neumann algebra. *Communications in Mathematical Physics*, 105(1):123–131, Mar 1986.

[97] Hyukjoon Kwon and M. S. Kim. Fluctuation Theorem for an Arbitrary Quantum Process. *ArXiv e-prints*, page arXiv:1810.03150, Oct 2018.

[98] Leslie E. Ballentine. *Quantum mechanics: A modern development.* World scientific, 1998.

[99] Eugen Wigner. Die gesamtquantenzahl. In *Gruppentheorie und ihre Anwendung auf die Quantenmechanik der Atomspektren*, pages 254–270. Vieweg+Teubner Verlag, Wiesbaden, 1931.

[100] E. Noether. Invariante variationsprobleme. *Nachrichten von der Gesellschaft der Wissenschaften zu Göttingen, Mathematisch-Physikalische Klasse*, 1918:235–257, 1918.

[101] Cristina Cirstoiu and David Jennings. Global and local gauge symmetries beyond lagrangian formulations, 2017.

[102] Thomas Hebdige and David Jennings. On the classification of two-qubit group orbits and the use of coarse-grained 'shape' as a superselection property. *Quantum*, 3:119, Feb 2019.

[103] E. Wigner. *Z. Phys.*, 133(101), 1952.

[104] Huzihiro Araki and Mutsuo M. Yanase. Measurement of quantum mechanical operators. *Phys. Rev.*, 120:622–626, Oct 1960.

[105] Mehdi Ahmadi, David Jennings, and Terry Rudolph. The wigner–araki–yanase theorem and the quantum resource theory of asymmetry. *New Journal of Physics*, 15(1):013057, jan 2013.

[106] William Feller. *An Introduction to Probability Theory and Its Applications, Volume 1*. Wiley, 2008.

[107] Erick Hinds Mingo and David Jennings. Superpositions of mechanical processes, decomposable coherence and fluctuation relations. *arXiv e-prints*, page arXiv:1812.08159, Dec 2018.

[108] Erick Hinds Mingo. *Irreversibility, Coherence and Quantum Fluctuation Relations*. PhD thesis, Imperial College London, 2020.

[109] D. Leibfried, R. Blatt, C. Monroe, and D. Wineland. Quantum dynamics of single trapped ions. *Rev. Mod. Phys.*, 75:281–324, Mar 2003.

[110] Robert Alicki. Model of quantum measurement and thermodynamical cost of accuracy and stability of information processing. *arXiv e-prints*, page arXiv:1305.4910, May 2013.

[111] James Binney and David Skinner. *The Physics of Quantum Mechanics*. Oxford University Press, 2013.

[112] Charles Kittel and Herbert Kroemer. *Thermal Physics*. W. H. Freeman, 1980.

[113] C. L. Clarke and I. J. Ford. Dissipation production in a closed two-level quantum system as a test of the obversibility of the dynamics. *ArXiv e-prints*, June 2018.

[114] Zoe Holmes, Erick Hinds Mingo, Calvin Y. R. Chen, and Florian Mintert. Quantifying athermality and quantum induced deviations from classical fluctuation relations. *arXiv e-prints*, page arXiv:2001.04926, Jan 2020.

[115] A. Perelomov. *Generalized Coherent States and Their Applications*. Theoretical and Mathematical Physics. Springer Berlin Heidelberg, 2012.

[116] F. T. Arecchi, Eric Courtens, Robert Gilmore, and Harry Thomas. Atomic coherent states in quantum optics. *Phys. Rev. A*, 6:2211–2237, Dec 1972.

[117] D. Stoler, B.E.A. Saleh, and M.C. Teich. Binomial states of the quantized radiation field. *Optica Acta: International Journal of Optics*, 32(3):345–355, 1985.

[118] A. Vidiella-Barranco and J. A. Roversi. Statistical and phase properties of the binomial states of the electromagnetic field. *Phys. Rev. A*, 50:5233–5241, Dec 1994.

[119] A Zavatta, V Parigi, M S Kim, and M Bellini. Subtracting photons from arbitrary light fields: experimental test of coherent state invariance by single-photon annihilation. *New Journal of Physics*, 10(12):123006, Dec 2008.

[120] Masahito Ueda, Nobuyuki Imoto, and Tetsuo Ogawa. Quantum theory for continuous photodetection processes. *Phys. Rev. A*, 41:3891–3904, Apr 1990.

[121] Stephen M. Barnett, Gergely Ferenczi, Claire R. Gilson, and Fiona C. Speirits. Statistics of photon-subtracted and photon-added states. *Phys. Rev. A*, 98:013809, Jul 2018.

[122] J. Hlou*š*ek, M. Je*ž*ek, and R. Filip. Work and information from thermal states after subtraction of energy quanta. *Scientific Reports*, 7(1):13046, 2017.

[123] Mihai D. Vidrighin, Oscar Dahlsten, Marco Barbieri, M. S. Kim, Vlatko Vedral, and Ian A. Walmsley. Photonic maxwell's demon. *Phys. Rev. Lett.*, 116:050401, Feb 2016.

[124] S. Weidt, J. Randall, S. C. Webster, E. D. Standing, A. Rodriguez, A. E. Webb, B. Lekitsch, and W. K. Hensinger. Ground-state cooling of a trapped ion using long-wavelength radiation. *Phys. Rev. Lett.*, 115:013002, Jun 2015.

[125] S. Weidt, J. Randall, S. C. Webster, K. Lake, A. E. Webb, I. Cohen, T. Navickas, B. Lekitsch, A. Retzker, and W. K. Hensinger. Trapped-ion quantum logic with global radiation fields. *Phys. Rev. Lett.*, 117:220501, Nov 2016.

[126] E. A. Hinds and Stephen M. Barnett. Momentum exchange between light and a single atom: Abraham or minkowski? *Phys. Rev. Lett.*, 102:050403, Feb 2009.

[127] A Roy, S De, Bindiya Arora, and B K Sahoo. Accurate determination of black-body radiation shift, magic and tune-out wavelengths for the 6s 1/2 to 5d 3/2 clock transition in yb +. *Journal of Physics B: Atomic, Molecular and Optical Physics*, 50(20):205201, 2017.

[128] Kevin J. Weatherill. *A C02 laser lattice experiment for cold atoms.* PhD thesis, Durham University, 2007.

[129] Nathanaël Cottet, Sébastien Jezouin, Landry Bretheau, Philippe Campagne-Ibarcq, Quentin Ficheux, Janet Anders, Alexia Auffèves, Rémi Azouit, Pierre Rouchon, and Benjamin Huard. Observing a quantum maxwell demon at work. *Proceedings of the National Academy of Sciences*, 114(29):7561–7564, 2017.

[130] Jürgen Eschner, Giovanna Morigi, Ferdinand Schmidt-Kaler, and Rainer Blatt. Laser cooling of trapped ions. *JOSA B*, 20(5):1003–1015, 2003.

[131] K. G. Johnson, J. D. Wong-Campos, B. Neyenhuis, J. Mizrahi, and C. Monroe. Ultrafast creation of large schrödinger cat states of an atom. *Nature Communications*, 8(1):697, 2017.

[132] C. T. Schmiegelow, H. Kaufmann, T. Ruster, J. Schulz, V. Kaushal, M. Hettrich, F. Schmidt-Kaler, and U. G. Poschinger. Phase-stable free-space optical lattices for trapped ions. *Phys. Rev. Lett.*, 116:033002, Jan 2016.

[133] D. von Lindenfels, O. Gräb, C. T. Schmiegelow, V. Kaushal, J. Schulz, Mark T. Mitchison, John Goold, F. Schmidt-Kaler, and U. G. Poschinger. Spin heat engine coupled to a harmonic-oscillator flywheel. *Phys. Rev. Lett.*, 123:080602, Aug 2019.

[134] Florian Mintert and Christof Wunderlich. Ion-trap quantum logic using long-wavelength radiation. *Phys. Rev. Lett.*, 87:257904, Nov 2001.

[135] M. Johanning, A. Braun, N. Timoney, V. Elman, W. Neuhauser, and Chr. Wunderlich. Individual addressing of trapped ions and coupling of motional and spin states using rf radiation. *Phys. Rev. Lett.*, 102:073004, Feb 2009.

[136] K. Lake, S. Weidt, J. Randall, E. D. Standing, S. C. Webster, and W. K. Hensinger. Generation of spin-motion entanglement in a trapped ion using long-wavelength radiation. *Phys. Rev. A*, 91:012319, Jan 2015.

[137] Niels Lörch, Christoph Bruder, Nicolas Brunner, and Patrick P Hofer. Optimal work extraction from quantum states by photo-assisted cooper pair tunneling. *Quantum Science and Technology*, 3(3):035014, 2018.

[138] Á. M. Alhambra, M. Lostaglio, and C. Perry. Heat-Bath Algorithmic Cooling with Thermal Operations. *ArXiv e-prints*, July 2018.

[139] Johannes Roßnagel, Samuel T. Dawkins, Karl N. Tolazzi, Obinna Abah, Eric Lutz, Ferdinand Schmidt-Kaler, and Kilian Singer. A single-atom heat engine. *Science*, 352(6283):325–329, 2016.

[140] Juliette Monsel, Cyril Elouard, and Alexia Auffèves. An autonomous quantum machine to measure the thermodynamic arrow of time. *npj Quantum Information*, (1):59, 2018.

[141] Hermann. Weyl. *Space-Time-Matter*. Dover, 1950.

[142] J.W. Gibbs. On the equilibrium of heterogeneous substances. *Connecticut Acad. Sci.*, 1875-1878.

[143] Martin Plesch, Oscar Dahlsten, John Goold, and Vlatko Vedral. Maxwell's daemon: information versus particle statistics. *Scientific reports*, 4:6995–6995, Nov 2014.

[144] J. Bengtsson, M. Nilsson Tengstrand, A. Wacker, P. Samuelsson, M. Ueda, H. Linke, and S. M. Reimann. Quantum szilard engine with attractively interacting bosons. *Phys. Rev. Lett.*, 120:100601, Mar 2018.

[145] Zoë Holmes, Florian Mintert, and Janet Anders. Gibbs mixing of partially distinguishable photons with a polarising beamsplitter membrane. *arXiv e-prints*, page arXiv:2006.00613, May 2020.

[146] Zoë Holmes, Janet Anders, and Florian Mintert. Enhanced energy transfer to an optomechanical piston from indistinguishable photons. *Phys. Rev. Lett.*, 124:210601, May 2020.

[147] C. K. Hong, Z. Y. Ou, and L. Mandel. Measurement of subpicosecond time intervals between two photons by interference. *Phys. Rev. Lett.*, 59:2044–2046, Nov 1987.

[148] E. T. Jaynes. The gibbs paradox. In C. R. Smith et al., editor, *Maximum Entropy and Bayesian Methods*. Kluwer Acad. Pub., 1991.

[149] Simon Saunders. The gibbs paradox. *Entropy*, 20:552, 2018.

[150] Dennis Dieks. The gibbs paradox and particle individuality. *Entropy*, 20:466, 2018.

[151] A. E. Allahverdyan and Th. M. Nieuwenhuizen. Explanation of the gibbs paradox within the framework of quantum thermodynamics. *Phys. Rev. E*, 73:066119, Jun 2006.

[152] V.L. Luboshitz and M.I. Podgoretskii. The Gibbs paradox. *Sov. Phys. Usp.*, 14:662, 1972.

[153] Claude Cohen-Tannoudji Bernard Diu and Franck Laloë. *Quantum Mechanics*. Wiley, 1973.

[154] E. Schrödinger. *Statistical Thermodynamics*. Cambridge University Press, 1952.

[155] A. Landè. *New Foundations of Quantum Mechanics*. Cambridge University Press, 1926.

[156] A. Landè. *Foundations of Quantum Theory*. Yale University Press, 1952.

[157] I.E. Tamm. *Usp. Fiz. Nauk*, 6:112, 1926.

[158] M.J. Klein. *Am. J. Phys.*, 26:80, 1958.

[159] A. Peres. *Quantum Theory: Concepts and Methods*. Springer, 1995.

[160] Koji Maruyama, ***C***aslav Brukner, and Vlatko Vedral. Thermodynamical cost of accessing quantum information. *Journal of Physics A: Mathematical and General*, 38(32):7175–7181, Jul 2005.

[161] A. E Allahverdyan, R Balian, and Th. M Nieuwenhuizen. Maximal work extraction from finite quantum systems. *Europhysics Letters (EPL)*, 67(4):565–571, Aug 2004.

[162] Alexander S. Holevo. Bounds for the quantity of information transmitted by a quantum communication channel. 1973.

[163] Michael A. Nielsen and Isaac L. Chuang. *Quantum Computation and Quantum Information*. Cambridge University Press, 2000.

[164] G. Weihs and A. Zeilinger. Photon statistics at beam-splitters: an essential tool in quantum information and teleportation. In J. Perina, editor, *Coherence and Statistics of Photons and Atoms*. Wiley and Wiley,, 2001.

[165] Florian Marquardt Markus Aspelmeyer, Tobias J. Kippenberg, editor. *Cavity Optomechanics*. Springer, 2014.

[166] Markus Aspelmeyer, Tobias J. Kippenberg, and Florian Marquardt. Cavity optomechanics. *Rev. Mod. Phys.*, 86:1391–1452, Dec 2014.

[167] J. D. Thompson, B. M. Zwickl, A. M. Jayich, Florian Marquardt, S. M. Girvin, and J. G. E. Harris. Strong dispersive coupling of a high-finesse cavity to a micromechanical membrane. *Nature*, 452:72 EP –, 03 2008.

[168] A M Jayich, J C Sankey, B M Zwickl, C Yang, J D Thompson, S M Girvin, A A Clerk, F Marquardt, and J G E Harris. Dispersive optomechanics: a membrane inside a cavity. *New Journal of Physics*, 10(9):095008, sep 2008.

[169] J. C. Sankey, C. Yang, B. M. Zwickl, A. M. Jayich, and J. G. E. Harris. Strong and tunable nonlinear optomechanical coupling in a low-loss system. *Nature Physics*, 6:707 EP –, 06 2010.

[170] D. Lee, M. Underwood, D. Mason, A. B. Shkarin, S. W. Hoch, and J. G. E. Harris. Multimode optomechanical dynamics in a cavity with avoided crossings. *Nature Communications*, 6:6232 EP –, 02 2015.

[171] Christoph Reinhardt, Tina Müller, Alexandre Bourassa, and Jack C. Sankey. Ultralow-noise sin trampoline resonators for sensing and optomechanics. *Phys. Rev. X*, 6:021001, Apr 2016.

[172] Cyril Elouard, Maxime Richard, and Alexia Auffèves. Reversible work extraction in a hybrid opto-mechanical system. *New Journal of Physics*, 17(5):055018, may 2015.

[173] M. Brunelli, L. Fusco, R. Landig, W. Wieczorek, J. Hoelscher-Obermaier, G. Landi, F. L. Semião, A. Ferraro, N. Kiesel, T. Donner, G. De Chiara, and M. Paternostro. Experimental determination of irreversible entropy production in out-of-equilibrium mesoscopic quantum systems. *Phys. Rev. Lett.*, 121:160604, Oct 2018.

[174] Michael Konopik, Alexander Friedenberger, Nikolai Kiesel, and Eric Lutz. Nonequilibrium information erasure below kTln2. *arXiv e-prints*, page arXiv:1806.01034, Jun 2018.

[175] Juliette Monsel, Cyril Elouard, and Alexia Auffèves. An autonomous quantum machine to measure the thermodynamic arrow of time. *npj Quantum Information*, 4(1):59, 2018.

[176] Subrahmanyan Chandrasekhar. *Radiative Transfer*. Oxford University Press, 1950.

[177] T P Purdy, R W Peterson, P-L Yu, and C A Regal. Cavity optomechanics with si3n4membranes at cryogenic temperatures. *New Journal of Physics*, 14(11):115021, nov 2012.

[178] D E Chang, A H Safavi-Naeini, M Hafezi, and O Painter. Slowing and stopping light using an optomechanical crystal array. *New Journal of Physics*, 13(2):023003, feb 2011.

[179] Yu Zhou, Fu-li Li, Bin Bai, Hui Chen, Jianbin Liu, Zhuo Xu, and Huaibin Zheng. Super-bunching pseudothermal light. *Phys. Rev. A*, 95:053809, May 2017.

[180] A. Nunnenkamp, K. Børkje, and S. M. Girvin. Single-photon optomechanics. *Phys. Rev. Lett.*, 107:063602, Aug 2011.

[181] P. Kammerlander and J. Anders. Coherence and measurement in quantum thermodynamics. *Scientific Reports*, 6:22174, Feb 2016.

[182] Martí Perarnau-Llobet, Elisa Bäumer, Karen V. Hovhannisyan, Marcus Huber, and Antonio Acin. No-go theorem for the characterization of work fluctuations in coherent quantum systems. *Phys. Rev. Lett.*, 118:070601, Feb 2017.

[183] Matteo Lostaglio. Quantum fluctuation theorems, contextuality, and work quasiprobabilities. *Phys. Rev. Lett.*, 120:040602, Jan 2018.

[184] Mark Fox. *Quantum Optics*. Oxford University Press, 2006.

[185] Rodney Loudon. *The Quantum Theory of Light*. Oxford University Press, 2000.

[186] R. M. A. Azzam. Simplified design of thin-film polarizing beam splitter using embedded symmetric trilayer stack. *Appl. Opt.*, 50(19):3316–3320, Jul 2011.

[187] Li Li and J. A. Dobrowolski. High-performance thin-film polarizing beam splitter operating at angles greater than the critical angle. *Appl. Opt.*, 39(16):2754–2771, Jun 2000.

[188] M. R. Vanner, I. Pikovski, G. D. Cole, M. S. Kim, ***C***. Brukner, K. Hammerer, G. J. Milburn, and M. Aspelmeyer. Pulsed quantum optomechanics. *Proceedings of the National Academy of Sciences*, 108(39):16182–16187, 2011.

[189] James S Bennett and Warwick P Bowen. Rapid mechanical squeezing with pulsed optomechanics. *New Journal of Physics*, 20(11):113016, Nov 2018.

[190] M. R. Vanner, J. Hofer, G. D. Cole, and M. Aspelmeyer. Cooling-by-measurement and mechanical state tomography via pulsed optomechanics. *Nature Communications*, 4(1):2295, 2013.

[191] Max Ludwig, Amir H. Safavi-Naeini, Oskar Painter, and Florian Marquardt. Enhanced quantum nonlinearities in a two-mode optomechanical system. *Phys. Rev. Lett.*, 109:063601, Aug 2012.

[192] Francesca Calegari, Giuseppe Sansone, Salvatore Stagira, Caterina Vozzi, and Mauro Nisoli. Advances in attosecond science. *Journal of Physics B: Atomic, Molecular and Optical Physics*, 49(6):062001, Feb 2016.

[193] Felix Binder, Sai Vinjanampathy, Kavan Modi, and John Goold. Quantum thermodynamics of general quantum processes. *Phys. Rev. E*, 91:032119, Mar 2015.

[194] Wojciech H. Zurek. Eliminating ensembles from equilibrium statistical physics: Maxwell's demon, Szilard's engine, and thermodynamics via entanglement. *Physrep*, 755:1–21, Oct 2018.

[195] Jan Klaers, Julian Schmitt, Frank Vewinger, and Martin Weitz. Bose–einstein condensation of photons in an optical microcavity. *Nature*, 468:545 EP –, 11 2010.

[196] Benjamin T. Walker, Lucas C. Flatten, Henry J. Hesten, Florian Mintert, David Hunger, Aurélien A. P. Trichet, Jason M. Smith, and Robert A. Nyman. Driven-dissipative non-equilibrium bose–einstein condensation of less than ten photons. *Nature Physics*, 14(12):1173–1177, 2018.

[197] L. Szilard. Uber die entropieverminderung in einem thermodynamischen system bei eingriffen intelligenter wesen. *Z. Phys.*, 53:840–856, 1929.

[198] James Clerk Maxwell. *Theory of heat.* Longmans, Green, and Co., 1908.

[199] Hector Manuel Moya-Cessa and Francisco Soto-Eguibar. *Introduction to Quantum Optics.* Rinton Press, 2011.

[200] Christopher Gerry and Peter Knight. *Introductory Quantum Optics.* Cambridge UP, 2005.

Appendix A

Evidence of hostility

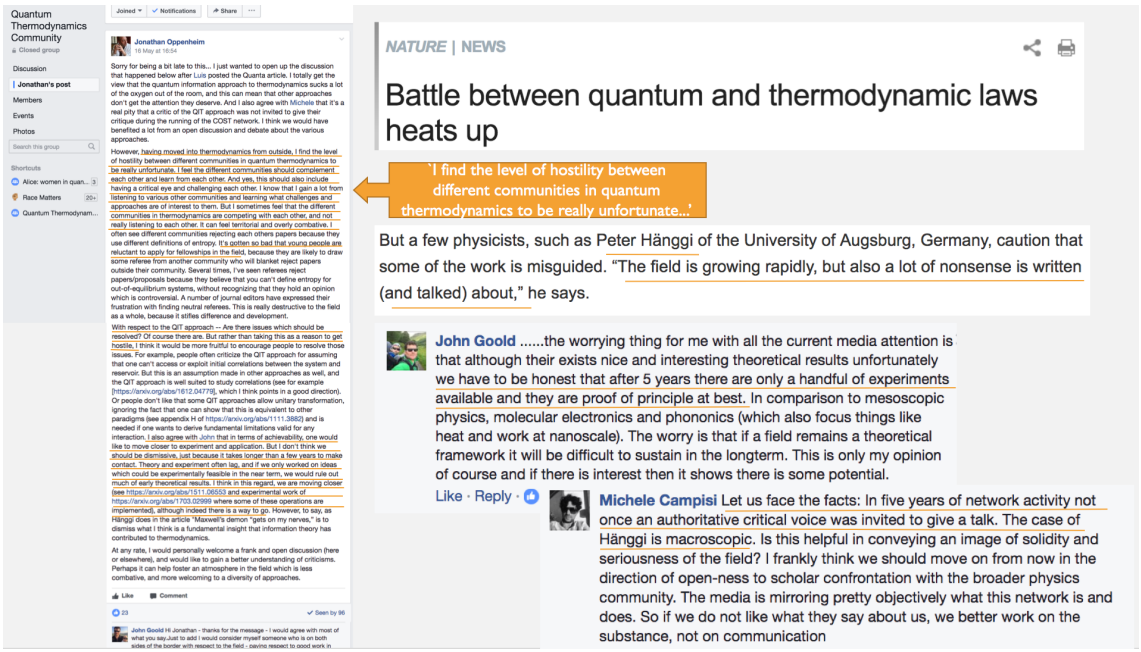


Figure A.1: **Quotes on quantum thermodynamics community.** These are a selection of quotes from physicists working in Quantum Thermodynamics on current tensions within the community. The facebook posts from Oppenheim, Goold and Campisi are taken from the COST network 2017 Quantum Thermodynamics conference page. The quote from Hänggi is taken from the a review of this conference that was published in Nature News.

Transcript of Oppenheim post: "Sorry for being a bit late to this... I just wanted to open up the discussion that happened below after Luis posted the Quanta article. I totally get the view that the quantum information approach to thermodynamics sucks a lot of the oxygen out of the room, and this can mean that other approaches don't get the attention they deserve. And I also agree with Michele that it's a real pity that a critic of the QIT approach was not invited to give their critique during the running of the COST network. I think we would have benefited a lot from an open discussion and debate about the various approaches.

However, having moved into thermodynamics from outside, I find the level of hostility between different communities in quantum thermodynamics to be really unfortunate. I feel the different communities should complement each other and learn from each other. And yes, this should also include having a critical eye and challenging each other. I know that I gain a lot from listening to various other communities and learning what challenges and approaches are of interest to them. But I sometimes feel that the different communities in thermodynamics are

competing with each other, and not really listening to each other. It can feel territorial and overly combative. I often see different communities rejecting each others papers because they use different definitions of entropy. It's gotten so bad that young people are reluctant to apply for fellowships in the field, because they are likely to draw some referee from another community who will blanket reject papers outside their community. Several times, I've seen referees reject papers/proposals because they believe that you can't define entropy for out-of-equilibrium systems, without recognizing that they hold an opinion which is controversial. A number of journal editors have expressed their frustration with finding neutral referees. This is really destructive to the field as a whole, because it stifles difference and development.

With respect to the QIT approach – Are there issues which should be resolved? Of course there are. But rather than taking this as a reason to get hostile, I think it would be more fruitful to encourage people to resolve those issues. For example, people often criticize the QIT approach for assuming that one can't access or exploit initial correlations between the system and reservoir. But this is an assumption made in other approaches as well, and the QIT approach is well suited to study correlations (see for example [https://arxiv.org/abs/1612.04779], which I think points in a good direction). Or people don't like that some QIT approaches allow unitary transformation, ignoring the fact that one can show that this is equivalent to other paradigms (see appendix H of https://arxiv.org/abs/1111.3882) and is needed if one wants to derive fundamental limitations valid for any interaction. I also agree with John that in terms of achievability, one would like to move closer to experiment and application. But I don't think we should be dismissive, just because it takes longer than a few years to make contact. Theory and experiment often lag, and if we only worked on ideas which could be experimentally feasible in the near term, we would rule out much of early theoretical results. I think in this regard, we are moving closer (see https://arxiv.org/abs/1511.06553 and experimental work of https://arxiv.org/abs/1703.02999 where some of these operations are implemented), although indeed there is a way to go. However, to say, as Hänggi does in the article "Maxwell's demon "gets on my nerves," is to dismiss what I think is a fundamental insight that information theory has contributed to thermodynamics.

At any rate, I would personally welcome a frank and open discussion (here or elsewhere), and would like to gain a better understanding of criticisms. Perhaps it can help foster an atmosphere in the field which is less combative, and more welcoming to a diversity of approaches."

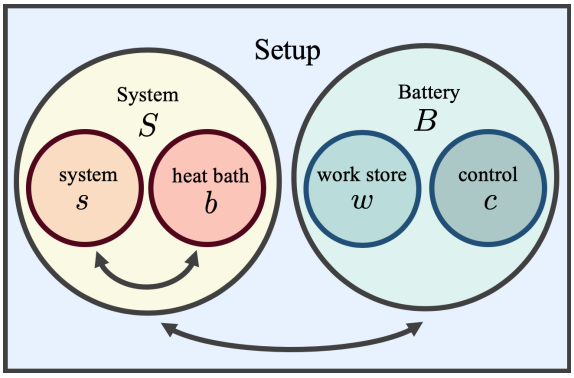


Figure B.1: **Enlarged system setup.** The total setup consists of a system, heat bath, work store, and control system (small circles). We can reduce this to a bipartite system (large circles) by using a single hybrid work store and control system, that we will call a 'battery' B and by viewing the system and heat bath as a composite enlarged system S. The arrows denote the systems which exchange energy.

Appendix B

Coherent fluctuation relations

B.1 Comment on role of heat bath

For the majority of the chapter on coherent fluctuation relations we have treated the thermal bath as implicit: a bath is a means of preparing the system in the thermal state but we do not model it. Effectively this amounts to assuming that the system and bath are sufficiently weakly interacting at the start of the protocols that they can be considered well defined independent systems at these times.

More rigorously, and as sketchd in Fig. B.1, we can think of the system (S) discussed in the bipartite case as an enlarged system consisting of some small system of interest (s) that is driven by a change in Hamiltonian H_s^i to H_s^f and a thermal bath (b) with a constant Hamiltonian H_b, i.e. $H_S^i = H_s^i \otimes H_b$ and $H_S^f = H_s^f \otimes H_b$. The FQC can be re-derived explicitly including the thermal bath if an additional factorisability condition is assumed to hold between the system and bath. The factorisability condition will hold if their shared Hamiltonian is non-interacting in the regions R_i and R_f, that is if

$$H_{sbB} = H_s^i \otimes H_b \otimes \Pi_B^i + H_s^f \otimes H_b \otimes \Pi_B^f + V_{sbB}^{\perp} \; + \mathbb{1}_{sb} \otimes H_B \tag{B.1}$$

where H_B, as before, is the battery Hamiltonian. Under these circumstances, the influence of the

bath 'factorises out'. The resulting equality explicitly quantifies the transition probabilities of the battery, when a system is driven with a change in Hamiltonian, in the presence of a thermal bath. This quantum Crooks equality takes exactly the same form as the usual FQC, Eq. (2.29), but with the relevant transition probabilities replaced by

$$\begin{aligned}\mathcal{P}(\phi_f|\phi_i,\gamma_i) &:= \langle\phi_f|\operatorname{Tr}_{sb}\left[U_{sbB}(\gamma(H_s^f)\otimes\gamma(H_b)\otimes|\phi_i\rangle\langle\phi_i|)U_{sbB}^\dagger\right]|\phi_f\rangle \quad \text{and}\\ \mathcal{P}(\psi_i|\psi_f,\gamma_f) &:= \langle\psi_i|\operatorname{Tr}_{sb}\left[U_{sbB}(\gamma(H_s^f)\otimes\gamma(H_b)\otimes|\psi_f\rangle\langle\psi_f|)U_{sbB}^\dagger\right]|\psi_i\rangle\end{aligned} \tag{B.2}$$

where $\gamma(H)$ is a thermal state with respect to Hamiltonian H.

This enlarged system perspective is perhaps a more rigorous way of thinking of the system in the bipartite case than simply treating the bath as an implicit means of preparing the system in a thermal state. We do not discuss this perspective in the main text only because it does not sit as well with the pedagogical spin example and trapped ion implementation. That is, it is hard to think of a two level system as representing both a system and a thermal bath!

A worthwhile extension to our research would be to explicitly simulate the bath in the experimental proposal and numerical analysis. One means of doing so would be to investigate the master equation fluctuation theorem that is proposed in the final version of [64]. Alternatively one could try and incorporate the bath using the quantum jump approach explored in [140].

B.2 Squeezed state Crooks equality derivation

The squeezed state FQC quantifies transition probabilities between battery oscillator states that are not only displaced but also squeezed. As such, the measured states $|\phi_f\rangle$ and $|\psi_i\rangle$ are set to the squeezed displaced states $|\alpha_f, r_f\rangle$ and $|\alpha_i^*, r_i\rangle$ respectively, i.e.

$$\begin{aligned}|\phi_f\rangle &= |\alpha_f, r_f\rangle = D(\alpha_f)S(r_f)|0\rangle \quad \text{and}\\ |\psi_i\rangle &= |\alpha_i^*, r_i\rangle = D(\alpha_i^*)S(r_i)|0\rangle\ ,\end{aligned} \tag{B.3}$$

where we have introduced the displacement operator $D(\alpha) = \exp(\alpha a^\dagger - \alpha^* a)$, the squeeze operator $S(r) = \exp(\frac{r}{2}(a^2 - {a^\dagger}^2))$, and for simplicity we assume from the outset that the squeezing parameters r_i and r_f are real. We calculate $|\phi_i\rangle$ and $|\psi_f\rangle$ using the relation between states $|\phi_{i,f}\rangle$ and $|\psi_{i,f}\rangle$ as specified in Eq. (2.28). This amounts to calculating the effect of applying the operator $\exp\left(-\chi a^\dagger a\right)$ to a squeezed displaced state, i.e.

$$\begin{aligned}|\phi_i\rangle &= \frac{1}{\sqrt{\tilde{Z}_{\alpha_i,r_i}}}\exp\left(-\chi\left(a^\dagger a+\frac{1}{2}\right)\right)D(\alpha_i)S(r_i)|0\rangle \equiv D(\mu_i)S(t_i)|0\rangle = |\mu_i,t_i\rangle \quad \text{and}\\ |{\psi_f}^*\rangle &= \frac{1}{\sqrt{\tilde{Z}_{\alpha_f,r_f}}}\exp\left(-\chi\left(a^\dagger a+\frac{1}{2}\right)\right)D(\alpha_f^*)S(r_f)|0\rangle \equiv D(\mu_f^*)S(t_f)|0\rangle = |\mu_f^*,t_f\rangle\ .\end{aligned} \tag{B.4}$$

We introduce $\mu_{i,f}$ and $t_{i,f}$ to denote the displacement and squeezing parameters respectively of the prepared states. (That the states $|\phi_i\rangle$ and $|\psi_f^*\rangle$ are also squeezed displaced states is a non-trivial result of the calculation.) To derive the FQC we will also need to calculate the $\exp\left(\frac{\Delta\tilde{E}}{k_BT}\right)$ term. It follows from the definition of $\Delta\tilde{E}$ in Eq. (2.30) that this can be written as

$$\exp\left(\frac{\Delta\tilde{E}}{k_BT}\right) = \frac{\tilde{Z}_{\alpha_f,r_f}}{\tilde{Z}_{\alpha_i,r_i}} = \frac{(\exp(-\chi a^\dagger a)D(\alpha_f)S(r_f)|0\rangle)^\dagger\exp(-\chi a^\dagger a)D(\alpha_f)S(r_f)|0\rangle}{(\exp(-\chi a^\dagger a)D(\alpha_i^*)S(r_i)|0\rangle)^\dagger\exp(-\chi a^\dagger a)D(\alpha_i^*)S(r_i)|0\rangle}\ . \tag{B.5}$$

To derive the FQC we thus need to calculate μ, s and $\tilde{Z}_{\alpha,r}$.

Useful Identities

To calculate μ, s and $\mathcal{N}_{\alpha,r}$ we will make use of the following equalities:

1. $\exp(ma^\dagger a)\exp(na^\dagger)\exp(-ma^\dagger a) = \exp(n\exp(m)a^\dagger)$

   Proof. This is derived using the Taylor expansion of the exponential followed by the Hadamard lemma [199],

   $$\exp(ma^\dagger a)\exp(na^\dagger)\exp(-ma^\dagger a) = \sum_k \frac{(n\exp(ma^\dagger a)a^\dagger \exp(-ma^\dagger a))^k}{k!} = \sum_k \frac{(na^\dagger \exp(m))^k}{k!} = \exp(n\exp(m)a^\dagger)\ .$$

   □

2. $\exp(ma)\exp(na^\dagger) = \exp(mn)\exp(na^\dagger)\exp(ma)$

   Proof. This is derived using the Baker-Campbell-Hausdorff formula [199] followed by the Zassenhaus formula [199],

   $$\exp(ma)\exp(na^\dagger) = \exp(ma+na^\dagger)\exp\left(\frac{mn}{2}\right) = \exp(na^\dagger)\exp(ma)\exp(mn)\ .$$

   □

3. $\exp(ma^2)\exp(na^\dagger) = \exp(mn^2)\exp(na^\dagger)\exp(ma^2)\exp(2mna)$

   Proof. This is again derived using the Baker-Campbell-Hausdorff formula followed by the Zassenhaus formula,

   $$\exp(ma^2)\exp(na^\dagger) = \exp\left(\frac{mn^2}{6}\right)\exp(ma^2+mna+na^\dagger) = \exp(mn^2)\exp(na^\dagger)\exp(ma^2)\exp(2mna)$$

   □

4. $\exp\left(\frac{1}{2}(ma^2+na^{\dagger 2})\right) = \frac{1}{\sqrt{\cos(\sqrt{mn})}}\exp\left(\frac{1}{2}\sqrt{\frac{n}{m}}\tan(\sqrt{mn})a^{\dagger 2}\right)\exp\left(-\ln\left(\cos(\sqrt{mn})\right)a^\dagger a\right)\exp\left(\frac{1}{2}\sqrt{\frac{m}{n}}\tan(\sqrt{mn})a^2\right)$

   Proof. To derive this equality it is helpful to first introduce the operators $K_+ := \frac{1}{2}a^{\dagger 2}$, $K_- := \frac{1}{2}a^2$, $K_z := \frac{1}{4}(aa^\dagger + a^\dagger a)$. These operators obey the commutation relations $[K_+, K_-] = -2K_z$ and $[K_z, K_\pm] = \pm K_\pm$. Next, we introduce the ansatz

   $$f := \exp((mK_+ + nK_-)t) = \exp(pK_+)\exp(qK_z)\exp(sK_-)\ . \tag{B.6}$$

   To find the coefficients p, q and s we differentiate f with respect to t,

   $$\begin{aligned} f' &= (mK_+ + nK_-)f \\ &= \left(p'K_+ + q'\exp(pK_+)K_z\exp(-pK_+) + s'\exp(pK_+)\exp(qK_z)K_-\exp(-qK_z)\exp(-pK_+)\right)f. \end{aligned} \tag{B.7}$$

   To simplify this expression we use the Hadamard lemma to obtain the following relations,

   $$\exp(pK_+)K_z\exp(-pK_+) = K_z - pK_+ \tag{B.8}$$

   and

   $$\begin{aligned} \exp(pK_+)\exp(qK_z)K_-\exp(-qK_z)\exp(-pK_+) &= \exp(pK_+)\exp(-q)K_-\exp(-pK_+) \\ &= \exp(-q)(K_- - 2pK_z + p^2K_+)\ . \end{aligned} \tag{B.9}$$

   Eq. (B.8) and Eq. (B.9) can be substituted into the right hand side of Eq. (B.7), from which it then follows that

   $$mK_+ + nK_- = p'K_+ + q'(K_z + pK_+) + s'\exp(-q)(K_- - 2pK_z + p^2K_+)\ . \tag{B.10}$$

   Equating coefficients in Eq. (B.10) we obtain a set of differential equations,

   $$\begin{aligned} p' - q'p + s'\exp(-q)p^2 &= m \\ q' - 2ps'\exp(-q) &= 0 \\ s'\exp(-q) &= n\,, \end{aligned}$$

   which can be solved, subject to the constraint that $p(0) = q(0) = s(0) = 0$, to find that

   $$\begin{aligned} p &= \frac{m}{n}\tan\left(\sqrt{mn}t\right) \\ q &= -2\ln\left(\cos\left(\sqrt{mn}t\right)\right) \\ s &= \frac{n}{m}\tan\left(\sqrt{mn}t\right)\ . \end{aligned} \tag{B.11}$$

   Identity 4 is obtained by substituting this solution, Eq. (B.11), back into the ansatz, Eq. (B.6). □

5. $\exp\left(\frac{1}{2}\left(ma^2+na^{\dagger 2}\right)\right)=\sqrt{\cos(\sqrt{mn})}\exp\left(\frac{1}{2}\sqrt{\frac{m}{n}}\tan(\sqrt{mn})a^2\right)\exp\left(\ln\left(\cos(\sqrt{mn})\right)a^\dagger a\right)\exp\left(\frac{1}{2}\sqrt{\frac{n}{m}}\tan(\sqrt{mn})a^{\dagger 2}\right)$

Proof. The proof here follows the same method as for identity 4. Using the ansatz $f=\exp((mK_+ + nK_-)t) = \exp(pK_-)\exp(qK_z)\exp(sK_+)$ it is possible to derive the same differential equations as in Eq. (B.11) but with $q\to -q$. □

6. $\exp\left(ma^2\right)\exp\left(na^{\dagger 2}\right)=\frac{1}{\sqrt{1-4mn}}\exp\left(\frac{n}{1-4mn}a^{\dagger 2}\right)\exp\left(\ln\left(\frac{1}{1-4mn}a^\dagger a\right)\right)\exp\left(\frac{m}{1-4mn}a^2\right)$

Proof. This is proven using identities 4 and 5. Let $p=\frac{1}{2}\sqrt{\frac{m}{n}}\tan(\sqrt{mn})$, $q=\frac{1}{2}\sqrt{\frac{n}{m}}\tan(\sqrt{mn})$ and $\exp(-2M)=\cos(\sqrt{mn})^2=\frac{1}{1-4pq}$, it follows that

$$\sqrt{M}\exp(pa^2)\exp(\ln(M)a^\dagger a)\exp(qa^{\dagger 2})=\frac{1}{\sqrt{M}}\exp(qa^{\dagger 2})\exp(-\ln(M)a^\dagger a)\exp(pa^2)\,,$$

which can be rearranged to give

$$\begin{aligned}\exp\left(-pa^2\right)\exp\left(qa^{\dagger 2}\right)&=M\exp(\ln(Ma^\dagger a)\exp(qa^{\dagger 2})\exp(-pa^2)\exp(\ln(M)a^\dagger a)\\&=M\exp(q\exp(-2M)a^{\dagger 2})\exp(2\ln(Ma^\dagger a)\exp(-p\exp(-2M)a^2)\ .\end{aligned}$$

The substitution $p\leftrightarrow -p$ then gives identity 6. □

Main Derivation

We are now in a position to calculate the effect of the operator $\exp\left(-\chi a^\dagger a\right)$ on a squeezed displaced state,

$$\exp\left(-\chi a^\dagger a\right)D(\alpha)S(r)\left|0\right\rangle=\exp\left(-\chi a^\dagger a\right)\exp(\alpha a^\dagger-\alpha^* a)\exp\left(\frac{r}{2}\left(a^2-a^{\dagger 2}\right)\right)\left|0\right\rangle\ . \tag{B.12}$$

We first use the standard factorised form of the displacement and squeeze operators [200],

$$D(\alpha)S(r)\left|0\right\rangle=\frac{\exp\left(-\frac{1}{2}|\alpha|^2\right)}{\sqrt{\cosh(r)}}\exp\left(\alpha a^\dagger\right)\exp\left(-\alpha^* a\right)\exp\left(-\frac{1}{2}\tanh(r)a^{\dagger 2}\right)\left|0\right\rangle \tag{B.13}$$

to rewrite Eq. (B.12),

$$=\exp\left(-\chi a^\dagger a\right)\frac{\exp\left(-\frac{1}{2}|\alpha|^2\right)}{\sqrt{\cosh(r)}}\exp\left(\alpha a^\dagger\right)\exp\left(-\alpha^* a\right)\exp\left(-\frac{1}{2}\tanh(r)a^{\dagger 2}\right)\left|0\right\rangle\ . \tag{B.14}$$

Eq. (B.14) is then rewritten using identity 3,

$$=\frac{\exp\left(-\frac{1}{2}|\alpha|^2\right)}{\sqrt{\cosh(r)}}\exp\left(-\chi a^\dagger a\right)\exp\left(\alpha a^\dagger\right)\exp\left(-\frac{1}{2}\tanh(r)\alpha^{*2}\right)\exp\left(\alpha^*\tanh(r)a^\dagger\right)\exp\left(-\frac{1}{2}\tanh(r)a^{\dagger 2}\right)\left|0\right\rangle\,, \tag{B.15}$$

followed by identity 1,

$$=\frac{\exp(-\frac{1}{2}(|\alpha|^2-\alpha^{*2}\tanh(r)))}{\sqrt{\cosh(r)}}\exp\left(\exp\left(-\chi\right)\left(\alpha+\alpha^*\tanh(r)\right)a^\dagger\right)\exp\left(-\frac{1}{2}\exp\left(-2\chi\right)\tanh(r)a^{\dagger 2}\right)\left|0\right\rangle\ . \tag{B.16}$$

By comparing Eq. (B.16) with itself in the limit that $\chi=0$, i.e. the limit in which $\exp\left(-\chi a^\dagger a\right)$ is not applied and Eq. (B.16) is simply a rewritten version of a squeezed displaced state, we identify the following modified displacement and squeeze coefficients μ and s,

$$\begin{aligned}\Re(\mu)&=\Re(\alpha)\frac{\exp\left(-\chi\right)\left(1+\tanh(r)\right)}{1+\exp\left(-2\chi\right)\tanh(r)}\,,\\\Im(\mu)&=\Im(\alpha)\frac{\exp\left(-\chi\right)\left(1-\tanh(r)\right)}{1-\exp\left(-2\chi\right)\tanh(r))}\quad\text{and}\\\tanh(s)&=\exp\left(-2\chi\right)\tanh(r)\ .\end{aligned} \tag{B.17}$$

It remains to calculate the $\exp\left(\frac{\Delta\tilde{E}}{k_BT}\right)$ term. This amounts to calculating,

$$\tilde{Z}_{\alpha,r}=\left(\exp\left(-\chi a^\dagger a\right)D(\alpha)S(r)\left|0\right\rangle\right)^\dagger\exp\left(-\chi a^\dagger a\right)D(\alpha)S(r)\left|0\right\rangle \tag{B.18}$$

The above equation can be immediately simplified using Eq. (B.16)

$$= \frac{\exp\left(-(|\alpha|^2 - \Re(\alpha)^2 \tanh(r))\right)}{\cosh(r)} \langle 0| \exp\left(ma^2\right) \exp\left(na\right) \exp\left(n^* a^\dagger\right) \exp\left(m^* a^{\dagger 2}\right) |0\rangle \tag{B.19}$$

where

$$\begin{aligned} m &= -\frac{1}{2} \exp\left(-2\chi\right) \tanh(r) \text{ and} \\ n &= \exp\left(-\chi\right) \left(\alpha^* + \alpha \tanh(r)\right) . \end{aligned} \tag{B.20}$$

Using 'Useful Identities' 6, 3, 1, and 2 in succession this can be rewritten to give,

$$\begin{aligned} &\langle 0| \exp\left(ma^2\right) \exp\left(na\right) \exp\left(m^* a^\dagger\right) \exp\left(n^* a^\dagger\right) |0\rangle \\ &= \frac{1}{r} \langle 0| \exp\left(na\right) \exp\left(\frac{m^*}{\exp(-2r)} a^{\dagger 2}\right) \exp\left(-\ln\left(\exp(-2r)\right) a^\dagger a\right) \exp\left(\frac{m}{\exp(-2M)} a^2\right) \exp\left(n^* a^\dagger\right) |0\rangle \\ &= \frac{1}{M} \exp\left(\frac{2\Re(n^2 m)}{\exp(-2M)}\right) \langle 0| \exp\left(na\right) \exp(-ln(\exp(-2M)) a^\dagger a) \exp\left(n^* a^\dagger\right) |0\rangle \\ &= \frac{1}{M} \exp\left(\frac{2\Re(n^2 m)}{\exp(-2M)}\right) \langle 0| \exp\left(\frac{n}{M} a\right) \exp\left(\frac{n^*}{M} a^\dagger\right) |0\rangle \\ &= \frac{1}{M} \exp\left(\frac{2\Re(n^2 m)}{\exp(-2M)}\right) \exp\left(\frac{|n|^2}{\exp(-2M)}\right) \end{aligned} \tag{B.21}$$

where $M = \frac{1}{\sqrt{1-4|m|^2}}$. It follows that,

$$\begin{aligned} &\tilde{Z}_{\alpha,r} := \frac{\exp(-(|\alpha|^2 - \Re(\alpha^2) \tanh(r)))}{\cosh(r) \sqrt{1 - \tanh(r)^2 \exp\left(-4\chi\right)}} \\ &\exp\left(\frac{\exp\left(-2\chi\right) \left(|\alpha|^2 (1 + \tanh(r)^2) + 2 \tanh(r) \Re(\alpha^2)\right) - \exp\left(-2\chi\right) \tanh(r) \left(\Re(\alpha^2) + \Re(\alpha^2) \tanh(r)^2 + 2|\alpha|^2 \tanh(r)\right)}{1 - \tanh(r)^2 \exp\left(-4\chi\right)}\right) , \end{aligned} \tag{B.22}$$

which can be simplified if we assume that the displacement parameters are real, $\alpha_{i,f} = \Re(\alpha_{i,f})$,

$$\tilde{Z}_{\alpha,r} := \frac{\exp\left(-|\alpha|^2 (1 - \tanh(r))\right)}{\cosh(r) \sqrt{1 - \tanh(r)^2 \exp\left(-4\chi\right)}} \quad \exp\left(|\alpha|^2 \frac{(1 + \tanh(r))^2 \left(1 - \tanh(r) \exp\left(-2\chi\right)\right) \exp\left(-2\chi\right)}{1 - \tanh(r)^2 \exp\left(-4\chi\right)}\right) . \tag{B.23}$$

This completes the derivation of the squeezed state FQC. The error-bounded squeezed state Crooks equality follows from the error bounded FQC, Eq. (2.115).

B.3 Cat state Crooks equality derivation

We take a cat state to be an equal superposition of two arbitrary coherent states, $|\text{Cat}\rangle \propto (|\alpha\rangle + |\beta\rangle)$. This is a more general definition than that sometimes seen in the literature where a cat state is taken to be only a superposition of a pair of coherent states $|\alpha\rangle$ and $|-\alpha\rangle$. To derive a cat state FQC the measured states $|\phi_f\rangle$ and $|\psi_i\rangle$ are set to

$$\begin{aligned} |\phi_f\rangle = |\text{Cat}_f\rangle &:= \frac{1}{\sqrt{2 + 2\Re(\exp(-\frac{1}{2}(|\alpha_f|^2 + |\beta_f|^2 - 2\beta_f^* \alpha_f)))}} (|\alpha_f\rangle + |\beta_f\rangle) \text{ and} \\ |\psi_i\rangle = |\text{Cat}_i^*\rangle &:= \frac{1}{\sqrt{2 + 2\Re(\exp(-\frac{1}{2}(|\alpha_i|^2 + |\beta_i|^2 - 2\beta_i^* \alpha_i)))}} (|\alpha_i^*\rangle + |\beta_i^*\rangle) , \end{aligned} \tag{B.24}$$

where the normalisation term is calculated using the fact that the overlap between two coherent states $|\alpha\rangle$ and $|\beta\rangle$ is given by $\langle\beta|\alpha\rangle = \exp(-\frac{1}{2}(|\alpha|^2 + |\beta|^2 - 2\beta^* \alpha))$. The prepared states $|\phi_i\rangle$ and $|\psi_f\rangle$ are calculated using the relation between states $|\phi_{i,f}\rangle$ and $|\psi_{i,f}\rangle$ as specified in Eq. (2.28).

Using operator algebra we find that

$$\begin{aligned}
|\phi_i\rangle &:= \exp\left(-\chi\left(a^\dagger a + \frac{1}{2}\right)\right)|\mathrm{Cat}_i\rangle \propto \left(\exp\left(-\chi a^\dagger a\right)|\alpha_i\rangle + \exp\left(-\chi a^\dagger a\right)|\beta_i\rangle\right) \\
&= \frac{1}{\sqrt{\tilde{Z}_{\mathrm{Cat}_i}}}\left(\eta_\chi^{|\alpha_i|^2}|\exp(-\chi)\alpha_i\rangle + \eta_\chi^{|\beta_i|^2}|\exp(-\chi)\beta_i\rangle\right) \quad \text{and} \\
|\psi_f\rangle &= \frac{1}{\sqrt{\tilde{Z}_{\mathrm{Cat}_f}}}\left(\eta_\chi^{|\alpha_f|^2}|\exp(-\chi)\alpha_f^*\rangle + \eta_\chi^{|\beta_f|^2}|\exp(-\chi)\beta_f^*\rangle\right)
\end{aligned} \tag{B.25}$$

where we have defined

$$\eta_\chi := \exp\left(-\frac{1}{2}\left(1-\exp(-2\chi)\right)\right) \tag{B.26}$$

and the normalisation term $\tilde{Z}_{\mathrm{Cat}_i}$ (and equivalently for $\tilde{Z}_{\mathrm{Cat}_f}$) takes the form

$$\tilde{Z}_{\mathrm{Cat}_i} = \frac{\eta_\chi^{2|\alpha_i|^2} + \eta_\chi^{2|\beta_i|^2} + \eta_\chi^{|\alpha_i|^2+|\beta_i|^2} 2\Re\left(\exp\left(-\frac{1}{2}\exp(-2\chi)(|\beta_i|^2+|\alpha_i|^2-2\beta_i^*\alpha_i)\right)\right)}{2+2\Re(\exp(-\frac{1}{2}(|\alpha_i|^2+|\beta_i|^2-2\beta_i^*\alpha_i)))} \ . \tag{B.27}$$

The normalisation terms $\tilde{Z}_{\mathrm{Cat}_i}$ and $\tilde{Z}_{\mathrm{Cat}_f}$ also provide the $\exp\left(\frac{\Delta\tilde{E}}{k_B T}\right)$ term. It follows from the definition of $\Delta\tilde{E}$ in Eq. (2.30) that

$$\exp\left(\frac{\Delta\tilde{E}}{k_B T}\right) = \frac{\langle\phi_f|\exp(-2\chi)|\phi_f\rangle}{\langle\psi_i|\exp(-2\chi)|\psi_i\rangle} = \frac{\tilde{Z}_{\mathrm{Cat}_f}}{\tilde{Z}_{\mathrm{Cat}_i}} \ . \tag{B.28}$$

As such, the cat state FQC follows from Eq.(B12 -B16). (We do not state the explicit form of $\exp\left(\frac{\Delta\tilde{E}}{k_B T}\right)$ in terms of $\alpha_{i,f}$, $\beta_{i,f}$, χ and η_χ as the expression does not simplify.)

Appendix C

An optomechanical piston setup to probe thermodynamic signatures of distinguishability

C.1 Displacement of PBS membrane for more realistic parameters

Here we include a plot of the time averaged displacement of the PBS membrane for slightly more realistic experimental parameters based broadly on Table 3.9.1. In contrast to Fig. C.1 we suppose here that the photons and the membrane are at different temperatures. While this means there is temperature gradient between the gas and piston, and therefore deviates from the spirit of the original Gibbs mixing thought experiment, it is perhaps a little more realistic since the mechanical and light modes may interact with different reservoirs.

C.2 Higher order effects

The effect of the back action of the membrane's motion on the photons dynamics can be incorporated by calculating the evolution of the membrane's displacement to second order in the optomechanical coupling strength.

The second order contribution to the work output, Eq. (3.20), vanishes and therefore the effect of the back action of the membrane on the photons for the work output is negligible. As a result the work output (both in the case of a PBS and BS membrane) is to high degree of approximation independent of the initial temperature of the membrane.

However, in contrast to the work output, the second order contribution to the energy transfer to the membrane does not vanish. In Fig. C.2 we plot the second order contribution to the energy transfer to the membrane for a BS membrane. We find that similarly to the first order case, the second order contribution also increases with the indistinguishability of the photons. In contrast to the first order contribution, the second order contribution depends on the initial state of the membrane. Assuming the membrane is initially thermal, the second order contribution increases with the initial temperature of the membrane as shown in Fig. C.2. Also, in contrast to the first order, the second order contribution to the energy of the membrane, once averaged over

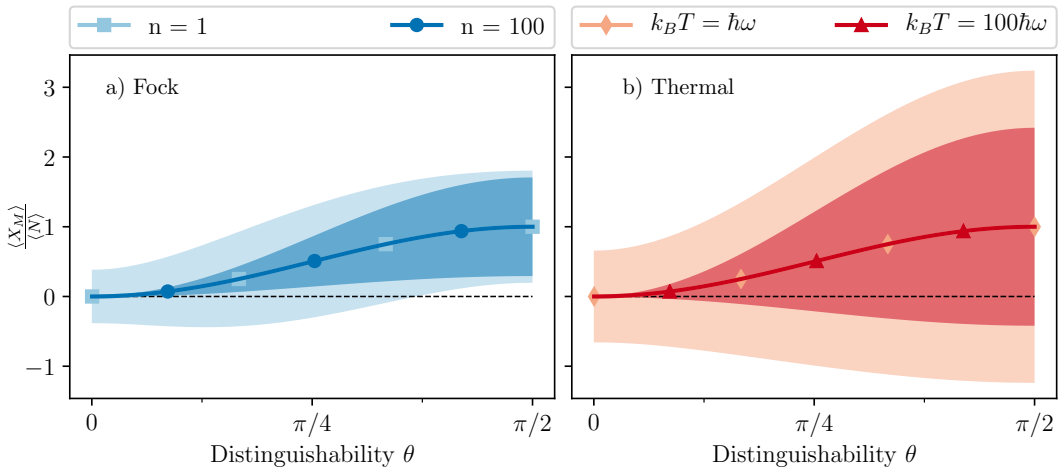


Figure C.1: **Time averaged displacement of PBS membrane.** Plot of $\langle X_M \rangle$ (directly related to the work output via (3.54)) normalised by the mean number of photons $\langle N \rangle$ per gas as a function of the distinguishability θ of the photon gases. a) Photons are initially in a Fock state with $n = 1$ photons per cavity (light blue squares) and $n = 100$ photons per cavity (dark blue circles). b) Photons are initially in a thermal state at temperature $T = \hbar\omega/k_B$ (peach diamonds) and $T = 100\hbar\omega/k_B$ (red triangles). For all four cases (light blue squares, dark blue circles, red triangles, peach diamonds) the displacement per photon is the same function over the distinguishability parameter θ. The shaded region shows the normalised standard deviation of the displacement. Parameters in both figures: $g_V x_{\text{zpf}} = 6 g_H x_{\text{zpf}} = 600\text{kHz}$, $\lambda = 10\text{GHz}$, $\omega = 1\text{THz}$, $\omega_M = 1\text{MHz}$, $m = 10\text{ng}$ and the membrane is at temperature $T_M = 5\hbar\omega_M/k_B$. All distances are given in units of $\frac{\hbar g_V}{m\omega_M^2}$.

oscillations, grows quadratically over time. In the case of a PBS membrane (data not shown) the second order contribution to the energy transfer also increases with indistinguishability. Thus the distinguishability dependence of the energy transfer to the membrane is softened for high temperature membranes in the long time limit. It would be interesting to explore such effects further.

Nonetheless, for both PBS and BS membranes, the effect of back action is negligible over the lifetime of the cavity, $1/\kappa$, as long as the initial thermal occupancy of the membrane, $\bar{n}_{th}$, is lower than ~ 50 phonons. This is therefore the regime of applicability for the results presented in the main text. Such low temperature regimes have been experimentally achieved [177].

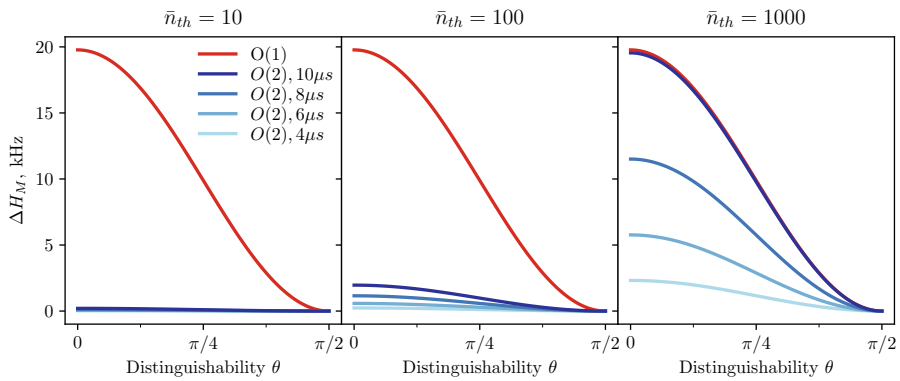


Figure C.2: **Second order contribution to energy transfer.** We plot the first and second order contributions to the time averaged energy transfer to a beamsplitter membrane as a function of the distinguishability of the photons in the cavity in the absence of damping effects ($\kappa = \kappa_C = 0$). Once the energy transfer to the membrane is averaged over fast oscillations the first order contribution to the energy transfer is constant in time, while the second order contribution has an amplitude that grows quadratically in time. Here we plot the second order correction up to $10\mu s$ (the cavity lifetime in the experimental setup of Ref[23]). The membrane is prepared in a thermal state containing on average $\bar{n}_{th}$ phonons, where $\bar{n}_{th} = 10$, $\bar{n}_{th} = 100$ and $\bar{n}_{th} = 1000$ in the left, centre and right plots respectively and the light field in both halves of the cavity is initially in a coherent state containing on average 10^6 photons. We utilise the following parameters from the experimental settings in [2, 3]: $\omega_M = 350$kHz, $\omega = 20$THz, $\lambda = 34$GHz, $m = 45$ng and $gx_{\text{zpf}} = 3.3$kHz, with similar behaviour expected for a range of parameters.